Filter criterion for granular soils based on the constriction size distribution

Feda Seblany

N° d'ordre : 2018LYSEC042 Année 2018

THÈSE

présentée pour l'obtention du titre de

DOCTEUR DE L'ÉCOLE CENTRALE DE LYON

École doctorale : MEGA
Spécialité : Génie Civil

par

Feda SEBLANY

FILTER CRITERION FOR GRANULAR SOILS BASED ON THE CONSTRICTION SIZE DISTRIBUTION

Soutenue à l'École Centrale de Lyon, le 17 Décembre 2018

devant le jury composé de

M. Didier MAROT	Professeur, Université de Nantes	Rapporteur
M. Laurent OXARANGO	Professeur, Université de Grenoble-Alpes	Président
M. Pierre PHILIPPE	Directeur de recherche, IRSTEA	Rapporteur
M. Christophe PICAULT	Ingénieur, Compagnie Nationale du Rhône	Invité
Mme. Nadège REBOUL	Maître de conférences, Université de Lyon 1	Examinatrice
M. Alexander SCHEUERMANN	Associate Professor, University of Queensland	Co-directeur de thèse
M. Eric VINCENS	Professeur, École Centrale de Lyon	Directeur de thèse

Thèse préparée au Laboratoire de Tribologie et Dynamique des Systèmes (CNRS-UMR 5513) de l'École Centrale de Lyon, Ecully, France

"I would rather be ashes than dust! I would rather that my spark should burn out in a brilliant blaze than it should be stifled by dry-rot. I would rather be a superb meteor, every atom of me in magnificent glow, than a sleepy and permanent planet. The function of man is to live, not to exist. I shall not waste my days trying to prolong them. I shall use my time."

Jack London

Acknowledgements

First, I would like to express my sincere gratitude to my supervisor, *Prof. Eric Vincens*. I have been amazingly fortunate to work with a supervisor who gave me the freedom to explore on my own and at the same time the guidance to recover when my steps faltered. Your patience, support, comments and engagement during the past three years helped me to achieve this work.

This research project has been funded by the *Compagnie Nationale du Rhône*. I gratefully acknowledge *CNR* for its interest and financial support. In particular, I would like to thank *Mr. Christophe Picault* for his precious time and for our inspirational discussions.

I am also grateful to the Univerity of Queensland for funding my stay in Australia for three months (spring 2018). It was a pleasure to work with such a talented group of researchers. In particular, special thanks go to my co-supervisor *Dr. Alexander Scheuermann* for following my research work and for his insightful comments.

I would like to sincerely thank *Prof. Didier Marot*, *Prof. Laurent Oxarango*, *Dr. Pierre Philippe* and *Dr. Nadège Reboul* for being members of the jury. I wish to extend my deepest thanks to *Ulrike Homberg* from *Zuse Institut Berlin* for her valuable contribution.

I am also thankful to the staff system at *LTDS-ECL* and *Centrale Innovation* who maintained all the requirements related to my work. Moreover, I am grateful to the friendly and cheerful group of colleagues and fellow students that I was blessed to meet in my daily work.

Furthermore, I would like to thank all my friends for their support and encouragement which drive me to give my best. Sincere appreciation is to *Matsa-Gamaleddyn* family for their warm welcome and hospitality at my arrival to Lyon and for their continuous help and accompany. I am so lucky to have so many wonderful and supportive friends.

My deepest gratitude goes to my family for their unconditional love and constant encouragement. In particular, I would like to thank my Mom and Dad who raised me with a love of science, inspired me to follow my dreams and supported me both financially and emotionally in all my pursuits. I have learned so much from you and I appreciate all of the sacrifices that you've made on my behalf. You are my role models and I would never have made it this far without you!

To my beloved sisters, brother and brother-in-law, I would like to express my warmest thanks for being my best friends. I love you dearly and thank you for all your advices and unbelievable support. And to the world's cutest kids ever, my nieces, *Melina* and *Elena*, thank you so much for being my source of happiness and for always cheering me up. Finally, I would like to dedicate this thesis to my grandfather. Although it has been years since you have passed, I still remember your encouraging words every day.

Table of Contents

Acknowledgements **iii**

Table of Contents **v**

List of Figures **ix**

List of Tables **xv**

Abstract **xvii**

Résumé **xix**

Introduction **1**

1 Context 1

2 Research objectives 4

3 Thesis outline 5

I Pores and constrictions in granular soils **7**

1 Introduction 7

2 Pore-network models 8

3 Methods for CSD computation 9

3.1 Experimental approaches 9

3.1.1 Background 9

3.1.2 Replica technique 10

3.1.3 Base suspension method 10
3.1.4 Micro-computerized tomography scanning (micro-CT) 13
3.2 Numerical approaches 14
3.2.1 Background 14
3.2.2 A brief review on the Discrete Element Method (DEM) 15
3.2.3 Delaunay tessellation 16
3.2.4 Voronoï diagram 17
3.2.5 Distance-mapping method 18
3.2.6 Pore merging criteria 19
3.3 Analytical approaches 22
3.3.1 Background 22
3.3.2 Model for the densest state 23
3.3.3 Model for the loosest state 24
3.3.4 Models for different relative densities 26
4 Conclusion 28

II Filter criteria for granular soils **29**

1 Introduction 29
2 Design of suitable filters 30
3 Experimental filtration tests 32
4 Particle-size based criteria 33
5 Permeability-based criteria 37
6 Constriction-based criteria 38
7 Internal stability of granular soils 40
8 Conclusion 43

III Pore and CSD computation for spherical materials **45**

1 Introduction 45

2 Discrete element modeling 46
2.1 Characteristics of numerical packings 46
2.2 Sample generation protocol 48
2.3 Representative Elementary Volume analysis 49
3 Void space characterization and pore merging criteria 51
3.1 Overlapping inscribed void spheres technique 52
3.2 Pore distributions derived from different merging criteria 54
3.3 CSD derived from different merging criteria 56
3.4 Conclusion 59
4 Analytical models 60
4.1 Validation of existing models 60
4.2 Improved model 62
5 Characteristic length of the pore space 63
5.1 Previous estimates 64
5.2 Influence of merging criteria 65
5.3 Statistics over DEM samples 68
6 Conclusion 71

IV CSD-based filter criterion for spherical materials 73

1 Introduction 73
2 Dry filtration tests 74
2.1 Objectives and principles 74
2.2 Results and discussion 75
2.3 Influence of the density 78
2.4 Comparison with existing controlling constriction sizes 78
3 Hydraulic filtration tests 80
4 Equivalent sieve opening size 82
4.1 A new analytical formula 82

4.2 Validation based on experimental data 84
5 A new constriction-based criterion 85
5.1 Verification of the criterion based on experimental data 87
6 Conclusion 91

Summary, conclusions and perspective **93**
1 General Summary 93
2 Main conclusions 94
3 Perspectives 97

Appendices **99**

A Pore distributions **101**

B CSD and probability density function of constriction sizes **103**

C Results of analytical models **107**

D *Granular Matter* Paper (Seblany et al., 2018) **109**

Résumé étendu en Français **131**
1 Contexte Général 131
2 Objectifs 132
3 Démarches et contributions 133
4 Perspectives 135

References **137**

List of Figures

1 (a): The catastrophic failure of the Teton dam (U.S., 1976); (b): The breach of the Ouches dam (France, 2001) 2

2 Sketch of a zoned core dam 2

I.1 The pore-network model of Witt (1993) 8

I.2 Cubic pore-network model (Schuler, 1996) 9

I.3 Void channel model (modified after Indraratna and Vafai (1997)) 9

I.4 Pore imprints of a gravel skeleton (Witt, 1986) 10

I.5 Constriction size distribution (CSD) and probability for a fine particle of diameter d to pass a constriction of its own size 11

I.6 Device of filtration tests from Soria et al. (1993) 12

I.7 Example of CSD determination according to Soria et al. (1993) (modified after Sjah and Vincens (2013)) 12

I.8 Volumetric visualization of a CT scan of a sample of sandstone with a resolution of 39 µm (Vincens et al., 2015) 14

I.9 Computation cycle of a DEM model 15

I.10 Interaction law used by Cundall and Strack (1979) 16

I.11 (a): Tetrahedron built from the centers of four neighbouring spheres; (b): Definition of a constriction: the largest empty disc included in the void space for a given face 17

I.12 2D representation of (a): Delaunay tessellation and; (b): Voronoï graph 18

I.13 Detail of a Voronoï graph; (a): red (larger) spheres at crossing indicate the centers of pores, while the blue (smaller) spheres represent the centers of constrictions on the edges; (b): The diameter is color-coded along the edges with yellow (large) to red (small) (Seblany et al., 2018) 18

I.14 Scheme of the Medial Axis method: medial axis with void nodes (large circles) and constrictions (small circles) (Taylor et al., 2015) 19

I.15 A 2D schematic of different configurations encountered in Delaunay triangulation; (a): separated pores; (b): interlocked pores; (c): highly interlocked pores. (d-f): Schematic of the throats on the common face of two neighbouring tetrahedra for different cases (3D) 20

I.16 A two-dimensional schematic diagram of merging of Delaunay cells with overlapping inscribed void spheres to form a single pore 20

I.17 Different neighbourhood levels for a Delaunay cell (In 2D) 21

I.18 A schematic of L_1 (In 2D) 21

I.19 A schematic of L_2 (In 2D) 22

I.20 A discretized particle size distribution (PSD) 23

I.21 Geometrical configurations for (a): the densest arrangement (Silveira, 1965); (b): the loosest arrangement (Silveira et al., 1975); (c): the arrangement of Schuler (1996) 24

II.1 Possible locations of initiation of internal erosion (Fell and Fry, 2007); (1): spillway wall interface; (2): adjacent to conduit; (3): crack associated with steep abutment profile; (4): desiccation on top of the core; (5): embankment to foundation; (6): foundation (if the foundation is made of soil or is an erodible rock); (7): embankment through poorly compacted layer and or crack 30

II.2 Stable base-filter interface during seepage (Locke and Indraratna, 2001) 32

II.3 Typical laboratory apparatus (Locke, 2001) 33

II.4 Filter and drainage criteria (Terzaghi et al., 1996) 34

II.5 Filters and base soils having different uniformity coefficients C_u but similar D_{15}/d_{85} ratio (Indraratna et al., 2007) 37

II.6 Graphical representation of the procedure from Kenney and Lau (1985) for internal stability assessment 42

III.1 Particle size distribution (ordinate on the left Y-axis) and cumulative particle size distribution (ordinate on the right Y-axis) for the considered samples (a): UG, (b): WG1, (c): GG1, (d): WG2, (e): GG2 47

III.2 CSDs obtained from samples prepared by different techniques (deposit under gravity, isotropic compression); (a): UGL, (b): WG1L 49

III.3 Evolution of porosity along the horizontal direction in each layer for UGL sample 50

III.4 CSDs over different layers for a sample width of $4D_{100}$ (UGL) 51

III.5 A configuration showing a constriction larger than the associated pores 52

III.6 Definition of different merging criteria associated to the overlapping inscribed void spheres technique 53

III.7 A schematic of $L_1(p\%)$ (In 2D) 53

III.8 Probability density functions for the equivalent pore diameter resulting from different definitions and corresponding to the overlapping inscribed void spheres technique; (a): UGL, (b): UGD 55

III.9 Probability density functions for the equivalent pore diameter resulting from different definitions and corresponding to the overlapping inscribed void spheres technique; (a): GG1L, (b): GG1D 55

III.10 Number of Delaunay cells per pore in L_1 for loose and dense states; (a): UG, (b): GG1, (c): WG2, (d): GG2 56

III.11 (a): CSDs for the UGL sample; (b): underlying probability density function for different merging criteria defined in the overlapping inscribed void spheres technique 57

III.12 (a): CSDs for the GG1L sample; (b): underlying probability density function for different merging criteria defined in the overlapping inscribed void spheres technique 57

III.13 (a): CSDs for the GG2L sample; (b): underlying probability density function for different merging criteria defined in the overlapping inscribed void spheres technique 57

III.14 Evolution of the relative number of constrictions for different merging criteria belonging to L_1, at loose and dense states; (a): UG, (b): GG1, (c): WG2, (d): GG2 58

III.15 Flow chart for the CSD computational procedure 61

III.16 Comparison of the CSDs calculated with the analytical method and the Delaunay method (L_0 computation) for (a): WG2; (b): GG2 62

III.17 Comparison of the CSDs calculated with the improved analytical method and the Delaunay method (L_1 computation) for (a): WG2; (b): GG2 63

III.18 Geometrical configurations; (a): cubic (8P); (b): pyramidal (4P) 65

III.19 Cubic pore network allowing unidirectional displacement of particles from a pore layer to another one (plain arrow) (modified after Sjah and Vincens (2013)) . . . 66

III.20 Scheme illustrating the impact of merging criteria on the mean pore spacing . . . 66

III.21 Different estimates of the mean pore spacing for (a): loose samples; (b): dense samples. All the quantities (D_{50M}, D_{50SA}, D_{50N}, mean void sphere and Eq. III.3) are normalized by the mean pore spacing based on DEM statistics (L_0) 69

III.22 Different estimates of the mean pore spacing for (a): loose samples; (b): dense samples. All the quantities (D_{50M}, D_{50SA}, D_{50N} and Eq. III.3 *) are normalized by the mean pore spacing based on DEM statistics (L_1) 70

IV.1 A schematic of the the filtration process 75

IV.2 Probability density function of constriction sizes (solid lines) depending on merging criterion L_0, L_1 and depth of penetration (dotted line) normalized by the sample thickness resulting from numerical filtration tests for: (a-b): UG, (c-d): WG1, (e-f): GG1 at loose (a-c-e) and dense (b-d-f) states. The vertical gray line identifies the largest mode of the constriction size distribution derived from merging criterion L_1 76

IV.3 Probability density function of constriction sizes (solid lines) depending on merging criterion L_0, L_1 and depth of penetration (dotted line) normalized by the sample thickness resulting from numerical filtration tests for: (a-b): WG2, (c-d): GG2 at loose (a-c) and dense (b-d) states. The vertical gray line identifies the largest mode of the constriction size distribution derived from merging criterion L_1 . . . 77

IV.4 Schematic of the finite volume formulation used in the DEM-PFV method (Catalano et al., 2014) (a): volume of fluid in a pore; (b): adjacent pores and local connections 80

IV.5 Probability density function of constriction sizes (solid lines) depending on merging criterion L_0, L_1, depth of penetration (dotted line) normalized by the sample thickness resulting from numerical dry filtration tests and critical diameters derived from hydraulic filtration tests for: (a-b): UG, (c-d): GG1 at loose (a-c) and dense (b-d) states. The vertical gray line identifies the largest mode of the constriction size distribution derived from merging criterion L_1 81

IV.6 Particle size distributions of the filters used by Sherard et al. (1984) for filtration analysis 84

IV.7 Comparison of the equivalent sieve opening size computed analytically with the controlling constriction size provided by Sherard et al. (1984) 85

IV.8 PSDs of three uniform filters from Indraratna et al. (1996) 87

IV.9 PSDs of two moderately graded filters (Indraratna and Vafai, 1997) 88

IV.10 PSDs of the well-graded filters used by Lafleur (1984) for filtration analysis . . . 89

IV.11 PSDs of uniform filters taken from the experimental study of Indraratna et al. (2007) 89

IV.12 Relation between the equivalent sieve opening size d_{OS} and the representative size D_{15} for various filters 90

A.1 Probability density functions for the equivalent pore diameter resulting from different definitions and corresponding to the overlapping inscribed void spheres technique; (a): WG1L, (b): WG1D 101

A.2 Probability density functions for the equivalent pore diameter resulting from different definitions and corresponding to the overlapping inscribed void spheres technique; (a): WG2L, (b): WG2D 101

A.3 Probability density functions for the equivalent pore diameter resulting from different definitions and corresponding to the overlapping inscribed void spheres technique; (a): GG2L, (b): GG2D 102

B.1 (a): CSDs for the UGD sample; (b): underlying probability density function for different merging criteria defined in the overlapping inscribed void spheres technique 103

B.2 (a): CSDs for the GG1D sample; (b): underlying probability density function for different merging criteria defined in the overlapping inscribed void spheres technique 103

B.3 (a): CSDs for the GG2D sample; (b): underlying probability density function for different merging criteria defined in the overlapping inscribed void spheres technique 104

B.4 (a): CSDs for the WG1L sample; (b): underlying probability density function for different merging criteria defined in the overlapping inscribed void spheres technique 104

B.5 (a): CSDs for the WG1D sample; (b): underlying probability density function for different merging criteria defined in the overlapping inscribed void spheres technique 104

B.6 (a): CSDs for the WG2L sample; (b): underlying probability density function for different merging criteria defined in the overlapping inscribed void spheres technique 105

B.7 (a): CSDs for the WG2D sample; (b): underlying probability density function for different merging criteria defined in the overlapping inscribed void spheres technique 105

C.1 Comparison of the CSDs calculated with the analytical method and the Delaunay method (L_0 computation) for (a): UG; (b): WG1; (c): GG1 107

C.2 Comparison of the CSDs calculated with the improved analytical method and the Delaunay method (L_1 computation) for (a): UG; (b): WG1; (c): GG1 108

List of Tables

II.1 Filter design criteria introduced by Sherard and Dunnigan (1989) 36

II.2 Comparison of capacities between particle-based and constriction-based filter criteria (Indraratna et al., 2008) 39

II.3 Filter design criteria introduced by Vakili et al. (2015) 40

II.4 Chronological progression of various filtration models related to constriction size distribution (modified after Indraratna et al. (2008) 41

II.5 Summary of internal stability criteria for granular soils 42

II.6 Internal stability criteria for granular soils as proposed by Chang and Zhang (2013) 43

III.1 Mechanical and numerical parameters for DEM simulations 48

III.2 Characteristics of numerical samples 48

III.3 The longest distance L_{max} traveled by a particle of diameter d = 1.16mm for different merging criteria defined in the overlapping inscribed void spheres technique 67

III.4 The longest distance L_{max} traveled by a particle of diameter d = 1.16mm for different merging criteria defined in the pore separation technique 67

IV.1 Comparison of the critical diameters with two characteristic constriction sizes (the modal value and D_{c35}) derived from L_1 calculation for the studied materials . . . 78

IV.2 Comparison of the critical diameters derived from numerical filtration tests with the controlling constriction sizes of Kenney et al. (1985) and Witt (1993) 79

IV.3 Typical hydraulic gradients (Giroud, 1996) 82

IV.4 Comparison of the numerical and analytical values for the equivalent sieve opening size d_{OS} (in mm) 84

IV.5 Comparison of the PSD-based criterion of Terzaghi et al. (1996) and the proposed CSD-based criterion with laboratory results taken from past studies 90

Abstract

The granular discontinuities in hydraulic structures or in their foundation constitute a major source of instabilities causing erosion phenomena, process by which finer soil particles are transported through the voids between coarser particles, under seepage flow. In the long term, the microstructure of the soil will change and the excessive migration become prejudicial to the stability of the structures and may also induce their failure. The safety of earth structures is mainly dependent on the reliability of their filter performance, i.e. the ability of the filter placed inside the structure during construction or outside during repair works, to retain fine particles. Indeed, the void space of a granular filter is divided into larger volumes, called pores, connected together by throats or constrictions. Recent researches showed that the distribution of throats (Constriction Size Distribution or CSD) between pores plays a key role to understand the filtration properties of a granular soil. This research is devoted to investigate the constriction sizes and their impact on the mechanisms of filtration in granular spherical materials. To achieve this objective, two approaches were followed in this work: numerical and analytical approaches. In the case of spherical materials, the Discrete Element Method (DEM) can help to compute the CSD using the Delaunay tessellation method. However, a more realistic CSD can be obtained by merging adjacent Delaunay cells based on the concept of the overlap of their maximal inscribed void spheres. Following this consideration and by extending the previously developed analytical models of CSD, a revised model is proposed to quickly obtain the CSD. The DEM data generated are then used to explore the potential of transport of fine particles through a filter of a given thickness by means of numerical filtration tests. A correlation has been found between the CSD and the possibility of migration of fine grains. Accordingly, an analytical formula has been proposed to calculate the controlling constriction size of a filter material. This characteristic size, which takes into account the particle size distribution (PSD) and the density of the material, has been used to reformulate a constriction-based criterion in a more physical manner. The proposed filter design criterion is verified based on experimental data from past studies and a good agreement has been found.

Key words: internal erosion - granular soils - sphere - DEM - pore - constriction - filtration - controlling constriction size

Résumé

Les discontinuités granulaires dans les ouvrages hydrauliques ou dans leur fondation constituent une source majeure d'instabilités à l'origine des phénomènes d'érosion. L'érosion interne est ainsi définie comme une migration de particules engendrée par un écoulement interne parasite, dans un sol ou dans un ouvrage en terre. A long terme, les conséquences de cette migration peut affecter la stabilité des ouvrages et peut même conduire à leur rupture. La sécurité des ouvrages en terre dépend principalement de la performance de leurs filtres, c'est-à-dire de la capacité du filtre, mis en interne en phase de conception ou en externe en phase de réparation, à retenir les particules fines. L'espace poral d'un filtre granulaire est divisé en volumes élémentaires, appelés pores, reliés entre eux par des étranglements plus étroits appelés constrictions. Des recherches récentes ont montré que la distribution des tailles de constriction (CSD) joue un rôle fondamental dans la compréhension des propriétés de filtration des sols granulaires. Ce travail vise à étudier la CSD et son impact sur les mécanismes de filtration dans les matériaux granulaires. Pour atteindre cet objectif, deux approches ont été suivies dans ce travail: l'une numérique et l'autre analytique. Dans le cas des matériaux de forme sphérique, la méthode des éléments discrets (DEM) permet de calculer la CSD en s'appuyant sur une partition de Delaunay en tétraèdres. Cependant, une CSD plus réaliste peut être obtenue par association des tétraèdres voisins selon un critère basé sur le chevauchement de leurs sphères de vide inscrites. A partir de cette considération et en se basant sur les modèles analytiques existants, un modèle révisé est proposé pour obtenir rapidement la CSD. Les échantillons DEM générés sont ensuite utilisés pour examiner le potentiel de transport des particules fines à travers un filtre d'épaisseur donnée. Les résultats des essais de filtration numériques menés ont montré une corrélation entre la CSD et la possibilité de migration des particules fines. En conséquence, une formule analytique a été proposée pour calculer le diamètre d'ouverture de contrôle des filtres granulaires. Cette taille caractéristique qui prend en compte la granulométrie et la densité du matériau granulaire, a été introduite dans un critère de filtre construit sur la base de la CSD, en vue de le représenter de manière plus physique. Le critère proposé reproduit correctement des résultats expérimentaux rapportés dans la littérature.

Mots clés: érosion interne - sols granulaires - sphère - DEM - pore - constriction - filtration - diamètre d'ouverture de contrôle

Introduction

1. Context

Particle retention within porous media is of great importance in numerous disciplines such as water and waste water treatment (McDowell-Boyer et al., 1986; Yuan et al., 2012), bacterial filtration (Logan et al., 1993; Martin et al., 1996), sand production in wells (Penberthy and Shaughnessy, 1992; Papamichos et al., 2001), leachate collection systems (Reddi et al., 2005; Rowe, 2005), producing oil from petroleum bearing reservoirs (Dullien, 1992; Ghanizadeh et al., 2015), retarding the transport of radionuclide in waste repositories (Painter et al., 2008; Xiong et al., 2016), internal erosion in earth structures (Reboul et al., 2010; Abdelhamid and El Shamy, 2015) and many others.

Past case studies have reported that internal erosion is one of the main factors affecting the safety and the serviceability of many levees and earth dams (Foster et al., 1998; Fell et al., 2003; Fell and Fry, 2007; Richards and Reddy, 2007; Zhang et al., 2009; Garner and Fannin, 2010; ICOLD, 2013). This phenomenon occurs when soil particles within the structure are washed out by seepage flow. If not carefully controlled, such a disorder can modify the hydraulic and mechanical characteristics of the earth structure leading, in the worst cases, to catastrophic damages and irreversible failure (e.g. the collapse of the Teton dam (Fread, 1988) as shown in Fig. 1a). The ICOLD (2013) reported that internal erosion has been responsible of about half of embankment dam failures over the world, and in France, every year, one hydraulic earthen structure is breached by this process (Fry et al., 2015), for example, the failure of the Ouches dam (Fig. 1b).

Indeed, earth structures are constructed with earthen materials primarily for flood control, water storage, power generation and irrigation. The construction and the design of such structures have resulted from different compromises where safety plays a major role. As earth structures age, maintenance costs and safety hazards often increase, making their continued reliability has becoming a growing concern.

There are four initiating mechanisms for internal erosion: concentrated leaks, backward erosion, contact erosion and suffusion (Fry, 2012; Fell and Fry, 2013; ICOLD, 2013). Concentrated leaks involve the formation of cracks or hydraulic fractures. Backward erosion piping occurs when soil particles are removed in a regressive way leading to the formation of a continuous pipe. Contact erosion is the erosion of particles at the interface between fine and coarse soils. Suffusion corresponds to the process of detachment and transport of finest particles within the matrix of coarse particles. In all cases, failure take place due to an uncontrolled seepage.

Fig. 1. (a): The catastrophic failure of the Teton dam (U.S., 1976); (b): The breach of the Ouches dam (France, 2001)

The most efficient way to stop the erosion process is to provide protective soil layers or geosynthetic layers, called filters in the downstream of hydraulic structures and in contact with the foundation. For example, in zoned dams, filter layers are required to prevent the wash out of the core materials consisting of fine-grained soils (Fig. 2).

Geotextiles are modern engineering materials that have gained recently an increasing attention in hydraulic applications, such as filtration and drainage (Giroud, 1982; Luettich et al., 1992; Sabiri et al., 2017). However, the geotextile fabric must be placed under strict specifications and its long term performance may be unsatisfactory (Locke and Indraratna, 2001). Granular filters made up of a suitable grading of coarse aggregates are more commonly used both for the design and for the repair.

The design of granular filters is critical for the safety of hydraulic structures since it implies that their role is warranted throughout the service life of these structures. In fact, the inability of granular filters to prevent the excessive migration of fine particles can be due to unsuitable soil gradation, segregation or poor compaction. It is then important to understand and interpret the role of grading and density in filtration processes for a better evaluation of soil erosion problems.

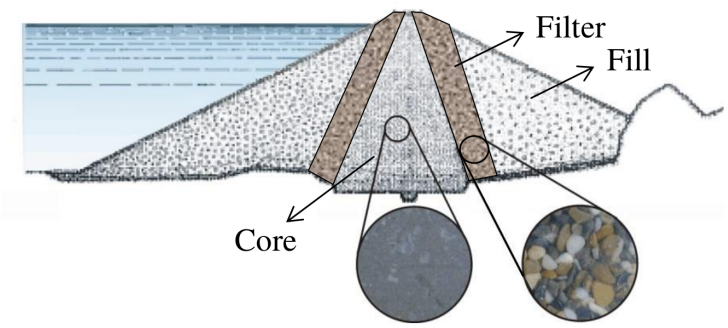

Fig. 2. Sketch of a zoned core dam

However, to achieve the retention function successfully, filters must have voids small enough to block the passage of fine materials but large enough to allow the escape of water without causing high hydraulic pressures. Consequently, filter designs must satisfy two criteria:

1. The geometrical criterion

   Studies on internal erosion originally focused on geometrical criteria, where primarily particle and equivalent opening sizes in the soil matrix allowing fine particle movement, were investigated. These criteria are based on the idea that the movement of fine particles through a filter is highly dependent on the geometry of filter grains and their pore structures. Fine particles can be eroded if they meet voids greater than their sizes. Consequently, the effectiveness of a filter to retain fine particles is governed by the way the pores are connected, more precisely by the narrowest paths linking pores, hereafter denoted constrictions.

   The commonly applied geometrical filter criteria are based on characteristic grain sizes of both base soil and filter materials where the filter grain size implicitly characterizes the constrictions within the filter (Sherard and Dunnigan, 1989; Terzaghi et al., 1996). Other studies directly used the controlling constriction size or the equivalent opening size, as the basis for a definition of a geometrical criterion (Kenney et al., 1985; Witt, 1993; Indraratna et al., 2007; Raut and Indraratna, 2008).

2. The hydraulic criterion

   Other methods relate the filter performance to the hydrodynamic conditions within the filter. In fact, a hydraulic load is needed to move a fine particle, even if the filter structure geometrically provides an opening size large enough for its displacement in the pore matrix.

   Some studies were based on the permeability of the filter which is regarded as being correlated to the constriction size (Vaughan and Soares, 1982; Vaughan et al., 2004; Delgado et al., 2006). The hydraulic criterion can also be described by the flow velocity, the flow direction, the hydraulic gradient and the conductivity. Internal erosion occurs when the hydraulic gradient and the flow velocity are large enough (higher than a critical value) to mobilize the fine particles through the voids between the coarse particles. In order to calculate the soil hydraulic parameters, new criteria based on the constriction size distribution of the soil have been developed (Scheuermann and Bieberstein, 2007; Goltz et al., 2009; Scheuermann et al., 2010).

In consequence, geometrical and hydraulic conditions should be fulfilled together to limit internal erosion. In the present study, we only focus on the geometric criterion.

In this regard, many researches showed that the internal pore structure, and more precisely the constriction size distribution (hereafter called CSD) is the key element to understand the filtration properties of a granular soil (Kenney et al., 1985; Witt, 1993; Locke et al., 2001; Indraratna et al., 2007). However, the validity of these findings rely on a precise description of the void space including pore and throat sizes.

Consequently, different methods to investigate the void space can be found in the literature (experimental, numerical and analytical methods). Experimental approaches are considered as practical tools to identify the pore characteristics, including the CSD of small samples. Besides, analytical approaches seem to be very convenient to obtain the CSD by using a conceptually simple procedure that assumes some geometrical arrangements to exist within the filter. Recently, with the

rapid increase in computer power, the discrete element method (DEM) has been proved to be an effective tool to model granular soils. This method allows to provide some measurements of pore structures if combined with specific void partitioning techniques.

However, the limits of pores cannot be comprehensively assigned due to the continuous and irregular nature of the void space, and thus, the throats cannot be easily defined. Therefore, the segmentation of the pore network into pores and constrictions remain inconclusive and further research is required to provide a more representative quantification of the void entities and to compute the CSD more accurately.

2. Research objectives

Current filter design procedures often include criteria based on particle size ratios. The feedback on earth structures performance has shown that empirically designed filters failed to prevent the loss of transported particles in some cases.

In order to solve common filtration design problems, the general concept of constriction-based criteria has recently been introduced as a useful adjunct to traditional concepts, and in this context, CSD investigations have been the subject of numerous studies in the past decade. Although these studies significantly contributed in this field, some aspects are not clearly specified and further insights are required to draw clearer conclusions.

Therefore, motivated by finding a simple tool that can be easily applied in engineering practices to control the retention of fine particles in earth structures given the grading and the density of the filter, this work, funded by the *Compagnie Nationale du Rhône*, provides a comprehensive approach relying on a fundamental study of the CSD. In particular, the role of the constriction size distribution in the filtration behaviour of granular soils is investigated based on numerical and analytical procedures using spherical particles. Two main objectives form the basic outline of this thesis:

- Adoption of a well-established model of CSD taking into account the grading and the relative density of the material.
- Derivation of an analytical formula to estimate the filter opening size which can be subsequently included in a rational filter retention criterion based on the CSD and considering the grading and the density of the material.

Previous researches carried out in *LTDS* were focused on CSD (Reboul et al., 2008, 2010; Wu et al., 2012; Sjah and Vincens, 2013; Li et al., 2014). The first part of this study particularly extends the results of Reboul et al. (2008) and Reboul et al. (2010). In their work, the DEM code PFC^{3D} was used to generate spherical packing for two materials with continuous gradings (a uniformly graded material and a widely graded material) and another material with a discontinuous grading curve; constrictions were identified in the samples using a void analysis algorithm and analytical models were developed for the design of the CSD.

Here, in addition to the materials above, further samples with a higher coefficient of uniformity will be tested, including one widely graded material and another gap-graded material. An updated

version of the void analysis algorithm will be used to derive the void characteristics, and analytical models will be revised accordingly.

3. Thesis outline

This manuscript is organized in four chapters grouped in two parts:

- **Part I** provides a synthesis of the main findings in the context of characterizing the void space in porous media and presents a summary of the chronological development of filter design criteria. It consists of two chapters:
  - **Chapter I** presents the pore network models for describing the void microstructure of a granular medium and provides a literature review of the CSD computation methods discussing their strengths and weaknesses.
  - **Chapter II** is dedicated to *"filter criteria for granular soils"*. Available filter design criteria (particle-size based criteria, permeability-based criteria and constriction-based criteria) and their limitations are briefly described. Criteria for internal stability of granular soils are also presented.
- **Part II** presents the results of the numerical and analytical analyses conducted to examine the void properties of granular filters and their implications on the filtration mechanisms within these materials. It comprises two chapters:
  - **Chapter III** mainly focuses on the characterization of pore and constriction size distributions in granular soils. Numerical simulations using the discrete element method have been conducted on assemblies of spheres. To better evaluate the effect of grading and density on the CSD, different grading have been studied at both loose and dense states. Then, to investigate the void entities, the Delaunay tessellation is combined with a specific void segmentation technique allowing to obtain a more representative CSD.

    In a second part, the analytical models developed by Locke et al. (2001) and Reboul et al. (2010) have been modified to fit the CSD resulting from a reasonable partition of the void network of numerical packings. Such models have the advantage of being based on simple geometrical and probabilistic considerations, and thus, constitute a promising tool that permits to quickly derive the CSD of a granular material on the basis of its grading curve and its density.

    Finally, a new formula is proposed for calculating the mean pore size. The estimate of this quantity is a discussing issue, and many proposals can be found in the literature. The DEM data has been used in this study to give a quantitative measurement of this characteristic of the void space which can be used in the probabilistic approaches capable of predicting the distance covered by a fine particles flowing through a filter.
  - **Chapter IV** is devoted to exploring the filtration properties of granular soils and to establish a clear relationship between the constriction size distribution which is the governing property of a filter and the transport of fine particles through this filter.

For this purpose, numerical filtration tests (Dry filtration under gravity and downward flow) have been carried out. A comparison is then made between the critical sizes derived from these tests and the controlling constriction sizes reported in the literature.

Moreover, an analytical formula is suggested to compute the equivalent sieve opening size of the filter which can be subsequently included in a constriction-based criterion. A validation study based on past experimental observations is conducted to judge the validity of the proposed criterion.

Finally, the conclusion summarizes the main outcomes of this thesis and outlines some perspectives for future research works.

Chapter I

Pores and constrictions in granular soils

1. Introduction

A granular soil is a three-dimensional assembly of particles that creates a complex void space. Because individual pores have no discrete boundaries like the soil particles, the characterization of the pore space is an ambiguous aspect of soil investigation. In general, the void space of a granular medium can be conceived as a collection of channels through which fluid can flow. The effective width of such channels varies along their lengths. Pore bodies are associated to the relatively wide portions and pore openings or pore throats are the relatively narrow portions that separate the pore bodies. These throats are also denoted constrictions.

Then, pores and constrictions constitute a partition of the void space helpful to define respectively its morphology and its topology (Vogel and Roth, 2001; Reboul et al., 2008). Such a partition can also help to build imbibition models for unsaturated materials (Mason and Mellor, 1995; Gladkikh and Bryant, 2005), models for the coefficient of permeability (Bryant et al., 1993; Chareyre et al., 2012) for fluid calculation, or geometrical filtration models for studying the migration of particles through granular media (Silveira, 1965; Schuler, 1996; Locke and Indraratna, 2001; Shire and O'Sullivan, 2017).

Indeed, constrictions play a major role in understanding the filtration properties of granular materials, because they are the main obstacles to be overcome by fine particles flowing under seepage through a granular filter. If a fine particle finds on its pathway a constriction size smaller than its proper size, it will be trapped in the filter.

When both constriction sizes and their occurrences are known, it is possible to define the cumulative constriction size distribution (CSD). Within the framework of the probability theory, there is a close relationship between the CSD and the probability for a fine particle to flow along a given length within a granular filter. Consequently, the CSD is indeed a key parameter to qualify the soil retention capability.

There are different techniques for the pore space characterization and the CSD computation, reported in the literature: through experiments, using numerical approaches or analytical approaches. In this chapter, we present these approaches pointing out their advantages and limits.

2. Pore-network models

The CSD has always been closely related to pore-network models which idealize the void space in porous media by considering a lattice of interconnected pores and throats following a respective size distribution. Such models have been widely used to simulate and understand the transport of fine particles in soils.

Silveira (1965) proposed a multi-layered constriction network involving one-directional movement of fine particles. These particles can cross a given layer if their sizes are smaller than the associated constriction size. Kenney et al. (1985) also used a one-dimensional infiltration model of a void network to determine the largest particle size that can be transported through a filter of a given thickness.

In Witt (1993), the void space is presented as a 3D network composed of spheres (pores) and pipes (links between pores) (Fig. I.1). For each pore, there is a number of possible exits or constrictions, and the smallest constriction size determines whether a fine particle flowing through the filter will be able to flow downstream or will be retained by the filter.

In a previous study, Witt (1986) found that the average number of constrictions per pore is 5.7. Based on this finding, Schuler (1996) adopted a cubic network model where each pore is modeled by a void cube having six exits (constrictions), one on each cube face, as shown in Fig. I.2. To pass from a layer i to another one (layer i+1), a particle has different possibilities: one direct path (plain arrow) and four sideways (dashed arrows).

An alternative model represents the filter voids as a series of parallel channels of varying diameter (Indraratna and Vafai, 1997) where the smallest constriction (D_0) within the pore channel governs the size of base particles that can cross the filter (Fig. I.3). The movement of particles is modeled by a finite difference analysis using flow laws and equations of conservation of mass. This model describes the time dependent changes of the particle size distribution (PSD), mass transfer, flow rate and porosity of filter and base soils. Later on, Indraratna and Locke (2000) and Reboul (2008) improved this model by incorporating the three-dimensional cubic model into their studies aiming at describing the phenomenon of particle migration within a base soil-filter system.

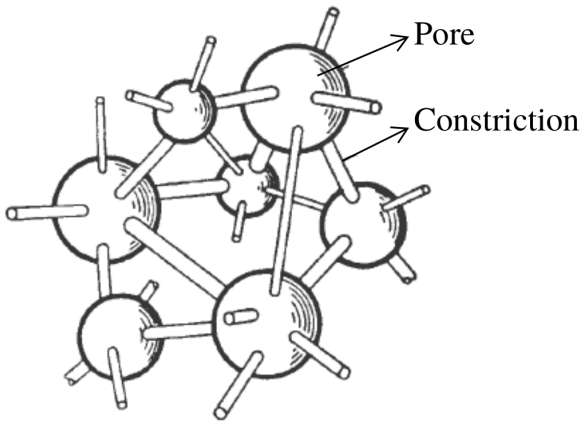

Fig. I.1. The pore-network model of Witt (1993)

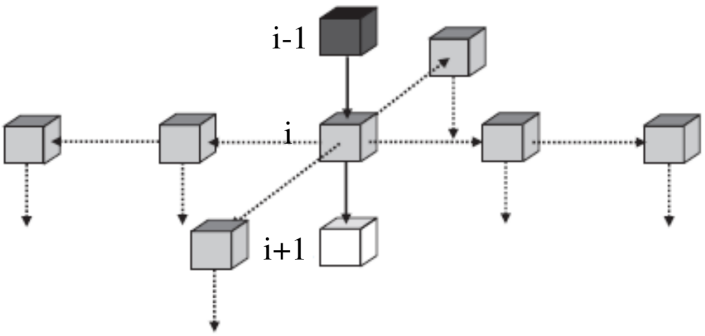

Fig. I.2. Cubic pore-network model (Schuler, 1996)

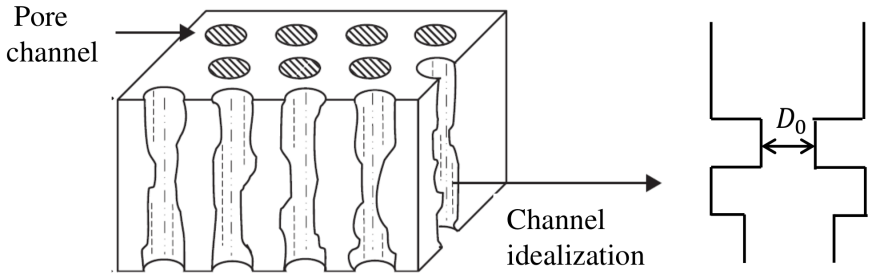

Fig. I.3. Void channel model (modified after Indraratna and Vafai (1997))

Following Schuler (1996), recent researches considered the regular cubic model (Locke et al., 2001; Sjah and Vincens, 2013; Vincens et al., 2015) to predict the probability of particle movement within granular filters. This prediction can be also used to estimate the infiltration depth of particles into the filters. More recently, Shire and O'Sullivan (2017) developed a pore-network model that uses an area-biased random walk approach to simulate the percolation of a base material through a given filter using the filter CSD and the base PSD.

3. Methods for CSD computation

3.1. Experimental approaches

3.1.1. Background

Several experimental methods can be used to quantify the void space of a granular soil and to determine its various characteristics. Although laboratory experiments have provided many insights and quantitative information about the organization of the pore structure, they are limited to small scales and are highly vulnerable to technical disturbances.

It must be noted that recent computerized technologies have brought a significant improvement in terms of performance and precision. Experimental approaches can be considered as a promising

tool since a wide range of characteristic parameters can be examined and some aspects of the soil behaviour can be reproduced leading to a better understanding of both the morphology and the topology of the void network.

3.1.2. Replica technique

The replica technique is a great qualitative tool to visualize the void space of a granular material and thus, to assess the morphology of the pore network, and the tortuosity of its pathways. In addition, this method is useful to estimate some void characteristics such as the pore connectivity and the CSD.

For this purpose, experimental investigations were carried out by Wittmann (1979), Witt (1986) and Witt (1993). A gravel material was filled with high elastic liquid rubber until its saturation. After hardening, all grains were extracted and the elastic matrix was dissected into single pores. A statistical study over these imprints permited to measure pore and constriction sizes. Fig. I.4 shows some typical pores of a natural gravel material (Witt, 1986). However, such a technique can be time consuming because enough pores must be analyzed to give an adequate statistical representation. Moreover, the application of this method to smaller particle sizes is impractical.

Beside this method, other experimental methods focused on the pore size characterization such as the mercury intrusion porosimetry (Giesche, 2006) and the gas adsorption (Thommes, 2010). Both methods are applicable over a wide range of pore sizes, but have a limitation in case of existence of closed pores (Xiong et al., 2016). In addition, the mercury intrusion porosimetry is based on simpler physiochemical principles and is much faster than the gas adsorption method which is rather characterized by its non-destructive nature.

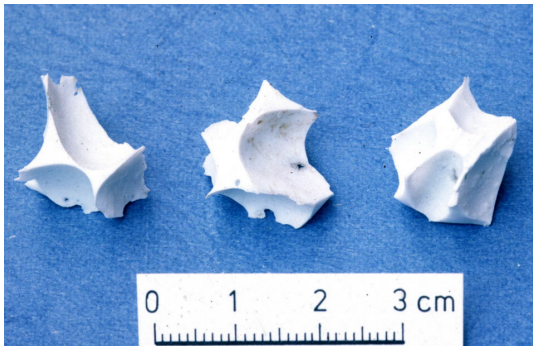

Fig. I.4. Pore imprints of a gravel skeleton (Witt, 1986)

3.1.3. Base suspension method

According to Silveira (1965), the number n of unit layers crossed by a base particle of diameter d moving forward through a multi-layered filter, with a fixed level of confidence P' ($P'\%$ of particles will be stopped after n confrontations) is defined as follows:

$$n = \frac{\log(1-P')}{\log P_u} \tag{I.1}$$

with P_u the probability to cross a unit layer. In the case of a unidirectional movement, P_u directly represents the probability P of passing a single constriction of diameter d_c $(d_c > d)$ (the fraction coarser than d from the CSD). However, in case of multi-directional pathways, another equation to predict P_u was developed by Locke et al. (2001). Then, if the average thickness of a unit layer is denoted s, the total penetration depth L of a fine particle in the filter is:

$$L = n.s \tag{I.2}$$

This equation relates the ability for a given particle to cover a certain distance within the filter with the constriction sizes encountered along its pathway. In particular, particles larger than the largest constriction size $d_{c_{max}}$ will not enter the filter (probability of passing = 0), and conversely, only particles smaller than the smallest constriction size $d_{c_{min}}$ will successfully cross the entire filter irrespective of its thickness (probability of passing = 1) (Fig. I.5).

As a consequence, if one states the filter thickness (hence a given infiltration depth covered by a particle of diameter d), a series of d and P values can be plotted producing a CSD curve (Soria et al., 1993; Silveira, 1993; Wu et al., 2012; Sjah and Vincens, 2013). Conversely, if the CSD is known, we can directly estimate the infiltration depth for a fine particle with a given diameter d (Silveira, 1965).

Experimental tests have been carried out by Soria et al. (1993) to estimate constriction sizes by evaluating the size of fine particles which can pass through a filter of a given thickness. The device used in such experiments is given in Fig. I.6.

First, fine particles in water suspension are poured over a granular filter with a given thickness submitted to a constant hydraulic head. Then, the base material that has successfully crossed the filter is collected and its PSD is derived. By repeating the procedure for several filter thicknesses, different PSDs for the collected material are obtained. Fig. I.7 presents the sequence of steps followed by these authors to obtain the CSD:

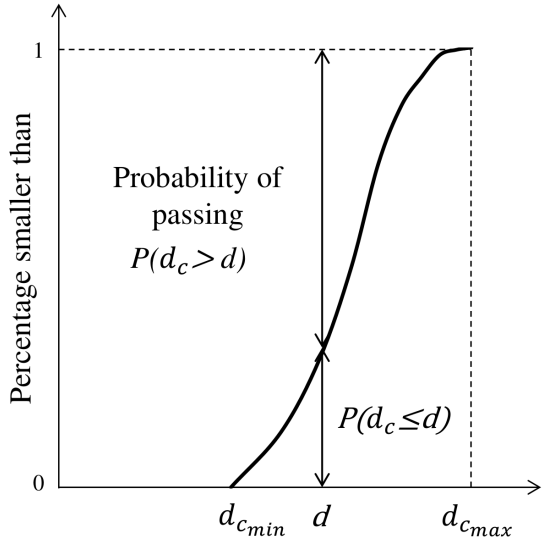

Fig. I.5. Constriction size distribution (CSD) and probability for a fine particle of diameter d to pass a constriction of its own size

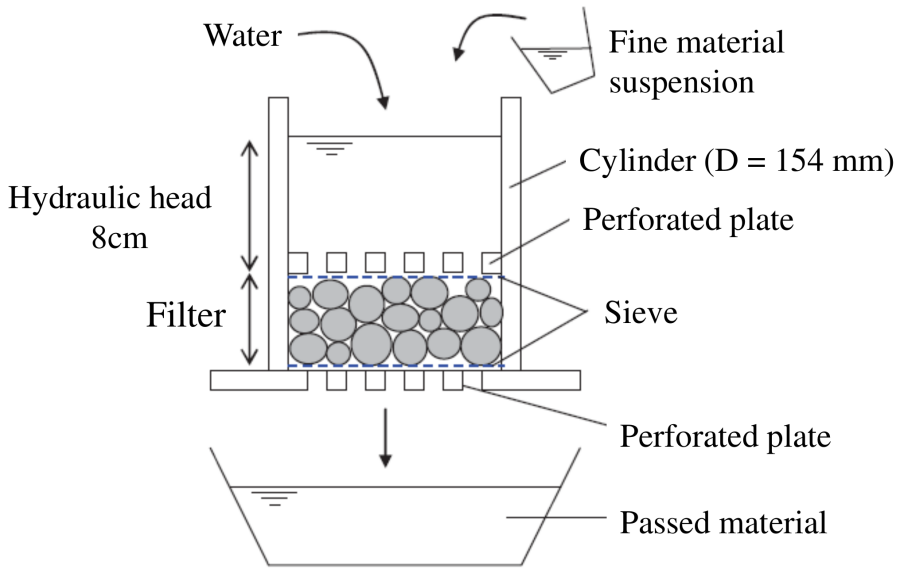

Fig. I.6. Device of filtration tests from Soria et al. (1993)

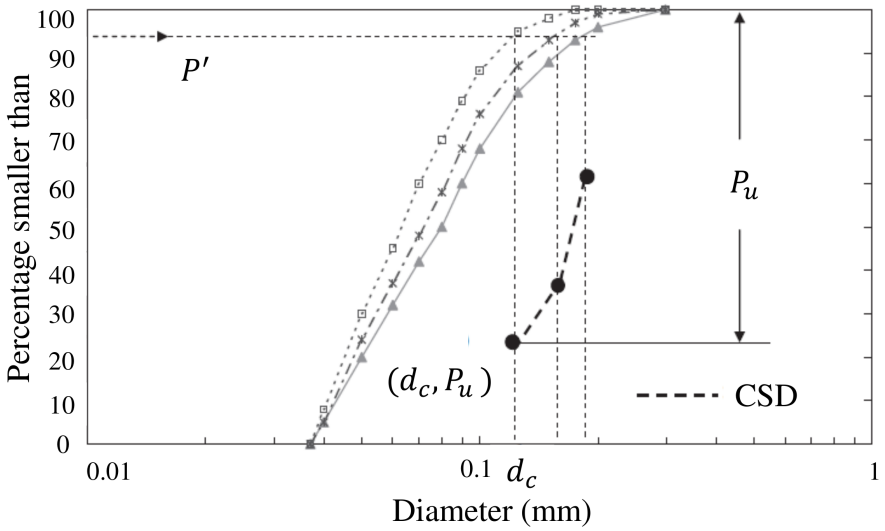

Fig. I.7. Example of CSD determination according to Soria et al. (1993) (modified after Sjah and Vincens (2013))

– Draw the PSDs of fine particles passed through the filter for different filter thicknesses L.

– With an assumed confidence level P', project a horizontal line intercepting the PSDs, and then downward to find the values of d_c. Different proposals for the confidence level can be found in the literature: 98% (Soria et al., 1993), and 95% (Locke et al., 2001; Wu et al., 2012; Sjah and Vincens, 2013).

– Assume a value for s, and compute P from Eq. I.2 for all filter thicknesses (a unidirectional movement is assumed herein).

  The estimate of s is a challenging problem and different proposals can be found in past studies. s is generally associated to the mean pore diameter which is stated to be equal to

the mean particle diameter (Silveira, 1965): D_{50M} by mass (Soria et al., 1993), D_{50N} by number (Locke et al., 2001), and D_{50SA} by lateral surface (Indraratna et al., 2007). Sjah and Vincens (2013) used the mean inscribed void sphere computed from a Delaunay tessellation applied to numerical packings of spheres. Another estimate of this quantity independent of the density and the shape of particles of the filter, was provided by Wu et al. (2012). In fact, there is little evidence so far for the choice of one between these options.

– For each thickness, enter P_u and intercept the vertical line representing d_c. The CSD points are then determined.

Concerning the base soil, Soria et al. (1993) chose a linear grading and take D_0 (0% passing for the filter) as the maximum diameter d_{100} (100% passing for the base soil). The smallest diameter d_0 of the base soil should be greater than the percolation diameter of the filter.

In general, the interactions between particles increase if they are numerous, and unstable cloggings may occur if they are too numerous. Consequently, the number and the grading of fine particles must be chosen to successfully reflect the properties of the pore space and to ensure representative results. For this purpose, Sjah and Vincens (2013) suggested some considerations for the choice of the base soil (grading, number and frequency of released particles) based on DEM filtration tests. More details can be found in Wu et al. (2012) and Sjah and Vincens (2013).

It is important to note that this technique generally only gives access to the central part of CSD curve and not to the smaller or the larger constriction sizes due to filter thickness constraints (too thin filter to be representative or too thick to be easily processed).

However, the experimental method described by Soria et al. (1993) has some limitations related to the size and the preparation of the apparatus, and the poor hydraulic control. In addition, it neglects the effect of the anisotropy of the constriction network. Here, the direction of the flow is taken parallel to the direction of the deposit; say the direction of the gravity while on site, the direction of the flow is perpendicular to the direction of the deposit.

3.1.4. Micro-computerized tomography scanning (micro-CT)

The micro-CT scanning of real soils (undisturbed soils) is another method used to predict the pore network characteristics including constriction sizes. This non-destructive tool provides high resolution 3D images of the void space irrespective of the grading and of the particle shape of the considered sample. Using this technique, Aste et al. (2005) investigated the geometrical and topological properties of packings of monosized spheres. Numerical dataset can also be converted to an image file, comprising voxels (Delaney et al., 2010; Seblany et al., 2017).

However, CT is only the first step towards determining the geometrical characteristics of the pore space and hence, a numerical post-processing technique must be applied to obtain the locations and the sizes of pores and constrictions from the image data. For this purpose, many numerical techniques can be used, and will be briefly described in the following section.

Contrary to the replica technique which is limited to coarse soils, CT scanning can be used for any type or shape of materials. Nevertheless, the specimen preparation and the image resolution (the ratio of voxel size to particle size) are the main limitations of CT technology. Indeed, the

associated voxelization may lead to an underestimation and incorrect identification of the throat sizes (Dong and Blunt, 2009; Li et al., 2018).
Seblany et al. (2017) compared the CSD derived from the Delaunay tessellation and the voxel-based method and found that they are almost congruent for a sufficient small voxel size (D_0/75, D_0 is the smallest grain size within the sample). The other limitation is the size of the data that must be stored and handled which requires limiting the size of the sample to be analysed when it is accompanied by a high resolution.

Moreover, pertinent algorithms are required to extract simplified networks of pores and throats from the images of the pore space. An example of a CT scan of a sample of sandstone is shown in Fig. I.8. A detailed review of the principles, advantages, limitations and applications of tomography in geoscience can be found in Ketcham and Carlson (2001) and Cnudde and Boone (2013).

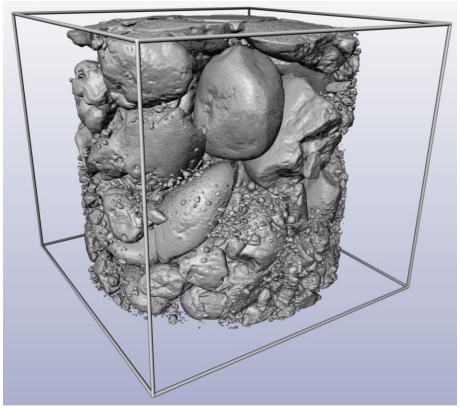

Fig. I.8. Volumetric visualization of a CT scan of a sample of sandstone with a resolution of 39 μm (Vincens et al., 2015)

3.2. Numerical approaches

3.2.1. Background

To overcome some limitations associated with experimental methods, and due to the continuous increase in computer power, numerical simulations are increasingly seen as a means to understand and predict the mechanical behaviour of granular soils.

In fact, a granular medium consists of distinct grains in contact. Their highly discontinuous nature requires a discrete numerical model that does not focus on the granular assembly as an entity, but rather deduces its global behaviour from the individual behaviour of each grain. The discrete element method (DEM) can model the complex behaviour of a granular medium and give access to the properties of the micro-structure of the granular assembly.

However, the void characteristics of numerical packings are not directly given by the DEM simulation data; rather it can be extracted by combining the DEM with spatial partitioning techniques (for example, the Delaunay tessellation and its dual Voronoï diagram).

On the other hand, and as highlighted in Section 3.1.4, numerical techniques are also needed to

obtain the pore space information from the images provided by micro-CT.

However, the void space of a granular medium (DEM sample or 3D image) forms a continuous network and cannot be addressed as a series of discrete objects of voids with definite physical boundaries and thus, the partitioning must be associated to an appropriate criterion to define individual local pores.

The following sections provide a brief literature review of the discrete element method and introduce the classical Delaunay and Voronoï tessellations as well as the distance-mapping method as common approaches for pore space partitioning. The associated pore merging criteria used in past studies are also presented.

3.2.2. A brief review on the Discrete Element Method (DEM)

The discrete element method (DEM) was initially developed by Cundall and Strack (1979) and became increasingly popular for modeling the granular materials with given grading and density.

This method is based on an explicit numerical scheme in which the interactions between particles are monitored contact by contact and the individual motion of particles is considered. The particles are considered as rigid and locally deformable elements that can interact by contact forces.

Ideal particle geometries (spheres) are generally used to control the computational cost of the DEM simulations. Originally, the simulations were performed for monosized sphere packings (Liu et al., 1999; Zhang et al., 2001; Yang et al., 2006) but polydisperse sphere packings (Lochmann et al., 2006; Reboul et al., 2010; Shire and O'Sullivan, 2016) are more representative of actual materials encountered on sites.

Each calculation cycle includes the application of Newton's second law of motion to each particle, and a force-displacement law governing particle interactions at the contacts. The DEM computational cycle is schematically represented in Fig. I.9.

At each time step, interaction forces between particles, and consequently the resulting forces acting on each of them, are deduced from sphere positions through the interaction law. Newton's second law is then integrated through an explicit second-order finite difference scheme to compute the new spheres positions. This process is repeated until the simulation is achieved.

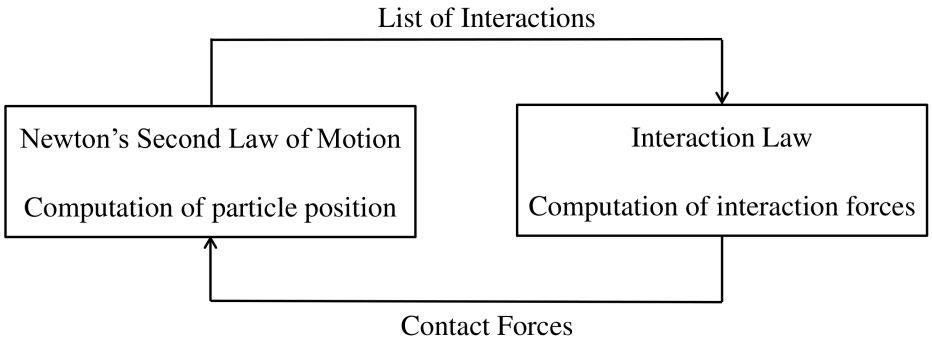

Fig. I.9. Computation cycle of a DEM model

Cundall and Strack (1979) use a simple constitutive model where the contact between two spheres is modeled by normal and tangential springs characterized, respectively, by normal (K_n) and tangential (K_s) constant stiffnesses, with a Coulomb shear slider of friction angle (ϕ_c) (see Fig. I.10). The normal contact force is proportional to the interpenetration between the two particles (δ_n). This law corresponds to a linear elastic-perfectly plastic behaviour.

Particles can be deposited by gravity or by the action of external compaction load. The density of the samples can be modified by changing the value of the inter-particle friction coefficient. The lower is this value, the denser is the sample. The introduction of a damping coefficient (local or global) is necessary to dissipate the energy in the system and to reach a steady state.

Different types of boundary conditions can be distinguished: rigid walls where the granular assembly is created in a deformable box with rigid walls, and periodic boundaries which extend the system to an infinite medium (Cundall, 1988). The periodic space is then created by repetition of parallelepiped-shaped cell. Such boundaries lead to the generation of homogeneous samples overcoming, thereby, the effect of rigid walls.

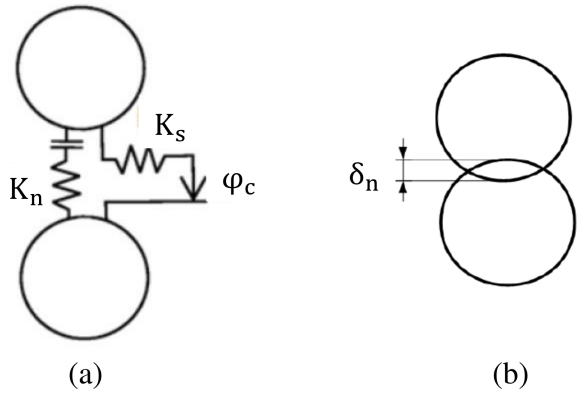

Fig. I.10. Interaction law used by Cundall and Strack (1979)

3.2.3. Delaunay tessellation

The Delaunay tessellation is usually processed on spherical DEM samples with known grain positions for characterizing their void network. It consists in partitioning the pore space into a set of tetrahedral volumes whose vertices are the centers of fours neighbouring spheres. In such a representation, each tetrahedron encloses a pore and the associated constrictions pass through the common faces between the adjacent cells (shaded face of the tetrahedron in Fig. I.11a) and a definition for them is chosen as the largest empty discs that can fit between the three particle vertices of a tetrahedron face (Al-Raoush et al., 2003; Reboul et al., 2008) (Fig. I.11b). Eventually, the inscribed void sphere between the four particles, vertices of a Delaunay cell is computed and is considered as a characteristic of the morphology of that cell. The weighted Delaunay tessellation or regular triangulation (Edelsbrunner and Shah, 1996) generalizes the classical Delaunay triangulation to weighted points, where weights account for the radius of spheres.

Another approach was developed by O'Sullivan et al. (2015) to extract throat sizes information where the contacts between particles are used as a basis for the triangulation (contact based triangulation). Valid constrictions are then defined by closed loops of either three or four contacts. The

Delaunay tessellation is a powerful tool for pore space characterization especially because a large number of particles can be considered; however, its application is restricted to spherical packings.

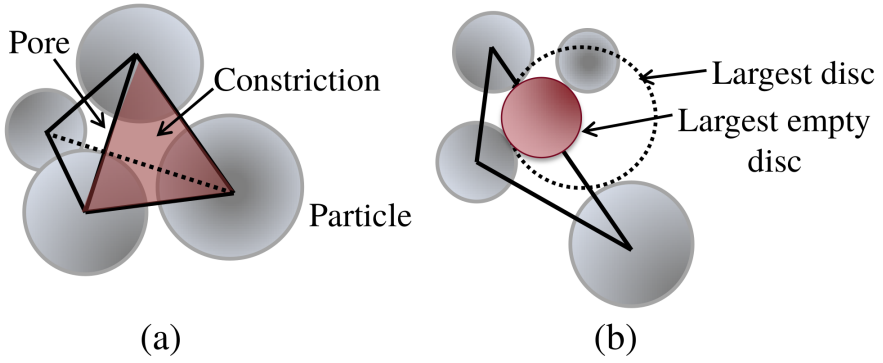

Fig. I.11. (a): Tetrahedron built from the centers of four neighbouring spheres; (b): Definition of a constriction: the largest empty disc included in the void space for a given face

3.2.4. Voronoï diagram

The Voronoï decomposition is a technique for spatial analysis used to describe the microstructure of granular media. This method has been extensively used to study the pore structure in packings of spheres (Richard et al., 1998; Gervois et al., 2002; Yang et al., 2006).

A Voronoï diagram consists of a set of Voronoï cells. Each Voronoï cell is defined as the region of space around a given sphere in which all points are closer to this sphere than to any other sphere in the packing. The points most distant from the surfaces of the neighbouring particles define the Voronoï nodes.

Due to the duality of the Delaunay and Voronoï decomposition, the Voronoï nodes correspond to the centers of the inscribed void spheres of the Delaunay tetrahedra and their distance to the surrounding solid spheres to the radius of these inscribed void spheres. The Voronoï graph and its dual, the Delaunay triangulation are illustrated in Fig. I.12.

Homberg et al. (2014) define the pore space elements (pores, constrictions, paths) for a spherical packing by applying a Voronoï computation based on the Euclidean distance to the solid spheres as described by Lindow et al. (2011). The edges between the Voronoï nodes are curved and describe the median path joining pore centers. The centers of constrictions correspond to the points having the minimal distance to the surrounding spheres along the edge (Fig. I.13).

In terms of duality, this is where the edges cut the common facet of the tetrahedra formed by joining particles centroids and, thus, correspond to the constrictions found in the Delaunay tessellation. Besides, Schaller et al. (2013) developed the set Voronoï diagram method based on a triangulation of the particles' bounding surfaces for configurations of aspherical particles.

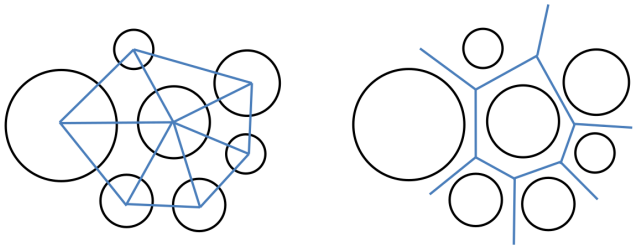

(a) (b)

Fig. I.12. 2D representation of (a): Delaunay tessellation and; (b): Voronoï graph

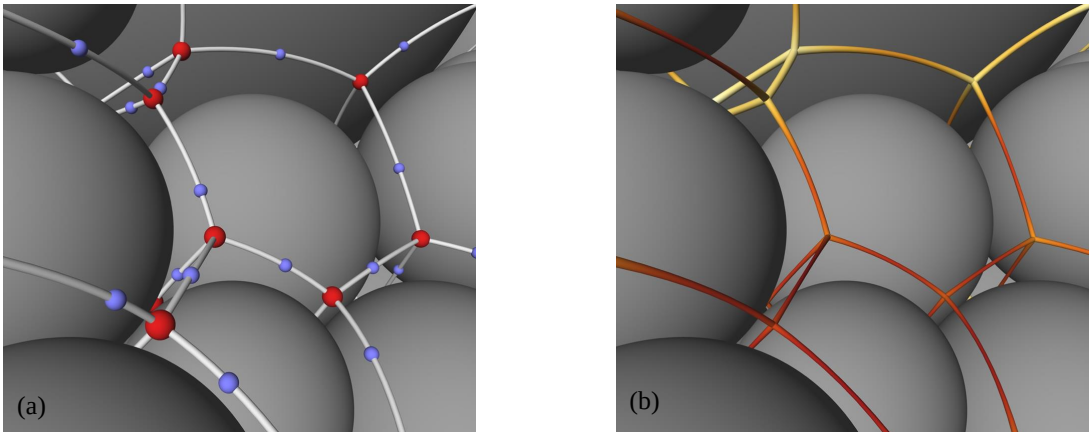

Fig. I.13. Detail of a Voronoï graph; (a): red (larger) spheres at crossing indicate the centers of pores, while the blue (smaller) spheres represent the centers of constrictions on the edges; (b): The diameter is color-coded along the edges with yellow (large) to red (small) (Seblany et al., 2018)

3.2.5. Distance-mapping method

Homberg et al. (2012) proposed an image-based method to measure the pore space characteristics of granular soils with irregular grain shapes, from micro-CT scans (voxelized images). This method called *Medial Axis method* identifies a medial axis running along the middle of the void space. By exploiting the distance information along this medial axis, pore centers (points where the void channel is widest) and constriction centers (points where the void channel is narrowest) can be determined (Fig. I.14). This approach was also used to characterize the transport possibilities of particles within the pore space of a granular soil (Vincens et al., 2015).

In a similar way, the maximal ball algorithm, developed by Dong (2008), divides the inscribed balls (the largest inscribed void spheres which can fit at each point of the void space) into clusters depending on the fact of being master or slave and assigns the local minimum of ball size to the constriction size and the local maximum of ball size to the pore size.

An equivalent technique (the watershed segmentation (Rabbani et al., 2014; Taylor et al., 2015; Raeini et al., 2017)) can be also applied to extract the pore-throat network from tomography images of real soils. A 3D distance map is defined allowing the identification of constrictions at

the boundaries between voids. Gueven et al. (2017) used this method to obtain the porosity field and other properties such as particle sizes, pore throats and permeability.

Such algorithms can handle DEM or micro-CT data as input (Al-Kharusi and Blunt, 2007; Arand and Hesser, 2017; Li et al., 2018). However, they produce fewer and smaller constrictions compared to Delaunay approach (Shire et al., 2012). This may be a consequence of inadequate image quality.

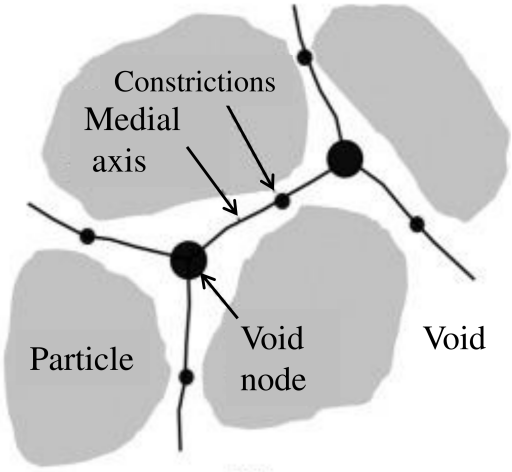

Fig. I.14. Scheme of the Medial Axis method: medial axis with void nodes (large circles) and constrictions (small circles) (Taylor et al., 2015)

3.2.6. Pore merging criteria

Using the above approaches, the pore structure can easily be accessed by a segmentation scheme of the whole void space. However, Al-Raoush et al. (2003) found that the tetrahedral tessellation leads to an artificial over-segmentation of the void space due to the underlying mathematical process for finding neighbours.

Indeed, the inscribed void sphere confined in each tetrahedron is not necessarily entirely included inside that tetrahedron, and two inscribed void spheres attached to two neighbouring tetrahedra may overlap. It signifies that the opening size between such tetrahedra may be wide enough to indicate a strong interconnection between them.

To illustrate that, a two-dimensional analogy of the three-dimensional Delaunay tessellation is given in Fig. I.15. In 2D, tetrahedral cells are represented by triangles, the sphere inscribed in each tetrahedron corresponds to the circle inscribed in each triangle and constrictions are found on triangle sides (tetrahedral faces in three dimensions).

The first schematic illustrates two completely separated pores (Fig. I.15a). In 3D, the constriction between them is found on their common face and corresponds to the narrowest passage formed by touching or nearly touching spheres (Fig. I.15d). In the other configurations (Fig. I.15b-c), the Delaunay triangles create a 'constriction' within the void pores due to their tight imbrication. In 3D, it can be observed that spheres forming such a constriction do not necessarily touch; as a result, this constriction do not certainly corresponds to a real throat (Fig. I.15e-f).

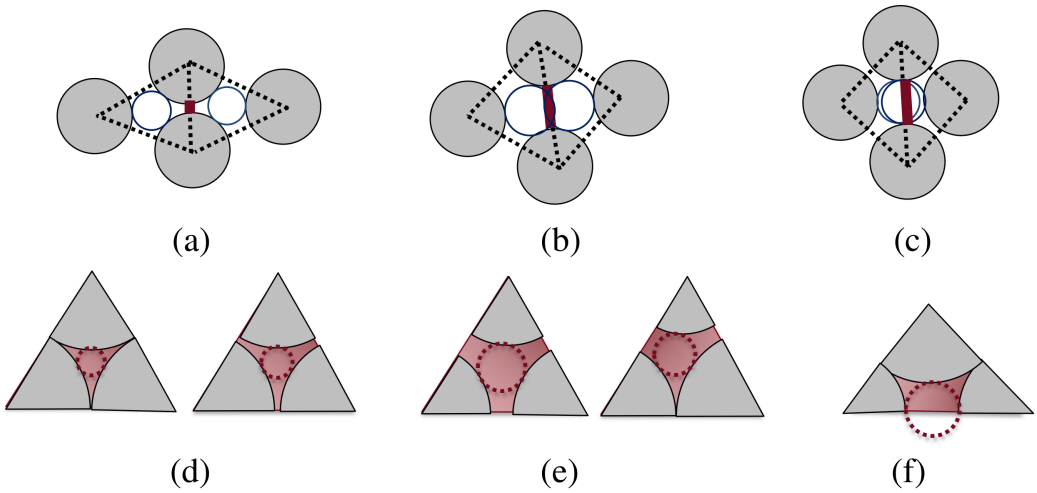

Fig. I.15. A 2D schematic of different configurations encountered in Delaunay triangulation; (a): separated pores; (b): interlocked pores; (c): highly interlocked pores. (d-f): Schematic of the throats on the common face of two neighbouring tetrahedra for different cases (3D)

Similarly, the voxelization of the void space and the irregular shape and arrangement of particles may produce spurious local maxima that give rise to an over-segmentation. Thus, and irrespective of the used technique for pore space characterization, a subsequent pore merging process must be performed to eliminate over-partitioning and to accurately set the boundaries between pores.

However, by definition, pore boundaries in porous media are uncertain since no rational definition can be set for them. Moreover, in actual granular materials with non smooth particles, any segmentation of the pore space leads to a very irregular network where pore entities are hardly distinguishable. Fore these reasons, not definite but rather reasonable proposals, can be made.

Until recently, several adaptive merging criteria have been proposed, but they did not completely account for the above artifacts. For example, Delaunay cells are usually merged using the criterion originally proposed by Al-Raoush et al. (2003). Merging takes place mainly if the overlap between two inscribed void spheres proceeding from two adjacent cells exceeds a certain degree (Fig. I.16).

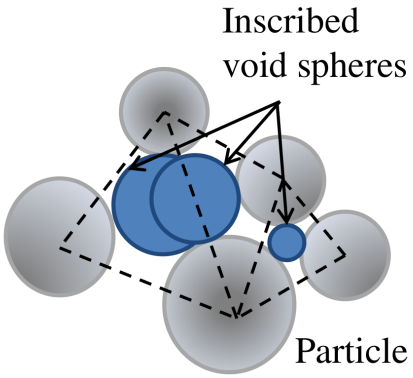

Fig. I.16. A two-dimensional schematic diagram of merging of Delaunay cells with overlapping inscribed void spheres to form a single pore

The selection of the critical degree of overlap is based on the user-judgment, but one should keep in mind that the correlation of two adjacent cells increases as the overlap increases. For example, and following Al-Raoush et al. (2003), the neighbouring cells should be merged if the center of one void sphere lies within the adjacent inscribed sphere. Reboul et al. (2008) and Sufian et al. (2015) merged Delaunay cells if their inscribed spheres overlap by any amount while Shire and O'Sullivan (2016) selected a merging overlap of 50% to generate the CSD.

According to Reboul et al. (2008), the initial computation of pores and constrictions derived from the weighted Delaunay tessellation is denoted Level 0 (L_0). Level 1 (L_1) corresponds to the modified Delaunay tessellation initially proposed by Al-Raoush et al. (2003): association of a tetrahedron with its nearest neighbour when their inscribed void spheres overlap each other (the maximum number of merged tetrahedra is 5); and a further level of merging (L_2) is processed, where merging is not only applied to the adjacent tetrahedron but also to the next adjacent tetrahedron if the inscribed void sphere of this latter overlaps that of the former pore. In this case, the maximum number of merged tetrahedra is 17. The three levels of neighbourhood for a Delaunay cell are shown in Fig. I.17.

A schematic of L_1 is given in Fig. I.18. The red triangle in 2D can be associated to its adjacent blue triangles if their inscribed void circles overlap each other. Here, the overlap between the inscribed circles corresponding to the red and right blue triangles induces the association of these two triangles and the removal of the constriction located on their common side, and so on for the other blue triangles.

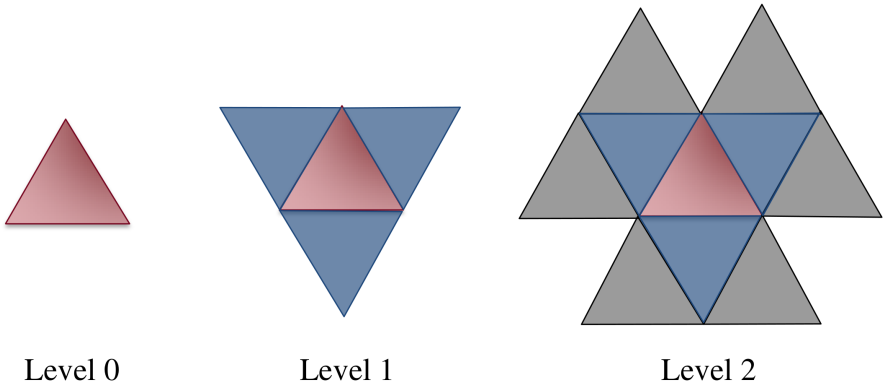

Fig. I.17. Different neighbourhood levels for a Delaunay cell (In 2D)

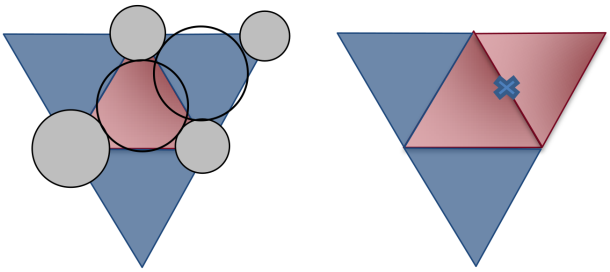

Fig. I.18. A schematic of L_1 (In 2D)

If L_2 is considered (Fig. I.19), after checking the overlap condition between the red and blue triangles as explained above, we check the overlap between the inscribed circles corresponding to the blue and grey triangles; and since this condition is verified, the three triangles will be merged and the constrictions formed on their common sides will be removed and so on for the other grey triangles.

A restriction of L_2 is also introduced and is denoted Level 2b (L_{2b}) (in Reboul et al. (2008), it was denoted Level 1b because the underlying CSD was comprised between the L_1 CSD and the L_2 CSD) where the inscribed void spheres must be arranged in decreasing order to induce a merging. This latter criterion takes into account the geometric constraints to define the pore entity. Indeed, the transition between pores is characterized by constricted regions followed by more expanded regions.

Rather than using an optimization algorithm to define the inscribed void spheres, van der Linden et al.(2016; 2018) suggested to merge two adjacent tetrahedra together when the areal porosity of their common face (the void area divided by the total area) exceeds a user-specified value. However, this simplified criterion is clearly subjective.

Based on the extremal structures of the distance map of the pore space, Homberg et al.(2012; 2014) defined a hierarchical merge strategy based on the significance of the pore separations. Accordingly, a merge between two adjacent pores is required when the size of the constriction linking these pores is very close to the smallest pore size since it tends to reveal that these two pores have a high degree of interaction to be considered as distinct entities.

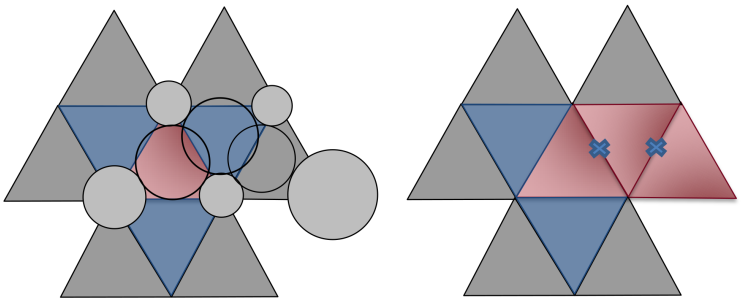

Fig. I.19. A schematic of L_2 (In 2D)

3.3. Analytical approaches

3.3.1. Background

The analytical approaches are based upon a probabilistic theory stating the existence of reference geometrical configurations involving some particles. For the sake of simplicity, the particles are generally approximated to spheres which may be a good approximation for many granular materials. The PSD of the granular material is divided into n classes as shown in Fig. I.20, each of them is characterized by a representative diameter d_i and a probability of occurrence (i.e. frequency) p_i. Note that Silveira (1965) highlighted that different discretization schemes of the filter PSD may affect the accuracy of the resulting CSD especially at the extremities of the curve. More recently,

Raut (2006) demonstrated that the CSD remains the same as long as the discretised data points do not modify the PSD. However, their conclusions have been derived from investigations involving uniform materials.

To define the constriction sizes, two geometrical configurations can be assumed depending on the density of the studied sample, one is denoted *three-particle configuration* (densest model) and the other one *four-particle configuration* (loosest model). One must remind that these configurations are purely geometrical and do not reflect the mechanical arrangements encountered in real materials. Indeed, a numerical sample can be highly heterogeneous in terms of space arrangement (Reboul et al., 2008). Shire and O'Sullivan (2016) showed that beside the idealized geometrical configurations, other particle-constriction configurations can be found in DEM samples.

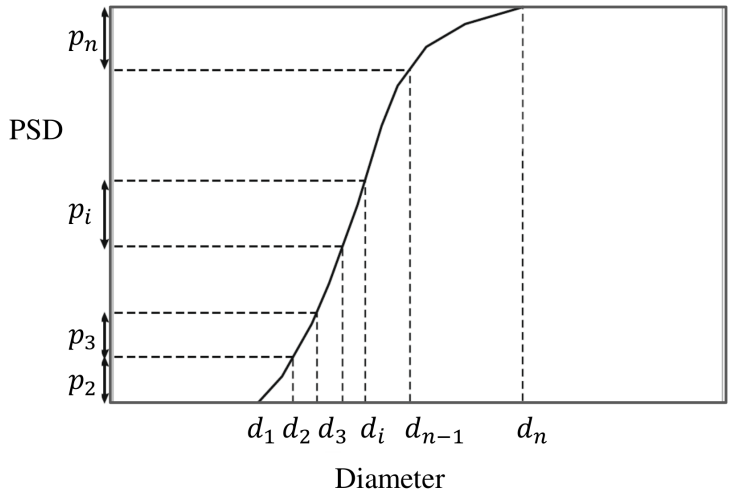

Fig. I.20. A discretized particle size distribution (PSD)

3.3.2. Model for the densest state

Based on the previous considerations, a mathematical model was initially proposed by Silveira (1965) to compute the CSD for a filter at its maximum density. In this model, all the constrictions are considered to be formed by three tangent spheres with respective diameters d_i, d_j, and d_k and respective probabilities of occurrence p_i, p_j and p_k (Fig. I.21a).

The constriction size d_{c3} is then defined as the diameter of the largest circle that can fit between the three circles resulting from the intersection of the spheres with the plane passing by their centers. d_{c3} is calculated from Descartes's theorem giving the relationship between the diameters of four tangent circles:

$$(\frac{2}{d_i})^2+(\frac{2}{d_j})^2+(\frac{2}{d_k})^2+(\frac{2}{d_{c3}})^2=0.5(\frac{2}{d_i}+\frac{2}{d_j}+\frac{2}{d_k}+\frac{2}{d_{c3}})^2 \tag{I.3}$$

By excluding the circumscribed circle, one solution can be derived from Eq. I.3. It corresponds to the inscribed circle which can be directly given by:

$$\frac{1}{d_{c3}}=(\frac{1}{d_i})+(\frac{1}{d_j})+(\frac{1}{d_k})+2\sqrt{(\frac{1}{d_i d_j})+(\frac{1}{d_j d_k})+(\frac{1}{d_k d_i})} \tag{I.4}$$

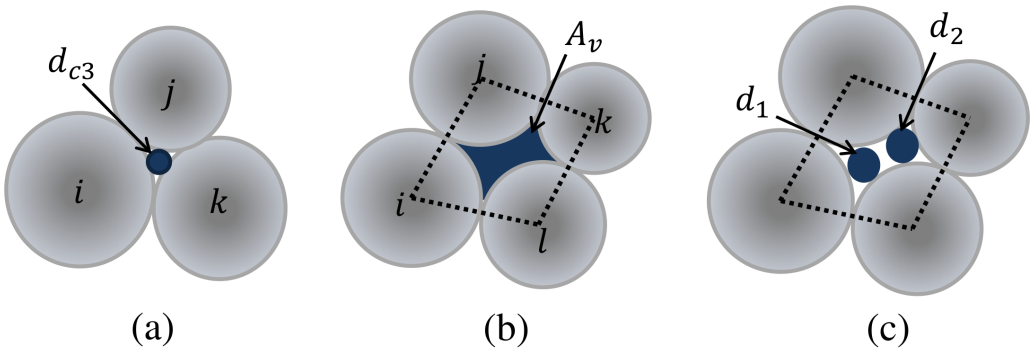

Fig. I.21. Geometrical configurations for (a): the densest arrangement (Silveira, 1965); (b): the loosest arrangement (Silveira et al., 1975); (c): the arrangement of Schuler (1996)

The probability of occurrence p_{c3} of the constriction size d_{c3} depends on the individual frequencies of the three particles constituting the group (p_i, p_j, and p_k), and can be computed from:

$$p_{c3} = \frac{3!}{r_i!r_j!r_k!} {p_i}^{r_i} {p_j}^{r_j} {p_k}^{r_k} \tag{I.5}$$

where r_i, r_j, and r_k denote the number of times that the diameters d_i, d_j, and d_k appear in the group respectively (r_i, r_j and r_k = 0, 1, 2 or 3; $r_i + r_j + r_k = 3$). The cumulative constriction distribution (by number) i.e. CSD, is obtained by considering all possible combinations within all representative diameters of the discretized PSD.

However, the mechanical densest state considering frictionless spherical particles is generally looser than what is predicted by the geometrical dense model and larger constriction sizes can be found in dense numerical samples (Reboul et al., 2010; Shire and O'Sullivan, 2016). Moreover, Reboul et al. (2008) showed that the three mutually touching spheres is unlikely to occur and there are still other configurations in a numerical packing of spheres even for very dense states ($\mu = 0$).

3.3.3. Model for the loosest state

For the sake of simplicity, many researchers have used the densest geometrical model to estimate the CSD of medium-dense to dense packings. However, real filters are not always compacted to their maximum density which implies that the three-particle arrangement is not conservative to address the problem.

Therefore, Silveira et al. (1975) developed an alternative model to calculate the CSD for a filter at its loose state, by considering a set of four tangent particles with respective diameters d_i, d_j, d_k and d_l and respective probabilities of occurrences p_i, p_j, p_k and p_l, as shown in Fig. I.21b.

The constriction size d_{c4} is given by the equivalent diameter of the maximum void area $A_{v,max}$ enclosed between the four touching filter particles:

$$d_{c4} = \sqrt{\frac{4A_{v,max}}{\pi}} \tag{I.6}$$

The area A_v is given by:

$$A_v = \frac{1}{8}[(d_i + d_j)(d_i + d_l)\sin\alpha + (d_j + d_k)(d_k + d_l)\sin\gamma - ({d_i}^2\alpha + {d_j}^2\beta + {d_k}^2\gamma + {d_l}^2\delta)] \quad \text{(I.7)}$$

where α, β, γ and δ represent the angles of the quadrilateral formed by the centers of the four tangent particles. β, γ and δ can be related to α by plane geometry and then $A_{v,max}$ can be found by an iterative process with respect to α.

Since we can rarely define a single plane passing through the centers of four particles in an actual sample, Schuler (1996) suggested to take the mean chord length through the circular particle rather than its diameter to represent the constriction size. Eq. I.6 is then corrected by a factor equal to 0.82.

Eq. I.8 gives the probability of occurrence p_{c4} associated with d_{c4}:

$$p_{c4} = \frac{4!}{r_i!r_j!r_k!r_l!}{p_i}^{r_i}{p_j}^{r_j}{p_k}^{r_k}{p_l}^{r_l} \quad \text{(I.8)}$$

where r_i, r_j, r_k and r_l are the number of occurrence of d_i, d_j, d_k and d_l in the group of four particles respectively (r_i, r_j and r_k = 0, 1, 2, 3 or 4; $r_i + r_j + r_k + r_l = 4$). By considering all possible groups, all possible constrictions and their respective probabilities can be estimated, and the whole CSD can be derived.

The experiments carried out by Witt (1986) showed that most constrictions are formed by four particles. Accordingly, Schuler (1996) adopted the four-particle arrangement to compute the CSD at any relative density, but two distinct constriction sizes are considered herein as depicted in Fig. I.21c. This model was also used in other studies (Scheuermann et al., 2010; Wang and Dallo, 2014).

The probability of a filter particle to form a constriction is related to its frequency in the PSD (either by mass, number or surface area). The models of Silveira (1965) and Silveira et al. (1975) are based on the PSD by mass (the usual PSD obtained by sieve analysis) which is adequate for uniform filters. But in case of well-graded materials, the PSD by mass may overestimate the influence of large particles (with high individual mass but low number) since it is unlikely that these particles will meet together to form a large constriction (De Mello, 1977).

For similar reasons, the PSD by number used by Kenney et al. (1985) over-represents the finer constrictions (Humes et al., 1996). Eq. I.9 can be used to convert the PSD by mass to a PSD by number.

$$P_{N,i} = \frac{\frac{P_{M,i}}{{d_i}^3}}{\sum_{i=1}^{n}\frac{P_{M,i}}{{d_i}^3}} \quad \text{(I.9)}$$

With $P_{M,i}$ the mass frequency of the i^{th} class of particles, and $P_{N,i}$ the associated number frequency.

To overcome these limitations, another approach is adopted: the PSD by surface area (Humes et al., 1996; Schuler, 1996; Locke et al., 2001). This choice can be explained by the fact that as the total lateral surface area of a class of particles increases, its probability to belong to an arrangement that will create a constriction, increases as well. The PSD by surface area can be

obtained as follows:

$$P_{SA,i} = \frac{\frac{P_{M,i}}{d_i}}{\sum_{i=1}^{n} \frac{P_{M,i}}{d_i}} \tag{I.10}$$

Thus, the resulting CSD varies depending on the imposed PSD, but one should keep in mind that different models give similar results for uniform filters, while the derived CSDs are considerably different for non-uniform filters.

3.3.4. Models for different relative densities

The models of Silveira (1965) and Silveira et al. (1975) only take into account extreme density states, but actual filters are likely to exist in intermediate state between the loosest and densest states. Therefore, alternative models have been developed to determine the CSD for any given relative density R_d (Eq. I.11).

$$R_d = \frac{e_{max} - e}{e_{max} - e_{min}} \tag{I.11}$$

where e is the actual void ratio and e_{max} (respectively e_{min}) denotes the maximum (respectively minimum) void ratio. The minimum void ratio corresponds to the maximum density of the soil (R_d = 1) while the maximum void ratio corresponds to the minimum density of the soil (R_d = 0).

– Model of Locke et al. (2001)

According to Schuler (1996), the CSD curves of a granular material at varying densities have approximately the same shape. Moreover, three particles arrangements may also exist even in a medium-dense soil (Giroud, 1996). Based on these observations, Locke et al. (2001) proposed a weighted contribution of the loosest and densest geometrical configurations to design a model valid for any other density. The constriction size d_c at any relative density R_d is given by the following equation:

$$d_c(P_c, R_d) = d_{c3}(P_c) + P_c(1 - R_d)(d_{c4}(P_c) - d_{c3}(P_c)) \tag{I.12}$$

where P_c is the fraction smaller of the CSD, d_c is the constriction size at P_c, d_{c3} and d_{c4} are the constriction sizes for the densest geometrical model (three-particle arrangement) and the loosest geometrical model (four-particle arrangement) respectively, for the same P_c.

This equation implies that, whatever the soil density, the smallest constriction size is the same and is equal to the smallest constriction provided by the dense geometric model.

Locke et al. (2001) suggested to use a regraded PSD to eliminate the coarse particles that in fact do not contribute to the CSD. Indeed, constrictions formed between such particles may be filled with finer particles and thus, no large voids remain. This was also highlighted by Shire and O'Sullivan (2016) for broadly graded materials.

At the densest state ($R_d = 1$), the three-particle configuration is only considered in Eq. I.12, and consequently, the model of Locke et al. (2001) tends to become inaccurate. This drawback poses a major problem because the materials in hydraulic structures are generally compacted to high densities to ensure the stability of soils.

– Models of Reboul et al. (2010)

For Continuously Graded Material *(1-parameter model)*

The analytical equation proposed by Locke et al. (2001) allows obtaining the constriction diameter at the loosest state d_{cL}, for each value of P_c, by setting R_d to zero. Based on the resulting equation, Reboul et al. (2010) validated their numerical studies performed on spherical packings. A correction factor was introduced to minimize the relative errors (Eq. I.13).

$$d_{cL}(P_c) = 1.11(d_{c3}(P_c) + P_c(d_{c4}(P_c) - d_{c3}(P_c))) \tag{I.13}$$

For dense samples (R_d = 1), Reboul et al. (2010) found that the Delaunay method gives constriction sizes that are much larger than those obtained using the model of Locke et al. (2001), and thus, they proposed another methodology to quickly and accurately compute the CSD, for any relative density. The constriction size d_c corresponding to a percentage P_c of the desired cumulative CSD can be found by using the following formula:

$$d_c(P_c, R_d) - d_{c_{min}} = \frac{e(R_d)}{e_{max}}(d_{cL}(P_c) - d_{c_{min}}) \tag{I.14}$$

where $d_{c_{min}}$ is the diameter of the smallest constriction formed between the three smallest particles of the sample, in mutual contact. $d_{c_{min}}$ is given by:

$$d_{c_{min}} = (-1 + \frac{2}{\sqrt{3}})D_0 \tag{I.15}$$

with D_0 the minimum particle diameter of the filter. At the loosest state (e = e_{max}), Eq. I.14 corresponds to d_{cL} obtained by Eq. I.13.

However, this analytical form and the one proposed by Locke et al. (2001) are only valid for materials with continuous grading according to Reboul et al. (2010).

For Gap-Graded Material *(2-parameter model)*

A more sophisticated model (Eq. I.16) is given by Reboul et al. (2010) to improve the prediction of the CSD at any density for uniformly graded, well-graded and also for gap-graded materials. The last case is critical in filtration modeling because a filter with a continuous grading curve tends to become gap-graded as fine particles coming from a base material infiltrate it.

$$d_c(P_c, R_d) - d_{c_{min}} = (1 - (\frac{e_{max} - e_{min}}{e_{max}})(AP_c + B)R_d)(d_{cL}(P_c) - d_{c_{min}}) \tag{I.16}$$

with A and B two parameters depending on the PSD of the material. The identification procedure of these parameters is given in Reboul et al. (2010).

The analytical models allows to quickly obtain the CSD, but they are derived from geometrical analyses considering the grains as spheres. In fact, real soil grains may not be associated to spherical materials and may hold irregular shapes (angular, flat, rounded and sub-rounded). For example, fluvial gravels which have flat and elongated particle shapes cannot be addressed with the same procedure. Moreover, these models were only validated for the studied types of grading.

4. Conclusion

A granular medium includes a set of large volumes of voids between solid particles (pores) connected by narrowest channels denoted as constrictions. The cumulative constriction size distribution (CSD) governs the filtration performance of granular soils.

Hence, different methods have been proposed in the literature to obtain the CSD. Among these methods, we can cite: experimental techniques, numerical approaches and analytical models. All methods can be considered as powerful tools to compute the constriction size distribution of granular soils, but all of them show their particular limitations related to the absolute size of grading, the type of grain size distribution, the particle shape, the accuracy and the computer time consumption.

However, some limitations associated with complex and time consuming experimental and numerical approaches can be addressed through the use of simple analytical models which can provide a quick estimate of the CSD for soil erosion assessment.

To ensure their validity, such geometrical models must be calibrated on the basis of numerical methods allowing to reproduce the correct mechanical state of granular soils underlying the void space structure.

In this regard, the micro-CT scans combined with appropriate algorithms can provide insight into the void network of a granular medium. One advantage of this method is its applicability to real soils including non-spherical particles. However, the voxelization of the space is the primary limitation of this technique, since the voxel size is directly linked to the smallest particle size within the sample and thus, abundant computer power must be expended or just small samples can be processed.

On the other hand, a DEM creation of samples combined with a Delaunay/Voronoï approach can potentially be used for pore space partitioning in the case of packings composed of spheres.

However, using such techniques may lead to an over-segmentation of the void space and thus, a post-processing of the dataset may be required. Until recently, different attempts have been made to define pore merging criteria, but their relevance has not always been definitively established. In the light of this fact, additional effort must be undertaken for achieving a more rational segmentation of the pore space.

Chapter II

Filter criteria for granular soils

1. Introduction

Internal erosion is one of the most frequent causes of deterioration and failure of earth structures. Such a process can be successfully avoided by providing adequate filter material. To achieve this, the required filter must be well designed and properly positioned in the structures.

However, designing an effective filter requires that the voids within the filter are sufficiently small to prevent the erosion of base particles. Indeed, constrictions which are the narrowest throats linking pores, are responsible for trapping loose base particles.

The constriction sizes of a granular filter are mainly controlled by the finer particles of this material (Kenney et al., 1985; Indraratna et al., 2008). In view of this fact, many researches have been conducted to establish PSD-based criteria for granular filters involving characteristic grain sizes of both the filtering soil and the base soil in which the migration must be avoided.

Until recently, earth structures were designed based on these so-called empirical retention criteria which are mainly based on laboratory tests. Other empirical retention criteria based on a comparison between filter permeability and base soil particle sizes were also used.

However, the engineering literature illustrated the weakness of some empirical methods by reporting failures of some existing dams and levees (Jansen, 1983; Foster and Fell, 2001).

The rapid advancement of geotechnical engineering has resulted in the development of constriction-based criteria for the design of filters. These criteria provide a sound understanding of the fundamental processes that govern the transport of erodible particles in granular soils since constriction areas are always smaller than the cross-sectional areas of pores, and thus, the CSD is the key filter characteristics that influences the performance of filter.

This chapter presents a comprehensive review of existing filter design practices together with a discussion regarding their relevance or their limitations.

2. Design of suitable filters

Foster and Fell (2001) defined three sequential phases of erosion leading to the failure of earth dams: initiation, continuation, and progression. Initiation occurs when the soil begins to erode as a result of seepage forces and other causal factors. The erosion may continue if it is not stopped by an appropriate filtering action. In this case, voids begin to form and gradually progress leading to the formation of a pipe in the dam body (or in the foundation) and eventually to a dam breach. Fig. II.1 shows possible locations of initiation of internal erosion in earth dams (Fell and Fry, 2007).

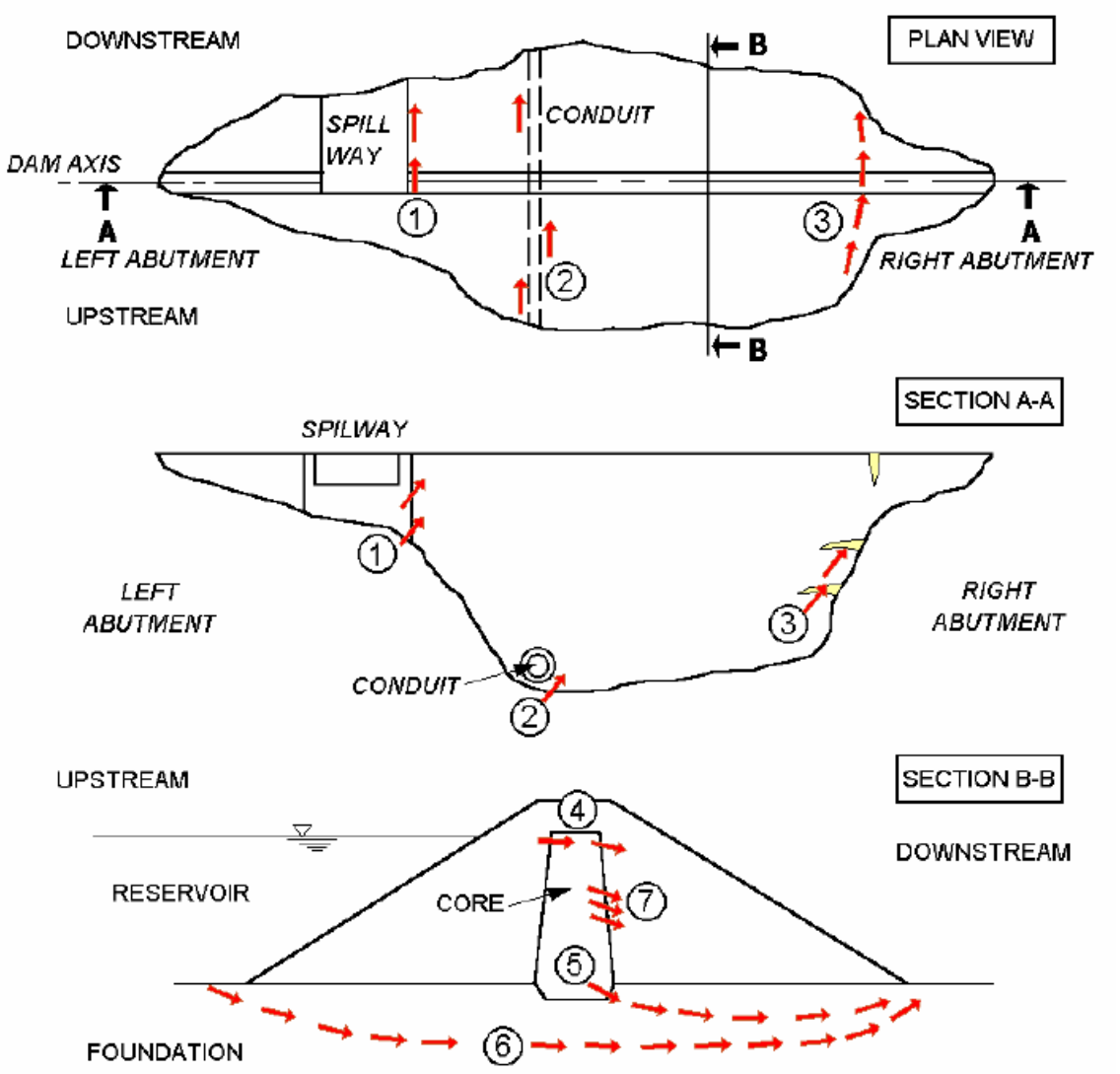

Fig. II.1. Possible locations of initiation of internal erosion (Fell and Fry, 2007); (1): spillway wall interface; (2): adjacent to conduit; (3): crack associated with steep abutment profile; (4): desiccation on top of the core; (5): embankment to foundation; (6): foundation (if the foundation is made of soil or is an erodible rock); (7): embankment through poorly compacted layer and or crack

Granular filters are generally used to prevent or mitigate such erosion processes. They are installed in zoned dams or on the downstream slope of levees to avoid the wash out of soil particles through the core of earth structures or through their foundation.

In order to have this ability, the International Committee on Large Dams (ICOLD, 2013) recommended that a filter has to satisfy five main requirements:

- **Retention**: the filter must restrain the transport of fine particles of the protected soil (base soil).
- **Drainage**: the filter must be sufficiently permeable in order to allow water to pass freely out of the base soil and to avoid the development of excessive pore water pressure on the filter-base soil interface.
- **Self-filtration or stability**: the filter must be internally stable and not subjected to suffusion. Suffusion is the process by which finer soil particles are progressively detached and eroded through larger soil particles by seepage forces.
- **No cohesion**: the filter must not hold cracks. Indeed, cracks may form in dam crests from desiccation or from a differential settlement (ICOLD, 2013). Such cracks can create a leakage path for particles to escape, thereby they reduce the filtration efficiency of the hydraulic structure.
- **Strength**: the filter must transfer the stresses within earth structures without particle crushing leading to the generation of finer grains. This is achieved by specifying the durability and the crushing strengths of the aggregates (ICOLD, 2013).

All these requirements should be taken into account to obtain a complete filter criterion. The research developed in this manuscript only deals with the first requirement.

Generally, the filter criteria are designed so that the base soil particles are not blocked at the filter-base soil interface. If not, clogging would take place inducing a high pore pressure rise likely to degrade the stability of the overall hydraulic structure. In that case, the filter would act as a perfect filter (Vaughan and Soares, 1982; Vaughan et al., 2004).

In fact, a granular filter works like a sieve characterized by its average opening size. The filter opening size is a key entity to understand the process of retention of base particles flowing through it. Fine particles smaller than the opening size can cross the filter, and those larger than this critical size will be captured by the filter.

Fig. II.2 shows a stable base-filter interface where larger base particles flowing under seepage are trapped by the constrictions of the filter. Smaller constrictions are then formed by the retained particles allowing the retention of further base particles. After the formation of a stable interface (zone in the filter with a mixture of base particles and filter grains), no further particle loss will occur. Such a filter is denoted as effective filter. In contrast, when the filter material is too coarse, the base particle can move freely through the pores of the filter leading to the formation of an unstable interface and then the filter becomes ineffective.

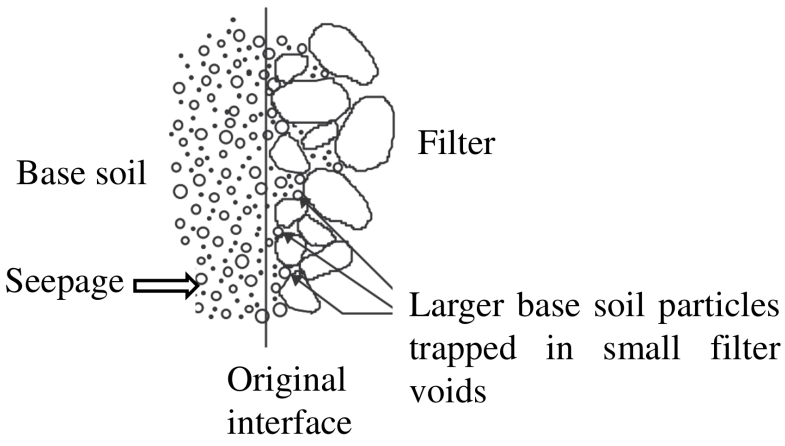

Fig. II.2. Stable base-filter interface during seepage (Locke and Indraratna, 2001)

3. Experimental filtration tests

As explained in Chapter I, stating individual pathways without interaction with other particles, the probabilistic methods can relate the base particles migration within a filter to the probability for a particle to encounter a constriction through which it can pass. This allows the determination of the retention efficiency for any kind of filter materials, including geotextiles (Elsharief, 1992).

The sizes of fine particles that can cross the filter are clearly affected by its thickness: as the filter thickness increases, the probability of coarser material to successfully cross the filter decreases since the probability that a grain will be captured by a smaller constriction increases as well.

Consequently, a filtration test can only allow to obtain, for a given material and a given density, the opening size of the filter, result that in fact depends on the filter thickness.

Conventional experimental approaches in filtration have usually been conducted using a vertical cylinder similar to that shown in Fig. II.3. The experiment involves a vertical flow of water through the base soil and filter. The apparatus is often vibrated or tapped with a rubber mallet to avoid the formation of arching within the sample. Generally, such tests allow a visual inspection of the base material passing through the filter, the measurement of the permeability changes throughout the test, the measurement of the changes of both filter and base soil materials and the determination of the PSD modification before and after the test. Test results will then be judged as failure cases if a significant quantity of base material passes through the filter (Sherard et al., 1984).

Using a random packing of glass spheres as the filter medium, Ghidaglia et al. (1996) carried out a series of experiments on deep bed filtration so that it was possible to visually determine the density of trapped particles inside the filter. Recently, the experimental tests conducted by Muresan et al. (2012) provide information on the dynamics of fines in the filters' pore network and changes of filters' efficiency.

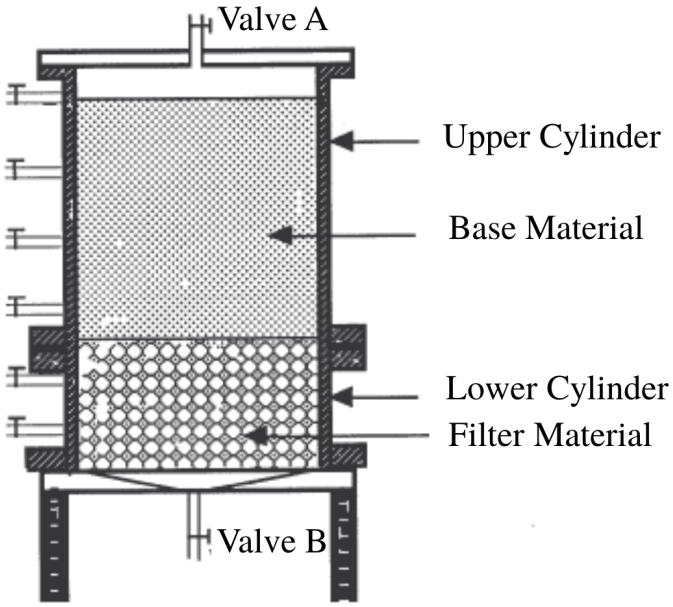

Fig. II.3. Typical laboratory apparatus (Locke, 2001)

In addition to experimental studies, few numerical studies are available to simulate the transport of fine particles within porous media. Roozbahani et al. (2014) investigated the mechanical trapping of fine particles in a bed of monosized packing of spheres. Their packing was firstly generated by means of the gravitational sphere algorithm. Then, by subsequently introducing fine particles into the bed, they computed the mass-rates of fine particles passing through and trapped in the packed bed.

Kerimov et al. (2018a) use the DEM to simulate packings of granular spherical particles under the action of gravitational forces. Then, they model the trapping and percolation of fine particles in the generated granular media. Sjah and Vincens (2013) also used the DEM to back-calculate the CSD curve from experimentally derived filter layers through which base particles may infiltrate. Besides, some numerical filtration tests include direct coupling between solid and liquid phases (Sari et al., 2011; Tejada et al., 2016)

4. Particle-size based criteria

Designing a suitable filter is not an easy task since filtration can be affected by several factors including geometric, hydraulic, chemical, physical and biological factors (Indraratna et al., 2008). However, filter criteria are usually expressed in two forms: the geometric criterion and the hydraulic criterion, while other aspects are ignored.

For the sake of simplicity, filter criteria are generally designed in terms of the PSD, and are presented in the form of filter-base soil grain sizes ratio derived from extensive laboratory tests.

The typical filter criterion of Terzaghi et al. (1996) stated that an effective filter should be sufficiently fine, relative to the particle sizes of the base soil to prevent fine particles from washing

through the filter material while being coarse enough to ensure adequate permeability, allowing the escape of flowing water and preventing the build-up of high internal pore pressures. To ensure this, two requirements must be fulfilled:

– **Retention requirement**:

$$d_{85} \geq \frac{D_{15}}{4} \tag{II.1}$$

– **Permeability requirement**:

$$d_{15} \leq \frac{D_{15}}{4} \tag{II.2}$$

where D_x is the representative filter particle diameter and d_x is the representative base particle diameter for which $x\%$ of the material (filter and base soil, respectively) by mass is finer.

An illustration of this design is given in Fig. II.4. In particular, the left-hand shaded area encloses all the grain-size curves for the base material; the right-hand area indicates the range within which the curves for the filter material must lie.

From a series of filtration tests, Honjo and Veneziano (1989) concluded that a filter material, herein modeled by a mechanical sieve, can be regarded as effective if at least 15% of base soil particles are larger than the sieve opening. By drawing an analogy, Terzaghi's retention criterion stated that a suitable filter characterized by an aperture equal to $D_{15}/4$ has to prevent the erosion of the larger sized base particles, represented by d_{85}.

In addition to the retention criterion, Honjo and Veneziano (1989) introduced a new index (d_{95}/d_{75}) which is related to the capability of base soil to form a satisfactory *self-healing* layer (interface layer). Terzaghi's retention criterion is then refined as follows, $D_{15}/d_{85} \leq 5.5 - 0.5 d_{95}/d_{75}$, for broadly graded soils.

More recently, large numbers of experiments have been carried out based on the original concepts initiated by Terzaghi et al. (1996) where D_{15} is selected as a representative filter size.

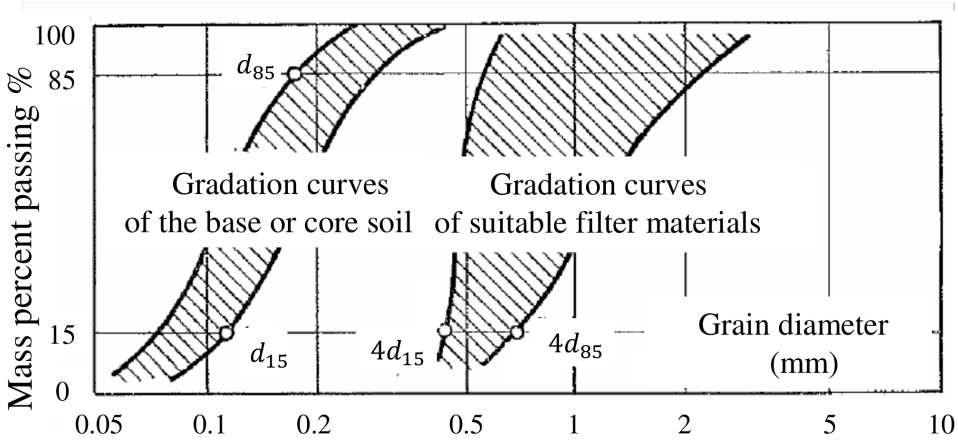

Fig. II.4. Filter and drainage criteria (Terzaghi et al., 1996)

Studies conducted by Kenney et al. (1985) over a wide range of gradings showed that the CSDs, for a given relative density, form a narrow band of similarly shaped curves when normalized by a characteristic filter diameter (D_5 or D_{15}). Thus, smaller filter grains seem to govern the controlling constriction size ${D_c}^*$, which has been found to be slightly influenced by the grading and the thickness of the filter.

Similar findings were also reported by Shire and O'Sullivan (2016). ${D_c}^*$ is here defined as the maximum possible size of particle that can be transported through a filter of a specific thickness. In other words, it measures the governing size of passable channels or pathways a particle can take in a porous medium. ${D_c}^*$ can be given by:

$$ {D_c}^* \leq \frac{D_{15}}{5} \tag{II.3} $$

$$ {D_c}^* \leq \frac{D_5}{4} \tag{II.4} $$

Using the concept of controlling constriction size, it was verified that filtration is most likely to occur if there are base particles larger than ${D_c}^*$. It must be noted that Kenney et al. (1985) findings provide a slightly smaller opening size than that implicitly given by Terzaghi et al. (1996). However, their relationship (Eq. II.3) supports the use of the filter design rule by Terzaghi.

By performing numerous filtration tests, Sherard and Dunnigan (1989) reformulated the commonly used filter criteria according to the considered base soil. The new design criteria are given in Table II.1. Here, the criteria are rewritten so that the controlling constriction size ${D_c}^*$ appears clearly. To design protective filters for fine cohesive base soils, Table II.1 indicates that the movement of particles is envisioned as a movement of clusters composed of glued grains rather than individual grains.

For the base soil, the representative diameter is often taken as d_{85} since particle loss is limited if the filter opening size is smaller than this value. However, this choice has been criticized by Lafleur et al. (1989) who recommended the use of $d_{50} - d_{85}$ as a representative range of base particle sizes for broadly graded base soils.

Similarly, the current design practice (NRCS, 1994) suggests to use a regraded d_{85} obtained by excluding the coarse fraction retained by the 4.75mm sieve size. Indraratna and Locke (1999) adopted this modification to reformulate the retention criterion of Sherard and Dunnigan (1989) (Table II.1). Kenney et al. (1985) also used a smaller base soil representative size (d_{50}) to address the ineffectiveness of the original filter criterion in the case of well-graded base soils.

Foster and Fell (2001) tested more types of soils and categorized the filter behaviour as follows: *"no erosion"*, *"some erosion"* and *"continuing erosion"*. According to these authors, D_{15}/d_{95} is more accurate than D_{15}/d_{85} to define the boundary between some and continuing erosion, since using a large characteristic base size (d_{85} or d_{95}) takes into account the self-filtration process where large particles trapped in the filter reduce progressively the porosity and the constriction sizes, and thus, prevent finer particles from penetration through.

Table II.1: Filter design criteria introduced by Sherard and Dunnigan (1989)

Base soil category	Fines content < 0.075mm	Filter criterion
1: Fine silt or clay	$85-100$	$D_{15}/5 \leq 1.8\ d_{85}$
2: Sandy silts/clays and silty/clayey sands	$40-85$	$D_{15}/5 \leq 0.14$mm
3: Sands, sandy gravels with few fines	$0-15$	$D_{15}/5 \leq 0.8\ d_{85}$
4: Soils intermediate between previous two categories	$15-40$	Intermediate between 2 and 3

Indeed, a rapid wash out of some fine particles will occur prior to the formation of a self-filtering layer at the base soil-filter interface. However, important losses may have negative impacts on the whole structure. To avoid such consequences, it is important to assess what kind of particle size is necessary to form this self-filtering zone.

In recent years, important advances have been made in the development of filter design criteria for geotextiles which was originally introduced by Giroud (1996). Beside permeability and retention criteria, two other criteria were also considered: the porosity criterion and the thickness criterion Giroud (2010).

However, in case of granular filters, no porosity or thickness requirements are needed since, firstly, a granular filter has enough opening per unit area to minimize the flow concentration at the soil-filter interface, and secondly, due to construction constraints, it has a sufficient thickness to stop a moving soil particle. A detailed overview of filter criteria for geotextiles can be found in Giroud (2010).

Terzaghi's approach has widely been used in engineering practice to describe, basically, the conflicting requirements on particle sizes of a suitable filter. However, these empirical criteria originally developed for cohensionless uniform base soil and filter materials, present obvious limitations when dealing with well-graded or gap-graded materials (Indraratna et al., 2008) since soil uniformity (C_u) was clearly not considered.

Fig. II.5 shows different set of filter-base soil combinations having a similar D_{15}/d_{85} ratio but various coefficients of uniformity C_u. From this figure, it is obvious that Terzaghi's ratio is not the appropriate term to evaluate the filtration characteristics of a filter-base soil system, since different behaviour can be expected depending on the grading of the filter or of the base soil material.

Furthermore, the effect of filter density was completely ignored. In fact, same filter materials in terms of PSD could have different CSD depending on their degree of compaction. The sensitivity of the CSD to the density (Schuler, 1996) shows that filter criteria based on a characteristic filter grain size are not accurate enough to assess the performance of granular soils. Therefore, applying such criteria does not explain the fundamental mechanics of filtration and hence, rigorous filter criteria must be explicitly based on physical considerations.

Nonetheless, and following the same framework as proposed by Terzaghi, the grain size distribution has also been used to assess the internal stability of soils (Kézdi, 1979) and to predict the permeability of porous media (Chapuis, 2012).

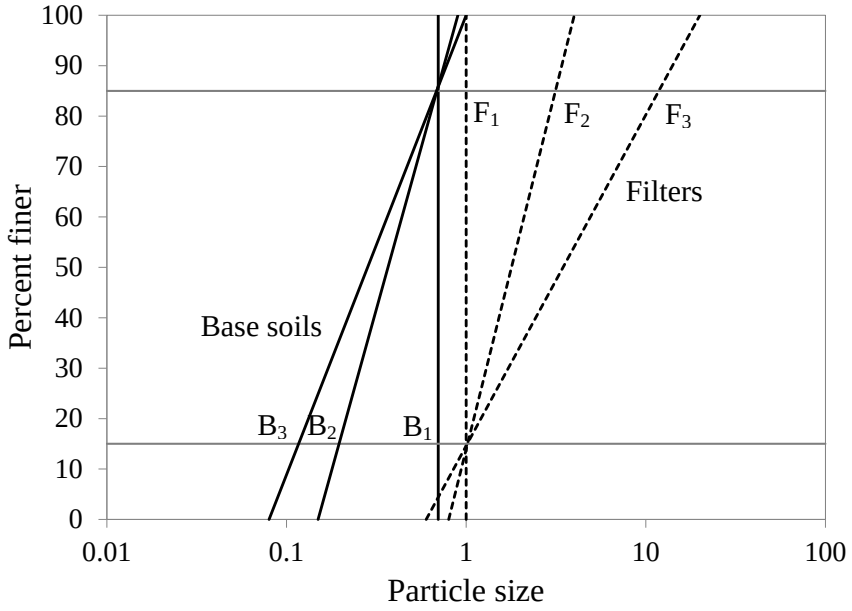

Fig. II.5. Filters and base soils having different uniformity coefficients C_u but similar D_{15}/d_{85} ratio (Indraratna et al., 2007)

5. Permeability-based criteria

Beside the classical PSD-based criteria, some researches introduced the permeability-based criteria to assess the retention capacity of granular filters by directly comparing filter permeability to base soil particle sizes.

Vaughan and Soares (1982) and Vaughan et al. (2004) developed an equation that links the permeability of a filter to the soil particle size to be retained (Eq. II.5). Alternative particle size-permeability relationships were also found by Indraratna et al. (1996).

$$\delta_R = 2.54.10^3 {K_{Filter}}^{0.658} \tag{II.5}$$

where K_{Filter} is the permeability of filter (m/s) and δ_R is the size of the smallest particle retained in microns.

Lately, Delgado et al. (2006) carried out extensive filtration tests to determine *No-erosion* filter criteria based on the filter permeability and the percentage of base soils passing the 0.075mm sieve. The permeability has been calculated from laboratory experiments (permeameter test) or estimated by applying the relation $K = 0.35D_{15}^2$ which relates the permeability K to the D_{15} filter size (Sherard and Dunnigan, 1989). Babu and Srivastava (2007) substituted the retention and permeability requirements of Terzaghi by a single equation taking into account the pore size, the permeability and the factor of safety against soil boiling conditions.

However, determining filter permeability is not easy and is even time-consuming. The standard

filter criteria based on grain sizes ratio are generally easier to apply. Although the permeability of a granular filter implicitly takes into account its PSD and other important characteristics such as the degree of compaction and the shape of particles, internal erosion seems to be more likely related to the openings of the filter (constrictions). Hence, the relevance of using CSD-based criteria has been highlighted in subsequent studies.

6. Constriction-based criteria

Empirical filter criteria, in particular Terzaghi's criteria, have been adopted in many simplified designs. However, these practices are only applicable to the range of tested soils. The results of filtration tests involving well-graded base soils make the efficiency of such criteria questionable.

Hence, it is more appropriate to develop filter criteria based on constriction sizes since within the filter, it is the size of constrictions rather than the size of particles that influences the filtration process Locke et al. (2001). Moreover, it is now well established that particle frequency based on the surface area is more adequate to model the properties of the void space in granular filters.

For this purpose, two representative diameters of the constriction size distribution were defined: the dominant constriction size D_{c95} (constriction size whereby 95% of the filter constrictions are finer than) (Indraratna and Raut, 2006; Raut and Indraratna, 2008) and the controlling constriction size D_{c35} (constriction size corresponding to finer = 35%) (Indraratna et al., 2007).

The first diameter can be used to disregard coarser base particles that do not influence the process of self-filtration since these particles cannot probably even enter the filter.

The second diameter is used as a control variable to assess the performance of the filter. Using a probabilistic method, Indraratna et al. (2007) indicated that there is a range of probabilities of constriction sizes (0.3-0.4) under which a small decrease in the probability of having $d > d_c$ enables the particle with diameter d to travel a large distance within the filter before being stopped. Thus, D_{c35} has been chosen as a control diameter. In other words, D_{c35} must be smaller than the large loose base particles, so these particles will not be eroded.

The CSD from which D_{c35} and D_{c95} are derived, is obtained following the calculations of Locke et al. (2001) (Eq. I.12). Note that the regrading rule proposed by these authors is not applied here.

Indraratna et al. (2007) argued that a filter can be conceived as a sieve with apertures equal to the controlling constriction size D_{c35}. Accordingly, a constriction-based criterion for base soil retention can be given by the following relationship:

$$d_{85SA} \geq D_{c35} \tag{II.6}$$

where d_{85SA} indicates that 85% by surface area of base particles are finer than this size.

Indraratna et al. (2007) proposed to reduce the representative diameter of base soil to d_{85SA} which can be more appropriate than the usually used value (d_{85} from the PSD by mass) when well-graded soils are considered. Indeed, applying the surface area concept for PSD and CSD quantification in this new criterion enables the removal of some limitations associated with the well-known Terzaghi retention criterion.

Furthermore, the above CSD-based criterion takes into consideration fundamental filter parameters including the coefficient of uniformity and the density contrary to Terzaghi's criterion which only considers the single filter grain size D_{15}. In this sense, it is more general. Nonetheless, it is worthy noting that obtaining D_{c35} is not as easy as assigning D_{15}. The construction of the whole CSD is herein required.

Later on, Raut and Indraratna (2008) proposed a new filter criterion based on the self-filtering base fraction and the controlling constriction size of the filter. The PSD of the base soil is then modified by ignoring all particles coarser than D_{c95}. Thus, for an effective base soil-filter combination, the following relationship must be fulfilled.

$$d_{85}{}^{*} \geq D_{c35} \tag{II.7}$$

where $d_{85}{}^{*}$ refers to d_{85} from the modified base soil PSD. The proposed criterion has a clear advantage in satisfying internal stability requirements (Raut and Indraratna, 2008).

Moreover, D_{c35} and D_{c95} models did not require the base soil to be regraded. It is worthy to note that these models involving dominant and controlling constriction sizes were verified based on extensive experimental data from various past filtration tests (Indraratna et al., 2007; Raut and Indraratna, 2008). Thus, one can conclude that constriction-based criteria give a more realistic approach and hold a more clear physical meaning compared to the conventional retention ratio based on particle sizes. Table II.2 illustrates the advantages of constriction-based models in comparison with the particle-based criteria (Indraratna et al., 2008).

More recently, Vakili et al. (2015) expanded the constriction-based criterion of Raut and Indraratna (2008) and carried out experimental tests on some dispersive and broadly graded base soils. They found that $d_{85}{}^{*} \geq D_{c35}/1.25$ is acceptable for base soils of Group 1 with high dispersivity. However, for base soils of Group 2, $d_{85}{}^{*} \geq D_{c35}/0.5$ is required for $C_u \geq 20$ and for a high degree of dispersion (more than 80%) (Table II.3). These authors stated that the dispersivity of base soils decreases the no-erosion filter boundary in agreement with previous researchers (Lafleur et al., 1993; Foster and Fell, 2001; Vakili and Selamat, 2014). A critical review on filter design criteria for dispersive base soils can be found in Vakili et al. (2018).

Table II.2: Comparison of capacities between particle-based and constriction-based filter criteria (Indraratna et al., 2008)

Criteria capabilities	Terzaghi	NRCS	D_{c35} Model	D_{c95} Model
No regrading is required	No	No	Yes	Yes
Inherent internal stability analysis	No	No	No	Yes
Enhanced design certainty due to self-filtration PSD	No	No	No	Yes
Clear distinction between effective and ineffective filter	No	No	Yes	Yes
Porosity, R_d and C_u considered	No	No	Yes	Yes
Analytical principles applied	No	No	Yes	Yes

Table II.3: Filter design criteria introduced by Vakili et al. (2015)

Fine content of base soil (%)	non dispersive base soil	highly dispersive base soil
≥ 85	${d_{85}}^* \geq D_{c35}/1.25$	${d_{85}}^* \geq D_{c35}/1.25$
$40-85$	${d_{85}}^* \geq D_{c35}$	${d_{85}}^* \geq D_{c35}/0.5$

A summary of all mathematical filtration models reported in the state of the art and related to constriction size distribution is presented in Table II.4 in a chronological order, which can be useful to have a general background on the progression of constriction-based retention criteria for granular filters.

7. Internal stability of granular soils

The internal stability of granular filters must be considered when designing earth structures. It refers to the ability for the coarse fraction of a granular material to prevent the loss of its own finer fraction due to seepage flow. This property is related to the soil particle-size distribution and to its density (Kenney and Lau, 1985). This concept is equivalent to prevent suffusion. Table II.5 summarizes the main internal stability criteria that are widely used in design practice to evaluate the internal stability of cohesionless soils.

Istomina (1957) used the coefficient of uniformity C_u as an indicator for the internal stability of sandy gravel soils. The coefficient of uniformity measures the range of particle diameters and is defined as the ratio of the diameter corresponding to 60% finer by weight to the diameter corresponding to 10% finer by weight. Accordingly, soils with $C_u \leq 10$ are considered to be internally stable and those with $C_u \geq 20$ are likely to be internally unstable. Those with C_u between 10 and 20 are situated in a transitional zone.

Kézdi (1979) extended the Terzaghi's criterion for the protection of a base soil by a filter to check the internal stability of granular soils. The PSD of the filter is then divided by an arbitrary diameter into coarse and fine fractions. The coarser fraction acts here as a filter and the finer fraction behaves as a base material and thus, D_{15} of the coarser component is compared to d_{85} of the finer component. The soil is considered to be internally stable if Eq. II.1 is satisfied. Sherard (1979) modified this criterion to $D_{15}/d_{85} \leq 5$.

Kenney and Lau (1985, 1986) performed some laboratory tests to define a threshold between stable and potentially unstable filters based on the shape of the gradation curve. The proposed criterion assesses a soil to be internally stable if $H/F \geq 1$, where F is the mass fraction of particles finer than an arbitrary particle size D, and H is the mass fraction of particles ranging from D to $4D$. H/F can be obtained from the PSD over a portion of its finer fraction given by $F \leq 20\%$ for soils with $C_u > 3$, and by $F \leq 30\%$ for soils with $C_u \leq 3$. Their method is shown graphically in Fig. II.6.

Burenkova (1993) uses new factors of uniformity (d_{90}/d_{15} and d_{90}/d_{60}) to define the boundaries for suffusive and non-suffusive soils. Wan and Fell (2008) subsequently found that this approach provides satisfactory predictions when analyzing cohesive soil specimens.

Table II.4: Chronological progression of various filtration models related to constriction size distribution (modified after Indraratna et al. (2008)

Reference	Highlight
Fuller and Thompson (1907)	Theoretical grading and the densest possible state of a packing of uniform spheres
Silveira (1965)	Simple filter void model composed of multi-layered constriction network involving one-directional movement of fine particles
Silveira et al. (1975)	Constriction sizes for filter materials at densest and loosest states
De Mello (1977)	Limitation of PSD by mass to model constrictions of well-graded filters
Wittmann (1979)	Modeling of flow path as a pore channel with irregular width
Kenney et al. (1985)	Multi-layered void network model: estimation of the number of confrontations with constrictions required to stop a base particle; using the PSD by numbers to model the CSD of well-graded filters
Honjo and Veneziano (1989)	Particle transport model based on conservation of mass in the solid and liquid phases
Soria et al. (1993)	Experimental results on CSD of a dense filter according to geometric-probabilistic filtration theory
Silveira (1993)	Enhancement of the 1975 model
Witt (1993)	3D pore-network model composed of spheres (pores) interconnected by pipes (constrictions)
Schuler (1996)	Regular cubic model of pores interconnected by six constrictions similar to the Witt (1993) model
Giroud (1996)	The densest state may exist even in a medium-dense soil
Indraratna and Vafai (1997)	Pore channel model showing that the smallest constriction within the pore channel governs the size of base particles that can pass through it
Indraratna and Locke (2000)	Improvement of the Indraratna and Vafai (1997) model by incorporating the cubic pore network model
Locke et al. (2001)	Analytical model for CSD taking into account the PSD by surface area and the relative density of the filter; time-dependent model based on a cubic network
Raut and Indraratna (2004)	CSD model: numerical evaluation of the effectiveness of non-uniform granular filters
Semar and Witt (2006)	A network model that explicitly considers the full CSD
Indraratna and Raut (2006)	D_{c95} Model: the use of the dominant constriction size D_{c95} to delineate effective from ineffective granular filters
Indraratna et al. (2007)	D_{c35} Model: development of a retention criterion based on the controlling constriction size D_{c35}
Reboul et al. (2010)	New analytical models for CSD computation at any relative density calibrated on the basis of numerical samples
Moraci et al. (2012)	A layer-based model comprising alternate layers of particles and constrictions
Shire and O'Sullivan (2017)	New network model taking into account the processes of clogging and self-filtering

Table II.5: Summary of internal stability criteria for granular soils

Reference	Internal stability criteria
Istomina (1957)	$C_u \leq 10$: internally stable $10 < C_u < 20$: transitional $C_u \geq 20$: internally unstable
Kézdi (1979)	$D_{15}/d_{85} \leq 4$: internally stable
Kenney and Lau (1985, 1986)	$(H/F)_{min} \geq 1.3$: internally stable (original) $(H/F)_{min} \geq 1.0$: internally stable (modified)

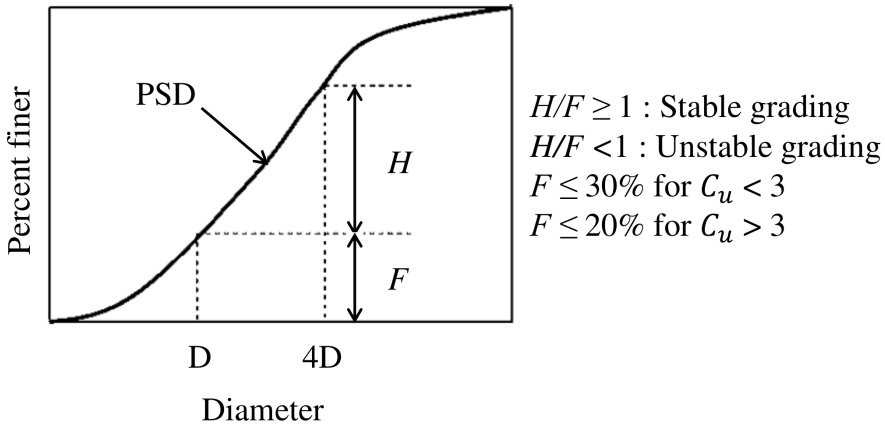

Fig. II.6. Graphical representation of the procedure from Kenney and Lau (1985) for internal stability assessment

The Natural Resources Conservation Service (NRCS, 1994) guidelines impose constraints on the choice of D_{100} and C_u of the filter to avoid its segregation (Indraratna et al., 2008). Later on, Li and Fannin (2008) proposed to use Kenney and Lau's criterion at $F < 15\%$, and Kézdi's criterion when F is larger than 15%.

According to Fell and Fry (2007), a soil with either discontinuous or upwardly concave grading is often internally unstable. For Kwang (1990), the stability criterion of gap-graded soils is governed by their gap ratio G_r which is defined as the ratio of the higher to lower sizes of the gap on the grain size distribution curve. G_r must be smaller than four. Indeed, a large gap ratio means that the coarse fraction cannot successfully retain the finer fraction, thus the fine particles can be easily eroded from the soil matrix.

Internal stability is also governed by stress conditions and hydraulic factors (Garner and Fannin, 2010). Besides, the shape of grains plays an important role. Marot et al. (2012) found that the angularity of coarse grains contributes to increase the suffusion resistance of the granular material.

Recently, Chang and Zhang (2013) identified other control variables such as the fine content (content smaller than 0.063mm) and the gap ratio to assess the internal stability of various types of gradation (well-graded and gap-graded soils), and accordingly proposed composite internal stability criteria (Table II.6).

Table II.6: Internal stability criteria for granular soils as proposed by Chang and Zhang (2013)

Type of gradarion	Fines content P(%)	Internal stability criteria
Well-graded	$P < 5$	$(H/F)_{min} > 1.0$: internally stable
	$5 \leq P \leq 20$	$(H/F)_{min} > -(1/15)\ P + 4/3$: internally stable for low plasticity soils
	$P > 20$	stable
Gap-graded	$P < 10$	$G_r < 3.0$: internally stable
	$10 \leq P \leq 35$	$G_r < 0.3P$: internally stable for medium plasticity soils
	$P > 35$	stable

8. Conclusion

The main matter discussed in this chapter was on the development of various filter design criteria for base soil retention. Empirical filter criteria are mainly based on characteristic grain sizes, ignoring the effect of compaction and shape of particles. These criteria have a wide recognition as a promising tool for internal erosion assessment. However, they are not fully adequate for the design of well-graded soils.

Within a granular filter, the size of pore channels can be controlled by the narrowest constriction along the percolation path and thus, the constriction size distribution dominates the void space characteristics. In this context, recent studies based on the constriction-size approach can provide considerable improvements from existing filter design criteria.

The integration of filter compaction and uniformity together in the analytical approach involving the PSD with surface area make these criteria more comprehensive. However, a complete filter criterion should take into account the internal stability of soils.

Many of the critical aspects of current design practices can be addressed by a thorough evaluation of filter CSD. This work focuses on improving analytical models for CSD and on extending constriction concepts of filters established in earlier studies (Kenney et al., 1985; Locke et al., 2001; Indraratna et al., 2007). In addition, a more accurate representation of the controlling constriction size in constriction-based criteria for filters, will be provided.

Chapter III

Pore and CSD computation for spherical materials

1. Introduction

It is now well established that a better insight into the problems of internal erosion in earth structures can be provided by investigating the void space within granular materials and more specifically by identifying their constriction size distribution.

The aim of this chapter is to provide a meaningful characterization of the void space in terms of pore and constriction size distributions. The samples preparation method of numerical packings will be described in the first part of this chapter. The numerical tools and the results of poral analyses will also be presented. Different gradings will be examined (Uniformly graded, well-graded and gap-graded materials) at extreme density states (Loose and dense).

The Discrete Element Method (DEM) was used here to generate packings of spheres, based on mechanical laws of motion and a weighted Delaunay tessellation was applied to compute the pore space properties. On the basis of this partition, the main void characteristics including the inscribed void spheres in local pores and the constriction sizes can be deduced.

However, this partitioning method generally induces an over-segmentation of the pore network and a merging step is usually added to mitigate such undesirable artifacts even if a precise delineation of a pore is somewhat subjective due to the complex and interconnected nature of the void space in porous media. This chapter provides a comparison between different merging criteria for pores in spherical packings, and a discussion about their implication on pore and constriction size distributions of the material is presented.

In a second part, the derived numerical CSD serves to re-examine the validity of the analytical models proposed by Reboul et al. (2010). Such models can be useful to build the CSD of a granular fiter. This information could help in understanding the transport mechanisms within granular materials.

Finally, we compare different definitions for the mean pore size based on statistical analyses performed on numerical samples with materials having different types of gradings at different density

states. This characteristic value of the void space can be used in pore-network models either to compute the CSD or to predict the longest path covered by a flowing fine particle through a granular filter.

2. Discrete element modeling

The Discrete Element Method (DEM) enables to investigate the mechanical behaviour of granular materials by modeling particles as rigid bodies whose dynamics is described by Newton's laws (Cundall and Strack, 1979). On the other hand, computation time increases considerably when a large number of particles or irregular shaped particles are considered, thus limiting the applicability of DEM to small scale problems (Shigeto and Sakai, 2011; Scholtès and Donzé, 2013). In our study, numerical samples composed of spheres are generated by means of an open source code, *YADE-DEM* (Šmilauer et al., 2010).

2.1. Characteristics of numerical packings

Referring to Fig. III.1, different types of soils (Uniformly Graded, Well-Graded and Gap-Graded) were studied. In addition to the materials studied by Reboul et al. (2010) (C_u = 1.7, 3.6, 3.9), further samples with a higher coefficient of uniformity (C_u = 6) were tested. Note that no higher coefficients of uniformity were investigated since such values would excessively penalize the computation time.

The labels of samples indicate the material type (for example, UG for Uniformly Graded material). A well-graded soil (WG) has a good representation of all sizes while a gap-graded soil (GG) has a range of under-represented or missing particles. The selected gradation was verified against internal stability requirements described in Chapter II and are internally stable.

The contact between particles is characterized by an elastic-frictional model with a normal and a tangential stiffness (respectively K_n and K_s) and a contact friction coefficient (μ). In this study, particle density (ρ) refers to the one of glass beads, and typical values for K_n and K_s of such materials are chosen. For the specific contacts between a particle and the bottom wall of the box, the contact friction coefficient (μ) is set to 0. Dissipation in the system is introduced by means of a global damping (α) proportional to the acceleration forces (Cundall and Strack, 1979).

In order to obtain representative statistical data, the considered number of particles varies from $2,000$ to $40,000$ depending on the filter gradation. Two coefficients of friction (μ) were used for each grading to generate samples with different void ratios: one corresponding to the loosest state and another one to the densest state (L and D denoting loose and dense respectively) for the material.

For the loosest samples, a value of 0.3 (0.15 for UG material) was selected as this value is approximately equal to the experimentally derived value for spherical glass beads (Barreto Gonzalez, 2010). The resulting void ratio matches the targeted value obtained through laboratory experiments by Biarez and Hicher (1994), for the same coefficient of uniformity and the same particle aspect ratio of 1 (difference between the largest and the smallest dimension of a particle). These

authors used the ASTM standard to determine both the maximum and minimum void ratio of actual granular materials having different gradings and particle aspect ratios.

For the densest samples, μ was assumed to be equal to zero. In fact, setting the inter-particles friction to zero is favorable for particle rearrangements, which in turn leads to the compaction of the packing (Thornton, 2000; Zhang et al., 2001; Sitharam et al., 2002). Table III.1 and Table III.2 summarize the input parameters used to obtain the numerical samples and their induced final properties.

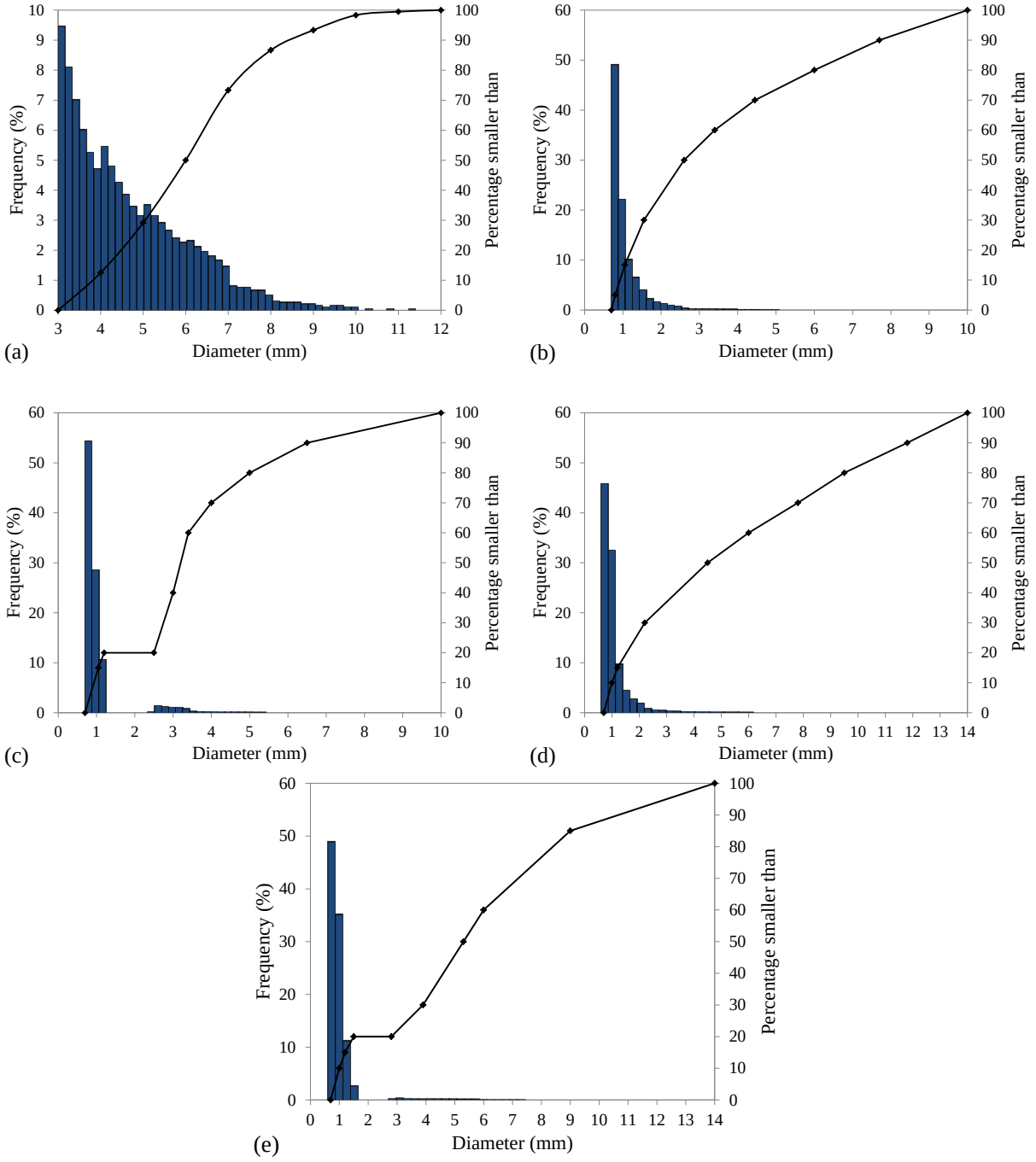

Fig. III.1. Particle size distribution (ordinate on the left Y-axis) and cumulative particle size distribution (ordinate on the right Y-axis) for the considered samples (a): UG, (b): WG1, (c): GG1, (d): WG2, (e): GG2

Table III.1: Mechanical and numerical parameters for DEM simulations

Parameter	Magnitude
Normal stiffness (K_n)	10^4 kN/m
Tangential stiffness (K_t)	10^4 kN/m
Specific weight of spheres (ρ)	2530 kg/m^3
Global damping (α)	0.7
Inter-particle friction (μ)	0.3 (loosest state) 0 (densest state)

Table III.2: Characteristics of numerical samples

Material	Coefficient of uniformity (C_u)	$D_0 - D_{100}$ (mm)	Number of particles	Void ratio e_{max}/e_{min}
UG	1.7	$3-12$	650	$0.61/0.52$
WG1	3.9	$0.7-10$	25000	$0.49/0.33$
GG1	3.6	$0.7-10$	25000	$0.52/0.33$
WG2	6	$0.7-14$	40000	$0.41/0.27$
GG2	6	$0.7-14$	40000	$0.43/0.27$

2.2. Sample generation protocol

The samples are generated by a deposit under gravity since this process can better reflect the current engineering practices or lab techniques. Indeed, the sample preparation method can affect the characteristic organization of the generated packing (Benahmed et al., 2004; Roux and Chevoir, 2005) and thus, artificial structures that may not reflect actual structures within granular materials, are not recommended if one wants to derive general findings.

To provide a clear demonstration of the influence of sample preparation on the void microstructure and more precisely on the CSD, a comparative study of two techniques has been carried out: a deposit under gravity and an isotropic compression. Fig. III.2 gives the CSDs obtained from UGL and WG1L samples prepared by different techniques.

It has been highlighted that, when dealing with uniformly graded samples at loose density state, the same CSD can be obtained irrespective of the considered process (Fig. III.2a). However, for broadly graded samples, the influence of the preparation technique was more pronounced. In the case of a deposit under gravity, the CSD curve tends to cover a wider range of constriction sizes and thus diverges greatly from the curve obtained by an isotropic compression (Fig. III.2b). Even if the compaction procedure is adopted to prepare isotropic samples which can provide a well-defined structure of the material, a process of deposition under gravity is more appropriate to predict the mechanical behaviour in actual site conditions (Vincens et al., 2015).

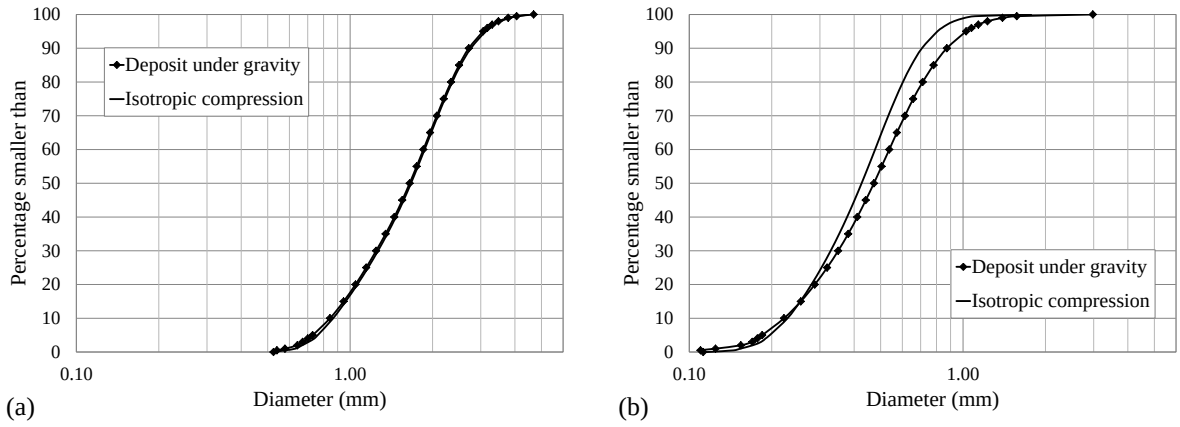

Fig. III.2. CSDs obtained from samples prepared by different techniques (deposit under gravity, isotropic compression); (a): UGL, (b): WG1L

To generate the samples, first, a loose cloud of particles with a prescribed particle size distribution is randomly placed, non-touching positions within a box having a horizontal size equal to that of the final sample but with a larger vertical size (about twice as more as the horizontal size). The base of the box is a square of 40mm to 60mm width (approximately $4D_{100}$). Periodic boundary conditions are imposed on the lateral sides of the box in order to avoid the undesirable rigid walls effects in the final samples (Allen and Wilson, 1989; Radjai and Voivret, 2011).

After this stage, the packing is subjected to gravity which induces the spheres to fall freely in the box. As a result, interactions that can occur between the particles are computed. The simulations are finished when all particles reach a quasi-static equilibrium state. The final equilibrium is supposed to be found when the unbalanced forces (the ratio of the mean resultant particle force to the mean contact force) goes below 0.05.

The densest sample is also obtained by gravitational deposition but under zero friction as described in Cui and O'Sullivan (2003) and Feng et al. (2003). The minimum porosity reached with such a process is equal to that obtained previously by Reboul (2008) for the same materials though the process of creation of their dense sample was different. In their work, spheres are initially released under gravity to create a loose sample and then, the densest state is obtained by means of shearing cycles with a contact friction value equal to zero.

It must be noted that such typical DEM densification processes lead to density states which are generally looser than those obtained for actual materials using the ASTM process (Bernhardt et al., 2016).

2.3. Representative Elementary Volume analysis

In order to obtain a representative homogenized medium, it is necessary to determine the Representative Elementary Volume (REV) of each sample. This latter corresponds to the minimum size of the sample that allows the stabilization of the statistical properties of the studied material.

Since the top and bottom boundaries of the sample are not periodic, any computation of pore-space characteristics for a given packing should be carried out within a volume smaller than the

total sample volume, while the vertical lateral limits of this measurement volume correspond to the periodic boundaries. Then, the limits of the top and bottom volume exclude a non-homogeneous region of thickness equal to D_{100} of the granular material.

Finally, as detailed by Reboul (2008) and Sjah and Vincens (2013), we checked that the final volume used for the statistics of the void space is greater than the REV. For this purpose, the sample is vertically divided into horizontal layers having a thickness equal to D_{100}. Then, the porosity is measured along the horizontal direction with a control width ranging from D_{100} to $4D_{100}$.

Fig. III.3 shows the REV analysis for UGL sample. The four layers are labeled from bottom to top. One can note that the porosity fluctuates initially until it reaches a constant value around 0.38 which is equal to the average porosity of the sample involving all layers. Therefore, this indicates that a sample width of $4D_{100}$ is considered to be an appropriate REV size.

Then, Fig. III.4 illustrates the constriction size distribution computed in each layer for a sample width of $4D_{100}$ and the CSD over the entire sample. As shown in this figure, all the CSDs are superimposed which implies that the selected REV for porosity can be considered as an adequate REV for constriction size distribution as well.

For other broadly graded samples, a large number of particles must be considered to achieve statistically reliable efficiency results. Al-Raoush and Papadopoulos (2010) stated that the minimum REV for the PSD is larger than the REV_{min} for porosity. For this reason, and starting with a small number of particles, DEM simulations were repeated using larger samples until a global stable state (REV) is reached in terms of porosity, CSD and PSD. This approach is similar to the work of Shire and O'Sullivan (2016).

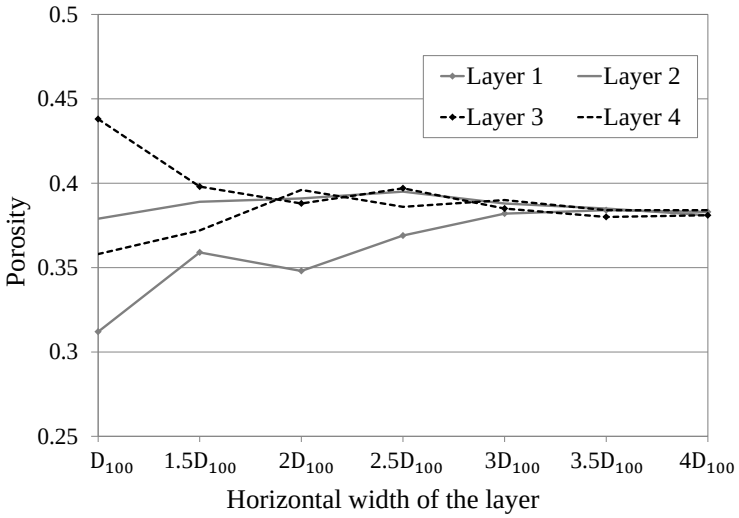

Fig. III.3. Evolution of porosity along the horizontal direction in each layer for UGL sample

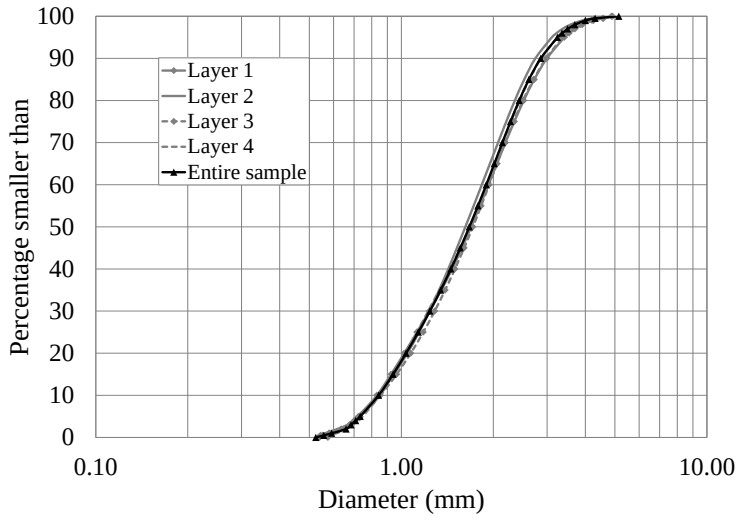

Fig. III.4. CSDs over different layers for a sample width of $4D_{100}$ (UGL)

3. Void space characterization and pore merging criteria

The Delaunay tessellation and its dual Voronoï graph are commonly used to discretize the void space of a granular material in order to derive its characteristics more easily. These partitioning methods help to characterize both the morphology and the topology of the pore network.

The CSDs extracted from a weighted Delaunay tessellation and a Voronoï graph for spherical packings (uniformly graded and well-graded materials) have been proven to be equivalent, which was expected (Vincens et al., 2015; Seblany et al., 2018). However, an excessive artificial segmentation of the void space is usually generated by such processes due, among others, to the creation of flat entities which are a signal of non-robustness of the mathematical process of finding the closest neighbour for a given particle. Other reasons arise from the arbitrary definition of a pore. For these reasons which origins are different, an additional merging step is expected.

Different techniques for merging pores can be found in the literature. Among them, we can cite the methods based on the overlap of inscribed void spheres (Reboul et al., 2008) and those based on the degree of separation of pores by their constriction (Homberg et al., 2012). The first technique lies in the computation of the inscribed void sphere associated to a local pore while the second technique hierarchically evaluates the degree of separation of local pores.

Without any algorithmic restriction, both techniques would produce over-merged entities similar to ducts. Then, the overlapping criterion is calibrated by the notion of neighbourhood level, while the degree of separation is strengthened by the existence of a threshold t that must be calibrated (Homberg et al., 2014).

Both approaches built on the data structures from the weighted Delaunay tessellation and the Voronoï decomposition, respectively, and provide tools to extract properties such as pore volumes and constriction sizes. The Voronoï-derived analysis associated to the pore separation technique was carried out by *Ulrike Homberg* from *Zuse Institute Berlin, Germany* and will not be presented hereafter, while the study related to the Delaunay sample analysis with the overlapping inscribed

void spheres technique belongs to the work presented herein. The conclusion of this work gave birth to an article that was published in the journal *Granular Matter* (Seblany et al., 2018). The full paper is attached in Appendix D.

In the following sections, we give a detailed definition for the overlapping inscribed void sphere technique and the associated merging criteria, and then we discuss their implications on the pore and constriction statistics of the considered material. Two generated samples (UG and GG1) are used as a data basis for this study.

3.1. Overlapping inscribed void spheres technique

Once the locations and radii of the solid spheres are known, a weighted tetrahedral tessellation of the space (Edelsbrunner and Shah, 1996) is performed using the CGAL Regular Delaunay algorithm (CGAL, 2010). Such a 3D partition provides an essential step for a spatial analysis of the packings.

The void volume included in each tetrahedron can be derived together with other characteristics including the inscribed void spheres. Accordingly, constrictions are identified on the faces of the tetrahedra. On each face, the constriction diameter is set as the largest empty circle that can be inscribed between the three particles forming the face (see Section 3.2.3 in Chapter I). These characteristics are obtained using the optimization algorithms originally developed by Reboul et al. (2008). A detailed algorithmic description can be found in Al-Raoush et al. (2003) and Reboul (2008). Therefore, the pore size distribution and the CSD can be computed by a statistical analysis over the whole sample.

However, this direct discretisation of the void space (L_0 Reboul et al. (2008)) includes some configurations where constrictions are larger than pores (constrictions formed by non-touching particles on the common face of two adjacent interlocked pores (Gao et al., 2012) (see Fig. III.5 for a 2D representation)) and other configurations where two adjacent inscribed void spheres are almost superimposed (the overlapping of these void spheres is greater than 99.9999%). Such cases correspond to tetrahedra of undesirable shapes (e.g. very flat tetrahedra with negligible volume). The constrictions resulting from these cases represent between 10% to 20% of the total number of constrictions, depending on the grading and on the density of the material. Thus, a L_0 description of the void space may include some artifacts due to the mathematical process used for the partitioning of the space. A post-processing of L_0 (Level L_0') guarantees the removal of these identified degenerated constrictions.

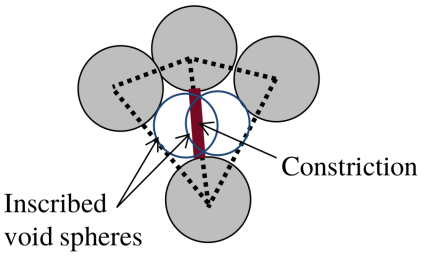

Fig. III.5. A configuration showing a constriction larger than the associated pores

Apart from these cases and as described in Chapter I (Section 3.2.6), the inscribed void spheres of two adjacent tetrahedra may greatly or just partly overlap. These cases should be then distinguished from those where the inscribed void spheres are completely separated. Indeed, such an overlapping may indicate a strong connection between these neighbouring pores justifying the non relevance of the throat statement between them as a true constriction. In that case, it would be appealing to merge these neighbouring pores.

In the case of overlapping, a merging of the corresponding adjacent pores is applied (Fig. III.6), giving birth to L_1 statistics. First, the tetrahedra derived from L_0' are sorted by increasing order of their inscribed void sphere. Then, for each tetrahedron, the overlap criterion is checked for the four adjacent tetrahedra having a common face with that one. At this stage, it should be noted that after merging two neighbouring pores, the process of merging is ended and did not go beyond the direct neighbour.

Further merging criteria belonging to L_1 are also studied. In addition to the overlap condition, these criteria (herein denoted $L_1(p\%)$, p is a defined-user threshold), evaluate the degree of separation between pores (Fig. III.6). A merging is applied when two adjacent inscribed void spheres with diameters d_{p_i} and d_{p_j} overlap each other and are connected by a constriction C_{ij} with a diameter $d_{C_{ij}} \geq (p/100).min(d_{p_i}, d_{p_j})$. The merging procedure is illustrated in 2D in Fig. III.7.

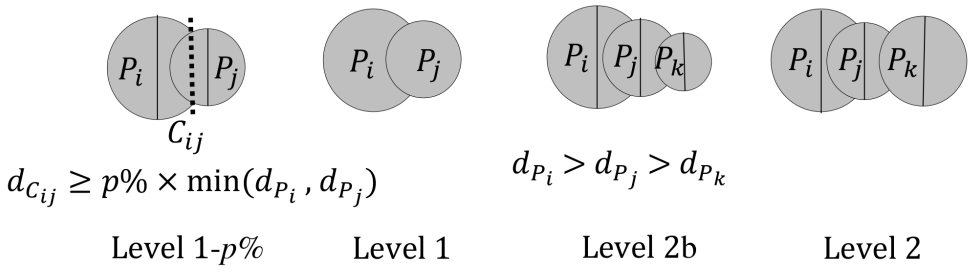

Fig. III.6. Definition of different merging criteria associated to the overlapping inscribed void spheres technique

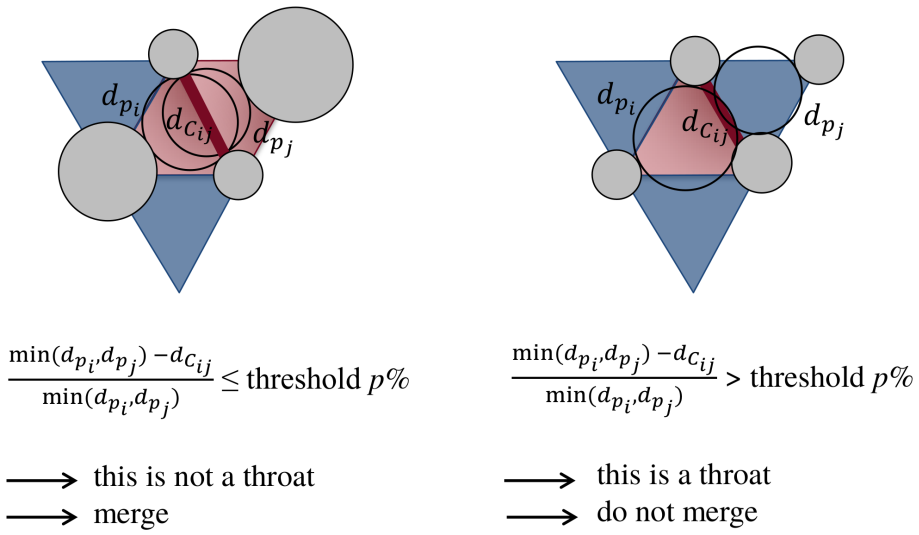

Fig. III.7. A schematic of $L_1(p\%)$ (In 2D)

L_2 and L_{2b} (Reboul et al., 2008) are also addressed where the next neighbouring local pores can also be merged with the two first ones in case of further overlap between the inscribed void spheres (Fig. III.6). No further level for merging pores is envisioned since in that case, the void space will tend to be characterized in terms of ducts.

Even if the overlapping inscribed void spheres technique seems relevant in the case of spherical packing where a partition of Delaunay can be processed, it may not be able to address the case of packing involving elongated particles which may produce more elongated pores than in a packing of spheres. In that case, by nature, few overlapping inscribed void spheres are expected to be found.

In the case of spherical packings, the proposed criteria imply that the persistence of a pore is limited in distance which can be both an advantage and a drawback. Thus, a pore can only be defined at a certain local scale involving a pore wall composed of maximum eight particles in the case of L_1 or of tens of particles in the case of L_2.

3.2. Pore distributions derived from different merging criteria

The tetrahedral cells which are mainly inscribed in the void space, will be used hereafter to evaluate the pore volumes for different merging criteria. For convenience, only L_1 and L_2 criteria will be considered in the following sections. The implication of using $L_1(p\%)$ will be discussed in Section 3.3.

As outlined previously, the pore size can be measured in terms of the largest inscribed void sphere associated to each tetrahedron but also by considering the sphere having a volume equal to that of the void within a Delaunay cell (L_0) or within merged Delaunay cells (L_1, L_2). This latter method is denoted in the following *equivalent void sphere* approach. Using these two definitions for characterizing pores, the distributions of pore sizes, for UG and GG1 materials, at loose and dense states, are plotted in Fig. III.8 and Fig. III.9 respectively. The corresponding data for the other samples are given in Appendix A.

It is interesting to note that the pore size distributions can be well described by a Log-Normal law in agreement with previous studies (Yang et al., 2006; Reboul et al., 2008). The correlation is almost perfect for L_0 (not shown herein); nevertheless, the statistical model tends to shift the mode towards larger pore diameters and to attenuate its frequency when L_1 and L_2 criteria are considered.

For UGL sample, accordingly to the work of Reboul et al. (2008) on the same grading, the distribution computed on the basis of the inscribed void spheres approach has a mode shifted towards the smaller diameters compared to the other distributions obtained by the equivalent void sphere approach, since this former approach disregards a part of the void space.

Moreover, the distribution obtained from L_1 is quite different than that corresponding to L_0, and a slight decrease in the modal value is also observed, thus showing that numerous pores around the mode in L_0 have been merged when processing L_1 merging. On the contrary, no significant difference in the equivalent pore diameter distribution is observed from L_1 to L_2 (Fig. III.8a). It tends to indicate that within the framework of this merging technique, the persistence of a pore is mainly limited to an adjacent tetrahedron for a given Delaunay cell.

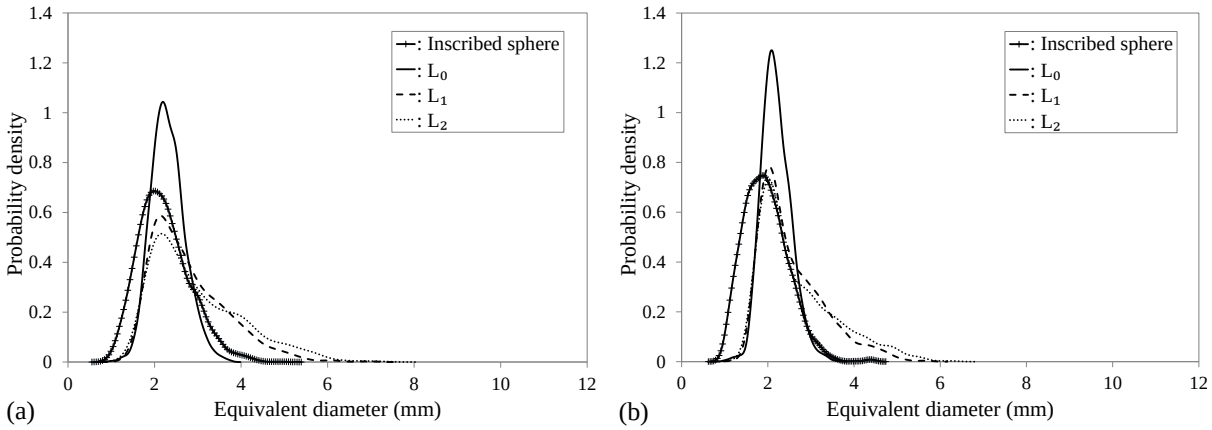

Fig. III.8. Probability density functions for the equivalent pore diameter resulting from different definitions and corresponding to the overlapping inscribed void spheres technique; (a): UGL, (b): UGD

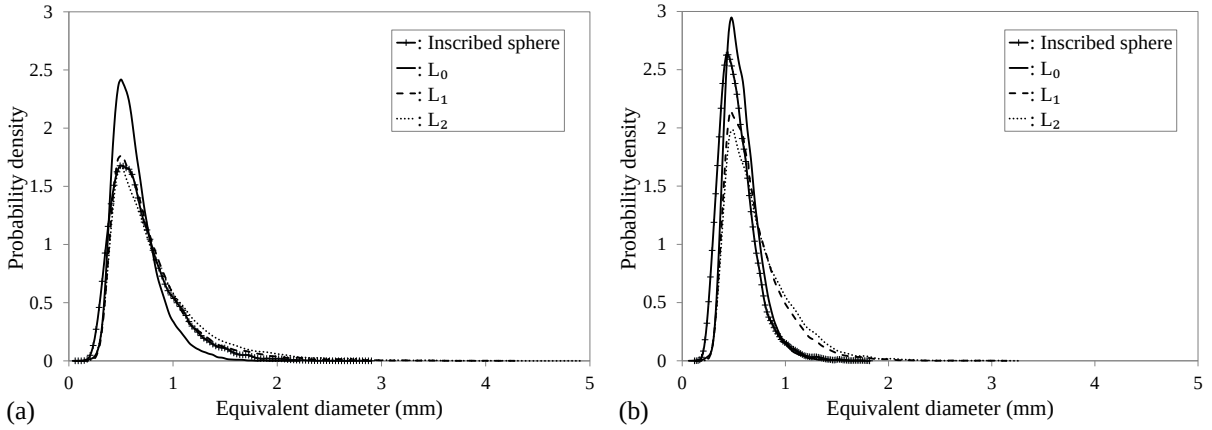

Fig. III.9. Probability density functions for the equivalent pore diameter resulting from different definitions and corresponding to the overlapping inscribed void spheres technique; (a): GG1L, (b): GG1D

For GG1L sample, the distribution and the modal value corresponding to the inscribed void sphere technique are only slightly shifted towards the smaller diameters. This may be a consequence of the wider range of particle sizes involved in this material, which tends to generate more flat tetrahedra with inscribed void spheres which are not entirely confined in these tetrahedra. Consequently, this would create the possibility of greater void spheres than in the case of UG material, the volume of which could match the volume of L_1 or L_2 distribution (Fig. III.9a). It must be noted that the other well and gap-graded materials (WG1, WG2, GG2) also exhibited this pattern (see Appendix A).

Moreover, one can note from Fig. III.8 and Fig. III.9 that the modal values for L_0, L_1 and L_2 are almost similar. Thus, the tetrahedral shape seems to be the main configuration represented within the sample, irrespective of the grading and porosity. The same findings were obtained by Reboul et al. (2008) for UGL sample.

For the densest states (Fig. III.8b and Fig. III.9b), as expected, the equivalent diameter distributions are narrower than those resulting from the loosest state (Fig. III.8a and Fig. III.9a); this is also accompanied by a decrease of the modal values. In fact, during the process of densification,

all the pores tend to reduce their volumes but the larger ones are more sensitive to this process. Indeed, arching that allows larger pores to be created in UGL and GG1L samples tends to be destroyed due to the reduction of the local friction ratio during the process of densification. The same pattern can be seen for the other three materials in Appendix A.

Fig. III.10 shows the number of Delaunay cells per pore in the case of L_1, for UG, GG1, WG2 and GG2 materials, at loose and dense states. Irrespective of the porosity and of the grading, about 50% of Delaunay cells are not affected by the merging in agreement with the results of Reboul et al. (2008) for UG material. The tetrahedral shape is then predominant, while more complex entities involving three or four tetrahedra (sharing a common face with a central tetrahedron) are poorly represented in the sample.

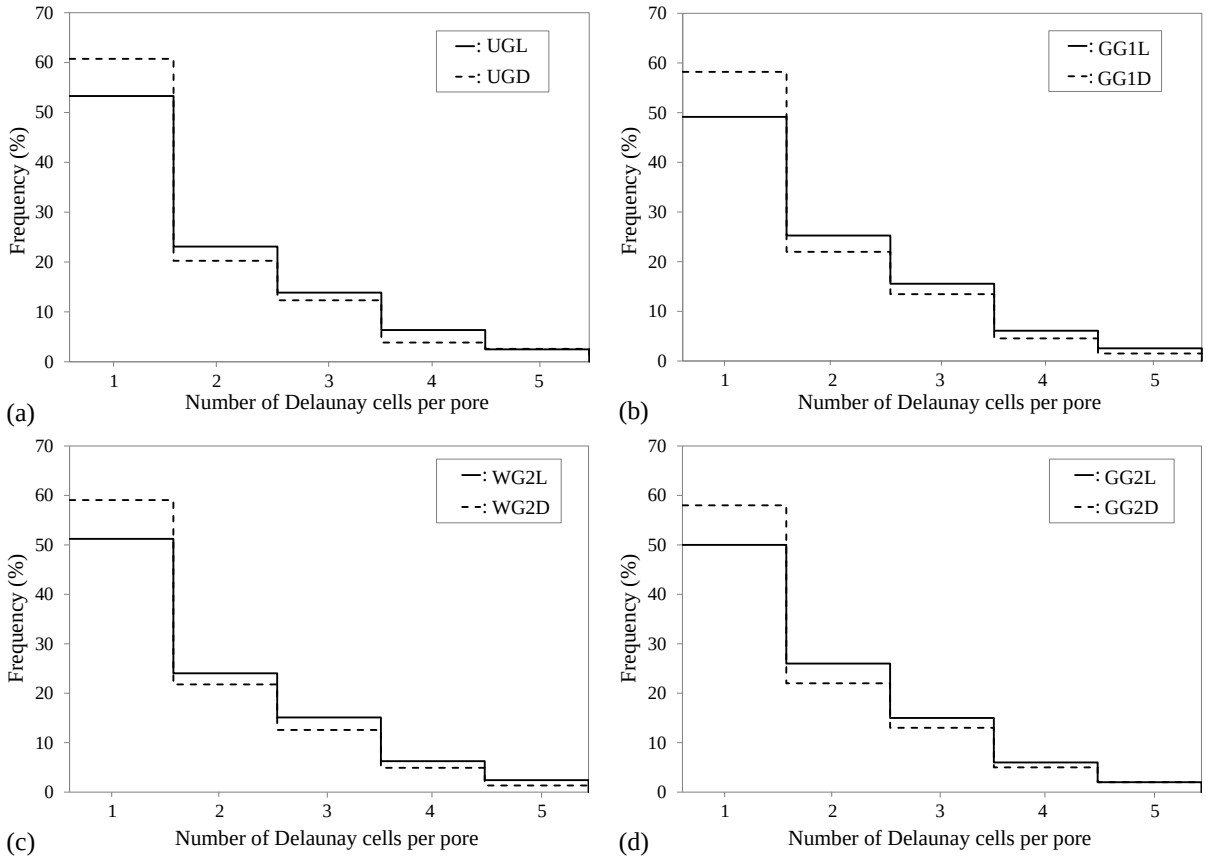

Fig. III.10. Number of Delaunay cells per pore in L_1 for loose and dense states; (a): UG, (b): GG1, (c): WG2, (d): GG2

3.3. CSD derived from different merging criteria

For the sake of simplicity, only the results corresponding to UGL, GG1L and GG2L samples are presented in this section, but similar results were also found for UGD, GG1D and GG2D samples (see Appendix B). The CSDs and the estimated probability density of constriction sizes for L_1 and L_2 merging are given in Fig. III.11, Fig. III.12 and Fig. III.13 for these loose samples. Appendix B also shows the CSDs and the estimated probability density of constriction sizes for WG1 and WG2 at loose and dense states.

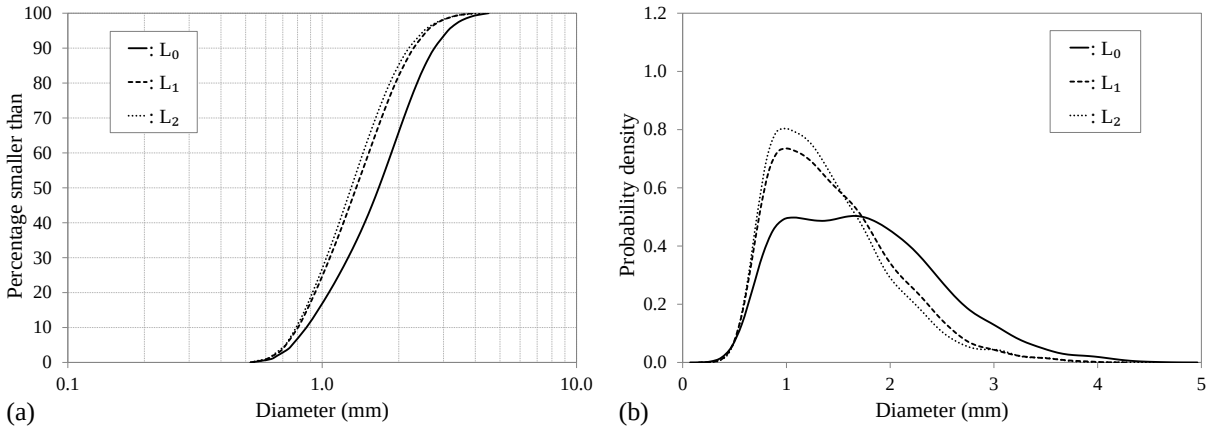

Fig. III.11. (a): CSDs for the UGL sample; (b): underlying probability density function for different merging criteria defined in the overlapping inscribed void spheres technique

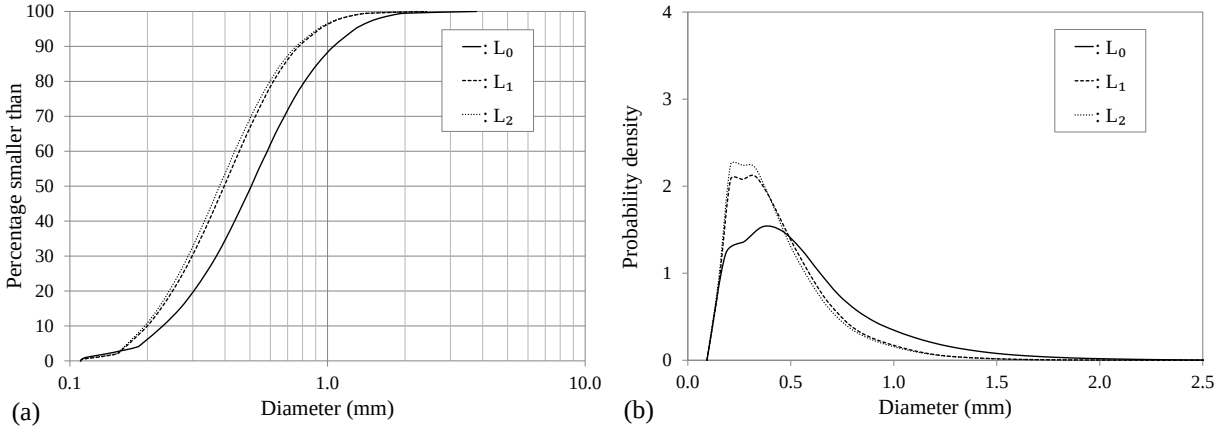

Fig. III.12. (a): CSDs for the GG1L sample; (b): underlying probability density function for different merging criteria defined in the overlapping inscribed void spheres technique

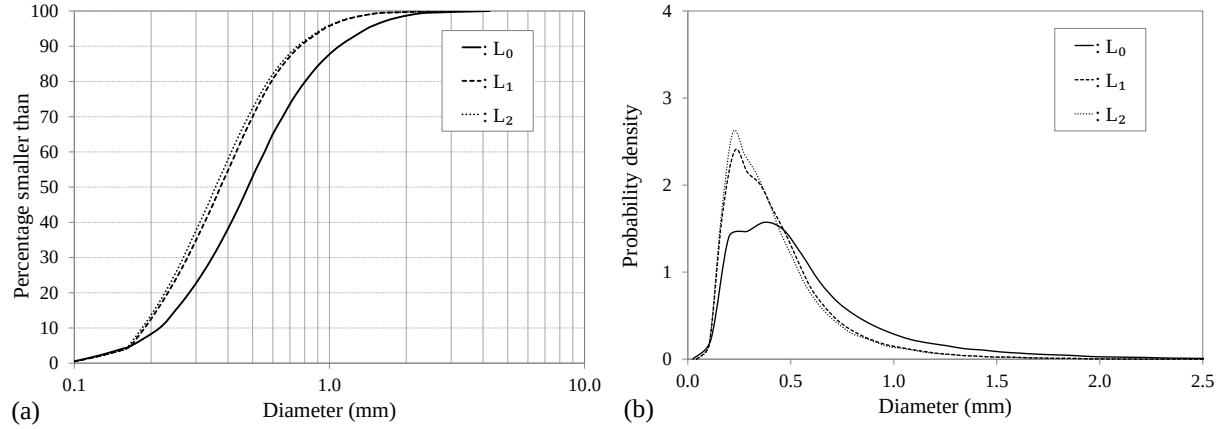

Fig. III.13. (a): CSDs for the GG2L sample; (b): underlying probability density function for different merging criteria defined in the overlapping inscribed void spheres technique

First, it has been noted that the number of constrictions decreases by more than 30% from L_0 to L_1. In fact, the initial computation (L_0) involves non negligible sets of tetrahedra with overlapping

inscribed void spheres that are merged in L_1. About half of them comes from odd configurations (that were removed in L_0' merging as described in Section 3.1), the other half comes from partly overlapping inscribed void spheres. Moreover, L_2 merging just provides few further merged pores than L_1 which means that such cases are not significantly present in the packing of spheres. Accordingly, a shift towards smaller constriction sizes is reported when comparing L_1 CSD with L_0 CSD (Fig. III.11a, Fig. III.12a and III.13a).

The evolution of the relative number of constrictions corresponding to different merging criteria belonging to L_1 (i.e. $L_1(p\%)$), for UG, GG1, WG2 and GG2 materials, at loose and dense states, is shown in Fig. III.14. It can be noted that the configurations involving a low degree of separation (more precisely $p \leq 10\%$) are well represented within the samples. Any less restrictive criterion does not provide further merging and the resulting pore-constriction structure is similar to that provided by L_1. Then, L_1 criterion generally induces the merging of highly interconnected pores. Furthermore, the decrease in the number of remaining constrictions is most significant in the case of well and gap-graded materials (Fig. III.14b-d) and at loosest state in general.

Another feature is observed in Fig. III.11b. Merging tends to let appear a clear and single mode while vanishing a second coupled mode which was also found by Reboul et al. (2008). When merging, the first mode for the constriction size almost stabilizes irrespective of the merging level (L_1, L_2). Similarly, WG1 and WG2 materials show the same trend (see Appendix B).

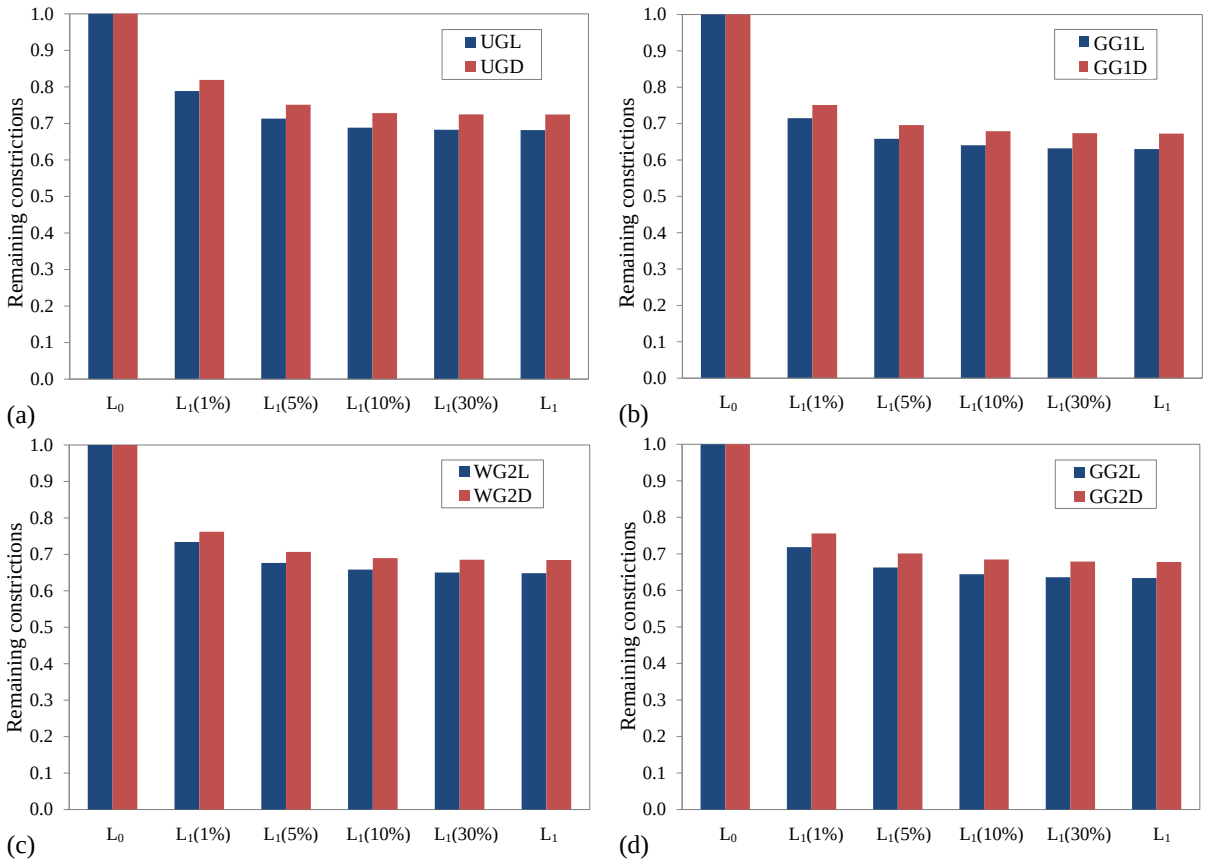

Fig. III.14. Evolution of the relative number of constrictions for different merging criteria belonging to L_1, at loose and dense states; (a): UG, (b): GG1, (c): WG2, (d): GG2

According to Yang et al. (2006), the first mode corresponds to the constriction formed by nearly contacting particles while the second one corresponds to that formed by non-touching particles. By merging interlocked pores, the constrictions formed on the common face of the tetrahedra associated to these pores are eliminated, and consequently, the first mode becomes more significant. It must be noted that the CSD, for dense packing, has a strong first mode and a rather weak second mode since, in this case, the Delaunay cells are mainly formed by touching particles (Fig. B.1b).

The same trend was also observed with the pore separation technique by *Homberg* while t is equal or smaller than 5% (Seblany et al., 2018). However, for larger threshold values, they found that the constriction size corresponding to the mode tends to shift to the smaller diameters. The reader can refer to Appendix D for further details.

For GG1L, the distribution of constriction sizes exhibits also two distinct modes. In contrast to UGL, the distribution resulting from L_1 or L_2 remains bimodal (Fig. III.12b). In such a case, the smaller mode which is approximately not affected by the merging is probably related to constrictions between fine particles in contact while the large one may include constrictions involving at least one particle of diameter greater than the gap. Therefore, the second mode which holds a physical meaning is not destroyed when merging.

However, one can note that the merging associated to GG2 material is similar to the one shown for UG material (Fig. III.13). Indeed, for gap-graded soils, the bimodal shape of the probability density function of constriction sizes is related to a significant contribution of particles larger than the gap size to the CSD. When the coarse content is sufficiently large, the possibility that such particles meet together with other finer particles to form a larger constriction size increases.

The shape of the PSD curve can also reflect this behaviour. A steep slope in the grain-size distribution of the coarse fraction together with a flat slope in the fine fraction is likely to characterize gap-graded soils showing two different modes of constriction size. The slope of the grading curve was also used to evaluate the internal stability of soils in previous studies (Wan and Fell, 2008; Chang and Zhang, 2013).

A statistical study involving different shapes of gap-graded grain size curve showed that a gap-graded material containing a significant coarse fraction (the surface area of the coarse fraction exceeds 50%) holds the same feature as GG1 material and has a two peaks CSD. Then, attention must be paid to gap-graded materials as minor differences in the shape of their particle size distribution can greatly affect the resulting CSD. In general, from the initial set of constrictions, irrespective of the grading, more than 60% of them correspond to exits of a single Delaunay cell and about 30% were removed from the statistics by the used merging criteria, which is significant.

Finally, *Homberg* found that the removal of constrictions, in the pore separation technique, is important for small thresholds ($t \leq 1\%$) irrespective of grading and density, and that the rate of removal of further constrictions tended to decrease as t increases (Seblany et al., 2018).

3.4. Conclusion

In summary, an appropriate pore merging criterion should be considered rather than L_0 for the computation of the pore size distribution and the CSD in order to guarantee the removal of non-physical aspects associated to the non-robustness of pore space partition.

The overlapping inscribed void spheres approach provides a predefined neighbourhood limit (L_1 and L_2) assuming a general maximum distance of correlation between pores and then a maximum pore size at a meso scale. This approach seems relevant for packing of spheres which may not be the case for granular materials with elongated particles since in this latter case, one expects to find elongated pores with scarce overlapping inscribed void spheres occurrences. In this case, other techniques may be available such as the pore separation technique used by *Homberg* in Seblany et al. (2018) (Appendix D).

Such a technique is more robust since it can be used for any granular material with any particle shape if a voxel representation of the material (solids and voids) is available. Moreover, it is possible to tune the value of the threshold involved in this technique to provide a result equivalent to L_1 and L_2 criteria irrespective of the considered void characteristics, pores or constrictions, the grading and the density (Seblany et al., 2018). More precisely, a threshold of about 2% (5% respectively) can be considered suitable to predict the pore and constriction size distributions corresponding to L_1 (L_2 respectively) (see Appendix D for more details). In the following, L_1 is considered sufficiently reasonable to describe the void characteristics.

4. Analytical models

Constriction size distribution is the key property to understand particle infiltration within porous media. However, the access to the constriction sizes is not easy and thus, there is a need to obtain this information using a simplified approach taking into account both the PSD and the relative density of the granular material. Accordingly, the analytical approach based on the pioneering works of Silveira (1965) and Silveira et al. (1975) is considered as a promising tool to quickly compute the CSD for any material at any relative density.

Some existing studies compared the analytical models with the results of experimental tests or numerical investigations coupling the DEM with a Delaunay tessellation (Soria et al., 1993; Locke et al., 2001; Reboul et al., 2010; Wang and Dallo, 2014; Shire and O'Sullivan, 2016). However, these models should be tested for more numerous types of grading. Furthermore, the analytical approach originally validated on the basis of L_0 computation (Reboul et al., 2010), should be re-assessed in the light of the recent findings suggesting the use of L_1 merging criterion for void space segmentation.

For this study, a Matlab routine for CSD computation (see Section 3.3 in Chapter I) has been developed. The implementation was successfully validated on an example from Raut (2006). The main steps of the CSD computational procedure are summarized in the flow chart given in Fig. III.15. For more algorithmic details, the reader may refer to Raut (2006) and Reboul (2008).

4.1. Validation of existing models

Reboul et al. (2010) compared the CSD generated with the weighted Delaunay tessellation method to the one calculated using the analytical approach (Locke et al., 2001) for UG, WG1 and GG1 materials and found that Eq. I.12 (R_d = 0%) gave a good match to the loose DEM samples. However, an error of 11% was recorded and subsequently corrected in Eq. I.13. This error may be

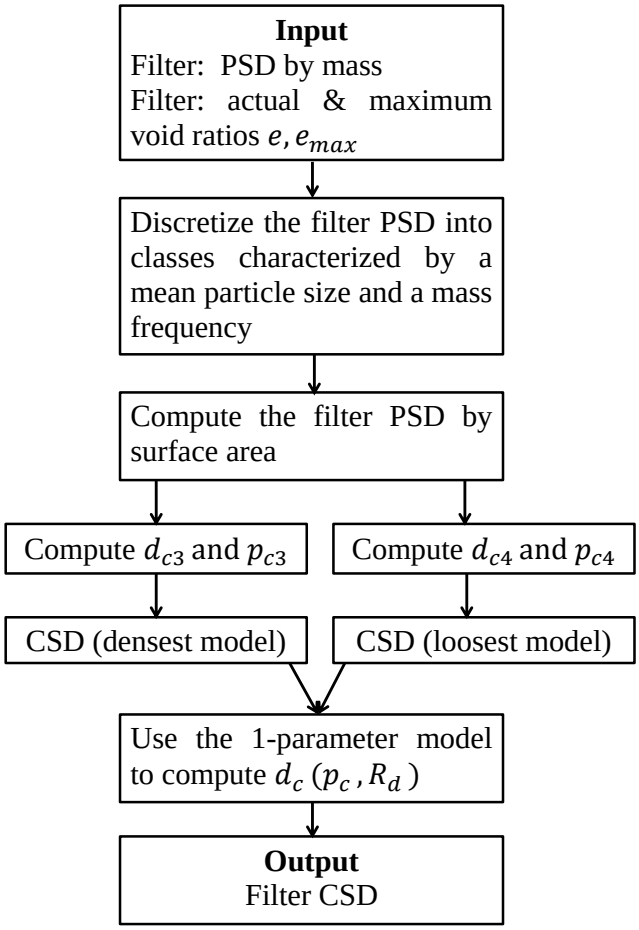

Fig. III.15. Flow chart for the CSD computational procedure

due to the imposed PSD discretization or to the use of a higher inter-particle coefficient of friction for loose samples preparation ($\mu = 0.7$) leading to a state different from the one taken into account by Locke et al. (2001).

A direct comparison of the CSD generated using the weighted Delaunay method and the analytical method *(inscribed circle method)*, for loose and dense DEM samples, was also conducted by Shire and O'Sullivan (2016) who found that the first method generates a much narrower range of CSDs than the second one. According to these authors, the divergence between these two methods become more significant as C_u increases. However, this result was expected since an isotropic compression was applied to create their loose samples which, in turn, will result in a less widely graded CSD than that obtained by a gravitational deposition.

Based on the prior study of Reboul et al. (2010), Fig. III.16 compares the CSDs obtained by means of analytical and numerical (Delaunay tessellation) approaches (L_0 computation is considered herein) for WG2 (Fig. III.16a) and GG2 (Fig. III.16b). One can refer to Appendix C to get the results for UG, WG1 and GG1 materials (Fig. C.1).

For the loosest state, Eq. I.12 (Locke et al., 2001) is considered. It can be seen from Fig. III.16 and Fig. C.1 that this equation gives a good estimate of the CSD in the loosest state for all the studied materials (the average relative error does not exceed 7%) in agreement with the results of

Locke et al. (2001).

For other densities, Reboul et al. (2010) proposed a *1-parameter model* taking into account the maximum and minimum void ratios of the material (Eq. I.14). For gap-graded materials, a more sophisticated model (*2-parameter model*) was considered (Eq. I.16). However, the lack of a rational justification for the process of identification of A and B, the constants involved in the 2-parameter model (Eq. I.16), makes this model difficult to process.

In our work, the 1-parameter model is considered sufficient since it gave a good match with the dense DEM samples irrespective of the grading (continuous or discontinuous grading) (Fig III.16 and Fig. C.1). More precisely, the mean relative error was found to be less than 7% which is reasonable (even if greater than the mean relative error of 5% found by Reboul et al. (2010) with the *2-parameter model*). Consequently, Eq. I.14 (Reboul et al., 2010) remains pertinent to model the variation of the L_0 CSD with relative density.

It must be noted that coarser particles (the sizes for which more than 90% of the particles by surface area are finer) were disregarded from the analytical calculations, since they do not really contribute to the skeleton forming the constrictions (Locke et al., 2001; Shire and O'Sullivan, 2016). Taking such particles into account will result in larger constriction sizes, which do not reflect the void space organization.

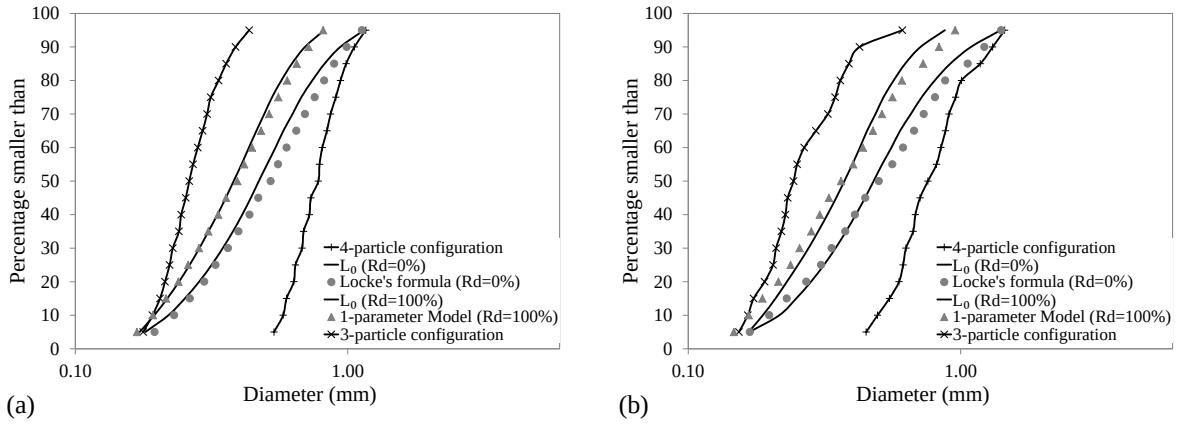

Fig. III.16. Comparison of the CSDs calculated with the analytical method and the Delaunay method (L_0 computation) for (a): WG2; (b): GG2

4.2. Improved model

The previous model is calibrated on the basis of the initial CSD resulting from a direct Delaunay triangulation (L_0). However, a CSD derived from L_1 is considered to be more representative than that derived from L_0 as it ignores non-physical values resulting from an excessive segmentation of the void space (Section 3).

When applying L_1 merging criterion, more cells are merged and fewer constrictions are considered. L_1 CSD is then shifted towards the smallest diameters irrespective of the type of grading. Indeed, larger constriction sizes are more affected by this merging, and thus, the contribution of the loosest geometrical configuration in Eq. I.12 should be corrected accordingly by multiplying d_{c4} by a coefficient of 0.72.

The updated equation (Eq. III.1) can be considered to estimate a more representative CSD (L_1 CSD).

$$d_{cL}(P_c) = (d_{c3}(P_c) + P_c(d'_{c4}(P_c) - d_{c3}(P_c))) \tag{III.1}$$

with $d'_{c4} = 0.72 d_{c4}$.

Accordingly, to compute the CSD for any relative density, the same equation proposed by Reboul et al. (2010) (Eq. III.2) can be used by replacing d_{cL} by the corresponding value calculated from Eq. III.1.

$$d_c(P_c, R_d) - d_{c_{min}} = \frac{e(R_d)}{e_{max}}(d_{cL}(P_c) - d_{c_{min}}) \tag{III.2}$$

The CSDs obtained using Eq. III.1 and Eq. III.2 are presented in Fig. III.17 for WG2 and GG2 materials. The results corresponding to the other studied materials are given in Fig. C.2 (Appendix C). The updated model accurately predicts the CSD for the five studied materials whatever the relative density (R_d=0% or R_d=100%), with an average relative error smaller than 7%. It must be noted that the updated model has also been validated for medium density states and has been shown to be a promising tool for CSD computation irrespective of the density (loose, medium or dense).

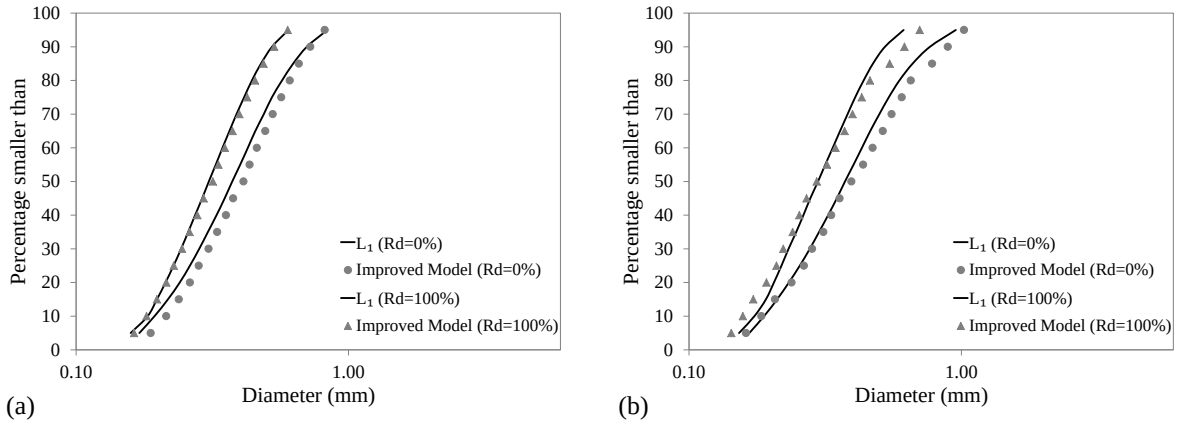

Fig. III.17. Comparison of the CSDs calculated with the improved analytical method and the Delaunay method (L_1 computation) for (a): WG2; (b): GG2

5. Characteristic length of the pore space

As previously reported, pore network-models have been developed to estimate the probable path length covered by fine particles flowing through a granular filter. For this calculation, two pieces of information are required: the constriction size distribution and the mean void spacing between two constrictions which can be associated to the mean pore diameter. The mean void spacing between two constrictions can also be associated to a characteristic length in the process of internal erosion since related to a free local movement of particles. If this movement is smaller than this quantity,

one can consider that erosion is not yet at the initiation stage.

Different assumptions have been previously made in the literature to determine this characteristic void spacing. However, they all neglect the influence of the density and very often they were not rigourously validated.

In this section, we give a brief summary of the previous estimates of the mean pore size considered in past studies, and we evaluate these assumptions by performing a statistical analysis over DEM samples. Since the characteristics of the void space including pores and constrictions are highly related to both the grading and the density of the filter, a relevant estimate for the void spacing should involve these two features.

5.1. Previous estimates

Since actual granular soils are composed of polydisperse and randomly arranged particles and since direct measurements are difficult to carry out, estimating the mean pore size is a challenging task.

Witt (1986) deduced the mean pore size by defining the mean pore volume which is equal to the porosity divided by the mean grain volume. Silveira (1965) and Soria et al. (1993) used D_{50} by mass (D_{50M}). Locke et al. (2001) proposed to take the mean diameter D_{50} by number (D_{50N}). Referring to Indraratna et al. (2007), D_{50} of the PSD by lateral surface area (D_{50SA}) is adopted.

Such values can be derived from the filter grain size distribution by mass, by number or by surface area. As previously explained, the PSD by mass may overestimate the role of coarser grains in the organization of the void space, and conversely, the PSD by number may overestimate the role of the finer particles (Humes et al., 1996). The use of the PSD by surface area can be considered as the best compromise between these two choices. However, all these estimates were proposed without a clear proof of their validity or have been validated only for the tested soils at their densest state.

Sjah and Vincens (2013) showed that the diameter of the mean void sphere inscribed within the four particles forming the tetrahedra in a Delaunay partition can give a good estimate of the mean pore size. However, their study was restricted to a uniformly graded granular filter at its loosest state and could not give a general and convenient framework for the study of actual granular materials.

To provide a better estimate of the mean pore size s, for an assembly of spheres at a given density, Wu et al. (2012) used a simplified equation based on the hypothesis of isotropy of the sample. It states that any change of the void ratio can be associated to a variation of the diameter of the mean pore size:

$$s = \sqrt[3]{\frac{e}{e_{max}}} s_{max} \tag{III.3}$$

where s_{max} is the mean pore size at the loosest state for the material and can be computed following an analytical methodology similar to the one used for the determination of the CSD (Locke et al., 2001). More precisely, it has been stated that the pores within the sample result from two main ge-

ometrical configurations: one involving eight particles (8P: cubic arrangement (Fig. III.18a)) and another one involving four particles (4P: pyramidal arrangement (Fig. III.18b)), and an estimate of s_{max} can be found by a weighted contribution of these two configurations:

$$s_{max} = P d_{p8} + (1 - P) d_{p4} \tag{III.4}$$

For simplicity, D_{50SA} is the characteristic particle size involved in this calculation. In this case, $s_{max} \approx 0.5 D_{50SA}$.

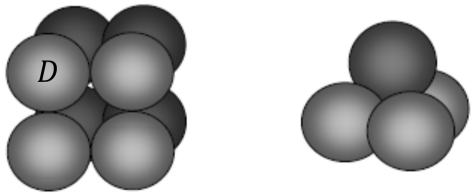

$d_{p8} = (\sqrt{3}$ -1) D $\quad$ $d_{p4} = (\sqrt{3/2}$ -1) D

(a) (b)

Fig. III.18. Geometrical configurations; (a): cubic (8P); (b): pyramidal (4P)

5.2. Influence of merging criteria

After comparing different merging criteria in Section 3, it is important to study how the choice of a certain criterion impacts the processing of the probabilistic filtration theory which assigns the coordinate of the CSD curve to the probability for a fine particle to be captured by a constriction smaller than its own size (Fig. I.5).

In the framework of the filtration theory proposed by Silveira (1965), filter constriction sizes are significantly related to the possibility of transport of base particles having a given diameter.

Stating that the pore network is organized according to a regular cubic model forming unit layers (Schuler, 1996) and that the displacement of particles is mainly unidirectional (Fig. III.19), we can associate the probability of passing one unit layer P_u with that of passing one constriction P. In that case, the average unit layer thickness s corresponds to the average distance between two confrontations.

A quick estimate of s can be given by the mean distance between centers of adjacent pores computed from the initial statistics over the entire sample (non-directional approach). When applying a merging criterion, the number of constrictions is reduced (Section 3.3), bigger pores (clusters of pores) are created and then the value of s tends to increase. Referring to Fig. III.20, a fine particle can pass from layer i-1 to layer i+2 by crossing three consecutive constrictions (left side). However, when a merging criterion is considered (right side), this particle will follow the same path by confronting only two constrictions.

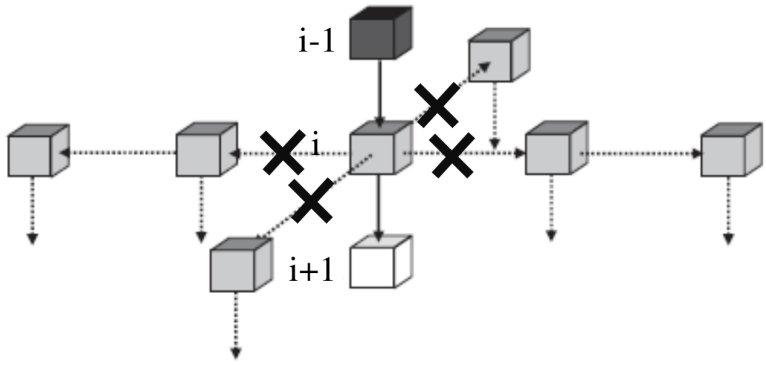

Fig. III.19. Cubic pore network allowing unidirectional displacement of particles from a pore layer to another one (plain arrow) (modified after Sjah and Vincens (2013))

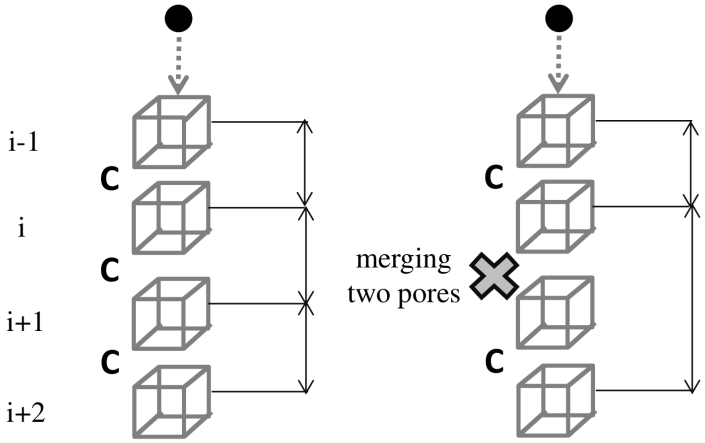

Fig. III.20. Scheme illustrating the impact of merging criteria on the mean pore spacing

Thus, each merging criterion must be associated to a consistent and corresponding average pore size. The results of this calculation are given in the second column of Table III.3 and Table III.4 for the merging criteria associated to the overlapping inscribed void spheres technique (Section 3.1) and the pore separation technique (in this case, s is obtained from the data given by *Homberg* in Seblany et al. (2018); the Voronoï approach is used herein to derive the void space properties), respectively. For this computation, only UGL sample is considered.

First, it can be seen from the second column of these tables that the estimated s corresponding to L_0 derived from Delaunay and Voronoï approaches (2.0mm compared to 1.9mm respectively) are quasi-equal while those corresponding to different merging criteria (L_1 - $t = 2\%$ and L_2 - $t = 5\%$)[1] are slightly different. This can be justified by the fact that the statistics resulting from various merging criteria (overlapping inscribed void spheres technique and pore separation technique) are not strictly identical. Moreover, the use of a specified merging criterion leads to a different value

[1]In Seblany et al. (2018), it has been shown that the pore size distribution and the CSD derived from L_1 and L_2 merging criteria correspond to the ones obtained by the separation technique if t is set to 2% and 5% respectively.

of s which can be greater than the reference s value found for L_0 by an amount of 65%, which is significant.

On the other hand, the maximum path length L_{max} for a particle of a given diameter d (e.g. 1.16mm herein), using Eq. I.2 was computed. We consider a confidence level of $P' = 95\%$ (Locke et al., 2001) and P (equal to P_u if a unidirectional pathway is stated) is obtained directly from the CSDs associated to different merging criteria (Fig. I.5). Thus, for the different merging criteria mentioned in Table III.3 (fourth and fifth columns), P is equal to 0.65 and 0.62 for L_1 and L_2 respectively. In Table III.4, P corresponds to 0.65 and 0.62 for $t = 2\%$ and $t = 5\%$ respectively.

A consistent method would imply to use the s value compatible with a merging criterion to compute L_{max}, which is not generally the case in the literature. In Table III.3 and Table III.4, one can note that if a consistent value for s is used, the maximum length L_{max} computed by the probabilistic approach is rather stable (around 21mm for the overlapping inscribed void spheres technique (see the diagonal line in Table III.3) and 19mm for the pore separation technique (see the diagonal line in Table III.4).

On the contrary, L_{max} is considerably underestimated ($L_{max} = 12.6$mm) if P value corresponding to L_2 ($P = 0.62$) is combined with s value estimated from L_0 ($s = 2$mm) in Eq. I.2 (Table III.3), which is generally done. The same holds true in the case of the pore separation technique (Table III.4). If the s value ($s = 1.9$mm) for L_0 is used together with a CSD computed with a merging threshold $t = 5\%$, the error made for the estimate of L_{max} approximates 40%.

Therefore, if one needs to estimate, in the light of the probabilistic theory, the distance traveled by a fine particle through the filter based on he CSD, attention must be paid to the choice of a consistent spacing between constrictions. The preliminary results have shown that the CSD and s must be concertedly and properly chosen, otherwise, the probabilistic method leads to significant errors for the estimate of the maximum traveled distance L_{max}.

Table III.3: The longest distance L_{max} traveled by a particle of diameter d = 1.16mm for different merging criteria defined in the overlapping inscribed void spheres technique

Merging criterion		L_{max} (mm)		
		L_0	L_1	L_2
L_0	s = 2.0mm	21.2	14.2	12.6
L_1	s = 3.0mm		20.9	18.8
L_2	s = 3.3mm			20.7

Table III.4: The longest distance L_{max} traveled by a particle of diameter d = 1.16mm for different merging criteria defined in the pore separation technique

Merging criterion		L_{max} (mm)		
		L_0	t = 2%	t = 5%
L_0	s = 1.9mm	19.8	13.2	11.9
t = 2%	s = 2.7mm		18.8	16.9
t = 5%	s = 3.0mm			18.7

5.3. Statistics over DEM samples

In order to select the best estimate for the mean pore diameter from previous proposals (Section 5.1), a reference will be chosen. We chose the mean constriction spacing which may better reflect the distance crossed by a fine particle within a mean local pore as an estimate of the mean pore diameter. Knowing the number of constrictions in each sample (herein, the overlapping inscribed void sphere technique is considered), the constriction spacing will be estimated following the methodology described in the previous section. Then, a comparison has been established with statistics over DEM samples including the mean inscribed void sphere for both loose and dense samples.

Fig. III.21 shows the mean pore size computed from different approximations normalized by the mean constriction spacing computed from DEM samples (L_0 computation) for both loose (Fig. III.21a) and dense states (Fig. III.21b). In Fig. III.21, the mean constriction spacing corresponding to L_0 is systematically equal to 1 due to the chosen normalization process. It must be noted that as C_u increases, the mean void spacing (L_0 computation) decreases (not shown herein) which is in agreement with the results found by Reboul (2008). The influence of density is less pronounced than that of the grading (not shown herein) which was also expected (Reboul, 2008).

Secondly, the proposal by Sjah and Vincens (2013) to use the mean inscribed void sphere as an estimate of the mean pore spacing seems to be validated in this study since it led to the closest value to this latter. The other ones (D_{50N}, D_{50SA}, D_{50M}) overestimate the mean pore spacing by a factor that may reach 10. This result agrees with a recent work by Taylor et al. (2018) who estimated the constriction spacing by considering the constriction density in micro-computed tomography images and DEM samples.

Finally, the formula proposed by Wu et al. (2012) (Eq. III.3) which allows the density to be taken into account, was found to be in a good agreement with the mean pore spacing from DEM samples, for both loose and dense samples.

For lower C_u values, particularly in the case of UG, the discrepancy between the mean pore size using Eq. III.3 and the mean pore spacing from DEM samples can be due to the imposed void ratio in this case. Indeed, in order to match the actual void ratio from experiments by Biarez and Hicher (1994), a lower friction value is used for generating the loosest sample (UGL) contrary to the other loosest samples. The discrepancy was found much smaller if the same friction value as for the other samples is used to create the loosest state.

As highlighted in Section 5.2, a consistent choice for the mean pore size must be associated to a given choice for the computation of the CSD, since when applying L_1 merging criterion, the number of constrictions tends to be reduced. As a consequence, the value for the mean constriction spacing tends to increase. In this case, as the number of constrictions decreases by approximately 30% from L_0 to L_1 regardless of the grading and the density state of the sample, an amplification factor of 1.4 can be suggested and applied to Eq. III.3. The new equation can be then written as follows:

$$s = 1.4 \sqrt[3]{\frac{e}{e_{max}}} s_{max} \qquad \text{(III.3}^*\text{)}$$

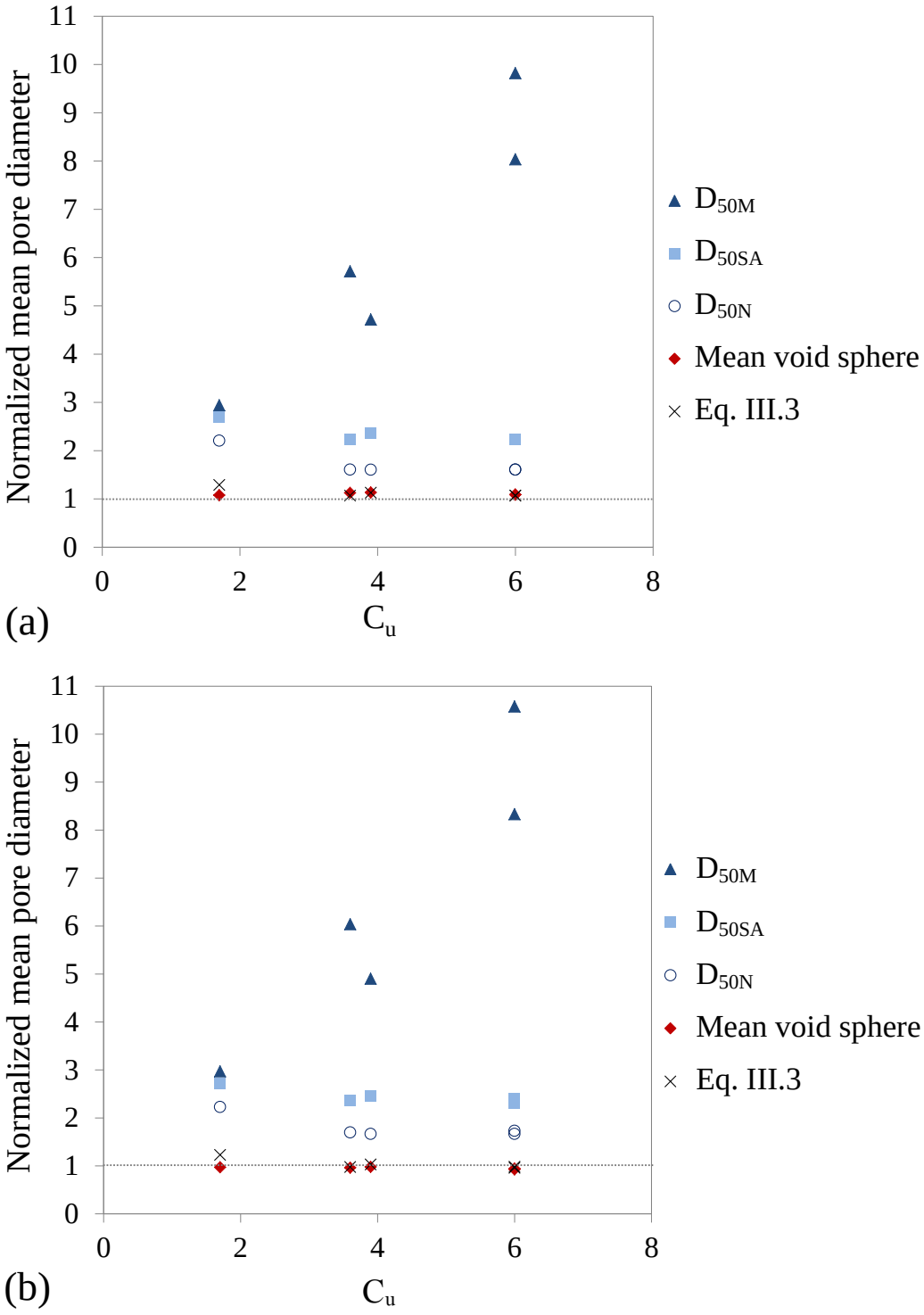

Fig. III.21. Different estimates of the mean pore spacing for (a): loose samples; (b): dense samples. All the quantities (D_{50M}, D_{50SA}, D_{50N}, mean void sphere and Eq. III.3) are normalized by the mean pore spacing based on DEM statistics (L_0)

The estimate of the mean void spacing resulting from this equation is normalized to that derived from DEM samples (L_1 computation) and shown in Fig. III.22. It seems that the new estimate is close to the mean void spacing derived from DEM data considering L_1 criterion since an estimate close to 1 was found in this case. The lesser quality of the result provided by Eq. (III.3*) in the

case of C_u smaller than 2 arises from the same reason that was previously mentioned for L_0.

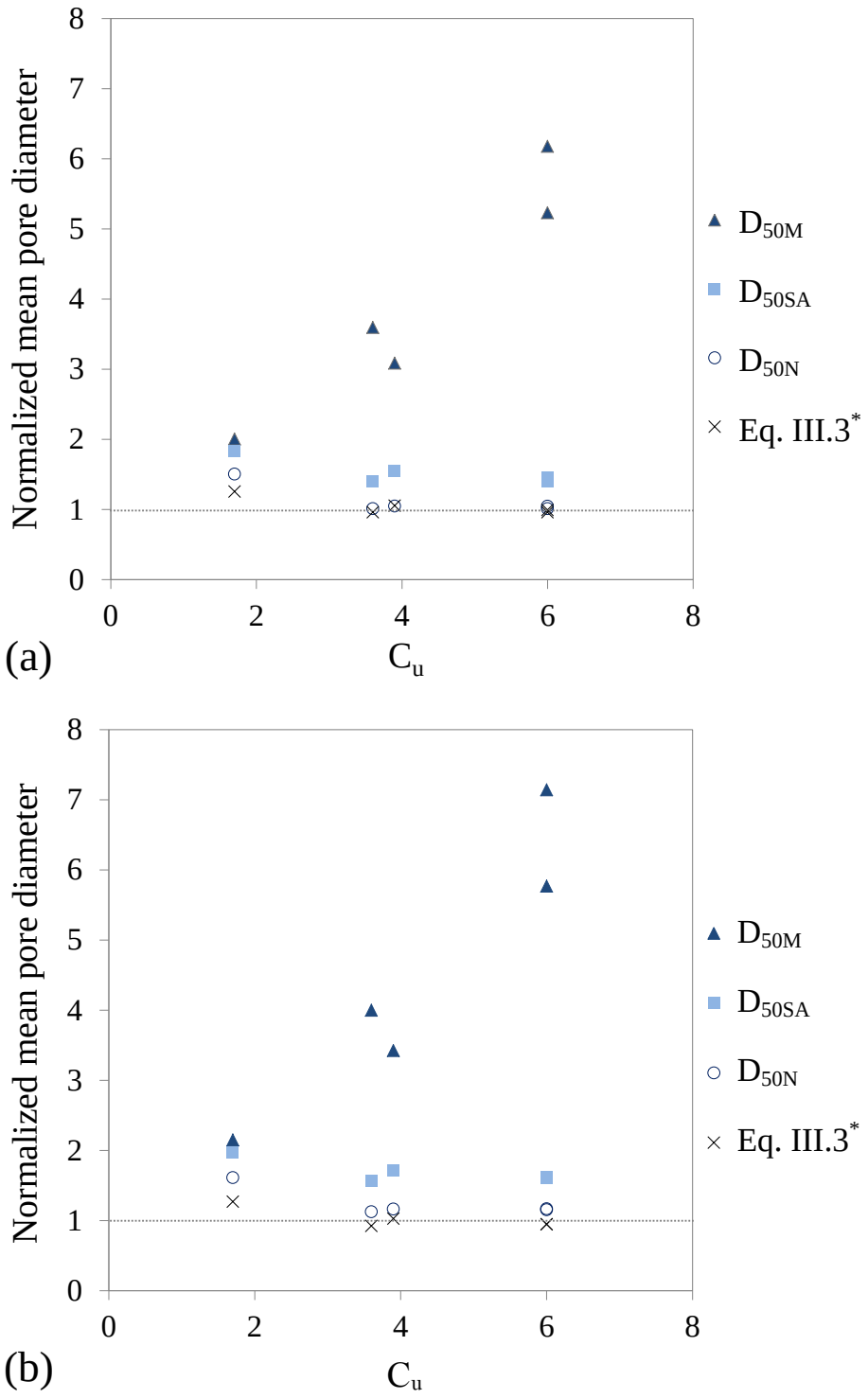

Fig. III.22. Different estimates of the mean pore spacing for (a): loose samples; (b): dense samples. All the quantities (D_{50M}, D_{50SA}, D_{50N} and Eq. III.3 *) are normalized by the mean pore spacing based on DEM statistics (L_1)

6. Conclusion

In this chapter, DEM data combined to a weighted Delaunay tessellation was used to quantify different void characteristics in packings of spheres such as the distribution of the void sphere diameter having a volume equal to that of the pore (equivalent void sphere) and that corresponding to the diameter of the largest inscribed void sphere associated to each tetrahedron, which characterizes the morphology of the void space, and the constriction size distribution (largest empty disc on the faces of tetrahedra) which characterizes its topology. Different materials were studied including uniformly graded, well-graded and gap-graded materials with different coefficient of uniformity, in a loose or in a dense state.

Since the usual weighted Delaunay partition may lead to an artificial over-segmentation of the pore space, the overlapping inscribed void spheres technique was used to merge local pores. Different criteria or levels have been defined and two criteria are mainly compared: a level 1 (L_1) where two direct neighbouring local pores are merged if their respective inscribed void spheres are overlapping, and a second level (L_2), where the next neighbouring local pores can also be merged with the two first ones to create a single pore in case of further overlapping of inscribed void spheres. It must be noted that a preliminary merging step (Level $L_0{}'$) is required to ensure the elimination of non-physical constrictions that result from geometrical artifacts and do not certainly correspond to real throats.

From a direct computation of pores and constrictions, L_1 merging induces the removal of more than 30% of constrictions irrespective of the grading and of the density. L_2 merging brings fewer new merging of local pores. Generally, merging tends to remove the larger constrictions and lets appear a clear single mode for the distributions of constriction sizes. However, in some gap-graded soils (herein, GG1 material), two close modes are obtained after merging which reveals a specific property of the studied grading.

One should keep in mind that different pore merging techniques may lead to different pore structures (different set of pore and constriction sizes) and, as a consequence, no definite poral structure can be derived for a DEM packing since the boundaries of a so-called pore is vague by nature. However, one should be conscious to the implication of using a given technique on the properties of the poral space.

The overlapping inscribed void sphere technique has its own advantages and limits: the associated merging criteria (i.e. L_1 or L_2 merging) can be considered as a reasonable procedure for defining pores at a meso scale and thus, for attaining more accurate pore network characteristics. However, this technique can only deal with spherical packings where elongated pores do not usually exist contrary to the packings composed of elongated particles.

In this latter case, the pore separation technique can be used if an appropriate threshold value is selected. In this context, a collaboration with *U. Homberg* from *Zuse Institute Berlin* allowed a correspondence between the criteria associated to both techniques to be given in Seblany et al. (2018) as a guide for the user (Appendix D).

The influence of the grading and of the density on the pore characteristics has been also analysed and the results have been found to be in a good agreement with the previous findings of Reboul et al. (2008). In addition to the uniform material studied in their work, an extended study involving a gap-graded material (GG1) has been carried out to better understand the effect of filter gradation.

On the basis of the work of Reboul et al. (2010), an analytical model was proposed to predict the CSD corresponding to L_1 merging, which allows a more reasonable representation of the pore space, compared to L_0. In addition, the results show that the 1-parameter model of Reboul et al. (2010) is precise enough to address both continuous and gap-graded materials.

Finally, an analytical approach was proposed to estimate a characteristic length of the void space: the mean pore diameter. The proposed estimate was found of very good quality irrespective of the grading and of the density of the sample.

Chapter IV

CSD-based filter criterion for spherical materials

1. Introduction

Since filters are commonly considered in earth structures design (dams, levees...) to protect base soils from erosion due to seepage, or involved in a repair aimed at stopping the development of internal erosion, a correctly designed filter must retain loose fine particles while allowing seepage to freely flow and thus preventing the build-up of high pore pressure.

Filter design criteria involving ratios of some specific grain sizes of filter and of base materials was firstly suggested by Terzaghi et al. (1996) to assess the effectiveness of uniformly graded granular soils. Subsequent studies either confirmed the validity of these criteria or extended such criteria to the study of other types of soils. However, the literature has proven that particle-based criteria exhibit serious limitations in dealing with broadly graded soils and are not adapted when the granular filter is not at its maximum density. These limitations can be overcome by an adaptive approach based on constriction size distribution rather than particle size distribution since constrictions are the main factor governing the filtration. Moreover, the density of the granular filter should be accounted for.

In this context, constriction-based criteria were proposed to describe the filter effectiveness in various types of soil (Indraratna et al., 2007). Although these criteria provide a deeper understanding of filtration mechanisms, the choice of the characteristic constriction diameter of the filter is not rationally established and requires further validation.

In the previous chapter, a detailed analysis of the pore network of granular soils, has been presented. This chapter focuses on the consequences of specific void properties on the particle transport within granular filters. The CSD will be used as a valuable parameter for a comprehensive description of filtration phenomena.

For this purpose, numerical filtration tests have been carried out to determine the equivalent sieve opening size of the filter, also denoted controlling constriction size. Indeed, particles having a diameter smaller than this size will cross large distances within the filter while particles larger than this size will be trapped somewhere in the filter. In this sense, it can be regarded as a critical

value for evaluating the filtration capacity of granular soils.

In a second part, an analytical formula is proposed to quickly estimate the equivalent sieve opening size of the filter based on some main physical properties, namely the grading and the density of the material. The proposed formula is then validated using experimental data from past studies.

Additionally, the idea of using this representative constriction size as a mean to assess the filtration capabilities of granular materials is developed. The filter opening size is then introduced in the constriction-based filter criterion of Indraratna et al. (2007). The predictions given by this criterion are then compared with a series of experimental data from the literature.

2. Dry filtration tests

2.1. Objectives and principles

The filtration capacities of the studied granular materials are checked by simulating the transport of fine particles through the coarse filters under the action of gravity (dry filtration). The numerical filtration tests aim at finding the longest filtration path covered by fine particles of a given diameter, for each grading at both its loosest and its densest states.

The minimal thickness of samples is stated to be equal to forty mean pore diameter (L_1 computation). This latter characteristic size takes into account not only the PSD of the filter but also its density. It means that the size of the reference samples are not related to a distance but to a number of confrontations with constrictions, which is more relevant.

Moreover, the proposed thickness seems to be a compromise between a too small filter thickness (and then a too short distance to travel for a fine particle through the filter) and a too large thickness. Indeed, thin filters do not trap sufficient base soil to form a stable filtration zone preventing soil erosion. On the contrary, thick filters can characterize the percolation threshold rather than the controlling size. In this sense, such filters are considered as inefficient since too many particles would be able to migrate within the filter with possible dramatic consequences upward.

This distance is supposed to let a gradual change of permeability operating within the filter due to the process of self-filtration when sufficient base soil particles enter the filter. It must be noted that the proposed filter thickness is in agreement with laboratory observations of $50D_5$ as suggested by Witt (1993) for coarse-grained filters ($D_5 > 0.5$ mm), and is much larger than the minimum filter thickness for effective filtration ($10D_{50N}$) as found by Locke et al. (2001). All these values vary in the range 30-150 mm and can serve as a preliminary guidance for the design of granular filters since a soil forms its own self-filtering zone within the initial few centimeters (Koerner and Koerner, 1992; Indraratna and Locke, 2000; Locke et al., 2001).

In the DEM numerical simulations of filtration performed in this work, filter particles are fixed while fine particles, initially at rest, are randomly positioned above the filter and then successively released in order to avoid group effects (Fig. IV.1). Only gravitational forces are considered to induce the movement of fine particles. For a conservative study of DEM filtration, the inter-particle friction is set to zero. Sari et al. (2011) showed that when the local friction between fine and coarse particles increases, the percentage of trapped fine particles increases as well. The

coefficient of restitution defined as the ratio of relative velocities after and before collision is set to 0.1 in order to prevent the rebounds of the dropped particles (Reboul, 2008).

Fine particles small enough to enter the filter can be either blocked in the material or can entirely cross the sample depending on the smallest constriction size encountered by the particle along its pathway. Fine particles that completely cross the filter are removed while particles being trapped inside the filter are kept in the sample until the end of the numerical simulation. It implies that interaction inducing the deviation of a fine particle entering in contact with another fine particle blocking a constriction, is made possible. Thus, this study does not address the true individual pathway of a fine particle which seems closer to the actual filtration process.

The number of released particles is chosen in such a way that there are no clogging problems on the top of the filter. However, a large number of fine particles must be used to explore a large number of paths and thus to increase the probability that one of the fine particles will take the longest possible filtration path. If this condition is not satisfied, an underestimation of the potential penetration depth would have altered the results.

For each sample, different filtration tests have been performed. The sizes of released particles correspond to the constriction diameters greater than the modal value of the underlying probability density (herein, L_1 is considered). It must be noted that smaller particles are released with a greater amount than that corresponding to larger particles since their pathway will be longer within the filter. Indeed, it implies that more pathways must be tested in this case. Then, for every particle size, five different releases are performed to reduce the randomness associated with the initial entry point of the fine particles within the filter. In this study, the number of fine particles varies from 200 to 4000 for each release depending on the considered base particle size.

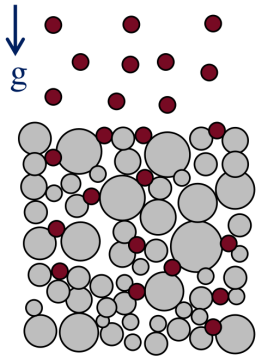

Fig. IV.1. A schematic of the the filtration process

2.2. Results and discussion

Fig. IV.2 and Fig. IV.3 show the maximum distance covered by fine particles of diameter d normalized by the thickness of the sample. In these figures, we have also included the probability density functions of constriction sizes for both L_0 and L_1.

These figures highlight the existence of a critical size under which the chance of penetration greatly increases leading particles to entirely cross the sample. Furthermore, it can be noted that the critical size from which the probability of a successful transit across the filter decreases

dramatically corresponds approximately to the mode of the constriction size distribution (L_1) independently of the grading and of the density.

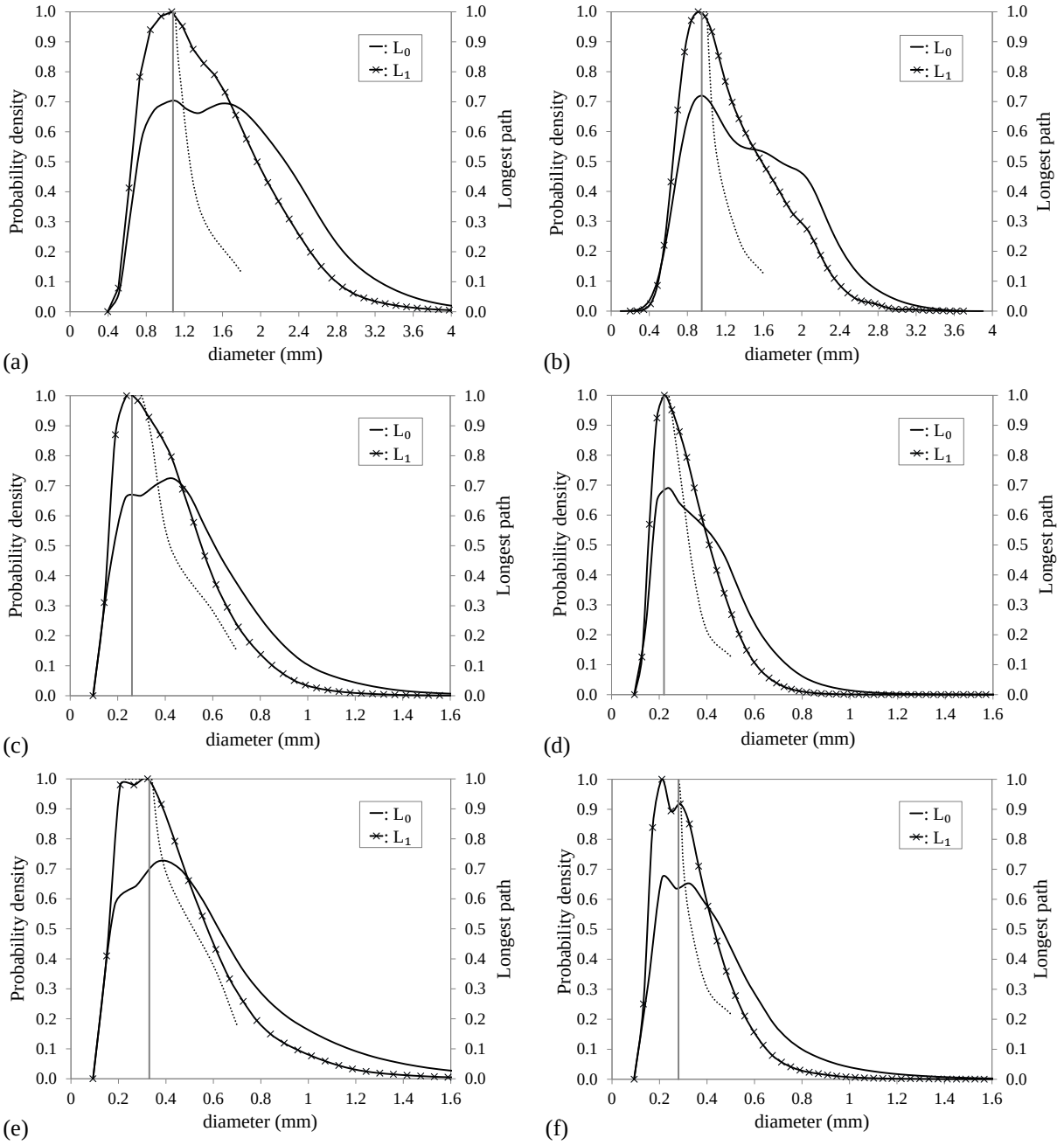

Fig. IV.2. Probability density function of constriction sizes (solid lines) depending on merging criterion L_0, L_1 and depth of penetration (dotted line) normalized by the sample thickness resulting from numerical filtration tests for: (a-b): UG, (c-d): WG1, (e-f): GG1 at loose (a-c-e) and dense (b-d-f) states. The vertical gray line identifies the largest mode of the constriction size distribution derived from merging criterion L_1

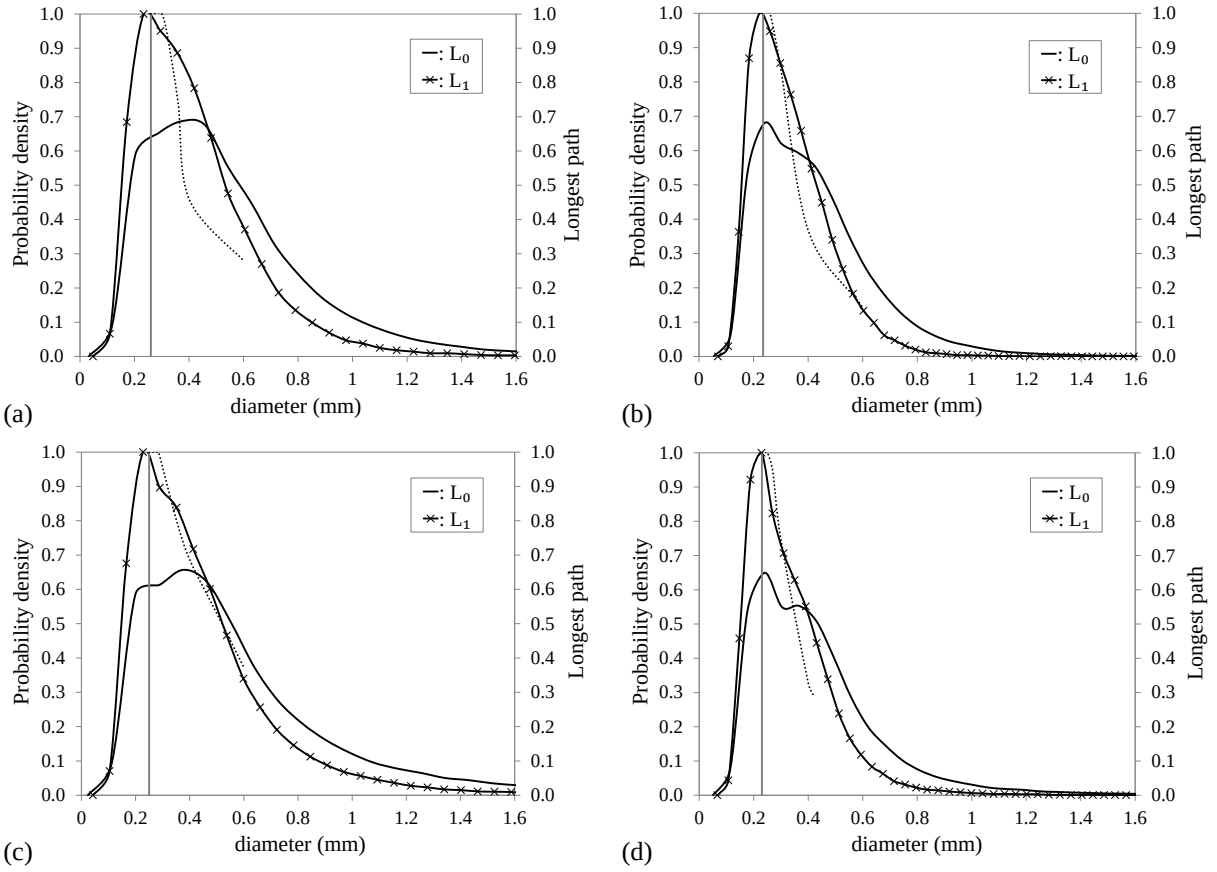

Fig. IV.3. Probability density function of constriction sizes (solid lines) depending on merging criterion L_0, L_1 and depth of penetration (dotted line) normalized by the sample thickness resulting from numerical filtration tests for: (a-b): WG2, (c-d): GG2 at loose (a-c) and dense (b-d) states. The vertical gray line identifies the largest mode of the constriction size distribution derived from merging criterion L_1

This can be explained by the fact that the mode is related to the most numerous constriction sizes within the granular material. A fine particle equal or smaller than this value will cross large distances when flowing in the filter since it will have a high chance to find constrictions equal or greater than its own size along its pathway. Conversely, a particle size larger than the modal value can be stopped more easily somewhere in the filter since it will have a higher chance to find a constriction smaller than its size in the medium.

Table IV.1 compares the critical diameters obtained by numerical filtration tests with the modal values of the constriction size distribution resulting from L_1 computation. In the case of GG1 material for which the probability density function showed two distinct modes, the largest modal value is identified as the significant mode for the filtration processes. The values for D_{c35}, the fractile 35 on the cumulative constriction curve, are also given in Table IV.1. According to the filter criterion of Indraratna et al. (2007), all particles smaller than D_{c35} cannot be retained by the filter. In their work, D_{c35} is obtained directly from the analytical model for CSD described by Locke et al. (2001).

One can note that the critical diameters are generally very close to D_{c35} but are slightly shifted from the mode towards larger sizes. This tends to discard the use of L_0 criterion to the benefit of L_1 criterion to obtain a meaningful CSD since the largest modal value corresponding to this

hierarchy is related to the filtration capabilities of the granular medium.

Furthermore, a new physical meaning can be attributed to the geometrical constriction-based criterion of Indraratna et al. (2007) supporting its use for the assessment of filter efficiency irrespective of the filter grading (either continuous or discontinuous).

Table IV.1: Comparison of the critical diameters with two characteristic constriction sizes (the modal value and D_{c35}) derived from L_1 calculation for the studied materials

Material	Loosest sample			Densest sample		
	$D_{critical}$	Mode	D_{c35}	$D_{critical}$	Mode	D_{c35}
UG	1.10	1.08	1.13	1.00	0.96	1.00
WG1	0.30	0.27	0.30	0.24	0.22	0.24
GG1	0.34	0.34	0.33	0.28	0.28	0.27
WG2	0.30	0.27	0.29	0.26	0.23	0.25
GG2	0.30	0.26	0.30	0.25	0.23	0.24

2.3. Influence of the density

The influence of the relative density on the filtration properties of a granular material can also be deduced from Fig. IV.2 and Fig. IV.3. Indeed, the number of constrictions crossed by a fine particle of a given size within a dense sample is always smaller or equal to that which can be crossed by the same particle within the loose sample. This can be explained by the fact that loose samples include larger pore and constriction sizes.

Furthermore, one can note that for the densest case, the traveled distance is more sensitive to a small variation of the fine particle size. As the density increases, the distribution of constriction sizes becomes tightened (Reboul, 2008), leading to different migration behaviour for small changes in the diameter of fine particles.

2.4. Comparison with existing controlling constriction sizes

In this section, a comparison is made between the critical diameters derived from the numerical filtration tests and the controlling constriction sizes reported in the literature.

Kenney et al. (1985) studied the retention capability of granular filters by determining analytically the controlling constriction size $D_c{}^*$. $D_c{}^*$ is defined as the size of the largest base particle that can potentially infiltrate through the filter. It can be related to the finest particle sizes by Eq. II.3 and Eq. II.4. In their work, the authors found experimentally that these relations hold true for all filters regardless of C_u value when the filter thickness is about $200D_5$.

However, these equations based on specific particle sizes of the filter (D_5, D_{15}) have limitations regarding the role of the filter relative density (R_d) and the coefficient of uniformity (C_u).

Similarly, Witt (1993) found through a probabilistic analysis of filter void sizes that as the number of confrontations with constrictions (i.e. the filter thickness) increases, the minimum throat size

$d_p{}^*$ for any path tends to stabilized, and for a depth of penetration L that can be given by:

$$d_p{}^* = 0.27D_G \qquad for \quad L \approx 50D_5 \tag{IV.1}$$

$$d_p{}^* = 0.23D_G \qquad for \quad L \approx 300D_5 \tag{IV.2}$$

D_G refers to the mean grain diameter of the soil (by number) which is ranging from D_5 to D_{10} (from D_{10} to D_{30} for very uniform filters ($C_u < 3$)).

The above equations highlight an important fact: with the increase of the thickness from $50D_5$ to $300D_5$, a small decrease in the effective opening size is observed which was expected. Another fact of interest is that if L increases beyond $300D_5$, the decrease in the minimum constriction size is negligible. This is similar to the findings reported by Kenney et al. (1985). Then, Eq. IV.1 refers to the critical particle sizes that can cross large distances within the granular filter (about $50D_5$).

Using the molten wax technique, Sherard et al. (1984) measured the minimum dimension of flow channels and found that the effective opening size was in the order of $0.18D_{15}$. Foster and Fell (2001) calculated the size of base particles transported through granular filters, and found that the larger particle size was equal to $0.20D_{15}$ while the median size was approximately equal to $0.16D_{15}$.

It must be noted that the role of the relative density is not included in these works since only dense samples ($R_d \approx 70-100\%$) were investigated. On the other hand, Kenney et al. (1985) used a multilayered constriction model to analytically determine the controlling constriction size of a filter. However, they mostly calculate the CSD based on the PSD by number, which has been criticized due to an over-representation of the finer fraction (Humes et al., 1996).

Table IV.2 compares the critical diameters obtained by numerical filtration tests with the controlling constriction sizes reported in previous studies. In a general manner, it can be seen that the critical diameters for dense samples, except the one corresponding to GG1 material, tend to be higher but are in the same order of magnitude as the controlling constriction sizes of Kenney et al. (1985) and Witt (1993) and the other stated upper bounds (not shown herein).

Indeed, this was expected since the critical diameter defined herein represents the size from which the depth of penetration of the fine particle increases rapidly to reach more than forty confrontations with constrictions. Moreover, GG1 represents a special case of gap-graded materials that was not being addressed in previous studies.

Table IV.2: Comparison of the critical diameters derived from numerical filtration tests with the controlling constriction sizes of Kenney et al. (1985) and Witt (1993)

Material	Kenney et al. (1985)		Witt (1993)		$D_{critical}$	
	$0.25D_5$	$0.20D_{15}$	$0.23D_G$	$0.27D_G$	Loose	Dense
UG	0.85	0.84	1.03	1.21	1.10	1.00
WG1	0.20	0.21	0.20	0.23	0.30	0.24
GG1	0.20	0.21	0.21	0.25	0.34	0.28
WG2	0.21	0.24	0.21	0.25	0.30	0.26
GG2	0.21	0.24	0.21	0.25	0.30	0.25

Finally, the numerical prediction of the critical diameters can be considered as in a good agreement with the effective opening size defined experimentally by Witt (1993) (Eq. IV.1).

3. Hydraulic filtration tests

Dry filtration tests have been widely used as an alternative to hydraulic filtration tests in order to simulate the migration of fine particles through granular filters in both experimental and numerical studies (Kenney et al., 1985; Kerimov et al., 2018a) since they can provide significant savings in computational time.

However, numerical or experimental procedures that do not include any hydrodynamic forces cannot totally reproduce the behaviour observed under real conditions where granular filters are subjected to hydraulic loads caused by internal and occasionally external seepage forces.

A complete analysis of the mechanical and hydraulic behaviour of particles and fluid flow can be then achieved by coupling the Discrete Element Method (DEM) for the modelling of the solid phase and the Pore-scale Finite Volume (PFV) formulation to solve the interstitial fluid flow. In the PFV framework, pore geometry and pore connections are defined locally through regular triangulation of the granular assembly, from which a tetrahedral mesh arises (Fig. IV.4). Finite volumes are tetrahedra whose vertices coincide with particle centers. This network simplifies the formulation and resolution of the flow problem. For the fluid phase, incompressible Stokes flow is considered. For more detailed information, the reader can refer to Chareyre et al. (2012), Tong et al. (2012) and Catalano et al. (2014).

In this section, we use the micro-hydromechanical model DEM-PFV implemented in *YADE*. The same kind of simulations is performed but gravitational forces are not included and replaced by a constant downward hydraulic flow. This may help to avoid any bridging phenomena and capture of particles near stagnation point induced by the gravity. Different concentrations of base soils in the seepage water and various hydraulic conditions have been tested to insure the movement of the largest possible number of particles. To deal with computation constraints, only UG and GG1 materials were involved in this study.

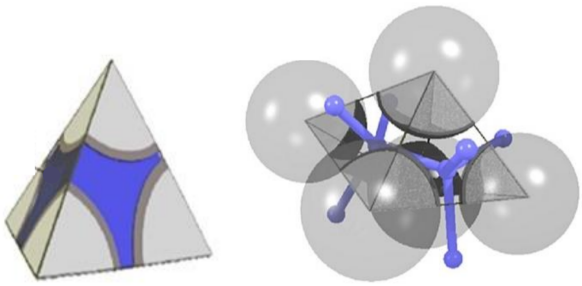

(a) (b)

Fig. IV.4. Schematic of the finite volume formulation used in the DEM-PFV method (Catalano et al., 2014) (a): volume of fluid in a pore; (b): adjacent pores and local connections

Fig. IV.5 compare the critical diameters obtained by filtration under gravity and under downward flow. The hydrodynamic condition within the filter was observed to improve particle mobility. Indeed, the largest base particles to be moved through the filters are likely to be smaller in the case of dry simulations. In this latter case, the displacement of particles is mainly unidirectional while the flow helps to reorient fine particles towards the larger paths where flow velocities are larger thereby allowing further displacement to occur. But we could not see any reason related to the anisotropy of constriction sizes orientations.

Furthermore, one can note that filtration pathways become less tortuous as density increases (Fig. IV.5b-d) since, in this case, the horizontal forces generated by the flow did not offered meaningful improvement in filtration capacity compared to the unique vertical force induced by the gravity. This is in accordance with the findings of Reboul et al. (2008) stating that dense samples exhibit more uniform properties than loose samples. Thus, if a fine particle can pass through one constriction, then it is likely to pass through the other constrictions delimiting the pore.

Besides, when the coefficient of uniformity increases (Fig. IV.5c-d), the smaller grain will fill the spaces between the larger particles leading to the clogging of some pores. The more clogged the medium, the more tortuous the filtration path.

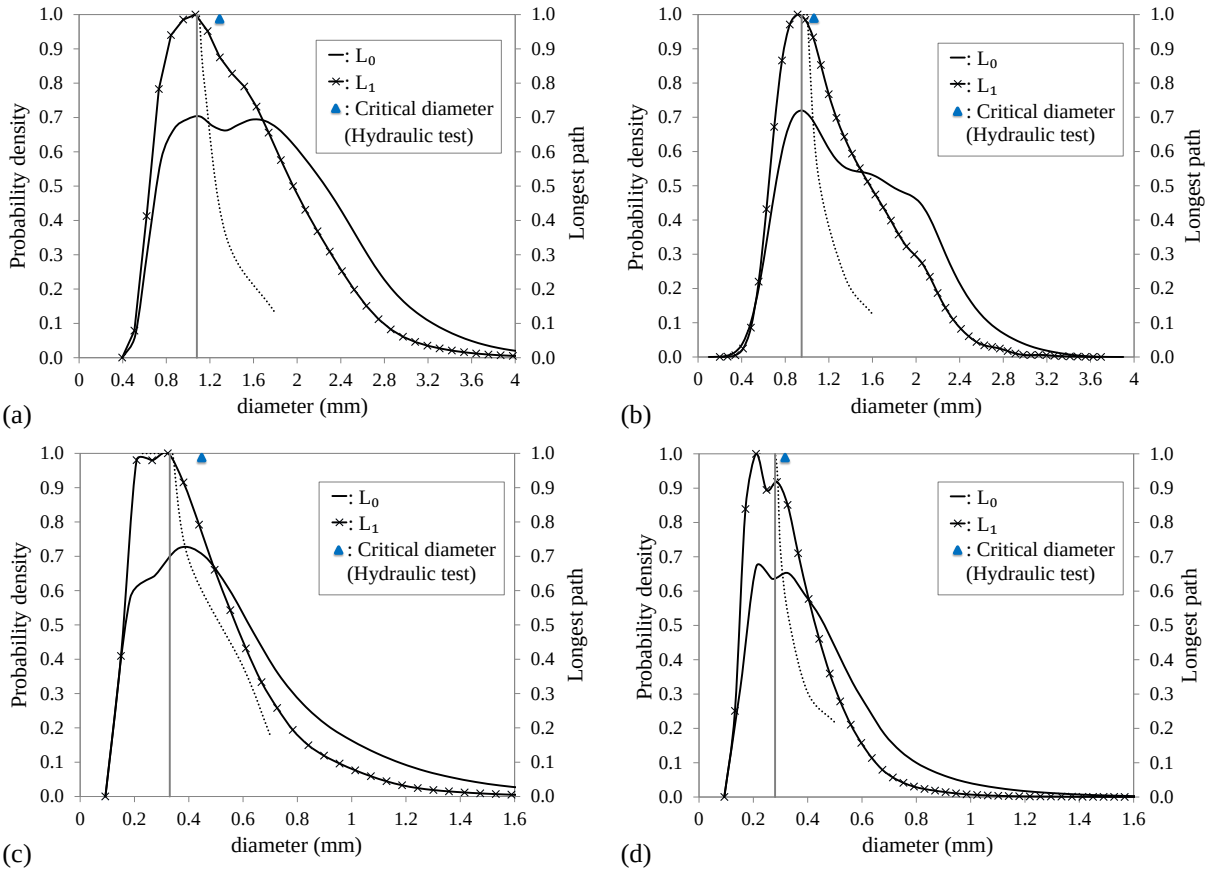

Fig. IV.5. Probability density function of constriction sizes (solid lines) depending on merging criterion L_0, L_1, depth of penetration (dotted line) normalized by the sample thickness resulting from numerical dry filtration tests and critical diameters derived from hydraulic filtration tests for: (a-b): UG, (c-d): GG1 at loose (a-c) and dense (b-d) states. The vertical gray line identifies the largest mode of the constriction size distribution derived from merging criterion L_1

Although the effect of hydraulic load cannot be neglected for a reliable filter design, one should keep in mind that the results presented herein correspond to a high hydraulic gradient (a constant gradient of 50) previously used in the experimental studies of (Sherard et al., 1984). However, the diameters of the largest particles passing through these filters are expected to be smaller than those shown in Fig. IV.5 if typical hydraulic gradients were imposed (see Table IV.3).

Table IV.3: Typical hydraulic gradients (Giroud, 1996)

Application	Typical hydraulic gradient
Ordinary dewatering trench	1
Vertical wall drain	1.5
Pavement edge drain	1
Landfill leachate collection/detection removal system	1
Landfill closure surface water collection removal system	1
Dam toe drains	2
Dam clay cores	3 to > 10
Inland channel protection	1
Shoreline protection	10
Liquid impoundment with clay liners	>10

Notes: Table developed after Giroud (1988). Critical applications may require designing for higher gradients than those given.

4. Equivalent sieve opening size

4.1. A new analytical formula

It is now clear that the CSD is a key factor for understanding the mechanisms of filtration in granular materials. Indeed, the notion of controlling constriction size was firstly introduced by Kenney et al. (1985) to evaluate the smallest constriction size that can be found along a filtration path. Sari et al. (2011) performed some numerical filtration tests and found that the finer part of the CSD curve and more precisely constrictions smaller than the mode are mainly responsible for trapping particles.

As previously outlined, the mode of the constriction size distribution can hold an important physical meaning being the most represented constriction size within the sample. Fine particles smaller than this value can easily cross the filter since the probability of finding constrictions larger than their own sizes, is significant.

Herein, the study does not focus on determining the characteristic constriction size corresponding to the mode of the distribution but rather on a value slightly larger by 5%. It implies that we take slightly into account that hydraulic forces may increase the value of the characteristic constriction size that was found closely related to the mode in dry filtration tests. Hereafter, we denote this characteristic size the equivalent sieve opening size d_{OS}.

The knowledge of this value may be useful to quickly evaluate the efficiency of a filter to retain a fine particle of a given diameter. In that way, the construction of an entire CSD curve (analytical models) is not necessarily required.

Hereafter, a quick and general estimate of the equivalent sieve opening size can be given following the method that allowed building analytical models for CSD (see Chapter I). Under this guidance, the size of the constriction formed by the densest or loosest arrangements (d_{c3} or d_{c4}) corresponds to the diameter of the circle that can fit between the three or four spherical particles of diameter D. d_{c3} and d_{c4} can be computed analytically by using Eq. IV.3 and Eq. IV.4 respectively.

$$d_{c3} = (\frac{2}{\sqrt{3}} - 1)D \tag{IV.3}$$

$$d_{c4} = (\sqrt{2} - 1)D \tag{IV.4}$$

The equivalent sieve opening size, at the loosest state, $d_{OS,L}$ associated to a cumulative probability P is eventually given by a weighted contribution of the two configurations within the sample (Locke et al., 2001) modified in order to take into account L_1 merging criterion:

$$d_{OS,L} = Pd'_{c4} + (1-P)d_{c3} \tag{IV.5}$$

For other densities, the 1-parameter model from Reboul et al. (2010) is considered sufficient for representing the CSD since it gave a good match with the dense DEM samples irrespective of the grading (continuous or discontinuous grading).

$$d_{OS}(P,e) = \frac{e}{e_{max}}(d_{OS,L}(P) - d_{c_{min}}) + d_{c_{min}} \tag{IV.6}$$

where $d_{c_{min}}$ is the minimum constriction size formed between the three smallest particles of the sample in mutual contact (Eq. IV.3).

Since smaller filter particles (D_{15} - D_{30}) are responsible for the formation of the finer fraction of the CSD curve, a trial and error process is applied to the lower range of the PSD by surface area to find the characteristic particle size that must be involved in these calculations which allows a direct determination of the equivalent sieve opening size. It was found that choosing D_{50SA} as a characteristic diameter for the grading can give a good estimate of the equivalent sieve opening size for all materials whatever their density state except for GG1 material which represents a special case of gap-graded soils. In such a case, it would be better to find the second mode of the constriction size distribution; a larger particle diameter must be then involved in the analytical calculation. In this special case, D_{55SA} can be considered as an adequate characteristic diameter of the grading.

Table IV.4 gives the values of the equivalent sieve opening size derived from the numerical distribution of constriction sizes and the calculated values obtained by using Eq. IV.5 and Eq. IV.6 for loose and dense states, respectively. The values of D_{c35} involved in the filter criterion of Indraratna et al. (2007) are also tabulated. One can note that the analytical values are very close to the numerically computed equivalent sieve opening sizes with a relative error of about 5%. The values of d_{OS} are also in the same range of those of D_{c35}.

Table IV.4: Comparison of the numerical and analytical values for the equivalent sieve opening size d_{OS} (in mm)

Material	Numerical value		D_{c35}		Analytical value	
	Loose	Dense	Loose	Dense	Loose	Dense
UG	1.13	1.01	1.13	1.00	1.20	1.07
WG1	0.28	0.23	0.30	0.24	0.28	0.23
GG1	0.36	0.29	0.33	0.27	0.36	0.28
WG2	0.28	0.24	0.29	0.25	0.29	0.23
GG2	0.27	0.24	0.30	0.24	0.28	0.23

4.2. Validation based on experimental data

Even if the numerical results showed a high accordance with the analytical estimates of the equivalent sieve opening size for the materials included in the current study (Section 4.1), the analytical procedure for computing the filter opening size must be validated using available experimental data. This section aims to compare the equivalent sieve opening size of various granular filters with other estimates provided in the literature.

The approaches that were developed to define the controlling constriction diameter are generally empirical and are based on many experimental trials (Sherard et al., 1984; Kenney et al., 1985; Witt, 1993; Foster and Fell, 2001) among other studies. Fig. IV.6 presents twelve filters (labeled from 1 to 12) used by Sherard et al. (1984) for the filtration analysis of sands and gravel materials. All these filters are compacted to high densities (R_d approaching 100%) and having a coefficient of uniformity $C_u < 3$, except filter 1 which is well-graded ($C_u > 3$).

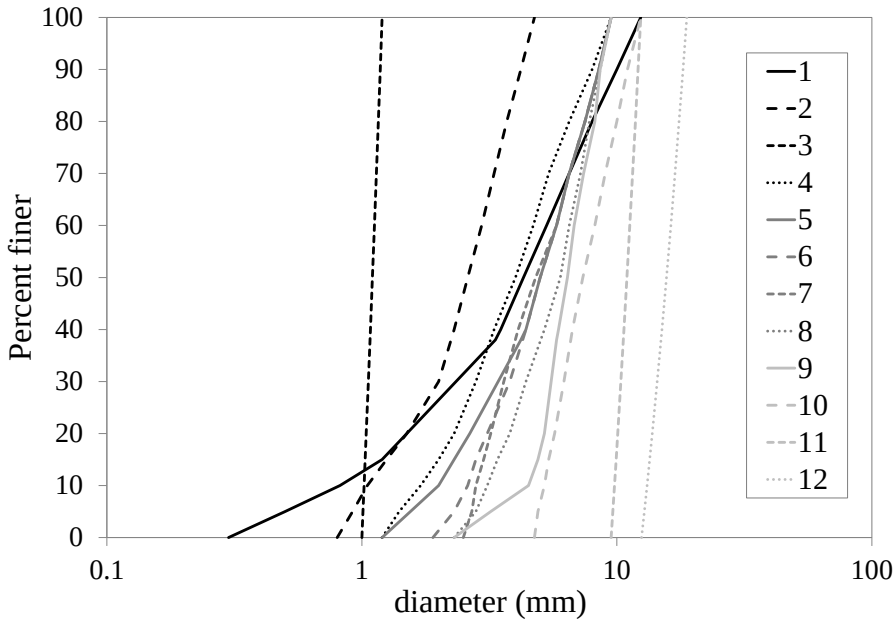

Fig. IV.6. Particle size distributions of the filters used by Sherard et al. (1984) for filtration analysis

The equivalent sieve opening sizes are then computed using Eq. IV.6 for $R_d = 100\%$. In the absence of precise measurements, the void ratios (e_{min} and e_{max}) are derived from the charts given by Biarez and Hicher (1994) based on experimental tests (rounded materials are herein assumed). A comparison is then made with the controlling constriction size reported by Sherard et al. (1984) (0.18-0.20D_{15}) as shown in Fig. IV.7.

A high correlation can be found between the analytical estimates (d_{OS}) and the experimental findings. In general, the analytical opening size are slightly shifted towards larger values but are still comparable to the controlling constriction sizes (0.20-0.25D_{15}) given in earlier studies such as Kenney et al. (1985) and Foster and Fell (2001). This was expected since the thickness of the experimental samples of Sherard et al. (1984) was smaller (about 12D_{15}) than the thickness used in this study (forty mean pore diameter).

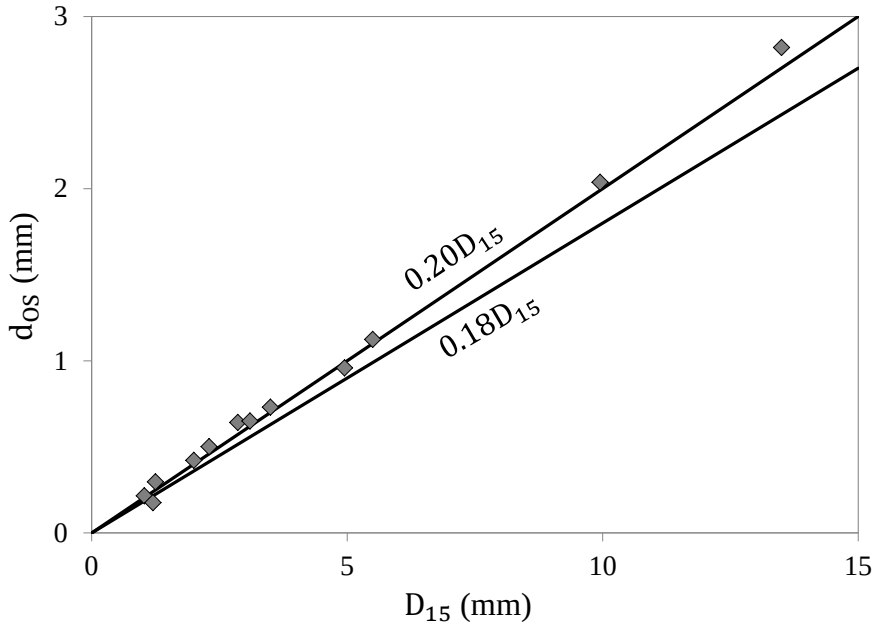

Fig. IV.7. Comparison of the equivalent sieve opening size computed analytically with the controlling constriction size provided by Sherard et al. (1984)

5. A new constriction-based criterion

Empirical filter design criteria initially developed by Terzaghi et al. (1996) have been widely used for assessing granular filter performance. However, these conventional retention criteria basically involves the PSDs of the base soil and the filter while neglecting the effects of the density and of the coefficient of uniformity (C_u).

In view of these limitations, constriction-based criteria have been introduced with D_{c35} and D_{c95} defining the controlling constriction size and the self-filtering constriction size respectively (Indraratna and Raut, 2006; Indraratna et al., 2007). These criteria have the advantage of being more comprehensive than the PSD-based criteria since they take into account the effects of density and C_u.

However, measuring the controlling constriction size is not as easy as appointing D_{15}. Constriction-based criteria were initially founded on the definition of the CSD curve. In their works, Indraratna and Raut (2006) and Indraratna et al. (2007) generate the CSD curve from which D_{c35} and D_{c95} can be determined by using the analytical model of Locke et al. (2001) that takes into account both the role of the PSD and that of the density (Eq. I.12). Their criteria have been validated on the basis of a large experimental data set involving highly compacted filters.

As revealed earlier in Chapter I (Section 3.3.4), the model of Locke et al. (2001) is not recommended since it assumes that only the densest configuration exists at higher densities which has proven to be incorrect (Reboul et al., 2008). Thus, the model is expected to loose its validity as the filter density increases.

Beside this main drawback, the analytical model of Locke et al. (2001) has been validated based on the results of two experiments for CSD computation: the base suspension method of Soria et al. (1993) and the replica technique of Wittmann (1979) (Chapter I). Both experiments have their own limitations associated to the assumption of the mean void spacing in the case of the first method and the representativeness of the sample in the case of the second experiment. Both these aspects may alter the quality of the validation.

To overcome these limitations, Reboul et al. (2010) proposed another model calibrated on the basis of statistical analyses over DEM samples. However, their numerical study ignores the effects of the over-segmentation of the void space introduced by the Delaunay tessellation which can lead to errors in the CSD computation.

Thus, analytical models need some enhancements to accurately predict the CSD curve. In this work, efforts have been made to adapt the analytical CSD to the numerically derived CSD for spherical packings (see Section 4.2 in Chapter III).

Although analytical models allow to estimate the full CSD curve based on simplified estimates of the particle sizes and their arrangements within the sample, the results may be dependent on the way the discretization of the PSD into classes is performed. A new formula (Eq. IV.6) is then proposed to rapidly calculate the effective opening size of a granular filter which can be subsequently involved in constriction-based criteria. The proposed estimate has been found to closely match the opening size obtained from both numerical and experimental filtration tests for different filters at their loose and dense states.

For base soils, d_{85} has generally been used as a representative size in conventional filter design criteria. As explained in Chapter I (Section 3.3), filters can be best modeled by the PSD based on surface area of particles. By analogy, base soils are expected to be modeled more adequately by the PSD based on surface area.

Indraratna et al. (2007) demonstrated that base soils having the same d_{85} by mass but different C_u values are not expected to be filtered in the same way through a mechanical sieve having an aperture equal to d_{85}. It means that the filtered mass will be different in each case for the same total initial mass of material. More precisely, the total amount of the retained particles will be reduced as the uniformity coefficient C_u increases. This is the reason for the non-effectiveness of common filter criteria especially for non uniform base soils.

Furthermore, large particles in broadly graded base soils have generally a non significant representation in the PSD_{SA} and thus do not influence the self-filtration phenomenon (Lafleur, 1984;

Indraratna et al., 2007). As a result, d_{85SA} is considered an acceptable representative size for base soils since it corresponds to smaller sizes as C_u increases.

Based on all these considerations, the constriction-based criterion proposed by Indraratna et al. (2007) (Eq. II.6) may continue to be used as a comprehensive criterion for evaluating the efficiency of granular filters if D_{c35} is appropriately computed. For the sake of simplicity, the equivalent sieve opening size calculated from Eq. IV.6 can substitute D_{c35} in Eq. II.6 leading to the following criterion.

$$d_{85SA} \geq d_{OS} \tag{IV.7}$$

5.1. Verification of the criterion based on experimental data

The proposed criterion implying a new definition for the filter opening size must be validated experimentally with the support of available database prior to its adoption into filter design practices. Hereafter, a comparison is made between the enhanced criterion results and available filtration tests results from previous studies.

A series of filtration tests involving a uniform base soil (lateritic) and three uniform and moderately compacted sand filters (coarse, medium, fine; $R_d = 100\%$) have been carried out by Indraratna et al. (1996). The PSDs of these filters are given in Fig. IV.8. Similarly, Fig. IV.9 presents the PSDs of two parallel graded filters (F1 and F2) corresponding to a medium-grained sand and a river gravel respectively (data taken from Indraratna and Vafai (1997)). The relative density of these filters was assumed to be 90%.

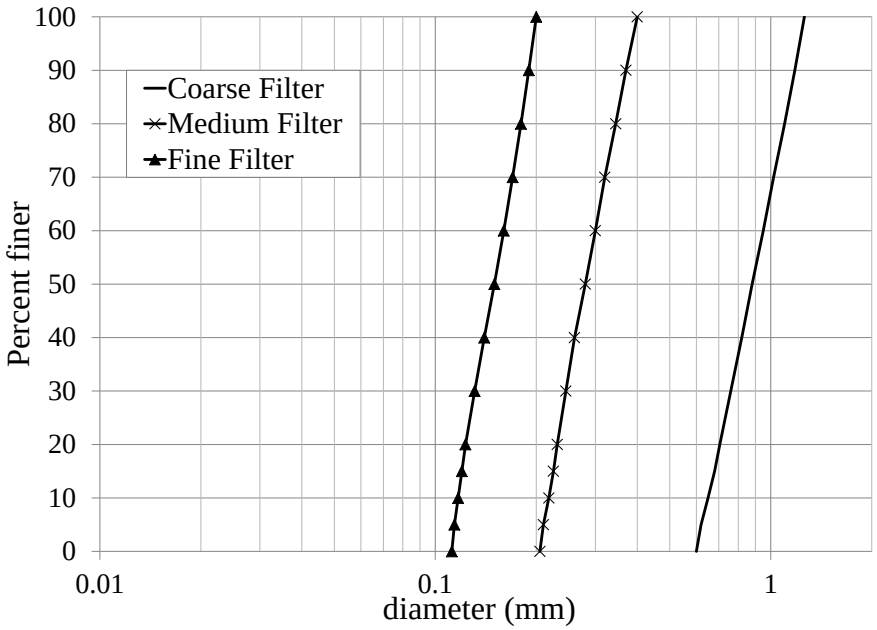

Fig. IV.8. PSDs of three uniform filters from Indraratna et al. (1996)

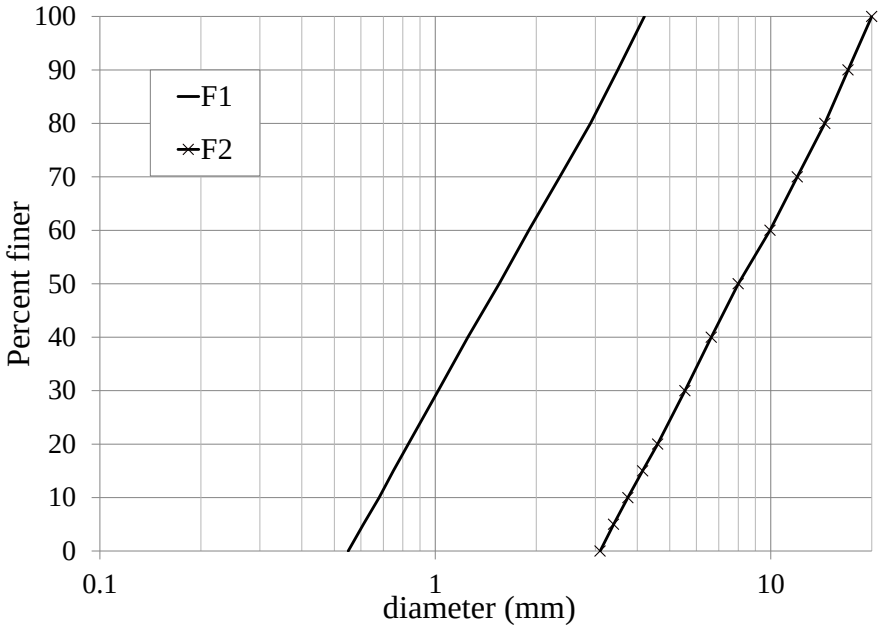

Fig. IV.9. PSDs of two moderately graded filters (Indraratna and Vafai, 1997)

Two well-graded filters (F-1 and F-5; $R_d = 70\%$) from Lafleur filtration tests (Lafleur, 1984) have been also considered in this comparative study. Fig. IV.10 depicts the corresponding PSD curves. Other data taken from recent experimental studies conducted by Indraratna et al. (2007) and involving very uniform sand filters (F4, F5 and F6) having a parallel gradation and a relative density less than 70%, can be shown in Fig. IV.11.

First, the equivalent sieve opening sizes of all these filters are computed and presented against D_{15} in Fig. IV.12. R_d is herein selected as the experimental value. The equivalent sieve opening sizes of the filters investigated in the current study are also shown. It can be noted that, for higher density states, the analytical calculations agree with the controlling constriction sizes (D_{15}/4 or 5) given in past studies (Kenney et al., 1985; Sherard and Dunnigan, 1989; Terzaghi et al., 1996). However, different d_{OS} values can be obtained at different compaction levels. One should expect higher values of d_{OS} at low densities. This correlation is then sensitive to the degree of compaction which has not been taken into account previously.

Furthermore, the opening size for broadly graded filters having a C_u larger than 6 (F1 from Sherard et al. (1984) and F-1 from Lafleur (1984)) shows a slightly inaccurate fit with the empirical values (d_{OS} larger than D_{15}/4-5). This was expected since the commonly used filter criteria were proven to have obvious limitations particularly with broadly graded filters and base soils.

On the other hand, Table IV.5 compares both the PSD-based criterion and the CSD-based criterion involving d_{OS} with experimental observations. First, one can note that the commonly used PSD-based criteria ($D_{15}/d_{85} < 4$ or 5) fail to distinguish effective filters from ineffective filters especially for well-graded filters (F-5 from Lafleur (1984)).

On the contrary, the predictions given by the CSD-based criterion ($d_{OS}/d_{85SA} < 1$) are in accordance with the experimental results for all filters except for two uniform filters (F6 and the medium filter) where D_{c35} is slightly larger than d_{85SA} (bold values). Such filters are classified herein as ineffective while experimental tests have shown their efficiency. According to Indraratna et al.

(1996), the self-filtration process will take place more rapidly in the case of uniform fine sand filters compared to uniform medium sand filters, possibly leading to this discrepancy. However, these filters are expected to be more effective at higher densities.

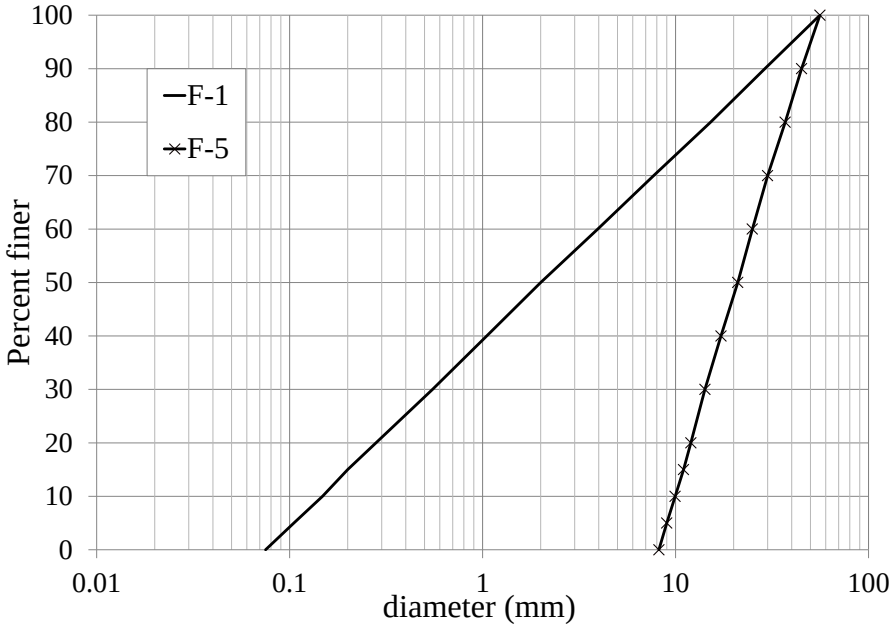

Fig. IV.10. PSDs of the well-graded filters used by Lafleur (1984) for filtration analysis

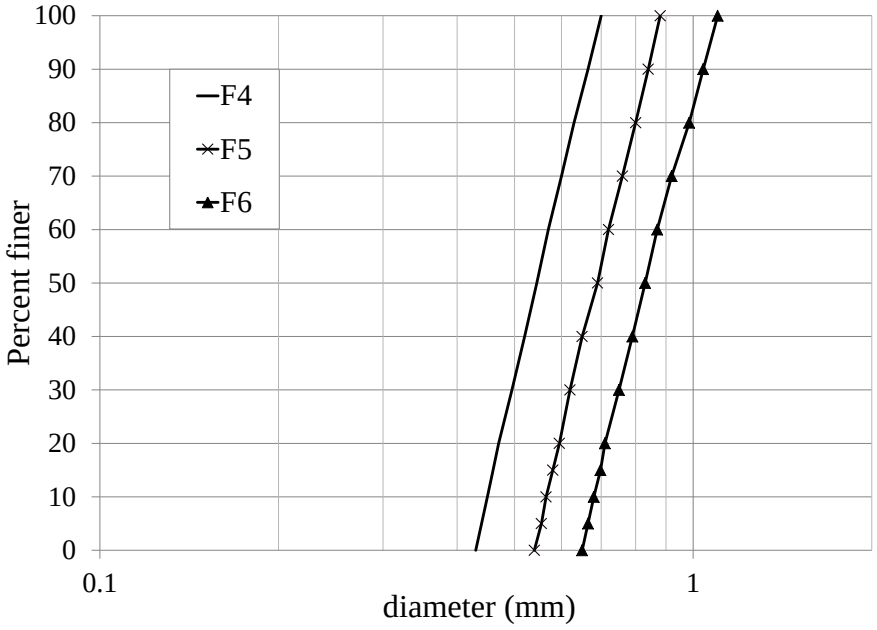

Fig. IV.11. PSDs of uniform filters taken from the experimental study of Indraratna et al. (2007)

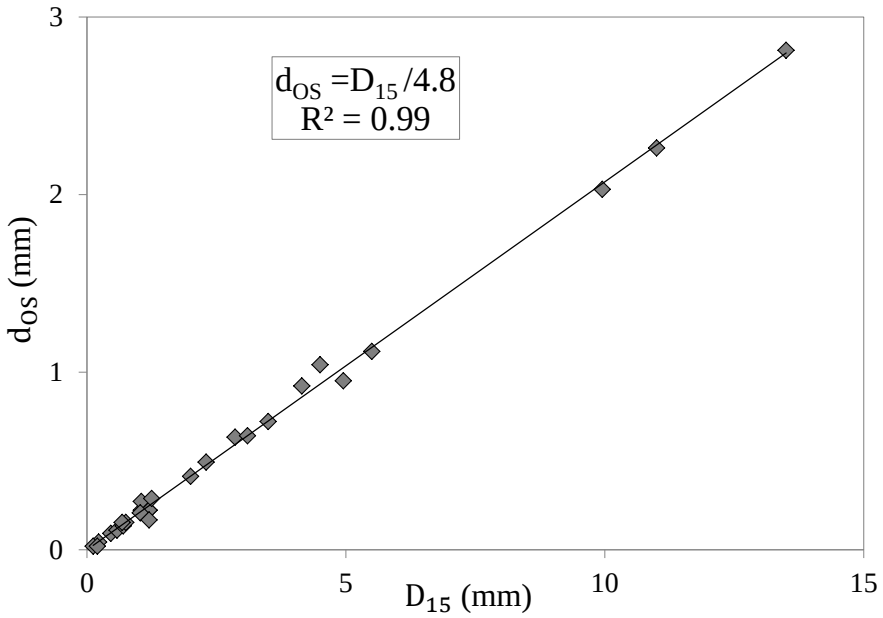

Fig. IV.12. Relation between the equivalent sieve opening size d_{OS} and the representative size D_{15} for various filters

Table IV.5: Comparison of the PSD-based criterion of Terzaghi et al. (1996) and the proposed CSD-based criterion with laboratory results taken from past studies

Filter	R_d (%)	C_u	D_{15} (mm)	D_{15}/d_{85}	d_{OS} (mm)	d_{OS}/d_{85SA}	Laboratory assessment
Very uniform base soils (fine sand) and filters (Indraratna et al., 2007):							
F4	70	1.3	0.46	3.96	0.10	0.85	Effective
F5	70	1.3	0.58	5.0	0.12	1.00	Effective
F6	70	1.3	0.70	6.0	0.14	**1.19**	**Effective**
Uniform base soils (lateritic) and filters (Indraratna et al., 1996):							
Coarse Filter	50	1.5	0.68	15.45	0.16	3.85	Ineffective
Medium Filter	50	1.4	0.23	5.14	0.05	**1.21**	**Effective**
Fine Filter	50	1.3	0.12	2.72	0.03	0.67	Effective
Moderately graded base soils and filters (Indraratna and Vafai, 1997):							
F1	90	2.8	0.75	1.78	0.16	0.54	Effective
F2	90	2.8	4.15	9.90	0.91	3.02	Ineffective
Well-graded base soils and filters (Lafleur, 1984):							
F-1	70	26.7	0.20	0.03	0.03	0.17	Effective
F-5	70	2.4	11.0	1.60	2.27	14.28	Ineffective

Moreover, the new predictions improve the results found earlier by Indraratna et al. (2007). Indeed, their criterion involving D_{c35} (obtained from the analytical model of Locke et al. (2001)) classified F5 as ineffective contrary to the experimental observations. Herein, F5 is considered to be effective since d_{OS} is equal to d_{85SA}. For F6 and medium filters, the same result has been

found by Indraratna et al. (2007), but the ratios (D_{c35}/d_{85SA}) were larger than d_{OS}/d_{85SA}. Thus, the constriction-based criterion herein modified seems to be reasonably satisfactory.

6. Conclusion

The transport of fine particles in granular media is mainly controlled by the constriction sizes encountered along their paths. The numerical filtration study presented in this chapter showed a rapid increase in the penetration depth within the filter, starting from a given critical particle size. Moreover, and whatever the grading and the density, a close relationship has been established between the potentiality for migration of fine particles and the largest mode of the constriction size distribution derived from L_1 computation which tends to confirm the validity of the chosen merging criterion.

Furthermore, a comparative analysis involving the critical diameter derived from the numerical filtration tests and the controlling constriction size obtained from past investigations, indicates a close agreement with the effective opening size of Witt (1993) as well as with D_{c35} highlighted in the work of Indraratna et al. (2007).

This result tends to support the use of this characteristic constriction size in filter design criteria as proposed by these latter authors since it discriminates fine particles able to travel large distances through the filter from those that will be trapped after a rather short distance.

However, to provide a quick estimate of the equivalent sieve opening size, an analytical formula was proposed. The calibration has been performed by means of statistics over DEM samples involving different materials at their loosest and densest state. The results of the analytical estimate have been found to be consistent with findings from past investigations.

Finally, a filter criterion based on this equivalent sieve opening size has been tested with a series of published experimental data. The predictions have been found to agree satisfactorily with experimental observations, thus supporting the efficiency of the proposed CSD-based criterion. However, further experimental investigations are needed to confirm this earlier conclusion.

Summary, conclusions and perspective

1. General Summary

Earthen dams and levees are prone to progressive failure due to internal erosion induced by seepage forces. Internal erosion refers to the migration of fine particles through the voids of a granular soil under seepage flow. With the loss of fine particles, local cavities and differential settlements may occur leading to possible instabilities and even to the creation of a breach in severe cases.

To avoid serious incidents, adequate filter materials must be provided in zoned dams or on the downstream slope of levees. Indeed, a filter must be sufficiently fine to perform the retention function and control the migration of fine particles caused by internal erosion. At the same time, it must have adequate permeability to drain seepage water.

However, designing a suitable filter is a complex task, requiring the attention to geometrical, physical, chemical and hydraulic factors among others. This research study focused on the geometrical criterion.

In this regard, a filter is usually designed in terms of the particle size distribution (PSD) of both base soil and filter materials. The famous Terzaghi's filter criterion, $D_{15}/d_{85} \leq 4$ (Terzaghi et al., 1996), initially developed on the basis of laboratory results on uniform cohesionless soils, leads to unsafe filter designs when applied to well-graded soils. However, current design practices are still based on these empirical criteria and thus, exhibit some limitations.

There are also some established criteria relating filter permeability to the PSD of the base soil. However, the migration of fine particles through a filter material is related to the pore connectivity. In particular, constrictions which are the narrowest channels between pores, represent the key characteristic of granular filters.

Following this reasoning, constriction-based criteria were introduced instead of either the PSD or the permeability criteria. The limitations associated with common filter criteria such as the effects of the density and the uniformity coefficient of soils, can be removed.

The filter criterion suggested by Indraratna et al. (2007), $d_{85SA} \geq D_{c35}$, compares the controlling constriction size, D_{c35} (the constriction size for which 35% of the constrictions of the granular assembly are finer than this size) with the specific representative base size, d_{85SA} (85% finer in the PSD by surface area of the base material). It is important to note that the assumption of D_{c35} was not clearly justified. For this reason, the physical meaning of this constriction-based criterion was questionable.

A better assessment of filtration performance requires an accurate representation of the constriction size distribution (CSD). The CSD can be obtained using experimental techniques, analytical models and numerical approaches. In this latter approach, the discrete element method (DEM) can particularly help to understand the dynamics of particle assemblies.

The particle representation in DEM modeling is fundamentally important to accurately describe the behaviour of the whole assembly. In this regard, spheres can be considered as a simple approximation of granular grains.

The objectives of this study were to improve the characterization of the void space of a granular material and more particularly the CSD and its impact on the filtration properties. This permitted on its turn to develop a filter criterion on the basis of the CSD. To achieve these objectives, the following steps have been performed:

- The DEM simulation has been used to generate packings of polysized spherical particles having different gradations and densities;
- A weighted Delaunay tessellation has been applied to characterize quantitatively the void space of the generated granular assemblies, including pore and constriction sizes;
- Pore merging criteria have been introduced to improve the definition of local pores and constrictions;
- By extending the previous work of Reboul et al. (2010), analytical models have been modified based on new findings;
- A new estimate of the mean pore diameter which characterizes filtration but also erosion processes, has been suggested following the same analytical procedure;
- Numerical filtration tests have been conducted to evaluate the possibility for transport of fine materials through the void space of granular filters;
- A new formula has been suggested to obtain the equivalent sieve opening size of the filter based on analytical considerations;
- A new filter criterion involving the equivalent sieve opening size has been proposed.

The main conclusions obtained from this study are summarized in the following section. Perspectives for future studies are also presented.

2. Main conclusions

- Sample preparation is a crucial first step in DEM simulation and can significantly affect the organization of the void space. In this study, it was clearly justified that the sample preparation technique greatly influences the accuracy of the resulted CSD especially in the case of well-graded soils. Samples subjected to isotropic compression has been found to have a much narrower range of constriction sizes compared to the samples prepared by a deposit under gravity which can reflect the process used in engineering practices more

precisely. The isotropic compression method extensively used in DEM studies, generate essentially dense specimens and its validity can be questionable for looser density states.

- In addition to the materials used in Reboul et al. (2010) (Uniformly-graded, well-graded and gap-graded), other materials with a higher value of uniformity coefficient ($C_u = 6$) have been studied, and two density states have been examined. This permits to better understand the influence of grading on both the morphology and the topology of the void space and to evaluate the validity of previous findings. Since gap-graded soils exhibit atypical behaviour and require a special attention (Reboul, 2008), another gap-graded material has been investigated.

- The weighted Delaunay tessellation offers a powerful tool for extracting the void network structures of a granular medium, i.e. the sizes of pores (largest inscribed void sphere, equivalent void sphere) and constrictions (largest empty disc on the faces of tetrahedra). This method can be only used with spherical packings where particle radii and locations are known.

- The tetrahedral partition tends to subdivide a single void structure into multiple ones leading to inaccurate predictions of void characteristics (Al-Raoush et al., 2003). To resolve this problem, pore merging criteria must be applied. The merging technique considered in this study is based on the overlap of inscribed void spheres, which is inspired from the work of Reboul et al. (2008). We advise to process a preliminary step (Level L_0') in order to remove the numerical artifacts resulting from the Delaunay Tessellation scheme. L_1 permits to remove further constrictions between highly connected tetrahedra.

- An important consideration has been addressed concerning the implications of pore merging criteria on pore and constriction statistics. In particular, it has been found that the number of constrictions is reduced by approximately 30% from L_0 to L_1 whatever the grading and the density of the material, while no much difference was observed between L_1 and L_2 which extends previous findings by Reboul et al. (2008). Moreover, the merging tends to eliminate larger constrictions. In addition, the second mode of the constriction size distribution will be destroyed while the first mode will be clearly highlighted for all types of materials except for some specific types of gap-graded soils where two close modes are must likely to appear.

- A comparative study including different gap-graded materials has shown that the void space of such materials is organized differently according to the percent of particles larger than the gap size with respect to particles smaller than the gap size.

- Although it is probably impossible to build a unique and valid network from a complex and continuum void space, L_1 merging which imposes a predefined neighbourhood limit for each pore appeared to give a reasonable void network for spherical packings.

- Concerning the influence of grading and density on pore and constriction sizes, the results show a good agreement with those obtained by Reboul et al. (2008) for a uniform grading.

- Analytical models have been widely used to quickly derive the CSD of a granular material which is considered to be the main property governing the transport of fine particle through this medium. To overcome the limitations associated with previous studies, Reboul et al. (2010) suggested new models requiring the knowledge of the grading curve (by surface area) and of the extreme void ratios of the material. These models have been calibrated on the basis of statistical analyses over numerical assemblies of spheres generated by DEM.

However, the effect of the over-segmentation of the void space introduced by the Delaunay tessellation was not taken into account which can affect the accuracy of the estimated CSD.

- The aim of this study was to reformulate the analytical model in order to obtain a more representative CSD. Firstly, the validity of the analytical models of Reboul et al. (2010) has been tested using numerous gradings. It has been found that the CSD for the loosest state can be directly obtained from Locke's model Locke et al. (2001), and the one-parameter model proposed by Reboul et al. (2010) can give good results for all types of materials (continuous and discontinuous grading) with a mean relative error less than 7%. The two-parameters model also proposed by these authors, has been excluded from this study since the parameters included in this model were not clearly established and thus, it cannot be applicable to all types of materials.

  Secondly, a correction factor, which is independent of grading, was suggested in the improved model to fit the numerical CSD curve corresponding to L_1.

- Statistics from numerical samples have been used to examine the validity of previous estimates of the mean pore diameter. It has been found that all the estimates failed to predict this characteristic length of the pore space. A new formula is then proposed taking into account the correlation between the selected merging criterion and the constriction spacing.

- Numerical filtration tests have been carried out to evaluate the maximal particle size that can infiltrate through a filter of a given thickness. The results of dry filtration tests have shown a critical size from which the probability of further movement through the filter increases rapidly. Moreover, a clear correlation has been found between this critical diameter and the largest mode of the constriction size distribution corresponding to L_1. Then, the modal value of L_1 CSD can be associated to the opening size of the granular filter, and a physical meaning can be attributed to L_1 justifying its use as a reasonable pore merging criterion. Besides, the numerically derived critical diameters are similar to the controlling constriction size found in the literature (Witt, 1993) for a similar thickness of filters. On the other hand, we tried to draw a relationship between the critical diameters and constriction sizes and we found that they correspond to the fractile 35% from the CSD curve (L_1) independently of the grading and of the density of the filter material. One should not confound this value with D_{c35}, the controlling constriction size suggested by Indraratna et al. (2007), which has been obtained following a different analytical procedure.

- From the numerical hydraulic tests, it seems that the flow redirect fine particles along the widest filtration paths which allow crossing larger distance than in dry filtration tests. In this case, the mode is less correlated to the opening size of the granular filter.

- Based on the results of numerical filtration tests, a simple analytical formula involving the grading and the density of the filter, is proposed to quickly estimate the equivalent sieve opening size of the filter d_{OS}. Laboratory data from past experimental studies have been used to verify the accuracy of the estimate, and good agreement has been observed between experimental and analytical values.

- A better description of the ability of a fine particle to be transported through a granular filter could be given by incorporating d_{OS} of the filter and d_{85SA} of the base soil in a new constriction-based criterion, $d_{85SA} \geq d_{OS}$. By surface area consideration, d_{85SA} can better represent the base soil material compared to the conventional d_{85} by mass. The predictions

of the proposed criterion are compared with experimental data taken from past studies, and are shown to be in a good agreement.

- This geometric criterion is based on a direct comparison of the representative grain size of the base soil with the equivalent sieve opening size of the filter material. The representative constriction size involved in this criterion was obtained through analytical calculation based on numerical simulation results, and validated by experiments. Hence, it is a more realistic approach compared to the original criterion given by Indraratna et al. (2007). Moreover, it takes into account the particle size distribution and the degree of compaction of the filter, thus overcoming the limitations inherent to common empirical filter criteria. Using such criterion in conjunction with the current established practices based on the particle size ratios can offer a consistently reliable tool for assessing the efficiency of filters.

3. Perspectives

This work is a continuous study from previous researches (Reboul et al., 2008, 2010; Wu et al., 2012; Sjah and Vincens, 2013; Li et al., 2014) carried out at *LTDS* of *Ecole Centrale de Lyon*. The contributions of this work will be useful to derive a general conclusion regarding the morphology of the void space, the characterization of the CSD, and the transport mechanisms within granular media. However, some further developments on these topics can still be envisaged in the near future. In this context, a cooperation between experimental and numerical approaches will be especially beneficial to validate the results reported in this study.

On the other hand, the granular samples used in this study, have been modeled with spherical discrete elements. However, particles encountered in nature and engineering practice may not be spherical but rather of irregular shapes. In particular, fluvial grains have more elongated forms. Because of the geometrical anisotropy of their particles, the pore network and the interconnectivity of the pores are expected to be modified which can have also an effect on the transport processes within such porous media.

In this context, the DEM can be considered as an effective method increasingly used to simulate irregularly shaped particles (Eliáš, 2014; Kerimov et al., 2018b) Moreover, the increasing performance of the micro-computed tomography (micro-CT) technique allows to obtain the 3D microstructure of non-spherical materials at sufficient resolution (Homberg et al., 2012; Taylor et al., 2018).

In view of these facts, future work will be devoted to a fundamental study on irregularly shaped materials. DEM simulations involving polyhedral particles having different gradings, density states and aspect ratios must be performed. Since the void structures of arbitrary-shaped particles cannot be easily handled by the Delaunay tessellation, the medial axis method proposed by Homberg et al. (2012) can advantageously be used as an alternative technique for partitioning the continuous void space.

In Seblany et al. (2018), which consisted in a collaboration between *Ecole Centrale de lyon*, *Zuse Institute Berlin* and *Bauhaus-Universität Weimar*, we have established, in the case of spherical packings, a correspondence between the criteria associated to different merging techniques (the overlapping inscribed void spheres technique and the pore separation technique), which can be

used to situate the CSD obtained by the pore separation technique with respect to the CSD that is expected to be obtained by the overlapping inscribed void sphere technique.

Then, analytical models for calculating the CSD of irregularly shaped granular materials can be deduced from the models originally developed for spherical materials by introducing shape factors. An extended investigation on the influence of particle shape on the potential transport of fine particles should be conducted by means of dry or hydraulic filtration tests. The role of anisotropy in the modification of the filtration properties of granular soils can be evaluated by changing the orientation of the flow direction with respect to the anisotropy. Another goal is to identify an analytical formula for calculating the opening size of a granular filter composed of elongated grains. This characteristic size can be subsequently included in a constriction-based filter criterion.

A preliminary study has been undertaken in an attempt to examine the effects arising from particle shape. Polyhedral packing that, apart from the particle shape, is identical in all respects (PSD, preparation technique, friction coefficients) to the previously studied spherical packing, has been generated. In accordance with previous studies (Wu et al., 2012; Taylor et al., 2017), the results have shown that such a particle shape gave a wider range of constriction sizes at the upper and lower ends of the CSD curve, compared to spherical particles. However, many directions are still quite unexplored and more investigations are to be carried out to fully understand the impact of particle shape on the CSD and on the filtration process. For all these reasons, this work was not included in this manuscript.

Appendices

Appendix A

Pore distributions

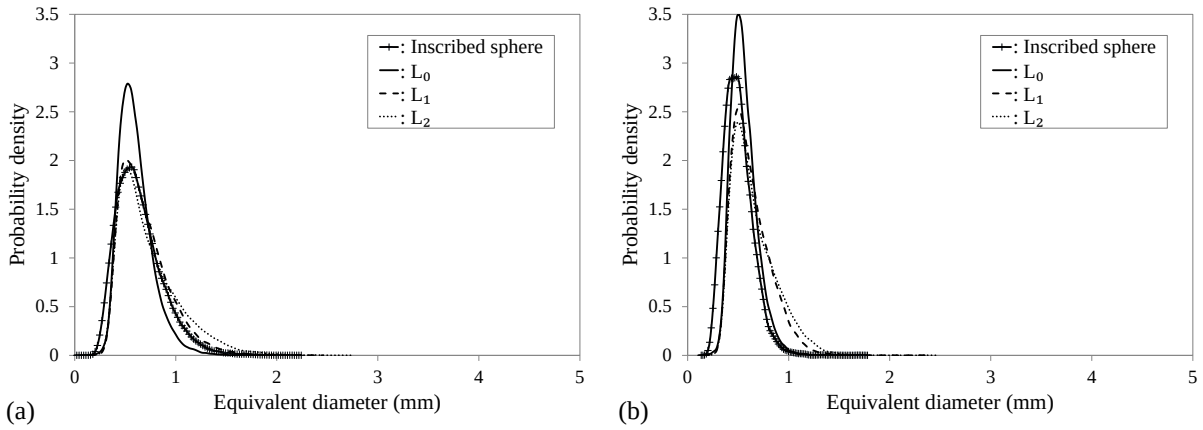

Fig. A.1. Probability density functions for the equivalent pore diameter resulting from different definitions and corresponding to the overlapping inscribed void spheres technique; (a): WG1L, (b): WG1D

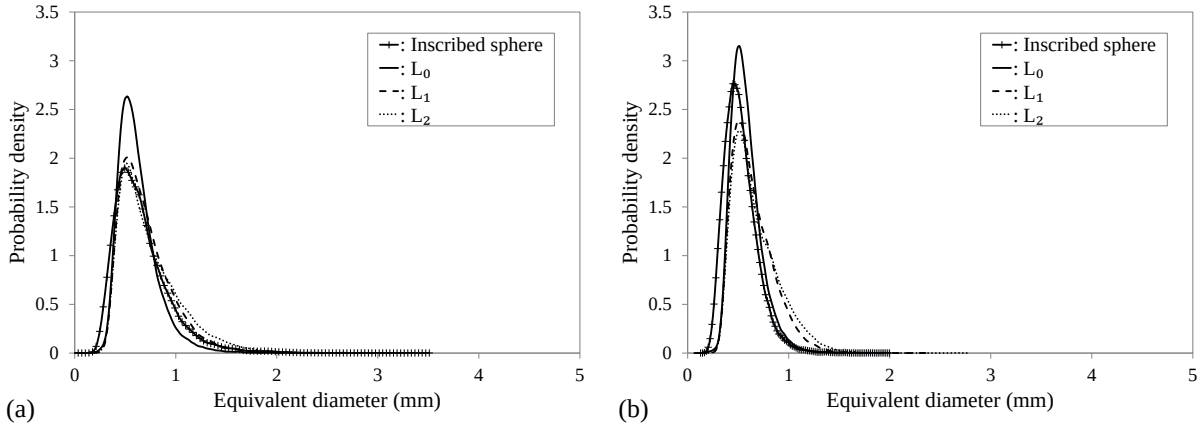

Fig. A.2. Probability density functions for the equivalent pore diameter resulting from different definitions and corresponding to the overlapping inscribed void spheres technique; (a): WG2L, (b): WG2D

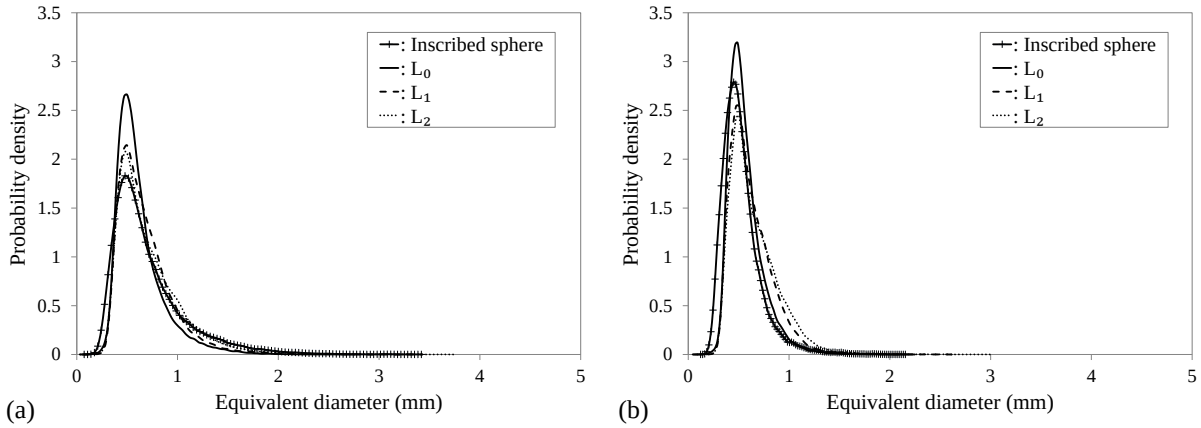

Fig. A.3. Probability density functions for the equivalent pore diameter resulting from different definitions and corresponding to the overlapping inscribed void spheres technique; (a): GG2L, (b): GG2D

Appendix B

CSD and probability density function of constriction sizes

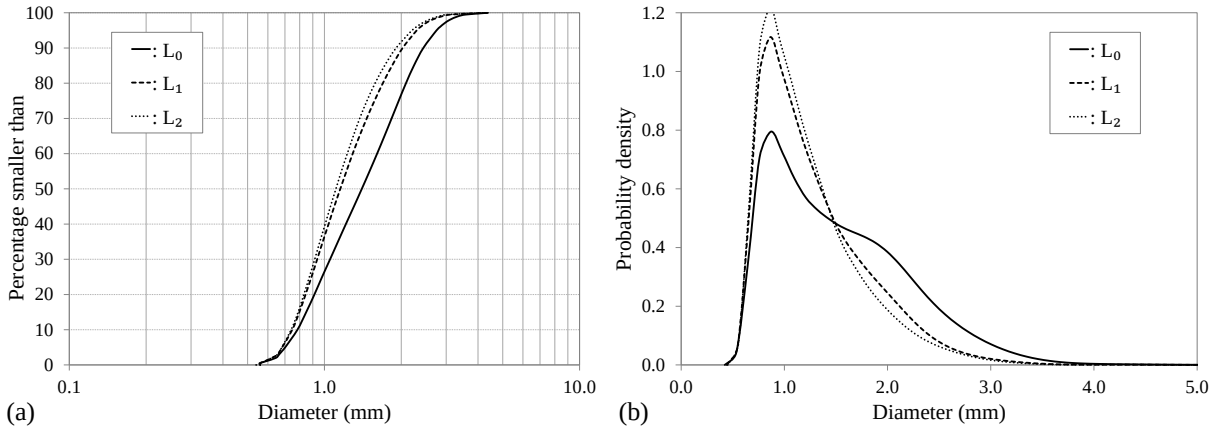

Fig. B.1. (a): CSDs for the UGD sample; (b): underlying probability density function for different merging criteria defined in the overlapping inscribed void spheres technique

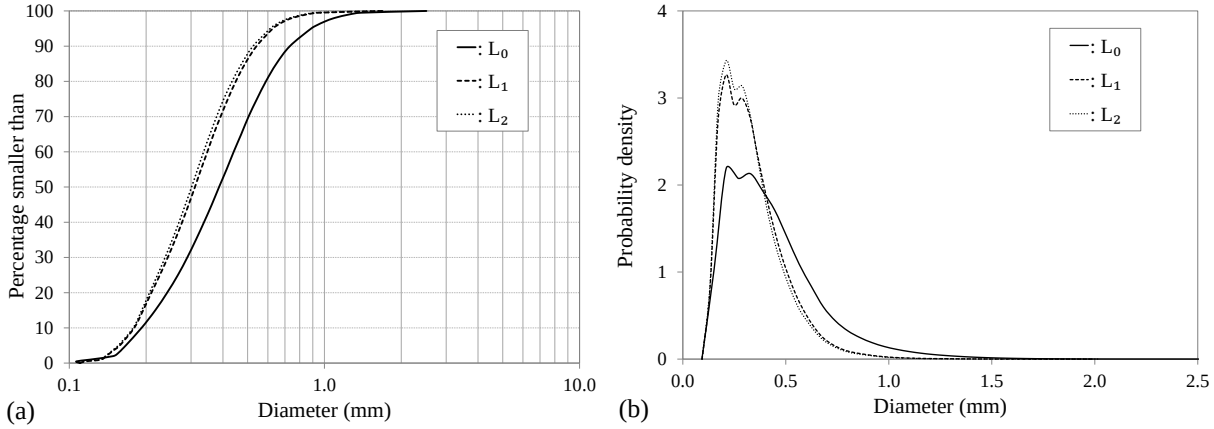

Fig. B.2. (a): CSDs for the GG1D sample; (b): underlying probability density function for different merging criteria defined in the overlapping inscribed void spheres technique

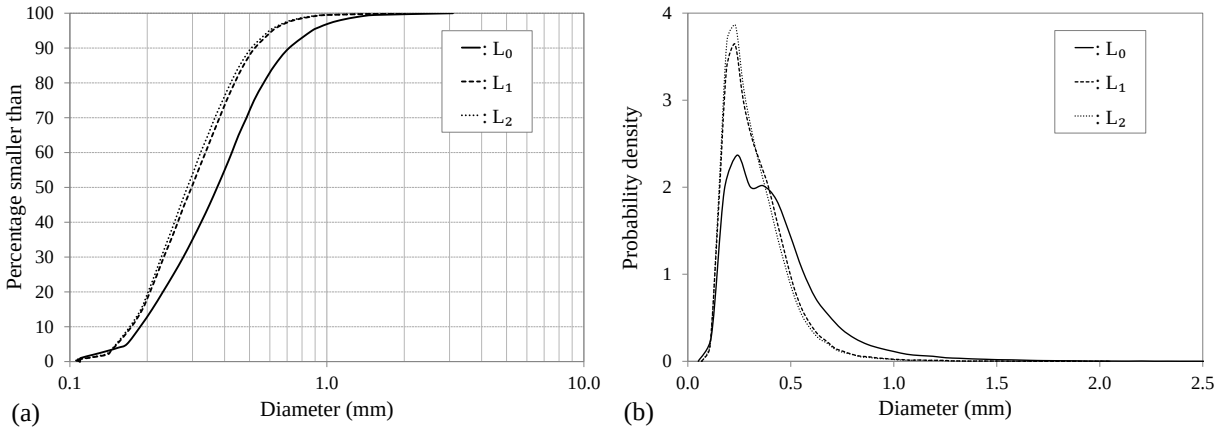

Fig. B.3. (a): CSDs for the GG2D sample; (b): underlying probability density function for different merging criteria defined in the overlapping inscribed void spheres technique

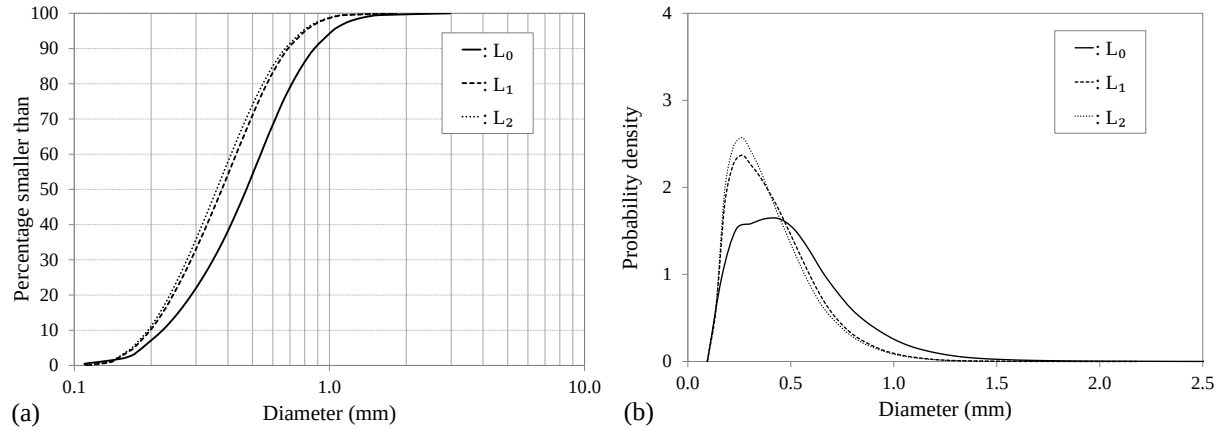

Fig. B.4. (a): CSDs for the WG1L sample; (b): underlying probability density function for different merging criteria defined in the overlapping inscribed void spheres technique

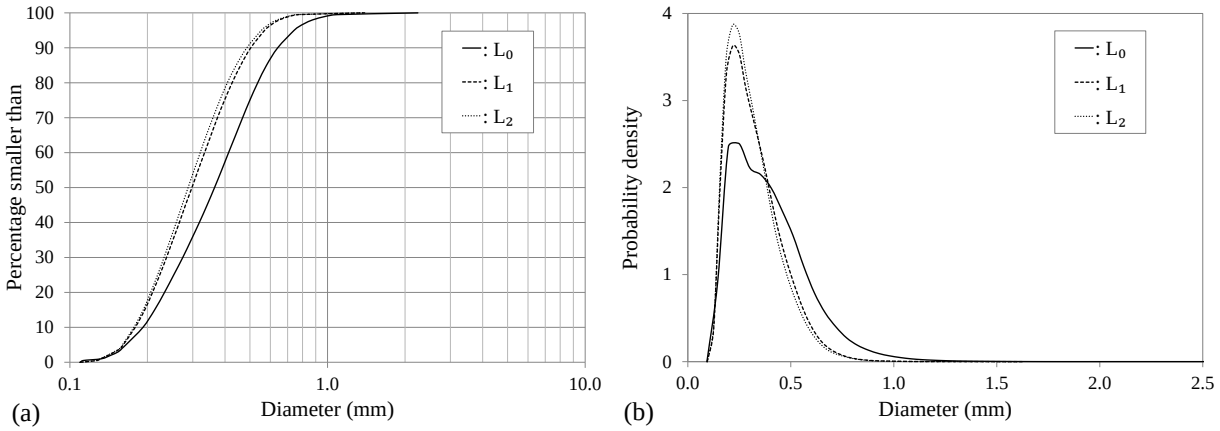

Fig. B.5. (a): CSDs for the WG1D sample; (b): underlying probability density function for different merging criteria defined in the overlapping inscribed void spheres technique

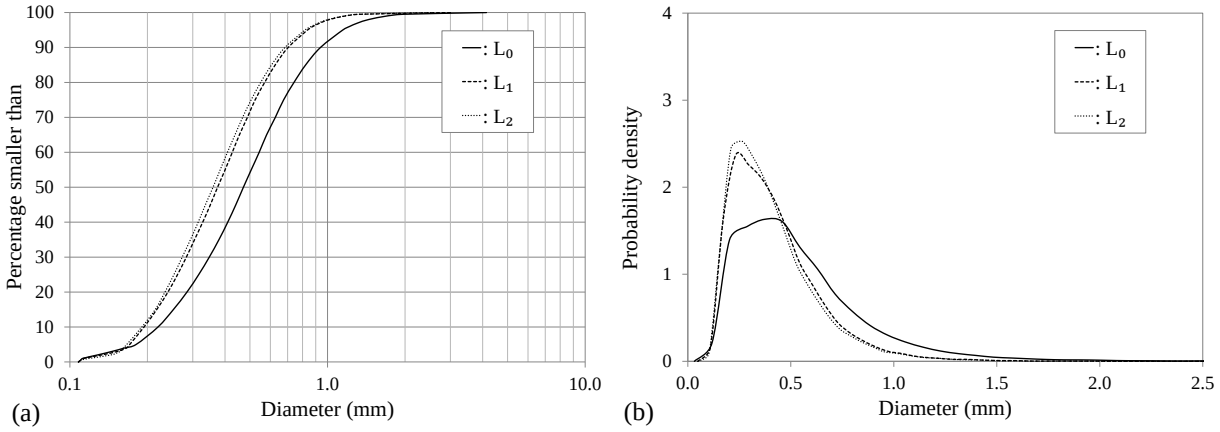

Fig. B.6. (a): CSDs for the WG2L sample; (b): underlying probability density function for different merging criteria defined in the overlapping inscribed void spheres technique

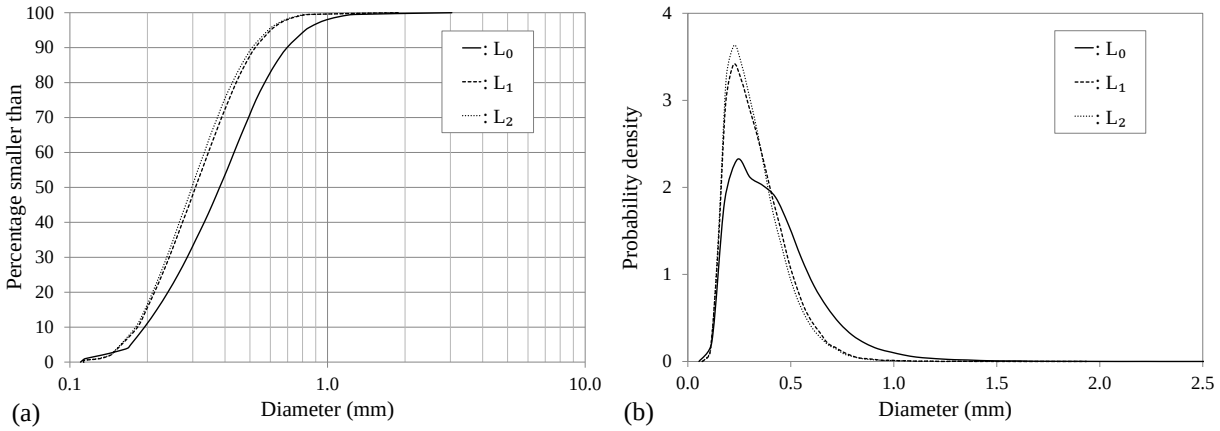

Fig. B.7. (a): CSDs for the WG2D sample; (b): underlying probability density function for different merging criteria defined in the overlapping inscribed void spheres technique

Appendix C

Results of analytical models

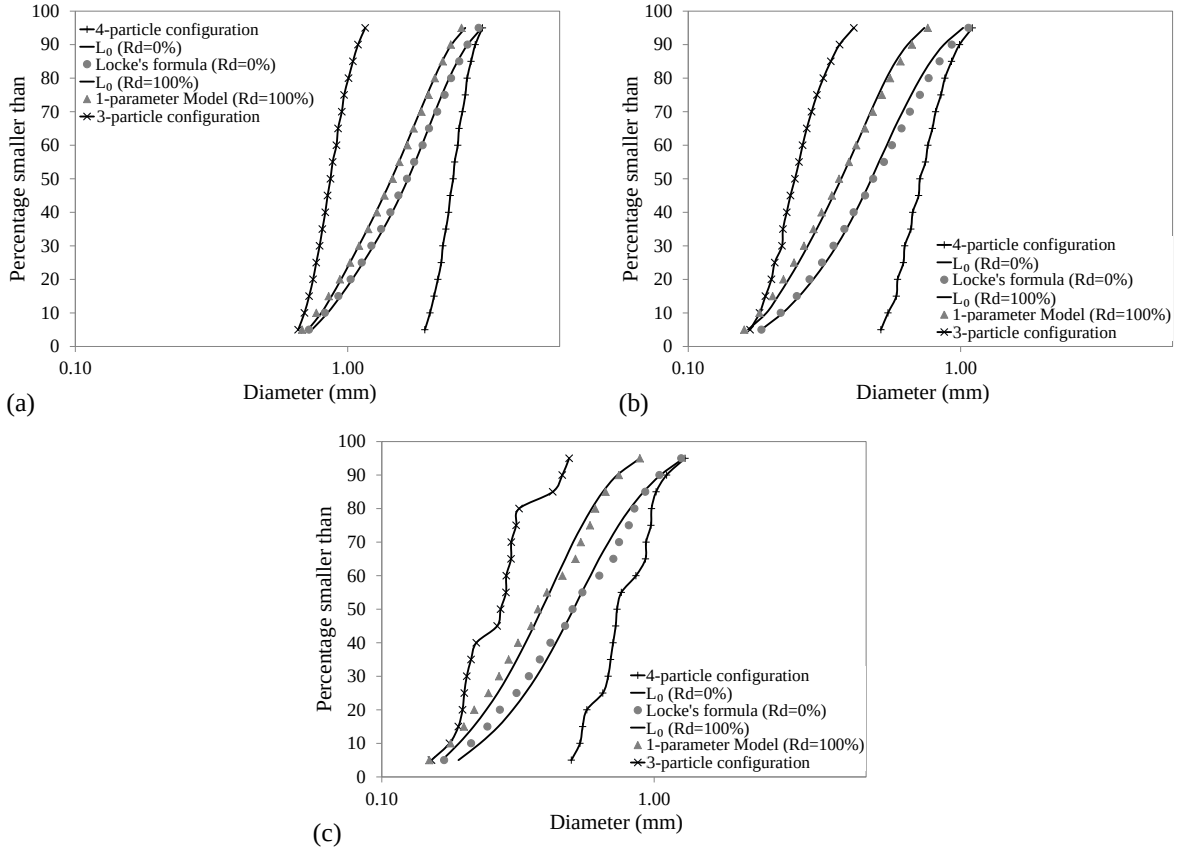

Fig. C.1. Comparison of the CSDs calculated with the analytical method and the Delaunay method (L_0 computation) for (a): UG; (b): WG1; (c): GG1

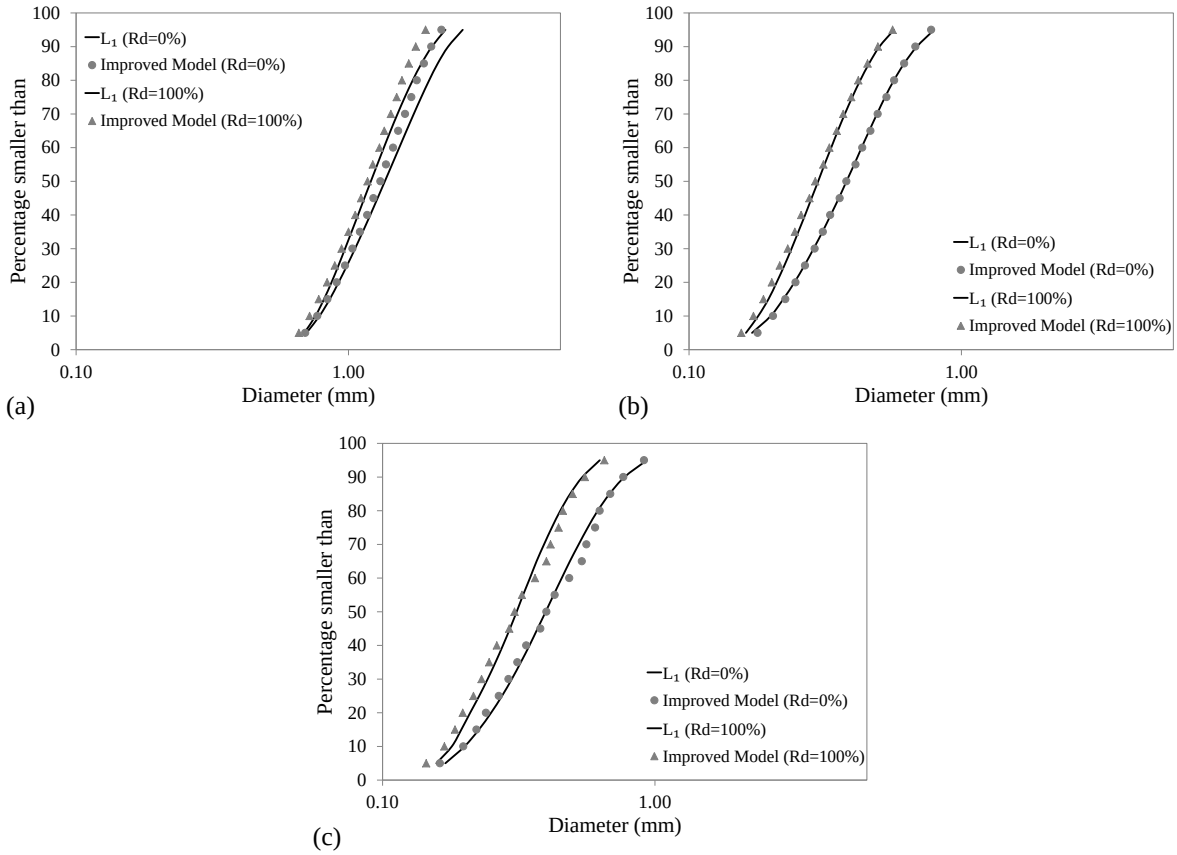

Fig. C.2. Comparison of the CSDs calculated with the improved analytical method and the Delaunay method (L_1 computation) for (a): UG; (b): WG1; (c): GG1

Appendix D

Granular Matter Paper (Seblany et al., 2018)

Seblany, F., Homberg, U., Vincens, E. et al. Granular Matter (2018) 20: 37.
https://doi.org/10.1007/s10035-018-0808-z

Merging criteria for defining pores and constrictions in numerical packing of spheres

Feda Seblany[1] . Ulrike Homberg[2] . Eric Vincens[1] . Paul Winkler[3] . Karl Josef Witt[3]

[1]Université de Lyon, Ecole Centrale de Lyon, LTDS, UMR CNRS 5513,
36 avenue Guy de Collongue, 69134 Ecully, France

[2]Zuse Institute Berlin, Department Visual Data Analysis,
Takustr. 7, 14195 Berlin-Dahlem, Germany

[3]Bauhaus-Universität Weimar, Chair of Geotechnical Engineering,
Coudraystraße 11c, 99423 Weimar, Germany

Seblany, F., Homberg, U., Vincens, E. et al. Granular Matter (2018) 20: 37.
https://doi.org/10.1007/s10035-018-0808-z

Abstract

The void space of granular materials is generally divided into larger local volumes denoted as pores and throats connecting pores. The smallest section in a throat is usually denoted as constriction. A correct description of pores and constrictions may help to understand the processes related to the transport of fluid or fine particles through granular materials, or to build models of imbibition for unsaturated granular media. In the case of numerical granular materials involving packings of spheres, different methods can be used to compute the pore space properties. However, these methods generally induce an over-segmentation of the pore network and a merging step is usually applied to mitigate such undesirable artifacts even if a precise delineation of a pore is somewhat subjective. This study provides a comparison between different merging criteria for pores in packing of spheres and a discussion about their implication on both the pore size distribution and the constriction size distribution of the material. A correspondence between these merging techniques is eventually proposed as a guide for the user.

Keywords: Delaunay tessellation . Voronoï graph . Void space . Granular materials

1 Introduction

A granular medium includes a set of large volumes of voids between solid particles (pores) connected by throats. The narrowest sections in these throats are generally denoted as constrictions. Pores and constrictions constitute a partition of the void space helpful to define respectively its morphology and its topology [28, 45]. Such a partition can also help to build imbibition models for unsaturated materials [16, 23], models for the coefficient of permeability [7, 8] for fluid-calculation, or geometrical filtration models for studying the migration of particles through granular media [21, 32, 34, 35].

There are different techniques for pore space characterization: through experiments [15, 19, 40, 42, 46], using analytical approaches [22, 29, 36] or numerical approaches [17, 26, 28]. To overcome some limitations associated with experimental methods, the Discrete Element Method (DEM) (among others [10]) can be helpful to draw some main tendencies for packings of spheres with a given grading and density. The pore space of such a packing can be extracted by combining the DEM with spatial partitioning techniques: the Delaunay tessellation [1, 28, 41] or its dual structure, the Voronoï diagram [14, 30, 47] among others.

In the Delaunay tessellation, the primary definition for a local pore is the Delaunay cell, i.e. a tetrahedron which vertices are located at the centers of spherical particles. Constrictions are found on the

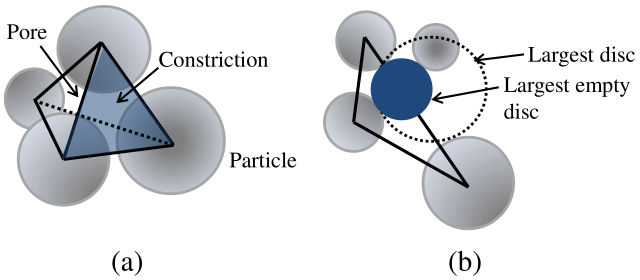

Figure 1: **(a)**: Tetrahedron built from the centers of four neighboring spheres; **(b)**: Definition of a constriction: the largest disc included in the void space for a given face

four faces of each tetrahedron and a definition for them is chosen as the largest empty discs that can be inscribed between the three particle vertices of a tetrahedron face [1, 28] (Fig. 1). Eventually, the inscribed void sphere between the four particles, vertices of a Delaunay cell is computed and is considered as a characteristic of the morphology of that cell. Obviously, the derived partition of the void space is somehow artificial since a Delaunay cell is merely related to the underlying mathematical process of finding the three closest neighbors of a given particle to generate a tetrahedron.

While the Delaunay tetrahedra constitute volumetric entities that cover pores or parts of pores, a Voronoï graph can complement the definition of the pore structures. Due to the duality of Delaunay and Voronoï decompositions, the Voronoï nodes should correspond to the centers of the inscribed void spheres of the Delaunay tetrahedra and their distance to the surrounding solid spheres to the radius of these inscribed void spheres. When applying a Voronoï computation that is based on the Euclidean distance to the solid spheres as described by Lindow et al. [20], the edges between the Voronoï nodes are curved and run along the maximal distance to the surrounding solid spheres. Then, they describe the median path joining pore centers. The centers of constrictions are located where the distance to the surrounding spheres is minimal along the edge. In terms of duality, this is where the edges cut the common facet of the tetrahedra of the connecting Voronoï nodes and, thus, correspond to the constrictions found in the Delaunay tessellation (Fig. 2).

Even if the equivalence of results for the constriction size distribution (CSD) extracted from a Delaunay tessellation and a Voronoï graph has been proven in the past for a packing of spheres [44], the question arises whether an excessive artificial partition of the void space is generated by both mathematical techniques and how to handle it.

Indeed, using a Delaunay tessellation, Al-Raoush et al. [1] found that the inscribed void sphere confined in each tetrahedron is not necessarily entirely included inside that tetrahedron, and two inscribed void spheres attached to these two neighboring tetrahedra may overlap. It signifies that the opening size between two adjacent tetrahedra may be high enough to indicate a strong interconnection between them. As a result, the tetrahedral tessellation would tend to abusively subdivide a complete pore structure into zones.

For the same reason, Homberg et al. [17] considered that a merge between two adjacent pores may be required when the size of the constriction linking these pores is very close to the smallest pore size (case where the Voronoï approach is used to derive the void space properties). In fact, in such a case, pores are interconnected and seem to belong to a single entity. Figure 3 illustrates a case where two adjacent pores (hatched and shaded area) are going to be merged.

Because different techniques may lead to different pore structures and, as a consequence, to a different set of pore and constriction sizes, this study aims to better understand the implications of using a given technique for merging pores on the properties of the poral space in packing of spheres. The problem that arises here is that no definite poral structure can be derived for a packing since the boundaries of a so-called pore is vague by nature. Within these limits, this paper tries to draw some advantages and limits of two techniques for merging pores. The influence of the proposed criteria for merging on the pore

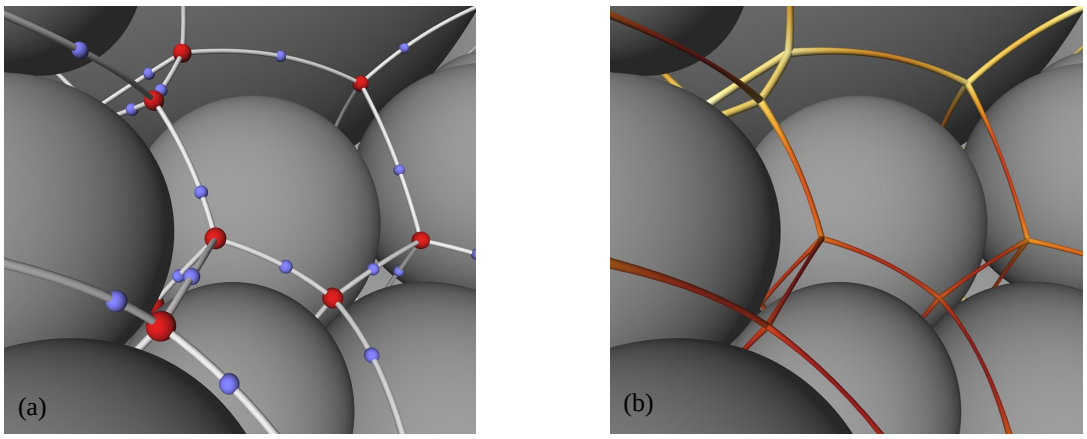

Figure 2: Detail of a Voronoï graph (GGD); **(a)**: red (larger) spheres at crossing indicate the centers of pores, while the blue (smaller) spheres represent the centers of constrictions on the edges; **(b)**: The diameter is color-coded along the edges with yellow (large) to red (small) (color figure online)

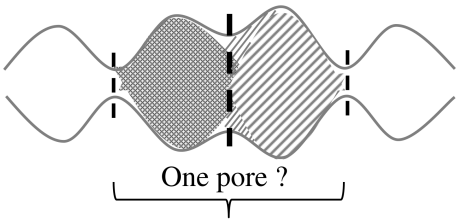

Figure 3: Scheme of a typical case encountered during pore merging

structures is also addressed and, as a guide for the user, a correspondence between the criteria associated to both techniques for merging pores is given.

2 Generation of numerical samples

The open-source code Yade-DEM [39] was used here to generate numerical samples composed of spheres. In this DEM code, the contacts between particles are deformable while the particles are considered as infinitely rigid bodies [10].

Two gradings are studied: a narrowly graded material (UG) and a gap-graded material (GG). The former grading is the one studied in previous studies [28, 38], ranging from $3mm$ to $12mm$ as shown in Figure 4a, with a coefficient of uniformity (C_u) equal to 1.7. The coefficient of uniformity measures the extent of particle diameters and is defined as the ratio of the diameter corresponding to 60% finer by weight to the diameter corresponding to 10% finer by weight. The latter grading is the one studied by Reboul et al. [29] and is given in Figure 4b. The minimum and maximum diameters (D_0 and D_{100}) for this material are respectively equal to $0.7mm$ and $10mm$, and C_u is equal to 3.6. Since different techniques for the sample creation may lead to different structures for the packing [4, 31], a deposit under gravity of particles, which is a technique that reflects the process used in actual experiments, is preferred.

To create the sample, a loose cloud of spheres with a prescribed particle size distribution is initially generated in a box having a horizontal size equal to that of the final sample but with a larger vertical size (about twice as more as the horizontal size). The base of the box is a square of $40mm$ width (ap-

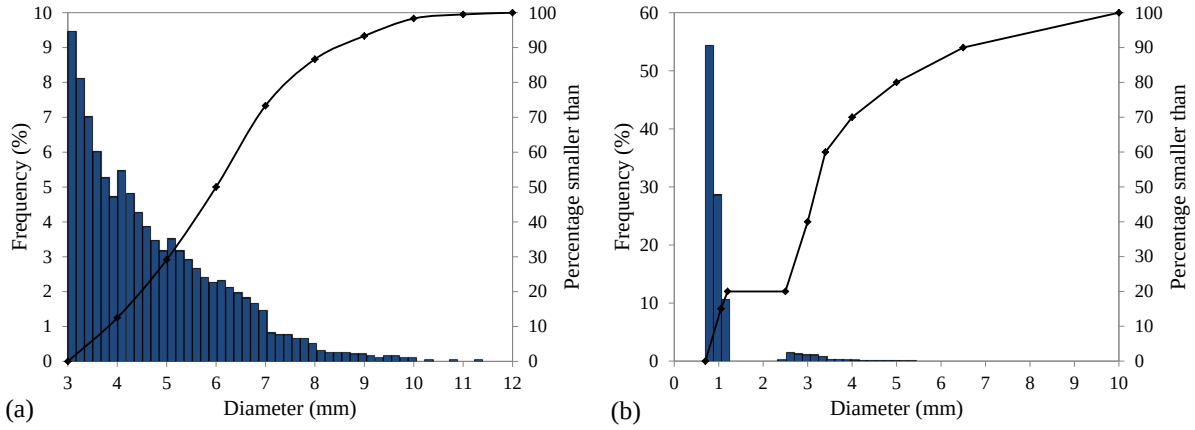

Figure 4: Particle size distribution (ordinate on the left Y-axis) and cumulative particle size distribution (ordinate on the right Y-axis) for **(a)**: UG material and **(b)**: GG material

proximately $4D_{100}$). The lateral boundaries of the box are associated to periodic conditions in order to avoid wall effects in the final samples [2, 27]. If a sphere overlaps any other existing spheres, another position is attributed to this sphere.

After this stage of particle generation, the packing is subjected to gravity which induces the spheres to fall freely in the box according to Newton's laws. Interactions between particles may occur as particles collide. The process is ended when all particles reach a quasi-static equilibrium state. The equilibrium is supposed to have been found when the unbalanced forces (mean resultant forces at contact divided by the mean contact force over the sample) goes below 0.05.

The contact between particles and that between particle and the bottom wall of the sample box (this wall is ruled as a particle with an infinite radius) is characterized by an elastic-frictional model. It includes a normal and a tangential stiffness (respectively K_n and K_t) and tangential forces are limited by the Coulomb criterion characterized by a contact friction coefficient (μ).

In this study, particle density is taken equal to the one of glass beads, and typical values for K_n and K_t of such materials are chosen. For the specific contacts between a particle and the bottom wall of the box, the contact friction coefficient (μ) is set to 0. Dissipation in the system is introduced by means of a global damping (α) proportional to the acceleration forces [10].

In the case of UG material, 650 particles have been used while for GG material, packings with 25000 particles were generated to obtain representative statistical data. For each grading, two samples are generated corresponding to the loosest state (respectively UGL and GGL) and to the densest state (respectively UGD and GGD). The inter-particle friction coefficient is set to 0.3 which is approximately equal to the value obtained by experimental test on spherical glass beads [3]. The resulting maximum porosities for UGL and GGL match the targeted values obtained through experiments by Biarez and Hicher [6], for the same coefficient of uniformity and the same particle aspect ratio of 1 (difference between the largest dimension and the smallest dimension of a particle). These authors used the ASTM standard to determine both the maximum and minimum porosity of actual granular materials having different gradings and particle aspect ratios.

The densest state is also obtained by gravitational deposition as described in [9, 12], but with a contact friction value between particles equal to zero. In fact, setting the friction to zero is favorable for particle rearrangements, which in turn leads to the compaction of the packing [37, 43, 49]. The minimum porosity reached with such process is equal to that obtained previously by Reboul et al. [28] for the same material (UG) though the process of creation of this dense sample was different. In their work, spheres are initially released under gravity to create a loose sample and then, the densest state is obtained by

means of shearing cycles with a contact friction value between particles equal to zero.

It must be noted that such typical DEM densification processes lead to density states which are generally looser than that obtained for actual materials using the ASTM process [5]. Table 1 and Table 2 summarize the set of parameters used to obtain the numerical samples and their induced final properties.

Since the top and bottom boundaries of the sample are not periodic, any computation of the poral characteristics of the packing is carried out within a volume smaller than the total sample volume. While the vertical lateral limits of this measurement volume correspond to the periodic boundaries. The limits of the top and bottom volume exclude then a zone of thickness equal to D_{100} of the granular material. Finally, we checked that the final volume used for the statistics of the void space is greater than the Representative Elementary Volume.

Table 1: Mechanical and numerical parameters for DEM simulations

Parameter	Magnitude
Normal stiffness (K_n)	10^4 KN/m
Tangential stiffness (K_t)	10^4 KN/m
Specific weight of spheres (ρ)	2530 Kg/m^3
Global damping (α)	0.7
Inter-particle friction (μ)	0.3 (loosest state)
	0 (densest state)

Table 2: Characteristics of numerical samples

Material	UG	GG
Coefficient of uniformity (C_u)	1.7	3.6
D_0 - D_{100} (mm)	3 - 12	0.7 - 10
Number of particles	650	25000
Maximum porosity	0.38	0.34
Minimum porosity	0.34	0.25

3 Merging techniques for pores

The generated samples will be used as data basis for the comparison of two different techniques: the overlap of inscribed void spheres and the degree of the separation of pores by their constrictions. Both techniques, without any algorithmic restriction, would produce over-merges in terms of ducts and less interlocked pores. Thus, the techniques are accompanied by algorithmic restriction: the overlapping criterion is based on levels of neighborhood as initially considered by Seblany et al. [33], while the degree of separation is strengthened by a hierarchical separation [18]. Both approaches build data structures from the Delaunay tessellation and the Voronoï decomposition, respectively, and provide tools to extract properties such as pore volumes and constriction sizes.

3.1 Overlapping inscribed void spheres technique

Once the locations and radii of the solid spheres are known, a modified (weighted) tetrahedral tessellation (Delaunay tessellation) of the space is performed [11].

Such a 3D partition induces a specific structure for the pore space. Indeed, each tetrahedron is herein supposed to represent a local pore associated to four exits. The void volume included in each tetrahedron can be derived together with other characteristics including the inscribed void sphere. Then, a statistical study over the whole sample can be computed for the properties of the local pores. Accordingly, constrictions defined as the largest empty discs on the tetrahedron faces can be obtained and the CSD can be deduced by means of a statistical study over the sample. All these characteristics are obtained using optimization algorithms (for the distance mapping) and more details can be found in [1, 28, 29].

The initial calculation of pores and constrictions corresponds to a level 0 (L_0) of analysis as proposed by Reboul et al. [28]. This direct computation from the Delaunay tessellation can include configurations where constrictions are larger than pores (constrictions formed by non-touching particles on the common face of two adjacent interlocked pores [13]), and other configurations where two adjacent inscribed void spheres are almost superimposed (The overlapping of these void spheres is greater than 99.9999%). Such cases correspond to tetrahedra of undesirable shape (e.g. very flat tetrahedra). The constrictions resulting from these cases represent between 10% to 20% of the total number of constrictions, depending on the grading and on the density of the material. Thus, a L_0 description of the void space may include some artifacts due to the mathematical process used for the partitioning of the space. A post-processing of L_0 (Level $L_0{}'$) guarantees the removal of these degenerated constrictions.

Apart from these cases, the inscribed void spheres of two adjacent tetrahedra may just partly overlap and these cases are distinguished from those where the inscribed void spheres are completely separated. In the case of overlapping, a merging of the corresponding adjacent pores is applied (Fig. 5), giving birth to a level 1 (L_1) characterization of the void space. First, the tetrahedra derived from $L_0{}'$ are sorted by increasing order of their inscribed void sphere, then for each tetrahedron, the overlap criterion is checked for the four adjacent tetrahedra. It should be noted here that after merging two neighboring pores, the process of merging is ended and didn't go beyond the direct neighbor.

A level 2 (L_2) is also processed where merging is not only applied to the adjacent local pore but also to the next adjacent local pore if the inscribed void sphere of this latter overlaps that of the former pore (Fig. 5). No further level for merging pores is envisioned since in that case, the void space will tend to be characterized in terms of duct.

Level 1 and level 2 can be envisioned as criteria for merging pores in the context of the overlapping inscribed void sphere technique. This technique and the proposed criteria hold some advantages and limits. First, even if this technique seems relevant in the case of packing of spheres where a partition of Delaunay can be processed, it may not be able to address the case of media with elongated particles which may give rise to more elongated pores than in packing of spheres. In that case, by nature, few overlapping inscribed void spheres are expected to be found. In the case of packing of spheres, the proposed two criteria imply that the persistence of a pore is limited in distance which can be both an advantage and a drawback. It implies that a pore can only be defined at a certain local scale involving a pore wall composed of maximum eight particles in the case of L_1 or of tens of particles in the case of L_2.

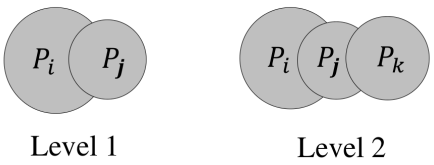

Figure 5: Definition of different merging criteria associated to the overlapping inscribed void spheres technique

3.2 Pore separation technique

The pore separation technique relies on the elements of the Voronoï graph that was computed from the spheres geometry based on the Euclidean distance to the solid spheres [20]. As described in Section 1, a Voronoï node P and its respective distance represent a pore and its size d_P in the initial decomposition, and a constriction C with its respective distance describe the narrowest location between two adjacent pores along a Voronoï edge (Fig. 6a).

The separation technique keeps track of this distance information and builds a hierarchical structure of these elements that follows the topology of the distance function. It evaluates the separation of each pair of pores P_i and P_j by their constriction C_{ij} based on the relative diameter difference $t_{\text{diff}}(P_i,C_{ij},P_j) = (d_P - d_{C_{ij}})/d_P$ with $d_P = min(d_{P_i},d_{P_j})$ and $i \neq j$. The value t_{diff} will be used to merge neighboring pores according to the degree of their separation, which is specified by a user-defined threshold t. This approach was initially developed for materials with irregular particles and does not consider sphere overlaps in order to include pairs within elongated pores.

The hierarchical manner arises from specifying tuples $T_{ij} = (P_i,C_{ij},P_j,t_{\text{diff}}(P_i,C_{ij},P_j))$ that are processed in a particular order. The approach starts from tuples of direct neighbors in the unmerged graph (Fig. 6b) and evaluates them in increasing order of the difference thresholds. Each step assigns the smaller pore to the larger one. Hereafter, the neighbor tuples that contain the newly merged pore will be updated by replacing this pore by the larger representative one as well as by re-computing t_{diff} accordingly. For example, if $d_{P_i} < d_{P_j}$, then all neighbor tuples T_{ik} with $k \neq j$ will be converted to $T_{jk} = (P_j, C_{jk}, P_k, t_{\text{diff}}(P_j,C_{jk},P_k))$ to be neighbors of P_j. P_i and C_{ij} are labeled on the graph as belonging to P_j (Fig. 6c) and will be discarded from further considerations. This step is then repeated until all (newly created) tuples with a difference threshold $t_{\text{diff}} \leq t$ have been processed. More algorithmic details can be found in [18].

The resulting tuples represent hierarchical neighbors rather than direct neighbors, where each pore represents all hierarchically assigned pores. They not only treat local information on the separation but also allow considering the separation between groups of local pores that are less significantly separated. The constriction and the difference relation t_{diff} of such a tuple represent then the most significant separation criterion between the two hierarchically neighbored pores. This can increase their life time as separated pores compared to the direct neighbor relations and avoids inappropriate merge propagation.

Voronoï approaches may produce additional pore centers in the graph that do not correspond to maxima in the distance function. In such cases, the diameter of constriction separating two adjacent pores is equal to that of the smaller pore ($t = 0\%$). This is similar to what was found with the weighted Delaunay tessellation (see Sect. 3.1). On the graph, such constrictions are then identical to the smaller pore (two edges in the center of Fig. 6a), which will be merged at the very beginning of the hierarchical merge.

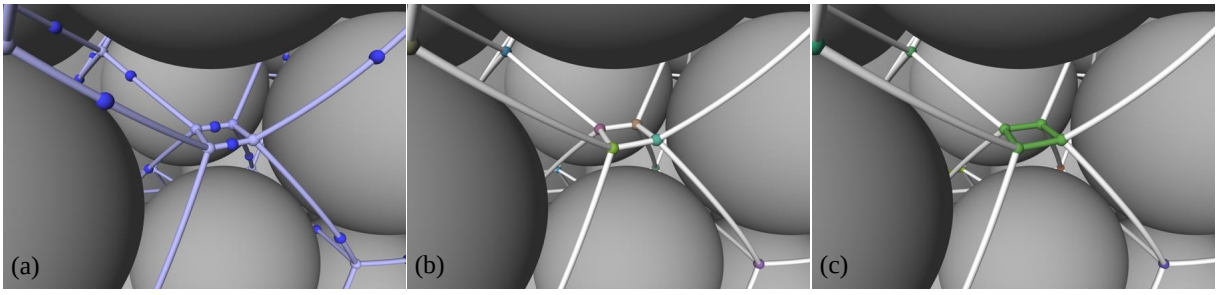

Figure 6: Detail of spheres and Voronoï graph extracted from the GGD sample; **(a)**: Bright spheres at crossings indicate pore centers, darker spheres indicate constrictions; **(b)**: Unmerged pore centers are randomly colored by their label ID; **(c)**: Merged pore centers and their connection paths and constrictions will be labeled as belonging together ($t = 1\%$) (color figure online)

4 Pore distributions derived from different merging criteria

The dual complexes of the Delaunay/Voronoï decomposition, as already described in Section 1, encode the elements of the pore space of a sphere packing. Herein, the Delaunay cells or tetrahedra are the entities that cover the pores or parts of pores and, thus, the appropriate entity to evaluate the pore volumes from both merging techniques.

4.1 Overlapping inscribed void spheres technique

The computational aspects of Delaunay tessellation involve tetrahedral cells mainly inscribed in the void space, which are more suitable than the Voronoï cells to characterize and quantify pore volumes [7, 24].

As explained previously in Section 3.1, the pore size can be measured in terms of the largest inscribed void sphere associated to each tetrahedron but also by considering the sphere having a volume equal to that of the void within a Delaunay cell (L_0) or within merged Delaunay cells (L_1, L_2). This latter method is denoted in the following *equivalent void sphere* approach. Using these two definitions for characterizing the pores, the distribution of pore sizes, for UG and GG materials, at loose and dense states, are plotted in Figure 7 and Figure 8. It is interesting to note that the pore size distributions can be well described by a Log-Normal law in agreement with previous studies [28, 48]. The correlation is almost perfect for L_0 (not shown herein); nevertheless, the statistical model tends to shift the mode towards larger pore diameters and to attenuate its frequency when L_1 and L_2 criteria are considered.

For UGL sample, accordingly to the work of Reboul et al. [28] on the same grading, the distribution computed on the basis of the inscribed void spheres approach has a mode shifted towards the smaller diameters compared to the other distributions obtained by the equivalent void sphere approach, since this former approach disregards a part of the void space. Moreover, the distribution obtained from L_1 is quite different than that corresponding to L_0, and a slight decrease in the modal value is also observed, thus showing that numerous pores around the mode in L_0 have been merged in L_1. On the contrary, no significant difference in the equivalent pore diameter distribution is observed from L_1 to L_2 (Fig. 7a). It tends to indicate that within the framework of this merging technique, the persistence of a pore is mainly limited to an adjacent tetrahedron for a given Delaunay cell.

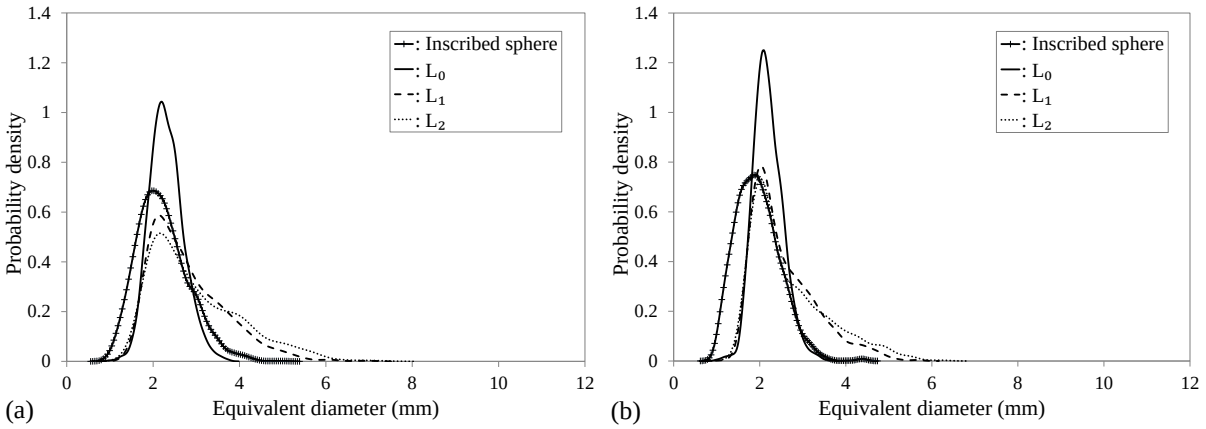

Figure 7: Probability density functions for the equivalent pore diameter resulting from different definitions and corresponding to the overlapping inscribed void spheres technique; **(a)**: UGL, **(b)**: UGD

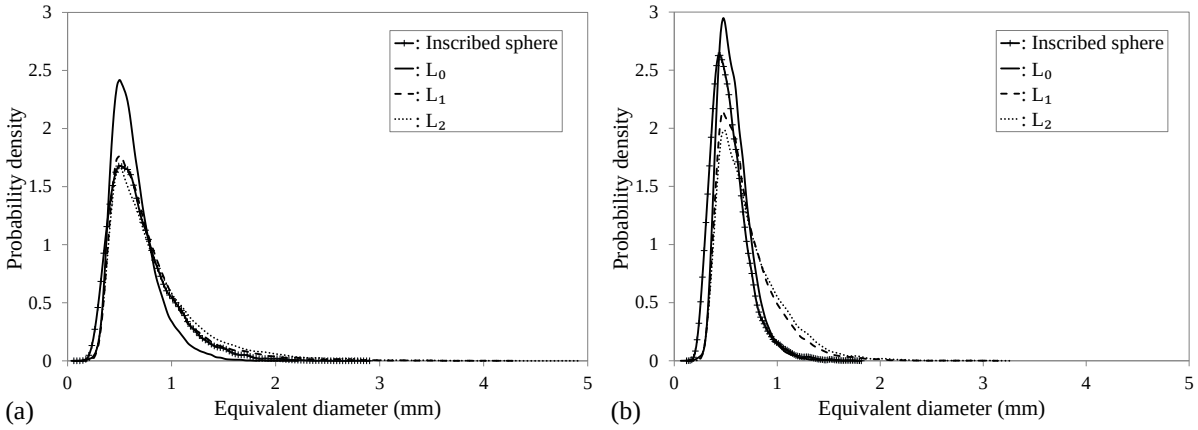

Figure 8: Probability density functions for the equivalent pore diameter resulting from different definitions and corresponding to the overlapping inscribed void spheres technique; **(a)**: GGL, **(b)**: GGD

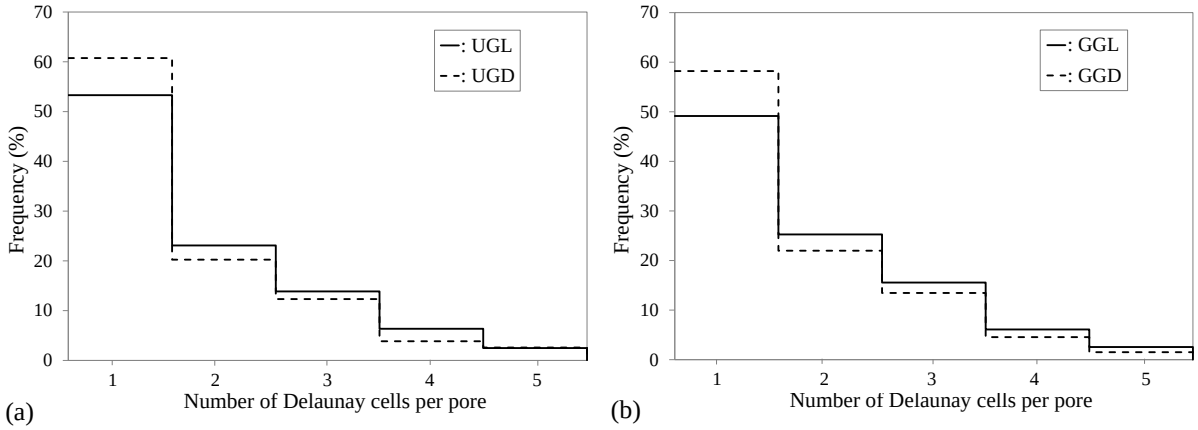

Figure 9: Number of Delaunay cells per pore in L_1 for loose and dense states; **(a)**: UG, **(b)**: GG

For GGL sample, the distribution and the modal value corresponding to the inscribed void sphere are only slightly shifted towards the smaller diameters. This may be a consequence of the wide range of particle sizes involved in this material, which tends to generate more flat tetrahedra with inscribed void spheres which are not entirely confined in these tetrahedra. Consequently, this would create the possibility of greater void spheres than in the case of UG material, the volume of which could match the volume of L_1 or L_2 distribution (Fig. 8a). It must be noted that other well graded materials that were studied (not shown herein) also exhibited this pattern. However, the tetrahedral shape seems to be the main configuration represented within the sample, irrespective of the grading and porosity, since the modal values for L_0, L_1 and L_2 are almost similar. The same finding was observed by Reboul et al. [28] for UGL sample.

For the densest states (Fig. 7b and Fig. 8b), as expected, the equivalent diameter distributions are narrower than those resulting from the loosest state (Fig. 7a and Fig. 8a); this is also accompanied by a decrease of the modal values. In fact, during the process of densification, all the pores tend to reduce their volumes but the larger ones are more sensitive to this process. Indeed, arching that allows larger pores to be created in UGL and GGL samples tends to be destroyed due to the reduction of the local friction ratio during the process of densification.

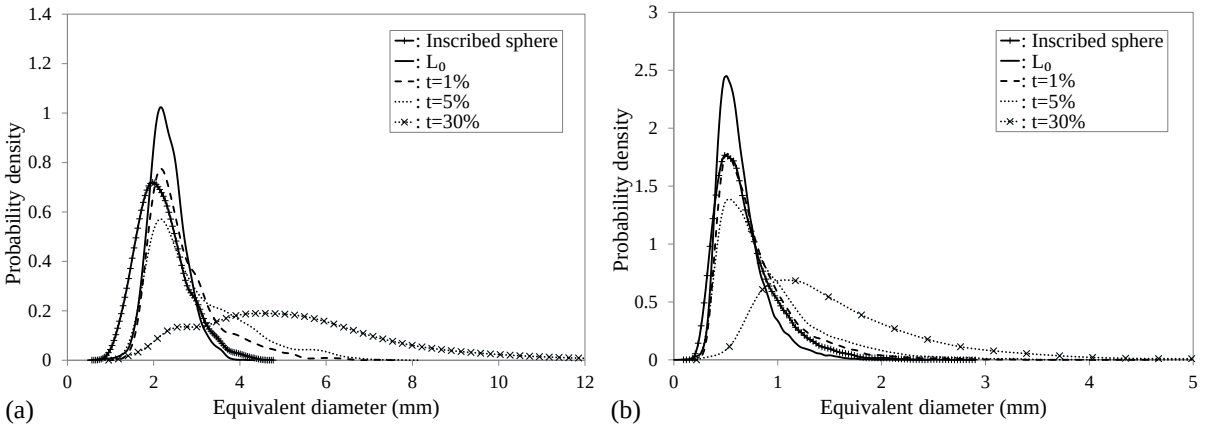

Figure 10: Probability density functions for the equivalent pore diameter resulting from different definitions and corresponding to the pore separation technique; **(a)**: UGL, **(b)**: GGL

Figure 9 shows the number of Delaunay cells per pore in the case of L_1, for UG and GG materials, at loose and dense states. Irrespective of the porosity and of the grading, about 50% of Delaunay cells are not affected by the merging. The tetrahedral shape is then predominant, while more complex entities involving three or four tetrahedra (sharing a common face with a central tetrahedron) are poorly represented in the sample.

4.2 Pore separation technique

As outlined previously, the pore separation technique is based on the pore-constriction size relations extracted from a Voronoï graph [20]. It computes the Voronoï nodes by determining their four generator spheres, which also are the spheres that build the corresponding tetrahedra in the Delaunay tessellation.

To measure the pore sizes for the comparison, an approximated method was applied to each tetrahedron and its bounding box. A set of quasi-random points (obtained from a Niederreiter sequence [25]) were spatially distributed within the bounding box. Knowing the volume of the bounding box, the void volume is estimated from the number of void points (points located inside the tetrahedron but outside the spherical particles) compared to the number of total points.

The underlying equivalent pore size distributions are given in Figure 10 for both UGL and GGL samples, and similar observations can be reported when the inscribed void sphere distribution is compared to that derived from L_0 (unmerged cells). Additionally, Figure 10 shows the behavior for large thresholds ($t = 30\%$): the difference between the equivalent pore size distributions become highly significant. The mode is very shifted towards the larger diameters. Such a large threshold merges pore clusters that already had been merged for smaller thresholds and, thus, massively increases the corresponding pore size.

4.3 Discussion

A comparison of the pore distributions associated to different merging criteria is developed in this section. As expected, the distributions of the inscribed void sphere diameter provided by the two tessellations of the void space are identical (Fig. 7a and Fig. 10a; Fig. 8a and Fig. 10b). The equivalent diameter of pores in the Delaunay cells derived from L_0 computation in both approaches was found quite similar which was also expected.

A correspondence between different merging criteria in terms of pore size distribution is given in Table 3 and Table 4, for respectively UG and GG materials, at loose and dense states. It can be seen from Table 3 that the minimum relative errors, for UG material, correspond to the couple L_1 and $t = 2\%$ as well as L_2 and $t = 5\%$ independently of the density. Similarly, Table 4 shows that the equivalent pore distribution corresponding to L_1 is close to that derived from $t = 1\%$, while the equivalent pore distribution derived from L_2 is closer to that resulting from $t = 3\%$. For GGD sample, the minimum relative error is found at $t = 2\%$ ($t = 4\%$ respectively) for L_1 (L_2 respectively).

For UG material, higher values of t are required to generate pore distributions similar to those obtained by the overlapping inscribed void spheres approach. This discrepancy is most likely caused by the nature of the pore network of the studied materials. Broadly graded material, notably at loosest state, more frequently produce clusters of dense inscribed spheres with large overlap, whereas inscribed spheres seem to be more distant with smaller overlap (higher separation) in the UG material. Furthermore, within broadly graded material, several solid spheres may build large voids containing large clusters of inscribed spheres. Such cases may exceed the expected maximum size given by the neighbor levels in the overlapping spheres approach and produce multiple pore instances within such a void. Late merges during the separation merge in UG material and underestimated volumes in GG during the L_1 and L_2 merges most likely lead to the drifting of the L_1 - t and L_2 - t correspondences between the UG and GG materials.

Each technique holds its own limits and holds some advantages. The overlapping inscribed void spheres approach provides a pre-defined neighborhood limit (L_1 and L_2) assuming a general maximum pore size at a meso scale. It may be artificial but seems relevant for packing of spheres. Nevertheless, in the case of granular materials with elongated particles, this technique may not be appropriate since one expects to find elongated pores with scarce overlapping inscribed void spheres occurrences. The separation technique allows tuning the pore structure more easily but the definition of the threshold is difficult and requires experience. One can note that this technique is more robust since it can be used for any granular material with any particle shape if a voxelization representation of the material (solids and voids) is available.

Table 3: Relative error (in %) between the pore size distributions derived from different merging criteria for UG

	$t(\%)$	1	2	3	4	5	6
UGL	L_1	3.9	3.0	3.1	3.8	5.6	8.2
	L_2	9.0	6.5	4.6	2.5	1.7	2.3
UGD	L_1	3.7	2.1	2.2	2.8	4.2	5.5
	L_2	7.5	5.6	3.9	1.8	1.0	1.2

Table 4: Relative error (in %) between the pore size distributions derived from different merging criteria for GG

	$t(\%)$	1	2	3	4	5	6
GGL	L_1	2.5	5.5	8.2	11.1	13.7	16.4
	L_2	5.5	3.4	3.2	5.5	7.8	10.2
GGD	L_1	3.5	2.2	3.0	4.7	6.4	8.1
	L_2	6.3	4.3	3.1	2.2	2.4	4.0

5 Constriction size distributions derived from different merging criteria

For convenience purposes, only the results corresponding to the UGL and GGL samples are presented in this section, but similar results were also found for UGD and GGD samples.

5.1 Overlapping inscribed void spheres technique

The CSDs and the estimated probability density of constriction sizes for L_1 and L_2 merging are given in Figure 11 and Figure 12 for both samples.

First, it has been noted that the number of constrictions decreases by approximately 40% from L_0 to L_1. In fact, the initial computation (L_0) involves non negligible sets of tetrahedra with overlapping inscribed void spheres that are merged in L_1. About half of them comes from odd configurations (that were removed in $L_0{}'$ merging as described in Section 3.1), the other half comes from partly overlapping inscribed void spheres. Moreover, L_2 merging just provides few further merged pores than L_1 which means that such cases are not significantly present in the packing of spheres. Accordingly, a shift towards smaller constriction sizes is reported when comparing L_1 CSD with L_0 CSD (Fig. 11a and Fig. 12a).

Indeed, further merging criteria belonging to L_1 were also studied [33]. In addition to the overlap condition, these criteria (herein denoted $L_1(p\%)$, p is the threshold denoted as t in the pore separation technique) evaluate the degree of separation between pores (see Sect. 3.2). The evolution of the relative number of constrictions corresponding to UG and GG materials, at loose and dense states, is shown in Figure 13. It can be noted that the configurations involving a low degree of separation (more precisely $p \leq 10\%$) are more represented within the samples. Furthermore, the decrease in the number of remaining constrictions is most significant in the case of GG material (Fig. 13b) and at loosest state in general.

Another feature is observed in Figure 11b. Merging tends to let appear a clear and single mode while vanishing a coupled second mode. When merging, the first mode for the constriction size almost stabilizes irrespective of the merging level (L_1, L_2). According to Yang et al. [48], the first mode corresponds to the constriction formed by nearly contacting particles while the second one corresponds to that formed by non-touching particles. By merging interlocked pores, the constrictions formed on the common face of the tetrahedra associated to these pores are eliminated, and consequently, the first mode becomes more significant. It must be noted that the CSD, for dense packing, has a strong first mode and a rather weak second mode since, in this case, the Delaunay cells are mainly formed by touching particles.

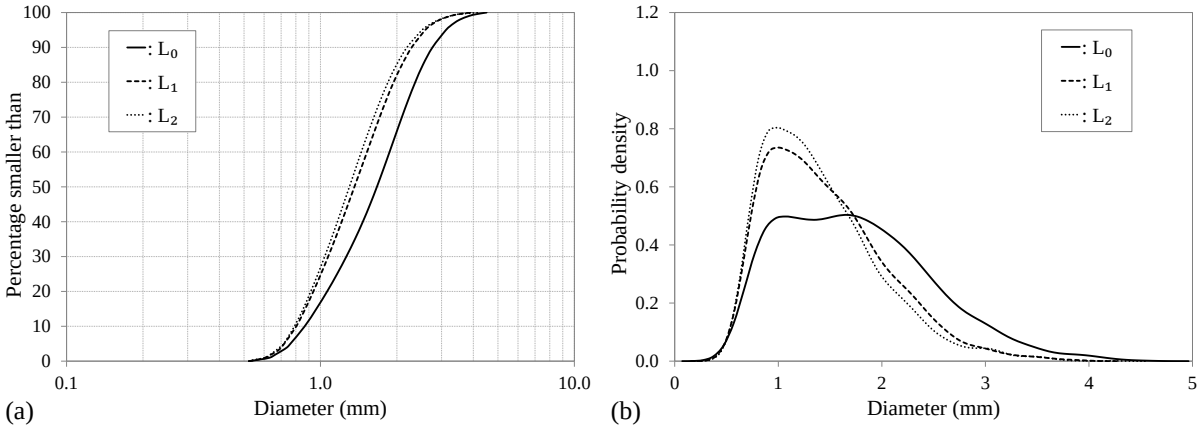

Figure 11: **(a)**: CSDs for the UGL sample; **(b)**: underlying probability density function for different merging criteria defined in the overlapping inscribed void spheres technique

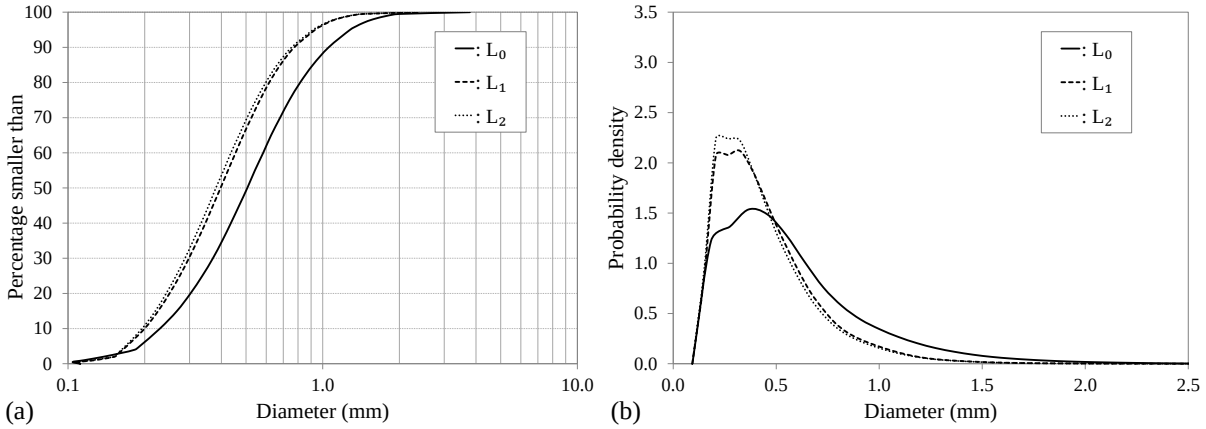

Figure 12: **(a)**: CSDs for the GGL sample; **(b)**: underlying probability density function for different merging criteria defined in the overlapping inscribed void spheres technique

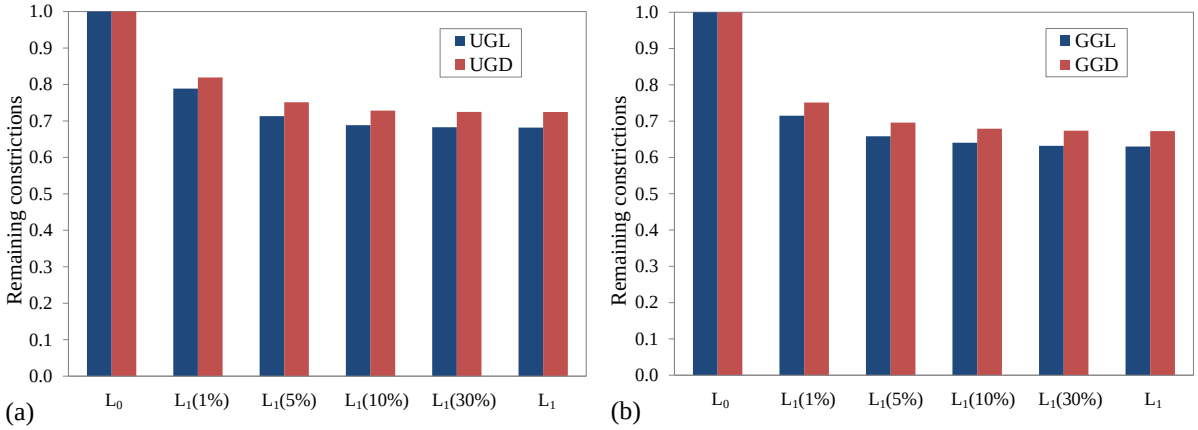

Figure 13: Evolution of the relative number of constrictions for different merging criteria belonging to L_1, at loose and dense states; **(a)**: UG, **(b)**: GG

For GGL, the distribution of constriction sizes exhibits also two distinct modes. In contrast to UGL, the distribution resulting from L_1 or L_2 remains bimodal (Fig. 12b). In such a case, the smaller mode which is approximately not affected by the merging is probably related to constrictions between fine particles in contact while the large one may include constrictions involving at least one particle of diameter greater than the gap. Therefore, the second mode is not destroyed when merging.

Another reason behind can be the large clusters exceeding the L_1 and L_2 neighborhood levels in the GG material as described in Section 4.3. Multiple L_1 or L_2 instances are created within such a void while keeping relatively large constrictions connecting these instances.

In general, from the initial set of constrictions, irrespective of the grading, more than 60% of them correspond to the exits of a single Delaunay cell and about 40% were removed from the statistics by the used merging criteria, which is significant.

5.2 Pore separation technique

Figure 14 and Figure 15 show the CSDs and the estimated probability density of constriction sizes for respectively UGL and GGL samples. One can note that the CSDs gradually shift towards the smaller diameters as the threshold value t increases, and this is accompanied by a progressive decrease in the number of constrictions. Small thresholds mainly merge larger constrictions between pores within voids, which are bounded by smaller constrictions that connect these void clusters. The hierarchical approach strengthens the separation value for the latter ones so that they persist longer. Large thresholds will also merge these cluster-connecting constrictions successively so that the deduced pore structure is highly affected as shown for $t = 30\%$, which can certainly be considered as a significant separation (Fig. 14a and Fig. 15a).

In the case of UGL, the probability density of constriction sizes has two modes for L_0, and then becomes unimodal when merging criteria are applied (Fig. 14b). Besides, the first mode is not affected by the merging steps for t lower than 5%. For GGL, the L_0 probability density (Fig. 15b) is similar to that obtained in Figure 12b but the bimodal character is not as pronounced. However, the distributions still exhibit a bimodal shape when merging, as described in Section 5.1.

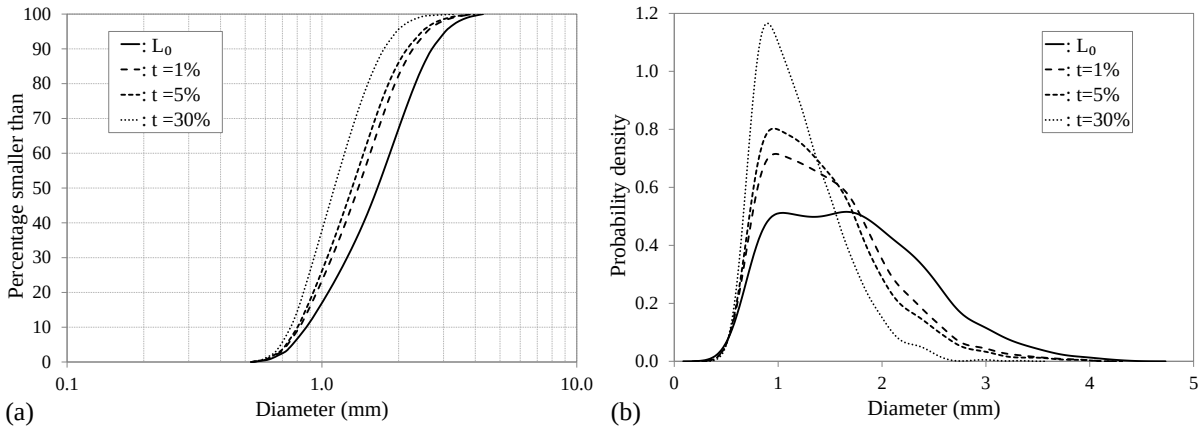

Figure 14: **(a)**: CSDs for the UGL sample; **(b)**: underlying probability density function of the constriction diameter for different merging steps associated to the pore separation technique

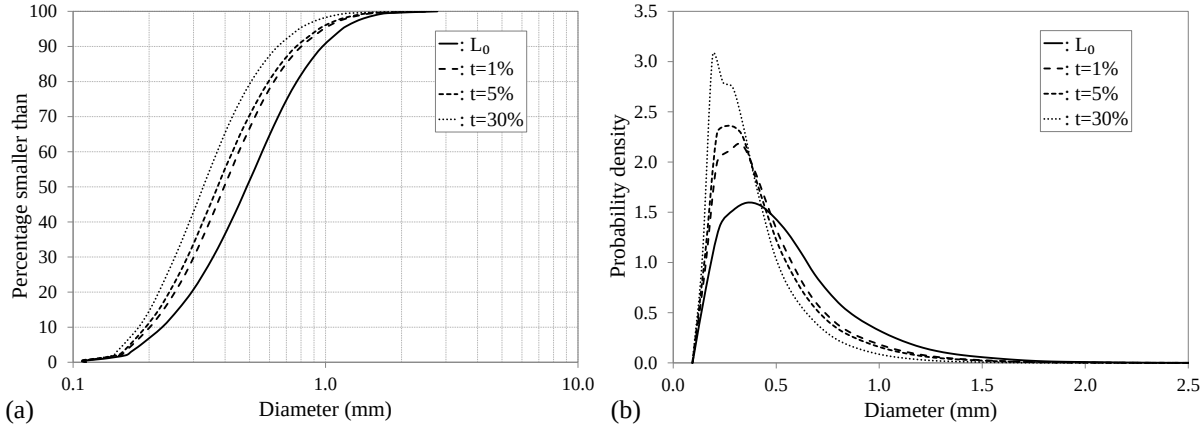

Figure 15: **(a)**: CSDs for the GGL sample; **(b)**: underlying probability density function of the constriction diameter for different merging steps associated to the pore separation technique

5.3 Discussion

It has been proven in a previous study involving UGL sample that the initial L_0 CSDs derived from the Delaunay and the Voronoï methods are almost congruent [44]. Herein, the proof is also given for the studied GGL sample (Fig. 16) even if it was expected.

The two different merge approaches are based on completely different techniques: overlapping spheres in a local manner and the pore separation in a hierarchical sense. This may lead to different merge behavior.

The overlapping inscribed void spheres approach implies a criterion based on the distance between the centers of adjacent pores which seems to be more reasonable according to Al-Raoush et al. [1] where neighboring pores are merged if the center of an inscribed void sphere lies within the adjacent inscribed void sphere. In fact, a statistical study over all tuples (P_i, C_{ij}, P_j) shows that more than 50% of overlap cases fulfil Al-Raoush et al. criterion and thus correspond to highly interconnected pores.

The separation technique evaluates the importance of the distance maxima and minima along the Voronoï graph: it fuses local pores that are insignificantly separated to their next larger pore, then evaluates the remaining more important pores among each other building up a hierarchy. That way, it detects significant constrictions and stops merging there for a given hierarchy level, which depends on a user-defined threshold.

For each material, the relative error between the CSDs derived from different merging criteria is calculated and given in Table 5 and Table 6. For UG material, the correspondence between the two merging techniques, previously found for the pore distribution, hold true for the CSD (L_1 and $t = 2\%$; L_2 and $t = 5\%$) (Tab. 5). For GGL sample, Table 6 indicates that the resulting CSDs provided by L_1 and L_2 are closer to those derived from $t = 1\%$ and $t = 4\%$ respectively. Furthermore, one can note that, for the densest state, the CSD associated to L_1 and that corresponding to $t = 2\%$ are approximately similar and it seems that a threshold value of 5% is more suitable to predict L_2. Nevertheless, satisfactory results can be obtained between $t = 1\%$ and $t = 2\%$ for L_1, and over the range of $4-6\%$ for L_2. More precisely, and irrespectively of density and grading, a threshold of about 2% (5% respectively) can be considered suitable to predict the pore and constriction size distributions corresponding to L_1 (L_2 respectively).

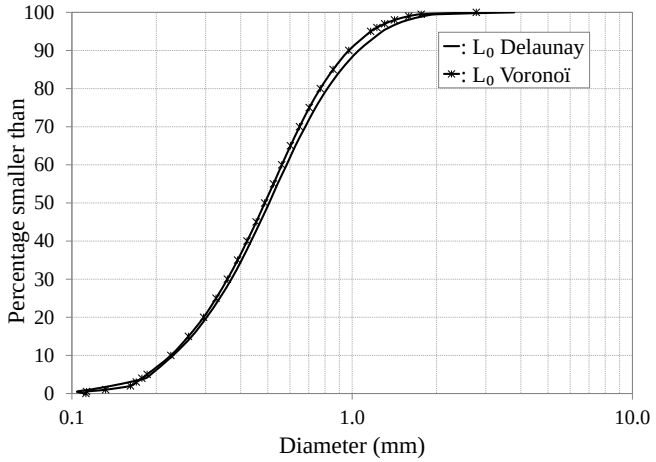

Figure 16: Initial CSD derived from Delaunay and Voronoï approaches for GGL sample

Table 5: Relative error (in %) between the CSD derived from different merging criteria for UG

	$t(\%)$	1	2	3	4	5	6
UGL	L_1	1.4	1.2	1.7	2.3	3.0	3.7
	L_2	4.2	3.1	2.4	1.8	1.4	1.5
UGD	L_1	2.2	2.0	2.3	3.2	4.0	4.8
	L_2	4.8	3.5	2.8	2.0	1.7	1.9

Table 6: Relative error (in %) between the CSD derived from different merging criteria for GG

	$t(\%)$	1	2	3	4	5	6
	$t(\%)$	1	2	3	4	5	6
GGL	L_1	2.1	2.1	2.6	3.0	3.6	4.0
	L_2	4.6	3.0	1.9	1.5	1.8	2.1
GGD	L_1	2.2	0.9	1.0	1.7	2.5	3.4
	L_2	4.6	2.9	1.7	0.9	0.8	1.5

6 Conclusion

In this paper, different void characteristics in packings of spheres are derived from a partition of the space. These characteristics are the distribution of the diameter of the void sphere having a volume equal to that of the pore, which characterizes the morphology of the void space, and the constriction size distribution which characterizes its topology. Since the usual Delaunay or Voronoï partitions may lead to an artificial over-segmentation of the pore space, two different techniques for merging local pores were studied and compared. These techniques, which lie on the computation of the inscribed void sphere associated to a local pore, are the overlapping void spheres technique and the pore separation technique.

In the overlapping void spheres approach, two criteria or levels are defined: a level 1 (L_1) where two direct neighboring local pores are merged if their respective inscribed void spheres are overlapping, and a second level (L_2), where the next neighboring local pores can also be merged with the two first ones to create a single pore in case of further overlapping of void inscribed spheres. The pore separation technique hierarchically evaluates the degree of separation indicated by the distance function of the void space for a given threshold t. To compare both approaches, different thresholds t were tested to show the impact of the merging criterion on the distribution of pore and constriction sizes.

Two materials were studied, one which can be considered as uniformly graded and another one which is widely graded but gap-graded, both in a loose or in a dense state. From a direct computation of pores and constrictions, L_1 merging induces the removal of about 40% of constrictions irrespective of the grading and of the density. L_2 level merging brings fewer new merging of local pores. In the pore separation technique, the removal of constrictions is important for small values of the threshold ($t \leq 1\%$) irrespective of grading and density, and the rate of removal of further constrictions tends to decrease as t increases.

In the case of the uniformly graded material, merging tends to remove the larger constrictions and lets appear a clear single mode for the distributions of constriction sizes. In the case of the studied gap-graded material, two close modes are obtained after merging which is just typical of the studied grading. The same trend is observed with the pore separation technique while t is equal or smaller than 5%. For larger threshold values, the constriction size corresponding to the mode tends to shift to the smaller diameters.

A correspondence is found between the two merging techniques irrespective of the considered void characteristics, pores or constrictions, the grading and the density. L_1 merging corresponds to a thresh-

old of about 2% and L_2 to a threshold of about 5%. It can serve as a guide for a user for the definition of pores at a meso scale even if a definite pore structure cannot be obtained due to subjective nature of these bodies.

Acknowledgements: Part of this work belongs to a project funded by *Compagnie Nationale du Rhône* (CNR). F. Seblany and E. Vincens acknowledge CNR for its interest and its financial support.

References

[1] R. Al-Raoush, K. Thompson, and C.S. Willson. Comparison of network generation techniques for unconsolidated porous media. *Soil Science Society of America Journal*, 67(6):1687–1700, 2003.

[2] M.P. Allen and M.R. Wilson. Computer simulation of liquid crystals. *Journal of Computer-Aided Molecular Design*, 3(4):335–353, 1989.

[3] D. Barreto Gonzalez. *Numerical and experimental investigation into the behaviour of granular materials under generalised stress states*. PhD thesis, Imperial College London, 2010.

[4] N. Benahmed, J. Canou, and J.C. Dupla. Structure initiale et propriétés de liquéfaction statique d'un sable. *Comptes Rendus Mécanique*, 332(11):887–894, 2004.

[5] M.L. Bernhardt and G. Biscontin. Experimental validation study of 3D direct simple shear dem simulations. *Soils and Foundations*, 56(3):336–347, 2016.

[6] J. Biarez and P.Y. Hicher. Elementary mechanics of soil behaviour, classification of and correlations between parameters. pages 81–106. AA Balkema: Rotterdam, 1994.

[7] S.L. Bryant, P.R. King, and D.W. Mellor. Network model evaluation of permeability and spatial correlation in a real random sphere packing. *Transport in Porous Media*, 11(1):53–70, 1993.

[8] B. Chareyre, A. Cortis, E. Catalano, and E. Barthélemy. Pore-scale modeling of viscous flow and induced forces in dense sphere packings. *Transport in Porous Media*, 94(2):595–615, 2012.

[9] L. Cui and C. O'Sullivan. Analysis of a triangulation based approach for specimen generation for discrete element simulations. *Granular Matter*, 5(3):135–145, 2003.

[10] P.A. Cundall and O.D. Strack. A discrete numerical model for granular assemblies. *Geotechnique*, 29(1):47–65, 1979.

[11] H. Edelsbrunner and N.R. Shah. Incremental topological flipping works for regular triangulations. *Algorithmica*, 15(3):223–241, 1996.

[12] Y.T. Feng, K. Han, and D.R.J. Owen. Filling domains with disks: an advancing front approach. *International Journal for Numerical Methods in Engineering*, 56(5):699–713, 2003.

[13] S. Gao, J.N. Meegoda, and L. Hu. Two methods for pore network of porous media. *International Journal for Numerical and Analytical Methods in Geomechanics*, 36(18):1954–1970, 2012.

[14] A. Gervois, L. Oger, P. Richard, and J.P. Troadec. Voronoï and radical tessellations of packings of spheres. In *Proceedings of the International Conference on Computational Science*, pages 95–104. Springer, Berlin, 2002.

[15] H. Giesche. Mercury porosimetry: a general (practical) overview. *Particle & particle systems characterization*, 23(1):9–19, 2006.

[16] M. Gladkikh and S. Bryant. Prediction of imbibition in unconsolidated granular materials. *Journal of Colloid and Interface Science*, 288(2):526–539, 2005.

[17] U. Homberg, D. Baum, S. Prohaska, U. Kalbe, and K.J. Witt. Automatic extraction and analysis of realistic pore structures from μCT data for pore space characterization of graded soil. In *Proceedings of the 6th International Conference Scour and Erosion (ICSE-6)*, pages 66–73, 2012.

[18] U. Homberg, D. Baum, A. Wiebel, S. Prohaska, and H.C. Hege. Definition, extraction, and validation of pore structures in porous materials. In *Bremer, P.T. and Hotz, I. and Pascucci, V. and Peikert, R. (eds.) Topological methods in data analysis and visualization III*, pages 235–248. Springer, Berlin, 2014.

[19] T. Kenney, R. Chahal, E. Chiu, G. Ofoegbu, G. Omange, and C. Ume. Controlling constriction sizes of granular filters. *Canadian Geotechnical Journal*, 22(1):32–43, 1985.

[20] N. Lindow, D. Baum, and H.C. Hege. Voronoï-based extraction and visualization of molecular paths. *IEEE Transactions on Visualization and Computer Graphics*, 17(12):2025–2034, 2011.

[21] M. Locke and B. Indraratna. A new model for the behaviour of granular filters. In *Proceedings of the Fourth Australia New Zealand Young Geotechnical Professionals Conference*, pages 147–151. University of Western Australia, 2001.

[22] M. Locke, B. Indraratna, and G. Adikari. Time-dependent particle transport through granular filters. *Journal of Geotechnical and Geoenvironmental Engineering*, 127(6):521–529, 2001.

[23] G. Mason and D.W. Mellor. Simulation of drainage and imbibition in a random packing of equal spheres. *Journal of Colloid and Interface Science*, 176(1):214–225, 1995.

[24] D.W. Mellor. *Random close packing (RCP) of equal spheres: structure and implications for use as a model porous medium*. PhD thesis, Open University, 1989.

[25] H. Niederreiter. Low-discrepancy and low-dispersion sequences. *Journal of Number Theory*, 30(1):51–70, 1988.

[26] C. O'Sullivan, J. Bluthé, K. Sejpar, T. Shire, and L.Y.G. Cheung. Contact based void partitioning to assess filtration properties in dem simulations. *Computers and Geotechnics*, 64:120–131, 2015.

[27] F. Radjai and C. Voivret. Periodic boundary conditions. In *Radjai, F. and Dubois, F. (eds.) Discrete Numerical Modeling of Granular Materials*, pages 181–198. Wiley-ISTE, 2011.

[28] N. Reboul, E. Vincens, and B. Cambou. A statistical analysis of void size distribution in a simulated narrowly graded packing of spheres. *Granular Matter*, 10(6):457–468, 2008.

[29] N. Reboul, E. Vincens, and B. Cambou. A computational procedure to assess the distribution of constriction sizes for an assembly of spheres. *Computers and Geotechnics*, 37(1):195–206, 2010.

[30] P. Richard, L. Oger, J.P. Troadec, and A. Gervois. Tessellation of binary assemblies of spheres. *Physica A: Statistical Mechanics and its Applications*, 259(1):205–221, 1998.

[31] J.N. Roux and F. Chevoir. Simulation numérique discrete et comportement mécanique des matériaux granulaires. *Bulletin des Laboratoires des Ponts et Chaussées*, 254:pp–109, 2005.

[32] U. Schuler. Scattering of the composition of soils. an aspect for the stability of granular filters. In *Proceedings of Geofilters*, volume 96, pages 21–34, 1996.

[33] F. Seblany, U. Homberg, E. Vincens, P. Winkler, and K.J. Witt. Merging criteria for the definition of a local pore and the CSD computation of granular materials. In *Proceedings of the 25th Annual Meeting of the European Working Group on Internal Erosion in Embankment Dams and their Foundations*, pages 150–159, 2017.

[34] T. Shire and C. O'Sullivan. A network model to assess base-filter combinations. *Computers and Geotechnics*, 84:117–128, 2017.

[35] A. Silveira. An analysis of the problem of washing through in protective filters. In *Proceedings of the 6th International Conference on Soil Mechanics and Foundation Engineering, Montréal, Que*, pages 551–555, 1965.

[36] A. Silveira, T. de Lorena Peixoto, and J. Nogueira. On void size distribution of granular materials. In *Proceedings of the 5th Pan American Conference on Soil Mechanics and Foundation Engineering, Buenos Aires*, pages 161–177, 1975.

[37] T. Sitharam, S.V. Dinesh, and N. Shimizu. Micromechanical modelling of monotonic drained and undrained shear behaviour of granular media using three-dimensional dem. *International Journal for Numerical and Analytical methods in Geomechanics*, 26(12):1167–1189, 2002.

[38] J. Sjah and E. Vincens. Determination of the constriction size distribution of granular filters by filtration tests. *International Journal for Numerical and Analytical Methods in Geomechanics*, 37(10):1231–1246, 2013.

[39] V. Šmilauer, E. Catalano, B. Chareyre, S. Dorofeenko, J. Duriez, A. Gladky, J. Kozicki, C. Modenese, L. Scholtès, L. Sibille, et al. *Yade reference documentation*. http://yadedem. org/doc/, 2010.

[40] M. Soria, R. Aramaki, and E. Viviani. Experimental determination of void size curves. In *Brauns, J. and Heibaum, M. and Schuler, U. (eds.) Filters in Geotechnical and Hydraulic Engineering*, pages 43–48. Balkema, Rotterdam, 1993.

[41] A. Sufian, A.R. Russell, A.J. Whittle, and M. Saadatfar. Pore shapes, volume distribution and orientations in monodisperse granular assemblies. *Granular Matter*, 17(6):727–742, 2015.

[42] M. Thommes. Physical adsorption characterization of nanoporous materials. *Chemie Ingenieur Technik*, 82(7):1059–1073, 2010.

[43] C. Thornton. Numerical simulations of deviatoric shear deformation of granular media. *Géotechnique*, 50(1):43–53, 2000.

[44] E. Vincens, K.J. Witt, and U. Homberg. Approaches to determine the constriction size distribution for understanding filtration phenomena in granular materials. *Acta Geotechnica*, 10(3):291–303, 2015.

[45] H.J. Vogel and K. Roth. Quantitative morphology and network representation of soil pore structure. *Advances in Water Resources*, 24(3):233–242, 2001.

[46] K.J. Witt. *Filtrationsverhalten und bemessung von erdstoff-filtern*, volume 104. Institut für Bodenmechanik und Felsmechanik der Universität Fridericiana, Karlsruhe, 1986.

[47] R.Y. Yang, R.P. Zou, and A.B. Yu. Voronoi tessellation of the packing of fine uniform spheres. *Physical Review E*, 65(4):041302, 2002.

[48] R.Y. Yang, R.P. Zou, A.B. Yu, and S.K. Choi. Pore structure of the packing of fine particles. *Journal of Colloid and Interface Science*, 299(2):719–725, 2006.

[49] Z.P. Zhang, L.F. Liu, Y.D. Yuan, and A.B. Yu. A simulation study of the effects of dynamic variables on the packing of spheres. *Powder Technology*, 116(1):23–32, 2001.

Résumé étendu en Français

1. Contexte Général

L'érosion interne est l'une des principales causes d'instabilité et de ruptures des ouvrages hydrauliques en terre (digue, levée, barrage). Elle correspond à des phénomènes d'arrachement et de transport des particules, au sein d'un matériau granulaire, sous l'action d'un écoulement parasite qui le traverse. Les désordres constatés sur des ouvrages existants soulignent la nécessité d'une meilleure compréhension des phénomènes qui régissent l'érosion interne.

Pour empêcher ces phénomènes de se propager excessivement, les ouvrages hydrauliques peuvent être protégés par des couches de transition ou des filtres installés dans le corps de l'ouvrage en phase de conception ou sous la forme de recharge en réparation.

Pour accomplir son rôle avec succès, un filtre doit être caractérisé par une granulométrie appropriée pour retenir les particules de sol d'une part, et pour maintenir une bonne perméabilité d'autre part.

En d'autres termes, si les ouvertures de filtre sont trop fines, toutes les particules érodées se retrouveront bloquées à l'interface pouvant générer ainsi de fortes pressions interstitielles et un claquage hydraulique. De même, si les ouvertures de filtre sont trop importantes, toutes les particules érodées traverseront le filtre qui ne jouera plus son rôle. Un filtre effectif doit donc laisser passer en partie la fraction la plus fine des particules érodées mais piéger les plus grosses. Les particules ainsi piégées dans le réseau des pores forment progressivement une interface stable contribuant au processus de filtration des particules plus fines. Ce phénomène se réfère à l'auto-filtration.

En s'appuyant sur une campagne d'essais expérimentaux, Terzaghi et al. (1996) a proposé des règles granulométriques pour guider la mise en œuvre des filtres dans les ouvrages hydrauliques. Suivant ces règles, la couche de transition doit être assez fine pour éviter l'érosion de la couche filtrante tout en restant suffisamment perméable.

Par la suite, de nombreuses études empiriques et expérimentales ont été menées afin d'évaluer l'efficacité de ces critères. En effet, les expériences de Terzaghi ont été effectuées sur des matériaux de granulométrie uniforme, leur validité est supposée ainsi être restreinte à des sols ayant des coefficients d'uniformité plutôt faibles.

La filtration dans un matériau granulaire est contrôlée par les resserrements connectant les différents pores, aussi appelées constrictions. En fait, si une particule traversant un pore est plus grosse que toutes les constrictions permettant de sortir de ce pore, elle y reste piégée indépendam-

ment de la valeur du gradient hydraulique imposé (dans la mesure où celui-ci ne déstructure pas tout le matériau).

Aussi, de nouveaux critères s'appuyant sur la distribution des tailles de constriction (CSD) ont été proposés par le passé (Indraratna et al., 2007). Ces critères permettent de s'affranchir des problèmes liés au coefficient d'uniformité du matériau et du fait que la plupart des règles empiriques ont été obtenues sur des matériaux denses.

Ces recherches se sont appuyées sur une volonté de mieux comprendre et décrire les phénomènes en jeu dans l'espace poral lors du processus de filtration.

Les études expérimentales permettant de définir la CSD pour un matériau granulaire sont généralement difficiles à mettre en œuvre. Les techniques de tomographie récentes peuvent constituer un moyen performant de visualisation de la morphologie de l'espace poral et peuvent être appliquées à tout type de matériaux. Cependant, elles nécessitent d'être combinées avec des algorithmes appropriés de traitement d'images pour aboutir à une quantification de cet espace. Ainsi, les méthodes analytiques semblent être une alternative intéressante pour obtenir la CSD à partir de variables facilement mesurables (granulométrie du matériau et densité), suivant une approche géométrique simplifiée qui doit être validée sur des cas bien documentés. Dans ce cadre, la méthode aux éléments discrets (DEM), introduite par Cundall and Strack (1979) permet de modéliser finement les matériaux granulaires. Des outils de partition de l'espace poral sont alors indispensables pour obtenir la CSD, mais ces techniques peuvent être sources d'artefacts qu'il faut savoir repérer et éliminer.

Ce travail s'appuie ainsi principalement sur une approche numérique basée sur DEM pour contribuer à une meilleure connaissance de l'espace poral de matériaux granulaires sphériques et une meilleure validation de critères de filtre associés à ces matériaux.

2. Objectifs

La recherche d'un critère de filtre basé sur la CSD et adapté pour différents types de sols granulaires (granulométrie, densité) constituera ainsi l'objectif principal de ce travail. Pour y parvenir, des approches numériques et analytiques sont envisagées:

- Une modélisation numérique (DEM) permettra de mieux contrôler les caractéristiques porales de milieux granulaires modèles. Des échantillons constitués des assemblages de sphères ayant différentes granulométries et différents états de densité seront générés.
- Une méthode de caractérisation de l'espace poral sera proposée pour obtenir une représentation plus précise des pores et de la CSD.
- Les modèles analytiques existants pour estimer la CSD seront testés et révisés sur la base d'une partition pertinente de l'espace poral.
- Des essais numériques de filtration seront menés pour corréler la topologie de l'espace poral, plus précisément la CSD d'un filtre granulaire, aux phénomènes de transport des particules à travers ce filtre.

- Un critère de filtre fondé sur la CSD sera proposé et validé sur la base des résultats expérimentaux rapportés dans la littérature.

3. Démarches et contributions

La méthodologie, les démarches suivies et les principales contributions de ce travail, sont explicitées ci-après.

Une attention particulière est premièrement accordée au processus de création de l'échantillon numérique qui peut influencer l'organisation de l'assemblage granulaire à l'échelle microscopique. Dans cette étude, les échantillons numériques de matériaux granulaires ont été générés par dépôt sous gravité des particules. Cette méthode est bien adaptée pour simuler le processus de mise en place des filtres dans les ouvrages hydrauliques.

La plupart des études numériques se concentrent sur des assemblages sphériques monodisperses, sur des granulométries continues et sur l'état le plus dense. Ici, les matériaux étudiés correspondent à des granulométries variées: granulométrie serrée, étalée et lacunaires, avec des coefficients d'uniformité allant de 1.7 à 6. Deux états de densité seront envisagés (lâche et dense).

Afin de caractériser la morphologie et la topologie de l'espace des vides au sein des assemblages numériques de sphères, une subdivision du milieu en tétraèdres, par une partition de Delaunay, est mise en place, permettant ainsi d'obtenir des tailles caractéristiques des pores (sphère maximale inscrite dans le pore, sphère ayant un volume équivalent à celui du vide au sein d'un tétraèdre) et des constrictions (le plus grand disque contenu dans l'espace des vides sur les faces des tétraèdres) en accord avec les travaux de Reboul et al. (2008).

La partition de Delaunay engendre une segmentation de l'espace poral en volumes élémentaires en accord avec son schéma mathématique interne; cette partition peut donc être qualifiée d'artificielle (Al-Raoush et al., 2003). Par la suite, ce schéma peut introduire une subdivision abusive de l'espace poral.

Pour affronter ce problème, une association des tétraèdres voisins selon des critères basés sur le chevauchement de leurs sphères inscrites de vide est construite. Plusieurs niveaux de fusion sont ainsi proposés à la lumière des travaux de Reboul et al. (2008). Un niveau de fusion primaire ($L_0{}'$) est introduit pour éliminer les constrictions résultantes des artefacts géométriques de segmentation.

Le choix d'un critère de fusion des pores peut influer de façon déterminante sur la distribution des tailles des pores et des constrictions. Une attention particulière est alors accordée à l'implication de ces critères sur les caractéristiques de l'espace poral. Dans ce contexte, le critère L_1 conduit à l'élimination d'environ 30% des constrictions par rapport à L_0 indépendamment de la densité et de la granulométrie et du matériau étudié. L_1 tend à éliminer un second mode parasite de la distribution des tailles de constriction et laisse apparaitre clairement le premier mode pour tous les matériaux étudiés à l'exception de GG1 (un matériau à granulométrie lacunaire) qui présente une distribution bimodale des tailles de constriction qui semble porter un sens physique. Une étude comparative de plusieurs granulométries lacunaires a montré que ce caractère bimodal est lié à une proportion importante des particules grossières. Enfin, ces résultats ne montrent pas de

différences importantes entre le critère fusion L_1 et L_2 qui est plus sophistiqué.

Il est illusoire de vouloir définir une CSD unique car le contour d'un pore est par définition incertain. Nous avons donc proposé une technique de calcul raisonnable où le critère de fusion L_1 semble permettre de délimiter, de manière satisfaisante et à l'échelle mésoscopique, les frontières géométriques des pores dans des assemblages sphériques.

En outre, une étude de l'influence de la granulométrie et de l'état de densité du filtre sur les distributions des tailles des pores et des constrictions a été menée. Les résultats permettent de valider ceux obtenus par Reboul et al. (2008) sur une granulométrie uniforme.

Certains modèles analytiques permettant d'obtenir rapidement la CSD existent dans la littérature (Locke et al., 2001; Reboul et al., 2010). Ils nécessitent la seule connaissance de la courbe granulométrique et de la densité du matériau. Une comparaison entre la CSD obtenue à partir de ces approches analytiques et celle qui résulte de l'analyse des échantillons numériques a permet d'ajuster ces modèles de façon à obtenir une CSD plus réaliste (CSD L_1). Plus précisément, trois conclusions ont été établies:

- La CSD (L_0) de l'état lâche résulte directement de la formule proposée par Locke et al. (2001).
- Le modèle à 1-paramètre proposé par Reboul et al. (2010) permet d'obtenir des résultats satisfaisants (CSD dense L_0) même pour les granulométries discontinues. Ce qui permet d'éviter l'utilisation du modèle à 2-paramètres proposé par ces auteurs et dont la procédure d'établissement est difficilement généralisable.
- Un facteur correctif doit être introduit dans le modèle à 1-paramètre pour reproduire la CSD (L_1).

Dans un deuxième temps, des études ont été menées sur les processus de filtration. Lié à ce phénomène, une formule a été proposée pour estimer le diamètre de pore moyen à partir des données statistiques obtenues sur les échantillons numériques. Plusieurs estimations de cette caractéristique de l'espace poral ont été proposées dans la littérature et sont incorporées dans les approches probabilistes pour estimer la distance parcourue par une particule fine dans un matériau granulaire.

Des essais numériques de filtration ont été réalisés pour établir une relation claire entre le transport des particules fines à travers un milieu granulaire et la CSD. Les essais sous gravité ont mis en évidence une taille critique à partir de laquelle la probabilité d'une particule à traverser la totalité de l'échantillon évolue rapidement. Cette taille critique correspond au plus large mode de la distribution des tailles de constriction (L_1) attribuant ainsi un sens physique à ce critère de fusion des pores. A noter que cette taille critique correspond au fractile 35% de la CSD (L_1) indépendamment de la granulométrie et de la densité du matériau.

D'autre part, cette taille critique a été comparée avec les valeurs des diamètres d'ouverture de contrôle relevées dans la littérature. Un bon accord a été trouvé avec le diamètre d'ouverture de contrôle rapporté dans l'étude expérimentale de Witt (1993).

Cependant, les essais de filtration hydrauliques ont montré que le flux réoriente les particules fines vers les chemins de filtration les plus larges, ce qui permet de parcourir une distance plus

importante. Dans ce cas, le mode est moins corrélé à la taille d'ouverture de contrôle du filtre granulaire.

Une formule analytique est ensuite proposée pour calculer rapidement cette taille caractéristique du matériau granulaire. Une validation a été réalisée sur des valeurs expérimentales.

Ce diamètre d'ouverture de contrôle est ensuite incorporé dans un critère de filtre basé sur la CSD, $d_{85SA} \geq d_{OS}$. Le critère proposé reproduit correctement des résultats expérimentaux rapportés dans la littérature.

Ainsi, le critère proposé offre une explication plausible concernant le choix de la taille représentative de l'ouverture du filtre et bien que proche du critère proposé par Indraratna et al. (2007) donne un éclairage plus rigoureux de sa construction.

4. Perspectives

Une des problématiques actuelles consiste à tenir compte de la complexité morphologique des particules composant les sols granulaires réels, qui s'éloignent souvent de la forme sphérique traditionnellement utilisée en DEM. Des travaux de recherche sont en cours afin de modéliser des assemblages de particules polyédriques, et d'évaluer l'influence de l'anisotropie induite par la forme irrégulière des particules sur la CSD et sur les chemins de filtration.

Une collaboration avec *Zuse Institute Berlin* est prévue afin d'obtenir la CSD de ces assemblages polyédriques. La méthode utilisée pour aboutir à la CSD s'appuie successivement sur une voxelisation de l'espace des vides, un post-traitement basé sur la méthode de l'axe médian pour obtenir une première morphologie et topologie de l'espace des vides et une technique de fusion des pores qui associe les pores voisins suivant le degré de séparation de leur constriction (Homberg et al., 2012).

Dans un article antérieur commun (Seblany et al., 2018), nous avons établi, dans le cas des assemblages sphériques, une correspondance entre les critères associés à différentes techniques de fusion des pores, qui pourra être utilisée comme un guide pour ces prochaines études.

Ce travail permet d'ouvrir d'intéressantes perspectives de recherche. Les formules analytiques et le critère de filtre proposés dans le cas des particules sphériques peuvent être réévalués pour s'adapter aux particules polyédriques allongées.

References

Abdelhamid, Y. and El Shamy, U. (2015). Pore-scale modeling of fine-particle migration in granular filters. *International Journal of Geomechanics*, 16(3):04015086.

Al-Kharusi, A. S. and Blunt, M. J. (2007). Network extraction from sandstone and carbonate pore space images. *Journal of Petroleum Science and Engineering*, 56(4):219–231.

Al-Raoush, R. and Papadopoulos, A. (2010). Representative elementary volume analysis of porous media using x-ray computed tomography. *Powder technology*, 200(1-2):69–77.

Al-Raoush, R., Thompson, K., and Willson, C. S. (2003). Comparison of network generation techniques for unconsolidated porous media. *Soil Science Society of America Journal*, 67(6):1687–1700.

Allen, M. P. and Wilson, M. R. (1989). Computer simulation of liquid crystals. *Journal of Computer-Aided Molecular Design*, 3(4):335–353.

Arand, F. and Hesser, J. (2017). Accurate and efficient maximal ball algorithm for pore network extraction. *Computers & Geosciences*, 101:28–37.

Aste, T., Saadatfar, M., and Senden, T. (2005). Geometrical structure of disordered sphere packings. *Physical review E*, 71(6):061302.

Babu, G. L. S. and Srivastava, A. (2007). A procedure for the design of protective filters. *Canadian Geotechnical Journal*, 44(4):490–495.

Barreto Gonzalez, D. (2010). *Numerical and experimental investigation into the behaviour of granular materials under generalised stress states*. PhD thesis, Imperial College London.

Benahmed, N., Canou, J., and Dupla, J. C. (2004). Structure initiale et propriétés de liquéfaction statique d'un sable. *Comptes Rendus Mécanique*, 332(11):887–894.

Bernhardt, M. L., Biscontin, G., and O'Sullivan, C. (2016). Experimental validation study of 3D direct simple shear dem simulations. *Soils and Foundations*, 56(3):336–347.

Biarez, J. and Hicher, P. Y. (1994). Elementary mechanics of soil behaviour, classification of and correlations between parameters. pages 81–106. AA Balkema: Rotterdam.

Bryant, S. L., King, P. R., and Mellor, D. W. (1993). Network model evaluation of permeability and spatial correlation in a real random sphere packing. *Transport in Porous Media*, 11(1):53–70.

Burenkova, V. (1993). Assessment of suffusion in non-cohesive and graded soils. *Filters in geotechnical and hydraulic engineering. Balkema, Rotterdam*, pages 357–360.

Catalano, E., Chareyre, B., and Barthélemy, E. (2014). Pore-scale modeling of fluid-particles interaction and emerging poromechanical effects. *International Journal for Numerical and Analytical Methods in Geomechanics*, 38(1):51–71.

CGAL (2010). Computational geometry algorithms library, 2011. *URL http://www. cgal. org*.

Chang, D. S. and Zhang, L. M. (2013). Extended internal stability criteria for soils under seepage. *Soils and Foundations*, 53(4):569–583.

Chapuis, R. P. (2012). Predicting the saturated hydraulic conductivity of soils: a review. *Bulletin of Engineering Geology and the Environment*, 71(3):401–434.

Chareyre, B., Cortis, A., Catalano, E., and Barthélemy, E. (2012). Pore-scale modeling of viscous flow and induced forces in dense sphere packings. *Transport in Porous Media*, 94(2):595–615.

Cnudde, V. and Boone, M. N. (2013). High-resolution X-ray computed tomography in geosciences: A review of the current technology and applications. *Earth-Science Reviews*, 123:1–17.

Cui, L. and O'Sullivan, C. (2003). Analysis of a triangulation based approach for specimen generation for discrete element simulations. *Granular Matter*, 5(3):135–145.

Cundall, P. (1988). Computer simulations of dense sphere assemblies. In *Studies in Applied Mechanics*, volume 20, pages 113–123. Elsevier.

Cundall, P. A. and Strack, O. D. (1979). A discrete numerical model for granular assemblies. *Geotechnique*, 29(1):47–65.

De Mello, V. F. (1977). Reflections on design decisions of practical significance to embankment dams. *Géotechnique*, 27(3):281–355.

Delaney, G. W., Di Matteo, T., and Aste, T. (2010). Combining tomographic imaging and dem simulations to investigate the structure of experimental sphere packings. *Soft Matter*, 6(13):2992–3006.

Delgado, F., Huber, N., Escuder, I., and De Membrillera, M. (2006). Revised criteria for evaluating granular filters in earth and rockfill dams. In *Transactions of the International Congress on Large Dams*, volume 22, page 445.

Dong, H. (2008). *Micro-CT imaging and pore network extraction*. PhD thesis, Department of Earth Science and Engineering, Imperial College London.

Dong, H. and Blunt, M. J. (2009). Pore-network extraction from micro-computerized-tomography images. *Physical Review E*, 80(3):036307.

Dullien, F. A. (1992). *Porous media: fluid transport and pore structure*. 2nd edn, Academic press, New York.

Edelsbrunner, H. and Shah, N. R. (1996). Incremental topological flipping works for regular triangulations. *Algorithmica*, 15(3):223–241.

Eliáš, J. (2014). Simulation of railway ballast using crushable polyhedral particles. *Powder Technology*, 264:458–465.

Elsharief, A. (1992). *Effects of the structural properties of non-woven geotextiles on their filtration behavior*. PhD thesis, Ph. D. Thesis, School of Civil Engineering, Purdue University, West Lafayette, IN, USA.

Fell, R. and Fry, J. J. (2007). *Internal Erosion of Dams and Their Foundations: Selected Papers from the Workshop on Internal Erosion and Piping of Dams and Their Foundations, Aussois, France, 25-27 April 2005*. Taylor & Francis Group.

Fell, R. and Fry, J. J. (2013). State of the art on the likelihood of internal erosion of dams and levees by means of testing. In *S. Bonelli (eds.) Erosion in geomechanics applied to dams and levees, Chapter 1*, pages 1–99. London, UK: ISTE-Wiley.

Fell, R., Wan, C. F., Cyganiewicz, J., and Foster, M. (2003). Time for development of internal erosion and piping in embankment dams. *Journal of geotechnical and geoenvironmental engineering*, 129(4):307–314.

Feng, Y., Han, K., and Owen, D. (2003). Filling domains with disks: an advancing front approach. *International Journal for Numerical Methods in Engineering*, 56(5):699–713.

Foster, M. and Fell, R. (2001). Assessing embankment dam filters that do not satisfy design criteria. *Journal of Geotechnical and Geoenvironmental Engineering*, 127(5):398–407.

Foster, M., Fell, R., and Spannagle, M. (1998). Analysis of embankment dam incidents. Report UNICIV No. *R-374, University of New South Wales, Sydney, Australia*.

Fread, D. (1988). *BREACH, an erosion model for earthen dam failures*. Hydrologic Research Laboratory, National Weather Service, NOAA.

Fry, J. (2012). Introduction to the process of internal erosion in hydraulic structures: embankment dams and dikes. In *S. Bonelli (eds.) Erosion of geomaterials, Chapter 1*, pages 1–37. London, UK: ISTE-Wiley.

Fry, J.-J., François, D., Marot, D., Bonelli, S., Royet, P., Chevalier, C., and Deroo, L. (2015). Etude de l'érosion interne: apport du projet eniroh. In *Vingt-cinquième congrès des Grands Barrages*, pages 486–507.

Fuller, W. B. and Thompson, S. E. (1907). The laws of proportioning concrete.

Gao, S., Meegoda, J. N., and Hu, L. (2012). Two methods for pore network of porous media. *International Journal for Numerical and Analytical Methods in Geomechanics*, 36(18):1954–1970.

Garner, S. and Fannin, R. (2010). Understanding internal erosion: a decade of research following a sinkhole event. *The international journal on hydropower & dams*, 17(3):93.

Gervois, A., Oger, L., Richard, P., and Troadec, J. P. (2002). Voronoï and radical tessellations of packings of spheres. In *Proceedings of the International Conference on Computational Science*, pages 95–104. Springer, Berlin.

Ghanizadeh, A., Clarkson, C., Aquino, S., Ardakani, O., and Sanei, H. (2015). Petrophysical and geomechanical characteristics of canadian tight oil and liquid-rich gas reservoirs: I. pore network and permeability characterization. *Fuel*, 153:664–681.

Ghidaglia, C., de Arcangelis, L., Hinch, J., and Guazzelli, É. (1996). Transition in particle capture in deep bed filtration. *Physical Review E*, 53(4):R3028.

Giesche, H. (2006). Mercury porosimetry: a general (practical) overview. *Particle & particle systems characterization*, 23(1):9–19.

Giroud, J. (1996). Granular filters and geotextile filters. In *Proceedings of Geofilters*, volume 96, pages 565–680.

Giroud, J. (2010). Development of criteria for geotextile and granular filters. In *Proceedings of the 9th International Conference on Geosynthetics, Guarujá, Brazil*, pages 23–27.

Giroud, J. P. (1982). Filter criteria for geotextiles. In *Proceedings of the Second International Conference on Geotextiles*, volume 1, pages 103–108. Industrial Fabrics Association International St Paul, MN.

Giroud, J. P. (1988). Review of geotextile filter criteria. In *Proceedings of the 1st Indian Geotextiles Conference on Reinforced Soil and Geotextiles, Bombay, India*, pages 1–6.

Gladkikh, M. and Bryant, S. (2005). Prediction of imbibition in unconsolidated granular materials. *Journal of Colloid and Interface Science*, 288(2):526–539.

Goltz, M., Etzer, T., Aufleger, M., and Muckenthaler, P. (2009). Assessing the critical seepage velocity causing transport of fine particles in embankment dams and their foundation. In *Proceedings of Long Term Behavior of Dams 2nd International Conference. Graz, Austria*, pages 479–484.

Gueven, I., Frijters, S., Harting, J., Luding, S., and Steeb, H. (2017). Hydraulic properties of porous sintered glass bead systems. *Granular matter*, 19(2):28.

Homberg, U., Baum, D., Prohaska, S., Kalbe, U., and Witt, K. J. (2012). Automatic extraction and analysis of realistic pore structures from μCT data for pore space characterization of graded soil. In *Proceedings of the 6th International Conference Scour and Erosion (ICSE-6)*, pages 66–73.

Homberg, U., Baum, D., Wiebel, A., Prohaska, S., and Hege, H. C. (2014). Definition, extraction, and validation of pore structures in porous materials. In *Bremer, Peer Timo and Hotz,Ingrid and Pascucci, Valerio and Peikert, Ronald (eds.) Topological methods in data analysis and visualization III*, pages 235–248. Springer, Berlin.

Honjo, Y. and Veneziano, D. (1989). Improved filter criterion for cohesionless soils. *ournal of Geotechnical Engineering*, 115(1):75–94.

Humes, C., Lafleur, J., and Rollin, A. (1996). A new approach to compute the void size distribution curves of protective filters. In *Proceedings of Geofilters*, volume 96, pages 57–66.

ICOLD (2013). *Bulletin on Internal Erosion of Existing Dams, Levees and Dikes and their Foundations*, volume 1. International Commission on Large Dams.

Indraratna, B., Dilema, E., and Vafai, F. (1996). An experimental study of the filtration of a lateritic clay slurry by sand filters. *Proceedings of the Institution of Civil Engineers-Geotechnical Engineering*, 119(2):75–83.

Indraratna, B. and Locke, M. (1999). Design methods for granular filters—critical review. *Proceedings of the institution of civil engineers-geotechnical engineering*, 137(3):137–147.

Indraratna, B. and Locke, M. (2000). Analytical modeling and experimental verification of granular filter behaviour. In *Filters and Drainage in Geotechnical and Environmental Engineering (Wolski & Mtynarek (eds.)), Balkema, Rotterdam*, pages 3–26.

Indraratna, B. and Raut, A. K. (2006). Enhanced criterion for base soil retention in embankment dam filters. *Journal of Geotechnical and Geoenvironmental Engineering*, 132(12):1621–1627.

Indraratna, B., Raut, A. K., and Khabbaz, H. (2007). Constriction-based retention criterion for granular filter design. *Journal of Geotechnical and Geoenvironmental Engineering*, 133(3):266–276.

Indraratna, B., Trani, L. D. O., and Khabbaz, H. (2008). A critical review on granular dam filter behaviour – from particle sizes to constriction-based design criteria. *Geomechanics and Geoengineering: An International Journal*, 3(4):279–290.

Indraratna, B. and Vafai, F. (1997). Analytical model for particle migration within base soil-filter system. *Journal of Geotechnical and Geoenvironmental Engineering*, 123(2):100–109.

Istomina, V. (1957). Filtration stability of soils. *Gostroizdat, Moscow, Leningrad*, 15.

Jansen, R. B. (1983). *Dams and public safety: a water resources technical publication*. US Department of the Interior, Bureau of Reclamation.

Kenney, T., Chahal, R., Chiu, E., Ofoegbu, G., Omange, G., and Ume, C. (1985). Controlling constriction sizes of granular filters. *Canadian Geotechnical Journal*, 22(1):32–43.

Kenney, T. and Lau, D. (1985). Internal stability of granular filters. *Canadian Geotechnical Journal*, 22(2):215–225.

Kenney, T. and Lau, D. (1986). Internal stability of granular filters: Reply. *Canadian Geotechnical Journal*, 23(3):420–423.

Kerimov, A., Mavko, G., Mukerji, T., and Al Ibrahim, M. A. (2018a). Mechanical trapping of particles in granular media. *Physical Review E*, 97(2):022907.

Kerimov, A., Mavko, G., Mukerji, T., Dvorkin, J., and Al Ibrahim, M. A. (2018b). The influence of convex particles' irregular shape and varying size on porosity, permeability, and elastic bulk modulus of granular porous media: Insights from numerical simulations. *Journal of Geophysical Research: Solid Earth*.

Ketcham, R. A. and Carlson, W. D. (2001). Acquisition, optimization and interpretation of x-ray computed tomographic imagery: applications to the geosciences. *Computers & Geosciences*, 27(4):381–400.

Kézdi, A. (1979). Soil physics–selected topics–developments in geotechnical engineering–25. Technical report.

Koerner, G. and Koerner, R. (1992). Leachate flow rate behavior through geotextile and soil filters and possible remediation methods. *Geotextiles and Geomembranes*, 11(4-6):401–430.

Kwang, T. (1990). Improvement of dam filter criterion for cohesionless base soil. *MEng thesis, Asian Institute of Technology, Bangkok, Thailand*.

Lafleur, J. (1984). Filter testing of broadly graded cohesionless tills. *Canadian Geotechnical Journal*, 21(4):634–643.

Lafleur, J., Mlynarek, J., and Rollin, A. (1989). Filtration of broadly graded cohesionless soils. *Journal of Geotechnical Engineering*, 115(12):1747–1768.

Lafleur, J., Mlynarek, J., and Rollin, A. (1993). Filter criteria for well graded cohesionless soils. In *Braun J, Helbaum M, Schuler U (eds.) Filters in geotechnical and hydraulic engineering*, pages 97–106. Balkema, Rotterdam.

Li, M. and Fannin, R. J. (2008). Comparison of two criteria for internal stability of granular soil. *Canadian Geotechnical Journal*, 45(9):1303–1309.

Li, W., Vincens, E., Reboul, N., and Chareyre, B. (2014). Constrictions and filtration of fine particles in numerical granular filters: Influence of the fabric within the material. In *Proceedings of the 7th International Conference on Scour and Erosion, Perth, Australia, 2-4 December 2014*, page 241. CRC Press.

Li, Z., Wang, Y., Chow, J., Su, Z., and Li, X. (2018). 3D pore network extraction in granular media by unifying the delaunay tessellation and maximal ball methods. *Journal of Petroleum Science and Engineering*, 167:692–701.

Lindow, N., Baum, D., and Hege, H. C. (2011). Voronoï-based extraction and visualization of molecular paths. *IEEE Transactions on Visualization and Computer Graphics*, 17(12):2025–2034.

Liu, L., Zhang, Z., and Yu, A. (1999). Dynamic simulation of the centripetal packing of mono-sized spheres. *Physica A: Statistical Mechanics and its Applications*, 268(3-4):433–453.

Lochmann, K., Oger, L., and Stoyan, D. (2006). Statistical analysis of random sphere packings with variable radius distribution. *Solid State Sciences*, 8(12):1397–1413.

Locke, M. and Indraratna, B. (2001). A new model for the behaviour of granular filters. In *Proceedings of the Fourth Australia New Zealand Young Geotechnical Professionals Conference*, pages 147–151. University of Western Australia.

Locke, M., Indraratna, B., and Adikari, G. (2001). Time-dependent particle transport through granular filters. *Journal of Geotechnical and Geoenvironmental Engineering*, 127(6):521–529.

Locke, M. R. (2001). *Analytical and laboratory modelling of granular filters for embankment dams*. PhD thesis.

Logan, B. E., Hilbert, T. A., and Arnold, R. G. (1993). Removal of bacteria in laboratory filters: models and experiments. *Water Research*, 27(6):955–962.

Luettich, S., Giroud, J., and Bachus, R. (1992). Geotextile filter design guide. In *Geosynthetics in Filtration, Drainage and Erosion Control*, pages 19–34. Elsevier.

Marot, D., Bendahmane, F., and Nguyen, H. H. (2012). Influence of angularity of coarse fraction grains on internal erosion process. *La Houille Blanche*, (6):47–53.

Martin, M. J., Logan, B. E., Johnson, W. P., Jewett, D. G., and Arnold, R. G. (1996). Scaling bacterial filtration rates in different sized porous media. *Journal of Environmental Engineering*, 122(5):407–415.

Mason, G. and Mellor, D. W. (1995). Simulation of drainage and imbibition in a random packing of equal spheres. *Journal of Colloid and Interface Science*, 176(1):214–225.

McDowell-Boyer, L. M., Hunt, J. R., and Sitar, N. (1986). Particle transport through porous media. *Water Resources Research*, 22(13):1901–1921.

Moraci, N., Mandaglio, M., and Ielo, D. (2012). A new theoretical method to evaluate the internal stability of granular soils. *Canadian Geotechnical Journal*, 49:45–58.

Muresan, B., Saiyouri, N., and Hicher, P.-Y. (2012). Dynamic behavior of straining in randomly packed beads: Experimental study. *Journal of Environmental Engineering*, 139(5):692–702.

NRCS (1994). *Natural Resources Conservation Services "Gradation design of sand and gravel filters." Part 633 national engineering handbook, Chap. 26,*. U.S. Dept. of Agriculture, Washington, D.C.

O'Sullivan, C., Bluthé, J., Sejpar, K., Shire, T., and Cheung, L. Y. G. (2015). Contact based void partitioning to assess filtration properties in dem simulations. *Computers and Geotechnics*, 64:120–131.

Painter, S. L., Cvetkovic, V., and Pensado, O. (2008). Time-domain random-walk algorithms for simulating radionuclide transport in fractured porous rock. *Nuclear Technology*, 163(1):129–136.

Papamichos, E., Vardoulakis, I., Tronvoll, J., and Skjaerstein, A. (2001). Volumetric sand production model and experiment. *International journal for numerical and analytical methods in geomechanics*, 25(8):789–808.

Penberthy, W. and Shaughnessy, C. (1992). *Sand control*. Henry L. Doherty Memorial Fund of AIME, Society of Petroleum Engineers.

Rabbani, A., Jamshidi, S., and Salehi, S. (2014). An automated simple algorithm for realistic pore network extraction from micro-tomography images. *Journal of Petroleum Science and Engineering*, 123:164–171.

Radjai, F. and Voivret, C. (2011). Periodic boundary conditions. In *Radjai, F and Dubois, F, (eds.) Discrete Numerical Modeling of Granular Materials*, pages 181–198. Wiley-Iste: London, United Kingdom.

Raeini, A. Q., Bijeljic, B., and Blunt, M. J. (2017). Generalized network modeling: Network extraction as a coarse-scale discretization of the void space of porous media. *Physical Review E*, 96(1):013312.

Raut, A. and Indraratna, B. (2004). Constriction size distribution of a non-uniform granular filter. In *Proc., 15th South East Asian Geotechnical Conf*, pages 409–414.

Raut, A. K. (2006). *Mathematical modelling of granular filters and constriction-based filter design criteria*. PhD thesis.

Raut, A. K. and Indraratna, B. (2008). Further advancement in filtration criteria through constriction-based techniques. *Journal of Geotechnical and Geoenvironmental Engineering*, 134(6):883–887.

Reboul, N. (2008). *Transport de particules dans les milieux granulaires. Application à l'érosion interne*. PhD thesis, Ecole centrale de Lyon.

Reboul, N., Vincens, E., and Cambou, B. (2008). A statistical analysis of void size distribution in a simulated narrowly graded packing of spheres. *Granular Matter*, 10(6):457–468.

Reboul, N., Vincens, E., and Cambou, B. (2010). A computational procedure to assess the distribution of constriction sizes for an assembly of spheres. *Computers and Geotechnics*, 37(1):195–206.

Reddi, L. N., Xiao, M., Hajra, M. G., and Lee, I. M. (2005). Physical clogging of soil filters under constant flow rate versus constant head. *Canadian geotechnical journal*, 42(3):804–811.

Richard, P., Oger, L., Troadec, J., and Gervois, A. (1998). Tessellation of binary assemblies of spheres. *Physica A: Statistical Mechanics and its Applications*, 259(1):205–221.

Richards, K. S. and Reddy, K. R. (2007). Critical appraisal of piping phenomena in earth dams. *Bulletin of Engineering Geology and the Environment*, 66(4):381–402.

Roozbahani, M. M., Graham-Brady, L., and Frost, J. D. (2014). Mechanical trapping of fine particles in a medium of mono-sized randomly packed spheres. *International Journal for Numerical and Analytical Methods in Geomechanics*, 38(17):1776–1791.

Roux, J.-N. and Chevoir, F. (2005). Simulation numérique discrete et comportement mécanique des matériaux granulaires. *Bulletin des Laboratoires des Ponts et Chaussées*, 254:pp–109.

Rowe, R. (2005). Long-term performance of contaminant barrier systems. *Géotechnique*, 55(9):631–678.

Sabiri, N.-E., Caylet, A., Montillet, A., Le Coq, L., and Durkheim, Y. (2017). Performance of nonwoven geotextiles on soil drainage and filtration. *European Journal of Environmental and Civil Engineering*, pages 1–19.

Sari, H., Chareyre, B., Catalano, E., Philippe, P., and Vincens, E. (2011). Investigation of internal erosion processes using a coupled dem-fluid method. In *Particles 2011 II International Conference on Particle-Based Methods, E. Oate and DRJ Owen (eds.), Barcelona*, pages 1–11.

Schaller, F. M., Kapfer, S. C., Evans, M. E., Hoffmann, M. J., Aste, T., Saadatfar, M., Mecke, K., Delaney, G. W., and Schröder-Turk, G. E. (2013). Set voronoi diagrams of 3d assemblies of aspherical particles. *Philosophical Magazine*, 93(31-33):3993–4017.

Scheuermann, A. and Bieberstein, A. (2007). Determination of the soil water retention curve and the unsaturated hydraulic conductivity from the particle size distribution. In *Experimental Unsaturated Soil Mechanics*, pages 421–433. Springer.

Scheuermann, A., Kiefer, J., et al. (2010). Internal erosion of granular materials – identification of erodible fine particles as a basis for numerical calculations. In *Proceedings of the 9th International Congress of the Hellenic Society of Theoretical and Applied Mechanics (HSTAM)*, pages 275–282. Hellenic Society for Theoretical & Applied Mechanics (HSTAM).

Scholtès, L. and Donzé, F.-V. (2013). A dem model for soft and hard rocks: role of grain interlocking on strength. *Journal of the Mechanics and Physics of Solids*, 61(2):352–369.

Schuler, U. (1996). Scattering of the composition of soils. an aspect for the stability of granular filters. In *Proceedings of Geofilters*, volume 96, pages 21–34.

Seblany, F., Homberg, U., Vincens, E., Winkler, P., and Witt, K. (2017). Merging criteria for the definition of a local pore and the CSD computation of granular materials. pages 150–159.

Seblany, F., Homberg, U., Vincens, E., Winkler, P., and Witt, K. J. (2018). Merging criteria for defining pores and constrictions in numerical packing of spheres. *Granular Matter*, 20(3):37.

Semar, O. and Witt, K. (2006). Internal erosion – state of the art and an approach with percolation theory. In *Proceedings of the 3rd International Conference on Scour and Erosion (ICSE-3)*, pages 602–606.

Sherard, J. L. (1979). Sinkholes in dams of coarse, broadly graded soils. In *Proceedings of 13th ICOLD, New Delhi, India*, pages 25–34.

Sherard, J. L. and Dunnigan, L. P. (1989). Critical filters for impervious soils. *Journal of Geotechnical Engineering*, 115(7):927–947.

Sherard, J. L., Dunnigan, L. P., and Talbot, J. R. (1984). Basic properties of sand and gravel filters. *Journal of Geotechnical Engineering*, 110(6):684–700.

Shigeto, Y. and Sakai, M. (2011). Parallel computing of discrete element method on multi-core processors. *Particuology*, 9(4):398–405.

Shire, T. and O'Sullivan, C. (2016). Constriction size distributions of granular filters: a numerical study. *Géotechnique*, 66(10):826–839.

Shire, T. and O'Sullivan, C. (2017). A network model to assess base-filter combinations. *Computers and Geotechnics*, 84:117–128.

Shire, T., O'Sullivan, C., and Gaudray, G. (2012). Comparison of two methods for measurement of soil constriction size distribution. In *Proceeding of the Sixth International Conference on Scour and Erosion, Paris*.

Silveira, A. (1965). An analysis of the problem of washing through in protective filters. In *Proceedings of the 6th International Conference on Soil Mechanics and Foundation Engineering, Montréal, Que*, pages 551–555.

Silveira, A. (1993). A method for determining the void size distribution curve for filter materials. In *Proceedings of GEOFILTERS'1992 International Conference on Filters and Filtration Phenomena in Geotechnical Engineering*, pages 71–73. Karlsrule, Germany.

Silveira, A., de Lorena Peixoto, T., and Nogueira, J. (1975). On void size distribution of granular materials. In *Proceedings of the 5th Pan American Conference on Soil Mechanics and Foundation Engineering, Buenos Aires*, pages 161–177.

Sitharam, T., Dinesh, S., Shimizu, N., et al. (2002). Micromechanical modelling of monotonic drained and undrained shear behaviour of granular media using three-dimensional dem. *International Journal for Numerical and Analytical methods in Geomechanics*, 26(12):1167–1189.

Sjah, J. and Vincens, E. (2013). Determination of the constriction size distribution of granular filters by filtration tests. *International Journal for Numerical and Analytical Methods in Geomechanics*, 37(10):1231–1246.

Šmilauer, V., Catalano, E., Chareyre, B., Dorofeenko, S., Duriez, J., Gladky, A., Kozicki, J., Modenese, C., Scholtès, L., Sibille, L., et al. (2010). *Yade reference documentation*. http://yadedem.org/doc/.

Soria, M., Aramaki, R., and Viviani, E. (1993). Experimental determination of void size curves. In *Brauns, J and Heibaum, M and Schuler, U, (eds.) Filters in Geotechnical and Hydraulic Engineering*, pages 43–48. Balkema, Rotterdam, The Netherlands.

Sufian, A., Russell, A. R., Whittle, A. J., and Saadatfar, M. (2015). Pore shapes, volume distribution and orientations in monodisperse granular assemblies. *Granular Matter*, 17(6):727–742.

Taylor, H., O'Sullivan, C., Shire, T., and Moinet, W. (2018). Influence of the coefficient of uniformity on the size and frequency of constrictions in sand filters. *Géotechnique*, pages 1–9.

Taylor, H., O'Sullivan, C., and Sim, W. (2015). A new method to identify void constrictions in micro-ct images of sand. *Computers and Geotechnics*, 69:279–290.

Taylor, H. F., O'Sullivan, C., Sim, W. W., and Carr, S. J. (2017). Sub-particle-scale investigation of seepage in sands. *Soils and Foundations*, 57(3):439–452.

Tejada, I., Sibille, L., and Chareyre, B. (2016). Role of blockages in particle transport through homogeneous granular assemblies. *EPL (Europhysics Letters)*, 115(5):54005.

Terzaghi, K., Peck, R. B., and Mesri, G. (1996). *Soil mechanics in engineering practice*. John Wiley & Sons.

Thommes, M. (2010). Physical adsorption characterization of nanoporous materials. *Chemie Ingenieur Technik*, 82(7):1059–1073.

Thornton, C. (2000). Numerical simulations of deviatoric shear deformation of granular media. *Géotechnique*, 50(1):43–53.

Tong, A.-T., Catalano, E., and Chareyre, B. (2012). Pore-scale flow simulations: model predictions compared with experiments on bi-dispersed granular assemblies. *Oil & Gas Science and Technology–Revue d'IFP Energies nouvelles*, 67(5):743–752.

Vakili, A. and Selamat, M. (2014). An assessment of veracity of filter criteria for earth dams. In *Proceedings of the Institution of Civil Engineers-Geotechnical Engineering*, volume 167, pages 574–584.

Vakili, A., Selamat, M., and Abdul Aziz, H. (2015). Filtration of broadly graded cohesive dispersive base soils. *Journal of Geotechnical and Geoenvironmental Engineering*, 141(5).

Vakili, A., Selamat, M., Mohajeri, P., and Moayedi, H. (2018). A critical review on filter design criteria for dispersive base soils. *Geotechnical and Geological Engineering*, 36(4):1933–1951.

van der Linden, J. H., Narsilio, G. A., and Tordesillas, A. (2016). Machine learning framework for analysis of transport through complex networks in porous, granular media: a focus on permeability. *Physical Review E*, 94(2):022904.

van der Linden, J. H., Sufian, A., Narsilio, G. A., Russell, A. R., and Tordesillas, A. (2018). A computational geometry approach to pore network construction for granular packings. *Computers & Geosciences*, 112:133–143.

Vaughan, P., Bridle, R., and Hewlett, H. (2004). An update on perfect filters. *Long-term Benefits and Performance of Dams (Hewlett H (ed.)). Thomas Telford, London, UK*, pages 516–531.

Vaughan, P. and Soares, H. F. (1982). Design of filters for clay cores of dams. *Journal of Geotechnical and Geoenvironmental Engineering*, 108(ASCE 16807).

Vincens, E., Witt, K. J., and Homberg, U. (2015). Approaches to determine the constriction size distribution for understanding filtration phenomena in granular materials. *Acta Geotechnica*, 10(3):291–303.

Vogel, H.-J. and Roth, K. (2001). Quantitative morphology and network representation of soil pore structure. *Advances in Water Resources*, 24(3):233–242.

Wan, C. F. and Fell, R. (2008). Assessing the potential of internal instability and suffusion in embankment dams and their foundations. *Journal of Geotechnical and Geoenvironmental Engineering*, 134(3):401–407.

Wang, Y. and Dallo, Y. A. (2014). On estimation of the constriction size distribution curve for cohesionless soils. *European Journal of Environmental and Civil Engineering*, 18(6):683–698.

Witt, K. J. (1986). *Filtrationsverhalten und bemessung von erdstoff-filtern*, volume 104. Institut für Bodenmechanik und Felsmechanik der Universität Fridericiana, Karlsruhe.

Witt, K. J. (1993). Reliability study of granular filters. *Filters in Geotechnical and Hydraulic Engineering*, pages 35–42.

Wittmann, L. (1979). The process of soil-filtration - Its physics in engineering practice. In *Proceedings of the 7th European Conference on Soil Mechanics and Foundation Engineering*, volume 1, pages 303–310.

Wu, L., Nzouapet, B. N., Vincens, E., and Bernat-Minana, S. (2012). Laboratory experiments for the determination of the constriction size distribution of granular filters. In *Proceedings of 6th International Conference on Scour and Erosion (ICSE-6)*.

Xiong, Q., Baychev, T. G., and Jivkov, A. P. (2016). Review of pore network modelling of porous media: experimental characterisations, network constructions and applications to reactive transport. *Journal of Contaminant Hydrology*, 192:101–117.

Yang, R., Zou, R., Yu, A., and Choi, S. (2006). Pore structure of the packing of fine particles. *Journal of Colloid and Interface Science*, 299(2):719–725.

Yuan, H., Shapiro, A., You, Z., and Badalyan, A. (2012). Estimating filtration coefficients for straining from percolation and random walk theories. *Chemical Engineering Journal*, 210:63–73.

Zhang, L., Xu, Y., and Jia, J. (2009). Analysis of earth dam failures: A database approach. *Georisk*, 3(3):184–189.

Zhang, Z., Liu, L., Yuan, Y., and Yu, A. (2001). A simulation study of the effects of dynamic variables on the packing of spheres. *Powder Technology*, 116(1):23–32.

dernière page de la thèse

AUTORISATION DE SOUTENANCE

Vu les dispositions de l'arrêté du 25 mai 2016,

Vu la demande du directeur de thèse

Monsieur E. VINCENS

et les rapports de

M. D. MAROT
Professeur - IUT de Saint-Nazaire - 58 rue Miche Ange - 44606 SAINT-NAZAIRE cedex

et de

M. P. PHILIPPE
Directeur de Recherche - IRSTEA - 3275 Route de Cézanne - 13100 Aix-en-Provence

Madame SEBLANY Feda

est autorisée à soutenir une thèse pour l'obtention du grade de **DOCTEUR**

Ecole doctorale MECANIQUE, ENERGETIQUE, GENIE CIVIL ET ACOUSTIQUE

Fait à Ecully, le 3 décembre 2018

P/Le directeur de l'E.C.L.
La directrice des Etudes

ECOLE CENTRALE DE LYON
Service Scolarité
ECULLY

M-A. GALLAND